Molecularly Imprinted Polymers: Towards a Rational Understanding of Biomimetic

Materials

A Thesis

Presented to

The Academic Faculty

by

Alexandra Molinelli

In Partial Fulfillment

of the Requirements for the Degree

Doctor of Philosophy in Chemistry

Georgia Institute of Technology

October 2004

Molecularly Imprinted Polymers: Towards a Rational Understanding of Biomimetic

Materials

Approved by:

Dr. Boris Mizaikoff, Advisor

Dr. Jiri Janata

Dr. Mira Josowicz

Dr. Marcus Weck

Dr. Ching-Hua Huang

October 14th 2004

ACKNOWLEDGMENT

My sincere thanks first and foremost go to my supervisor Professor Dr. Boris Mizaikoff, who gave me this great opportunity to do my PhD thesis at the Applied Sensors Laboratory, School of Chemistry and Biochemistry, Georgia Institute of Technology. He always has been a great scientific advisor and mentor.

I also would like to express my appreciation and thanks to the members of my committee who have followed me along these past years and provided knowledge, insight, and experience helping throughout my work.

Furthermore, I would like to offer my gratitude to the School of Chemistry and Biochemistry and to my colleagues and friends for their help and support, making this time at Tech an enjoyable one.

I acknowledge with thanks and appreciation Dr. Michael Jakusch for enabling use of the computing facilities at the Austrian Research Center Seibersdorf (ARC, Division of Environmental and Life Sciences) and helping with the molecular dynamics simulations.

Many thanks to all the members of the Applied Sensors Laboratory, for their help, support, friendship, and for the many interesting and useful discussions. Especially I would like to thank Manfred Karlowatz for the many discussions on the IR studies, and our collaborator John O'Mahony from Dublin City University for the great team work!

And last but not least, many thanks go to my friends in Atlanta, without whom I would not have enjoyed as much my time in the United States!

TABLE OF CONTENTS

LIST OF TABLES

LIST OF FIGURES

xiv

xviii

xix

LIST OF ABBREVIATIONS

AA	Acrylamide
3-ac-DON	3-Acetyl-DON
15-ac-DON	15-Acetyl-DON
APCI	Atmospheric Pressure Chemical Ionization
AU	Arbitrary Units
BET	Brunauer Emmett Teller
CCl_4	Carbontetrachloride
$CDCl_3$	Deuterated Chloroform
C-fla	2-Carbethoxy-5,7-dihydroxy-4'-methoxyisoflavone
$CHCl_3$	Chloroform
CTL	Control
2,4-D	2,4-Dichlorophenoxyacetic Acid
DAD	Diode Array Detector
DON	Deoxynivalenol
DVB	Divinylbenzene
ε	Molar Absorptivity
ECD	Electron Capture Detector
EGDMA	Ethyleneglycol Dimethacrylate
FLD	Fluorescence Detector
FTIR	Fourier Transform Infrared
G	Guest
GC	Gas Chromatography

H	Host
HPLC	High Pressure Liquid Chromatography
I.D.	Inner Diameter
IMP	Imprinted
IR	Infrared
ITC	Isothermal Titration Calorimetry
K_b or K	Binding Constant
K_{dim}	Dimerization Constant
K_d	Dissociation Constant
K_{OW}	Octanol-Water Partition Coefficient
L	Ligand
LC	Liquid Chromatography
LOD	Limit of Detection
MAA	Methacrylic Acid
MCT	Mercury-Cadmium-Telluride
MD	Molecular Dynamics
MIP	Molecularly Imprinted Polymer
MIR	Mid Infrared
MISPE	Molecularly Imprinted Solid Phase Extraction
MMA	Methyl methacrylate
MS	Mass Spectrometer
NMR	Nuclear Magnetic Resonance
NP	Nitrophenol
ppb	Part Per Billion
ppm	Parts Per Million

R	Relaxation Rate
RI	Retention Index
RSD	Relative Standard Deviation
S	Substrate
SFE	Supercritical Fluid Extraction
SPE	Solid Phase Extraction
T_1	Spin Lattice Relaxation Time
TFM	2-Trifluoromethylacrylic acid
V_B	Breakthrough volume
4-VP	4-Vinylpyridine
ZON	Zearalenone

SUMMARY

Within the last decade, interest in molecularly imprinted polymers (MIPs) has strongly increased, with potential applications ranging from solid phase extraction materials to antibody-like sorbent assays and selective recognition layers in sensing devices. Advantages such as chemical, mechanical and thermal stability together with high selectivity for the templated analyte render MIPs interesting alternatives to routinely applied separation materials or antibodies. While non-covalently imprinted MIPs have been extensively characterized and their viability in real world applications demonstrated, only recently the need of relating the MIP binding site heterogeneity to the basic mechanisms during MIP synthesis has been emphasized for the development of optimized recognition materials. It is assumed that complex formation based on non-covalent interactions between the template analyte, the functional monomer, and the cross-linker is ultimately responsible for a successful imprint. However, confirmation of the proposed mechanisms is essential for the development of optimized MIPs.

The research described in this thesis contributes to the development of new strategies facilitating advanced understanding of the fundamental principles governing selective recognition of molecularly imprinted polymers at a molecular level, which is a prerequisite for the rational optimization of biomimetic materials. The nature of non-covalent interactions involved in the templating process of molecularly imprinted polymers based on the self-assembly approach were investigated with a variety of analytical techniques addressing molecular level interactions. For this purpose, the concerted application of IR and ^{1}H-NMR spectroscopy enabled studying the complexation of template molecules with a variety of functional monomers in the pre-polymerization solution by systematically varying the ratio of the involved components.

- Molecular level interactions such as hydrogen bonding, π-π stacking, van der Waals, and electrostatic interactions governing complex formation of 2,4-dichlorophenoxyacetic acid (2,4-D) as well as the structural isomers o-, m-, and p-nitrophenol with the functional monomers 4-vinylpyridine and methacrylic acid were investigated in aqueous and non protic porogenic solvents. In each medium, information on the interaction types, thermodynamics, and complex stoichiometry was applied toward predicting the optimum imprinting building blocks and ratios. 4-vinylpyridine was the functional monomer of choice, as it revealed increased interactions with the templates 2,4-D and 4-nitrophenol compared to methacrylic acid. Both IR and NMR measurements demonstrated that hydrogen bonding was the main interaction involved in the association between the templates and 4-VP in aprotic solvents. Furthermore, NMR measurements confirmed the importance of hydrophobic effects combined with π-π stacking interactions in aqueous solutions, thus confirming the importance of simultaneous multiple-site interactions for a successful imprinting strategy. The studies were performed in aprotic solvents such as carbon tetrachloride, chloroform, and the more polar acetonitrile. Furthermore, interactions in polar protic solvents such as water and water/methanol mixtures were investigated, which corroborated the importance of solvent effects on the complexation. For the first time, spin-lattice relaxation time NMR measurements were applied in the field of molecular imprinting following the behavior of molecular binding sites involved in the complex formation along with changes in the micro-environment of the template in solution. In addition, Job's plot analysis was performed with both IR and NMR data providing concordant results on complex stoichiometries for 2,4-D:4-VP ranging from 1:1 in CCl_4 (IR) or $CDCl_3$ (NMR) to 1:3 in D_2O

(NMR). These results are in accordance with the 1:4 ratio used for successful imprinting of 2,4-D at experimental conditions enhancing complexation formation in porogenic solution. Furthermore, following the interactions of 2-, 3-, and 4-nitrophenol with commonly used functional monomers revealed the importance of the steric distribution of binding sites of the template molecule and the availability of these functional groups for multiple-site interactions. IR studies in pre-polymerization solution showed identical results to the HPLC characterization of MIPs imprinted for 2-, 3-, and 4-nitrophenol, thereby for the first time demonstrating the utility of IR investigations for pre-screening the optimum functional monomer/template combination in solution.

- In order to investigate the effect of the ratio between template, functional monomer, and cross-linker on the resulting MIP selectivity, quercetin was selected as template along with a systematic variation of the mixing ratio with the functional monomer. HPLC characterization of thus produced MIPs were compared to control polymers enabling a systematic approach to imprinting based on advanced understanding of the factors governing the formation of high-affinity binding sites during the polymerization. The ratio 1:8:40 (quercetin: 4-vinylpyridine:ethyleneglycol dimethacrylate) was found to result in optimal imprinting of quercetin. Varying the template-functional monomer ratio enabled tuning of polymer recognition properties while varying the cross-linker ratio affected polymer morphology determining the range of possible applications.

- Molecularly imprinted polymers for the mycotoxins deoxynivalenol (DON) and zearalenone (ZON) were developed using DON and 3-acetyl-DON as template as well as quercetin as dummy template for ZON and applied as separation materials for advanced sample preparation in beverage analysis. The obtained

results demonstrated the potential of MIPs for rapid one-step sample clean-up and pre-concentration of mycotoxins from beverages such as beer.

- HPLC characterization of the MIPs synthesized within this work using the template molecules quercetin, 2,4-dichlorophenoxyacetic acid, and deoxynivalenol along with their respective structural analogues enabled investigating the importance of the combination of size, shape, and molecular functionalities for the selective recognition properties of MIPs compared to non-selective control polymers.

- Molecular dynamics simulations of 2,4-dichlorophenoxyacetic acid and its interactions with the functional monomer 4-vinylpyridine in aqueous and aprotic explicit solvent allowed demonstrating the fundamental potential of computer MD simulations for predicting optimized pre-polymerization ratios and the involved interaction types, especially if interpreted in combination with experimental results obtained from IR and NMR studies. Simulation results indicated π-π stacking in aqueous solution and hydrogen bonding in chloroform, which are the main interaction types confirmed by the experimental results (IR/NMR) obtained in this study.

A direct comparison between the predicted optimum ratios of the involved building blocks and those obtained by trial-and-error leading to successfully imprinted polymers was performed throughout this work. The obtained results clearly demonstrate that the application of rapid IR/NMR pre-screening methods in combination with molecular modeling strategies is a promising strategy towards optimized imprinting protocols in lieu of the conventionally applied labor intensive and time-consuming trial-and-error approach.

1. INTRODUCTION

1.1 MIPs as Biomimetic Materials

Biologically inspired (biomimetic) recognition properties are nowadays widely engineered into synthetic materials and structures by mimicking motifs found in nature. The ability of many biomolecules to selectively recognize and bind to a specific substrate is a key process essential to every biological system. Selective molecular receptor recognition usually occurs via formation of non-covalent bonds. Accordingly, selective binding of a guest molecule is among the most desirable properties of man-made antibody and receptor mimics [1]. While antibodies are used in a wide variety of analytical applications many of them remain costly with comparatively short shelf-life. The synthesis of biomimetic recognition elements featuring synthetic receptor sites capable of selective target binding/rebinding with comparable efficiency to substrate-enzyme or antibody-antigen interactions is among the main goals of molecular imprinting.

1.2 Scope of This Work

In general, non-covalent templating techniques rely on the nature and stability of the complex formed between the target analyte and functional monomer building blocks prior to radical polymerization, which ultimately governs the amount of high-affinity binding sites and the binding site distribution obtained within the resulting polymeric recognition material. Therefore, molecular level understanding of the interactions responsible for complex formation and complex stability during the templating procedure

is crucial for rational understanding and development of designed biomimetic recognition materials. Furthermore, knowledge of strength of interactions and complex stoichiometry are necessary for further development of components involved in imprinting as well as choosing the optimum monomers for a given template. The aim of this thesis is to assess the factors responsible for a successful imprinting and to assess the applicability and feasibility of using IR and ^{1}H-NMR spectroscopy to characterize in pre-polymerization solution inter-molecular processes at a molecular level for the pre-screening of components involved in molecular imprinting for a chosen template analyte. Furthermore, the use of molecular dynamic simulations as a useful tool for functional monomer pre-screening in explicit solvent was investigated.

2. BACKGROUND

2.1 Molecularly Imprinted Polymers

2.1.1 Introduction

Molecular imprinting applied in the present work is based on non-covalent self-assembly of the template with functional monomers prior to polymerization. Free radical polymerization with a cross-linking monomer stabilizes the template-functional monomer complexes, resulting in a mechanically and thermally stable polymer. After extractive removal of the template, the remaining molecularly imprinted polymer matrix contains 3-dimensional binding cavities facilitating rebinding due to complementary shape and functionality for the template molecule.

While this imprinting strategy appears simple and straight forward, application of imprinted polymers in analytical chemistry is still limited as reality offers templated materials with low yields of high-affinity binding sites, trial-and-error approaches for MIP synthesis of new target molecules mainly following already established imprinting protocols, and – most importantly - lack of a rational understanding and tailoring of the molecular imprinting strategy. These considerations are contrasted by an exponentially increasing number of successful imprinting attempts reported in literature. In particular, the – at least at first sight - ease of preparation, along with superior chemical and mechanical properties render molecularly imprinted polymers an appealing alternative to natural receptors for a variety of applications ranging from analytical measurements to environmental clean-up, toxicant removal and selective filtration.

Given the controversy surrounding molecularly imprinted polymers, in depth understanding on how MIPs work, why they work or why they might not work in certain applications appears crucial to the future utility and more widespread use of molecular imprinting techniques.

2.1.2 Molecular imprinting strategies and procedures

During the molecular imprinting process highly cross-linked co-polymers are formed around analyte molecules acting as cavity-creating templates. The template molecules are then removed, providing binding sites ideally complementary in size, shape and functionality to the templated analyte. Upon re-introduction of the template preferential rebinding within the cavity should occur.

In the pre-polymerization mixture, the dissolved target analyte interacts by covalent, non-covalent, or metal coordination interactions with the functional monomer responsible for localizing the chemically active moieties of the target molecules during co-polymerization. Consequently, molecular imprinting is classified into covalent imprinting (pre-organized approach), non-covalent imprinting (self-assembly approach), and semi-covalent imprinting according to the type of interactions between functional monomer building blocks and target molecules in the pre-polymerization mixture and during rebinding (see Figure 1).
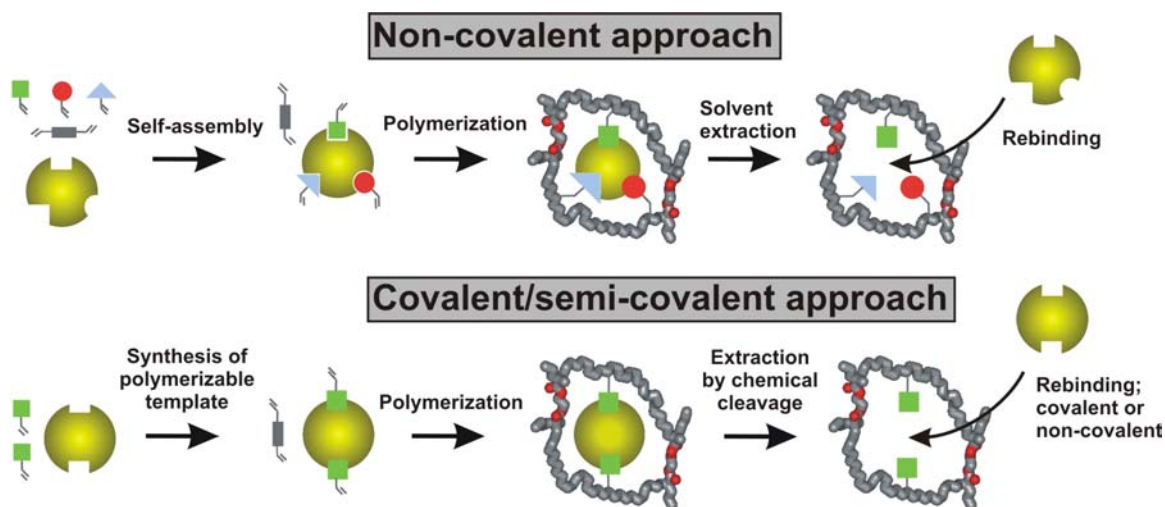
Figure 1 Principle of molecular imprinting.

The covalent approach to molecular imprinting promises the most homogeneous binding site distribution with largely identical binding pockets. The binding constants for the template molecule are high, since the interaction between template and functional monomer is based on covalent interactions sure to withstand polymerization conditions. A chemical synthesis step is necessary to bind the template to the functional monomer with bond types such as Schiff bases, boronates, ketals, carboxylic amides and esters. However, despite the high affinities of the polymeric material, the range of functional groups which can be targeted is restricted and removal of the template molecules is tedious (chemical cleavage) and limits the application of covalently prepared MIPs. Furthermore, slow binding kinetics restrict the analytical application of covalently imprinted MIPs, if rebinding is based on reversible covalent bonds. Alternatively, in the semi-covalent approach rebinding occurs via non-covalent interactions taking advantage of faster rebinding kinetics.

In non-covalent molecular imprinting, complexes assembled by non-covalent interactions are formed in the pre-polymerization mixture. Complexation is achieved by mixing

template, functional monomer, and cross-linker in a porogenic solvent matrix. As a consequence, sufficient complex stability is required to enable binding pocket formation during the polymerization process. In contrast to covalent imprinting, the self-assembly approach is characterized by a more heterogeneous binding site distribution. Resulting, sample overload may occur due to rapid saturation of the comparatively low amount of high-affinity binding sites, which results in a significantly decreased overall polymer performance. Nevertheless, the – again at least at first sight - simple preparation procedures, the wide range of imprintable compounds, and reversible host-guest binding based on non-covalent interactions ('biomimetic binding') render the non-covalent imprinting approach the most widespread method for MIP preparation. Given its versatility and closest resemblance of naturally occurring recognition mechanisms, the discussion in the remainder of this study will focus on non-covalent imprinting.

2.1.3 Non-covalent molecular imprinting

In recent years, two very important statements about MIPs have been made. In 2000 Nicholls et al. state that "… the extent of complexation governs the recognition properties of the imprinted polymer formed …"[2]. Even more striking are the findings reported by Andersson in 1997 that "… approx. 0.3-0.6% of template molecules successfully form complexes in pre-polymerization mixtures …" [3]. Though such numbers are occasionally conveyed in literature also by other groups, they usually receive much less attention than reports on successfully prepared new MIPs. The statements above summarize evident conditions, which appear to be less than favorable for a successful imprinting strategy. Throughout this thesis research, we would like to

focus most of our attention to these circumstances asking the question "If MIPs work – and apparently they do – can we understand why?"

2.1.3.1 Inherent problems to non-covalent molecular imprinting

In supramolecular host/guest chemistry a guest molecule fits the internal cavity of a correspondingly designed host structure. Bond fixation, coordination (self-assembly involving coordination chemistry), and molecular recognition are three important factors in this process. In the recognition step, spatial (shape/size) and chemical (functional groups) complementarity play a crucial role. Similarly, molecularly imprinted polymers provide biomimetic receptor sites, which may recognize and selectively rebind the templated analyte. Evidently, the performance of MIPs will depend on the quality of the binding pockets and binding sites. Consequently, an increasing number of interaction sites involved in the recognition process will improve the differentiation capabilities of a receptor between structurally analogous substrates. By the same argument, a 3-dimensional cavity with multiple interaction sites will provide superior binding to its guest molecule. Adverse to these considerations, the self-assembly approach inherently leads to a heterogeneous binding site distribution with only a small percentage of the binding sites exhibiting high affinity towards the template molecule. Hence, two effects need to be balanced: (i) if the binding constant is too high, the guest molecule will block the binding site and will prevent further use of the biomimetic polymer; (ii) if the binding constant is too low, the MIP will show limited selective recognition. These simple initial considerations already lead to a very important conclusion: without knowledge on and deliberate control over intermolecular forces involved in non-covalent molecular imprinting, no reliable predictions on structure and properties of the formed pre-

polymerization complexes and, consequently, on the recognition properties of the resulting MIP can be made.

Information associated with the binding pockets resulting from the imprinting process includes conformational information on size, shape, and polarity of the surrounding polymer matrix, along with evidence on the steric arrangement of functionalities and the electronic properties (charge, polarity, Van der Waals forces; see Table 1).

Table 1 Parameters contributing to molecular recognition.

Parameters involved in molecular recognition events
Size
Shape (conformation, configuration)
Functionality (shape + functionality → chirality)
Electronic properties of binding analyte
Electronic properties of surrounding polymer matrix (polarity, functionalities)
Reactivity of binding site (ionic interactions)
Accessibility of binding site (polymer porosity, density)
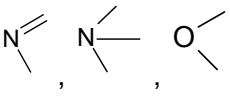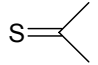
Evidence for shape selectivity in MIPs synthesized via non-covalent interactions has been found using molecular probes of different sizes [4]. In the self-assembly approach, the cross-linker may be a third component influencing the properties of the formed pre-polymerization complexes. The binding constants of different possible complex configurations ultimately determine their ability to 'survive' the polymerization process, which results in the formation of binding pockets or binding sites. In consequence, it is expected that polymers with a heterogeneous binding site distribution will be formed with

affinity distributions ranging from binding sites with high affinity for the template, to non-specific binding to the cross-linked polymer matrix, including multi-site recognition (multimers) [5]. Results on studies related to the nature of recognition in MIPs are widely contradictive and range from indications towards recognition taking place in cavities and not by interaction with residual template molecules, to recognition due to residual template interaction [6,7].

2.1.3.2 Molecular interactions involved in non-covalent imprinting

The main non-covalent interactions responsible for molecular recognition in biomimetic systems are hydrogen bonding, ion-pairing, and π-π interactions (see Table 3). Furthermore, Coulombic attraction, charge transfer, induction, dispersion, and exchange-repulsion contribute to the complex formation. The driving forces of ion-pairing interactions (ion-ion, dipole-ion, dipole-dipole) are Coulombic interactions. Hydrogen bonding is a strong interaction playing an important role in naturally occurring non-covalent interactions. Complexes based on hydrogen bonding typically exhibit comparatively high stability constants. Table 2 gives examples of hydrogen bonding donor and acceptor groups.

Table 2 Hydrogen bonding donor and acceptor groups.

Donor	Acceptor
O—H	O$=$P
N^{+}—H	O$=$S
N—H	O$=$C , O$=$C
S—H	N$\diagdown$, N$-$, O$<$
C—H	S$=$
	aromatic π-e^{-} cloud

These interactions are favored in weakly polar aprotic solvents such as acetonitrile. In contrast, more polar protic solvents support interactions such as metal-ion coordination of the template molecule. Comparatively weak electrostatic interactions such as π-π stacking may occur between aromatic rings in polar solvents such as water and methanol. Hydrophobic interactions are only facilitated in highly polar solvents or solvent mixtures such as water/methanol.

Table 3 Types and estimated bond energies of non-covalent interactions.

Bond type	Bond energy [8,9,10] [kJ/mol]	Relative strength
Hydrogen bond	20[8] 4-60[9] 2-5[10]	weak/medium
Hydrophobic effects	1-3[8]	weak
Ion-ion (1/r)	250[8] 100-350[9]	strong
Dipole-ion ($1/r^2$)	15[8]	weak
Dipole-dipole ($1/r^3$)	2[8] 5-50[9]	weak/medium
π-π stacking	0-50[9]	weak/medium
Dispersion (London) ($1/r^6$) (attractive van der Waals)	2[8] <5[9]	weak
Cation-π	5-80[9]	medium

The wide variety of possible interactions implies that molecular recognition of a guest molecule may be dominated by one mode of molecular interaction or controlled by a combination of different recognition mechanisms, which are enabled or disabled depending on the polarity of the selected protic or aprotic porogen. In general, the combination of two or more interaction modes can be expected.

2.1.3.3 Role of the porogen

The solvent matrix plays a crucial role during the process of molecular imprinting. Besides influencing the polymer morphology, the solvent properties govern the types and the strength of non-covalent interactions available for the self-assembly processes. By the same argument, in depth understanding of these processes enables control of the recognition efficiency of the resulting MIP by appropriate selection of the solvent matrix and tuning of its dielectric properties. In general, optimum recognition during the application of MIPs occurs in the same solvent used as porogen during the polymerization. Nevertheless, MIPs prepared in aprotic solvents have also demonstrated recognition in entirely aqueous solutions [11,12]. The capability of operating in aqueous environments and organic solvents is a distinct advantage of MIPs in contrast to natural receptors. Despite successful applications in aqueous environments, exchanging the apolar organic solvent used during the imprinting step for a polar aqueous solvent during rebinding applications usually involves a loss of interactions favored in weakly polar aprotic solvents and leads to a decrease in overall performance of the MIP. According to literature, only few attempts of imprinting in the presence of polar solvents such as methanol and water were successful [13]. Nevertheless, imprinting at aqueous conditions would allow maintaining the same conditions during the rebinding step and - most importantly – operating in aqueous environments would facilitate imprinting of biomolecules.

2.1.3.4 Role of the polymer morphology

The polymer morphology and structure resulting from the imprinting process is important for the dynamic binding properties of the synthetic receptor sites. The ideal properties of the cross-linked polymer matrix with embedded binding sites are a compromise between structural rigidity of the matrix maintaining the integrity of the binding sites and sufficient flexibility facilitating access to the binding pockets. The recognition properties of MIPs ultimately depend on a variety of factors, including the diffusion/permeation properties of the synthesized polymer structure, binding to selective binding pockets and non-selective retention. These effects are schematically summarized in Figure 2 considering as an example the application of MIPs as stationary phase material in a separation column for liquid chromatography.
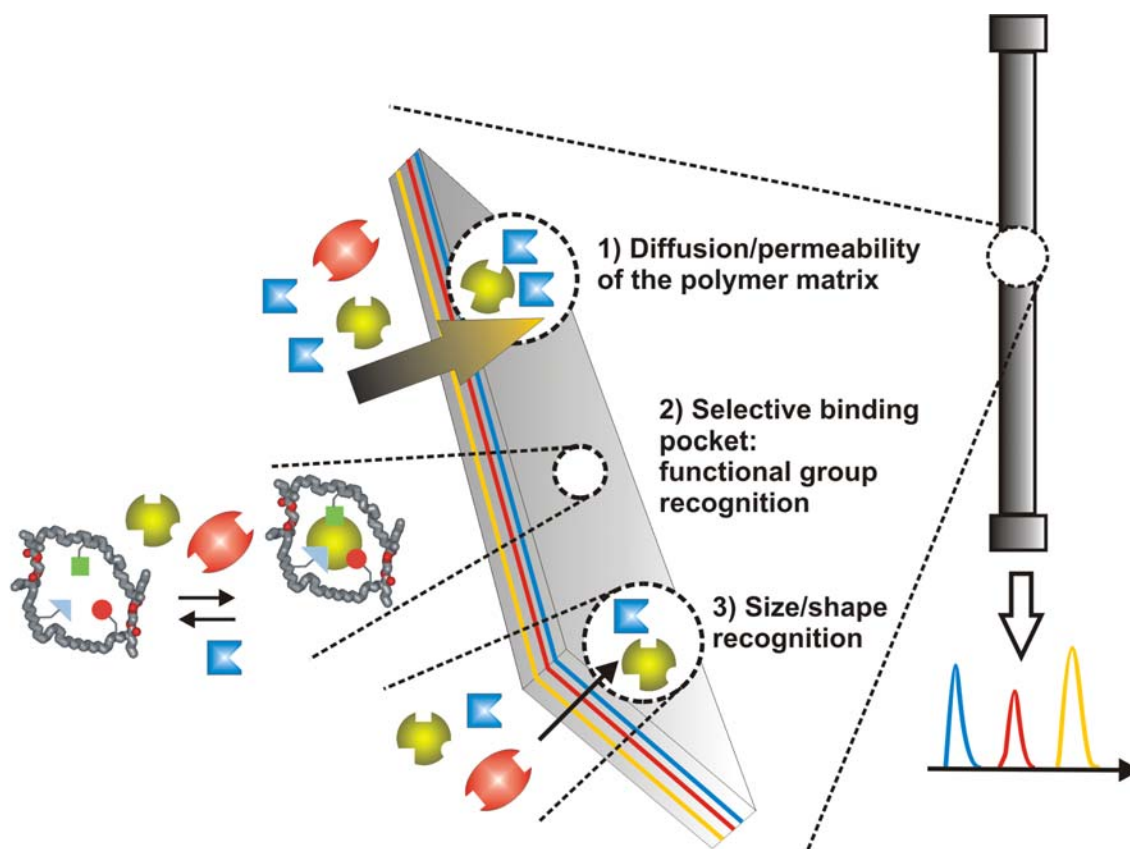
Figure 2 Schematic overview on factors affecting the recognition properties of a molecularly imprinted polymer for the example of a chromatographic separation phase. Next to diffusion properties and permeability of the stationary phase, effective separation of structural analogues will be governed by the availability of selective binding pockets next to retention by molecular size and shape.

In general, there are two main models for receptor behavior: (i) a rigid guest fitting into a rigid host structure according to E. Fischer's concept of lock-and-key [14], and (ii) conformational flexibility of both host and guest upon complexation following the concept of induced fit by D. E. Koshland [15]. Following the latter concept, structural plasticity of antigen-antibody complexes has been demonstrated by high-resolution crystal structure analysis [16]. In the synthetic case, the amount of cross-linker present during co-polymerization with a functional monomer will largely determine the rigidity of the imprinted polymer matrix. A high degree of cross-linker is necessary maintaining the

structural integrity of cavities formed during imprinting of the target analyte. However, due to the rigid polymeric structure steric obstruction of the template molecule certainly affects the association and dissociation rate of host-guest complexes formed within the embedded cavity. In contrast, sufficient flexibility of the polymer matrix facilitates access to the binding pockets.

The main driving force for a molecule to diffuse into and migrate through a polymer is its affinity to the matrix/binding pockets. While the affinity is related to chemical equality, dipole-dipole interactions and Van der Waals forces, the friction forces within the cross-linked polymer will determine the rate at which the molecules permeate. The initial friction force (diffusion coefficient) is determined by the size of the permeant and the dimensions of the void spaces of the strongly cross-linked polymer matrix. Furthermore, with increasing permeant volume, the internal stress imposed onto the polymer chains will cause the dimensions of the polymer to change resulting in polymer swelling effects, which may affect the integrity of the binding pockets.

Besides the structural flexibility of the polymer matrix, tuning of the void volume, i.e. porosity, is another parameter affecting access to embedded binding pockets. Selecting the appropriate polymerization method allows preparation of MIPs in different formats ranging from monolithic block polymers to micro- and nanospheres and polymer films.

During block-copolymerization a rigid polymer monolith is obtained, which is usually characterized by a multitude of micro- (< 2 nm), meso- (2 - 50 nm), and macropores (> 50 nm). The polymer monolith is then crushed, grinded and sieved to obtain particles with a well defined particle size distribution (see Figure 3).
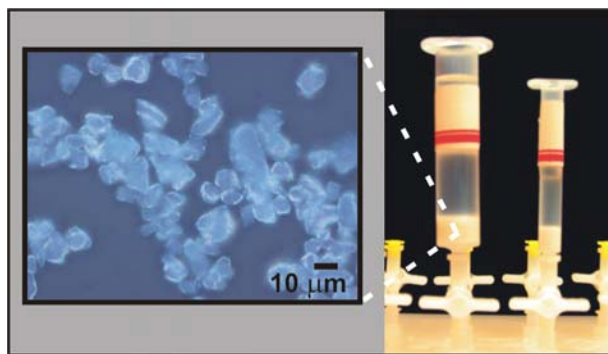
Figure 3 (left) Optical microscopy image (magnific. 50x) of molecularly imprinted polymer selective for quercetin used in solid phase extraction. Images of the MIP particles were acquired after block-copolymerization, crushing, grinding and sieving. (right) Solid phase extraction cartridge packed with 50 mg of quercetin-imprinted MIP.

Crushing of the monolith results in material loss and induces problems such as decreased interparticular volume and reduced mass transfer after packing into columns or cartridges. Nevertheless, this method of preparation is among the most commonly used formats for molecularly imprinted polymers. The porous MIP structure provides a high surface area and facilitates access to the binding pockets. Therefore, in case of a block polymer providing less flexibility of the cross-linked polymer matrix the pore size distribution is a key quality factor, which can be tuned by variables such as temperature, the nature and properties of the porogenic solvent, and the amount and type of cross-linker [17,18]. The effect of these variables on co-polymer porosity can be directly investigated by methods such as the BET method for surface area determination (see 2.2.3) and liquid extrusion porosimetry.

However, the generation of selective binding sites within the polymer matrix depends on the same variables and, hence, does not necessarily allow for concurrent tuning of the pore size. Furthermore, given a highly cross-linked polymer matrix a high degree of porosity facilitates but does not necessarily warrant for the required access to the embedded binding sites.

2.1.3.5 Thermodynamic considerations

In analogy to protein-peptide binding, enthalpy and entropy are highly correlated in a molecular recognition event using MIPs and contribute to the observed differences of thermodynamic results during MIP binding/rebinding events. Furthermore, the solvent structure plays a crucial role in these considerations.

Binding of a guest molecule to a host pocket should involve a measurable enthalpy change, which can be probed by methods such as isothermal titration calorimetry (ITC) or reliable assays determining binding affinities. However, due to the heterogeneous binding site distribution resulting from the self-assembly approach, the binding site structure strongly varies within the polymer. This is not the case in covalent imprinting, where template molecules and functional monomer building blocks are covalently linked prior to polymerization. Thus, the spatial arrangement of the involved components is pre-determined.

Recently, an elegant approach considerably reducing non-specific binding in non-covalent imprinting based on 'stoichiometric non-covalent imprinting' has been presented by Wulff et al. [19]. In this approach, a 1:1 or 1:2 molar ratio between template and functional monomer is used. It is shown that more than 90 % of the complex can be stabilized, if the association constants are in the range of $K_{ass} > 900$ M^{-1}. The development of new functional monomers enabling multiple-site functional group interactions with relatively high association constants for the template molecule in the pre-polymerization and during the polymerization steps, along with a spatially controlled arrangement of functional groups within the formed cavities benefits from both, the advantages of the covalent and the non-covalent imprinting approach.

Despite these synthetic considerations improving non-covalent imprinting strategies, the question remains, how favorable – from a thermodynamic point of view - is rebinding of the template molecule to the binding pocket?

In order to answer this question we may take advantage of the fact that the contributions of functional groups to drug/receptor interactions have already been widely studied. Average binding energies of common functional groups have been calculated providing a statistical estimate of the strength of non-covalent bonds associated with the investigated functional groups (see Table 2) [20]. While this information was initially used in drug design and for deriving structure-activity relationships, in a first approximation we can apply this knowledge to discuss molecular-level interactions in binding pockets of MIPs.

The Gibbs free energy change ΔG_{bind} of complex formation describing molecular recognition is given by [21-23:

$$\Delta G_{bind} = \Delta G_{t+r} + \Delta G_{r} + \Delta G_{hydr} + \Delta G_{vib} + \sum \Delta G_{polar} + \Delta G_{conf} + \Delta G_{vdWaals} \quad (1)$$

with ΔG_{t+r} translational and rotational

        ΔG_{r} restriction of rotors upon complexation

        ΔG_{hydr} hydrophobic interactions

        ΔG_{vib} residual soft vibrational modes

        $\Sigma(\Delta G_{polar})$ sum of interacting polar group contributions

        ΔG_{conf} adverse conformational changes

        $\Delta G_{vdWaals}$ unfavorable van der Waals interactions

Specifically, for studying template rebinding in MIPs equation (1) can be simplified to:

$$\Delta G_{bind} = \Delta G_{t+r} + \Delta G_r + \Delta G_{hydr} + \Delta G_{vib} + \sum \Delta G_{polar} \qquad (2)$$

Equation (2) assumes that (i) rebinding takes place in the solvent used as porogen during polymerization, (ii) that the conformational strain (ΔG_{conf}) of the template is minimal, and (iii) that no adverse van der Waals interactions ($\Delta G_{vdWaals}$) occur during rebinding to high-affinity binding sites. The detailed energetic contribution of these parameters to binding may help understanding molecular recognition events taking place during rebinding of a template molecule to a binding site embedded within a molecularly imprinted polymer matrix. Some contributions such as electrostatic interactions ($\Sigma\Delta G_{polar}$) may be evaluated by systematic studies varying the solvent polarity and using an array of structurally related compounds. However, in the self-assembly approach the distribution of resulting binding sites ranges from high affinity binding sites to low affinity binding sites, including e.g. induced binding sites, sites complementary to dimers or multimers, and shape selective cavities. Furthermore, non-selective binding contributes to the overall MIP performance. Heterogeneity of the binding site affinity and the number of high-affinity binding sites created in the resulting polymer matrix depend on the electronic properties of the building blocks and the types of interaction occurring between template, functional monomer, cross-linker, and porogen. Furthermore, they are influenced by polymerization variables such as temperature and pressure. In general, MIPs prepared with structurally rigid templates and functional monomers have shown higher selectivities compared to less-rigid templates affecting ΔG_r, as flexible molecules will have a variety of torsional degrees of freedom. Also, terms such as ΔG_{vib} are temperature dependent. Furthermore, the number and strength of interactions between template and functional monomer described by $\Sigma\Delta G_{polar}$ will determine the degree of selectivity of the resulting polymer [26]. In essence, the stability of the

template/functional monomer complex formed by self-assembly in the pre-polymerization solution will govern the number of high-affinity binding sites and, therefore, the performance of the synthesized non-covalent MIP. Hence, it is critical to the specificity of the prepared MIP that these pre-polymerization complexes are stabilized in order to withstand the polymerization conditions. Consequently, assessing the heterogeneity of the binding site distribution in MIPs by modeling of binding isotherms (see below) allows for better understanding of the imprinting procedure and provides insight for directed optimization of imprinting techniques.

2.1.3.6 Kinetic considerations

In order to approach the kinetics of MIP binding events we consider the kinetics of a binding reaction with H and G representing a pair of interacting molecules (e.g. antigen/antibody or host/guest in general):

$$H + G \overset{k_1}{\underset{k_{-1}}{\leftrightarrow}} HG \; ; \; K_1 = \frac{k_1}{k_{-1}} \qquad (3)$$
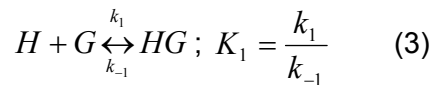
with k_1 association rate constant

      k_{-1} dissociation rate constant

The temporal progression of the binding reaction is described by:

$$\frac{d[HG]}{dt} = k_1[H][G] - k_{-1}[HG] \qquad (4)$$

Hence, different types of binding sites will be characterized by different rate constants k_i. Estimates of k_i are necessary to calculate the time to reach equilibrium conditions and we may ask the question, whether binding and/or release from binding sites in MIPs takes place within a reasonable period of time?

As a comparison, rate constants for antigen-antibody binding are in the range of 10^4 - 10^7 $M^{-1}s^{-1}$. Affinity constants for antibodies range from 10^6 to 10^9 M^{-1} (see Table 4) [24].

Table 4 Dissociation constants and sensitivity range for MIPs and natural antibodies.

Receptor	Range of dissociation constant K_d	Sensitivity range [$\mu g.L^{-1}$]
MIPs	nM-mM	0.1-100
Antibodies	nM-μM	0.01-10

In general, the amount of high-affinity binding sites in non-covalently prepared MIPs is estimated to be less than or around 1 % of the total number of binding sites. Hence, estimates of multiple host/guest interactions are difficult. However, dissociation constants in MIPs determined by modeling of binding isotherms yield results in the nM to mM ranges.

Thermodynamic and kinetic considerations certainly provide a better understanding of the parameters playing a governing role in obtaining a polymer with optimized recognition properties. Nevertheless, given the number of parameters with substantial impact on the resulting recognition properties it is evident that there is a tremendous need to analytically characterize each preparation step of molecularly imprinted polymers. Based on sufficient experimental evidence obtained by an array of analytical

methods suitable boundary conditions for modeling of molecular imprinting procedures can be established leading to rational design and optimization of MIPs.

2.1.4 Rational MIP design: analytical and computational approaches to understand how MIPs work

New insight into the mechanisms of molecular imprinting, which shall ultimately lead to rationally designed and improved polymers, can only be obtained by thorough analysis of the processing steps leading to the synthesis of an imprinted polymer.
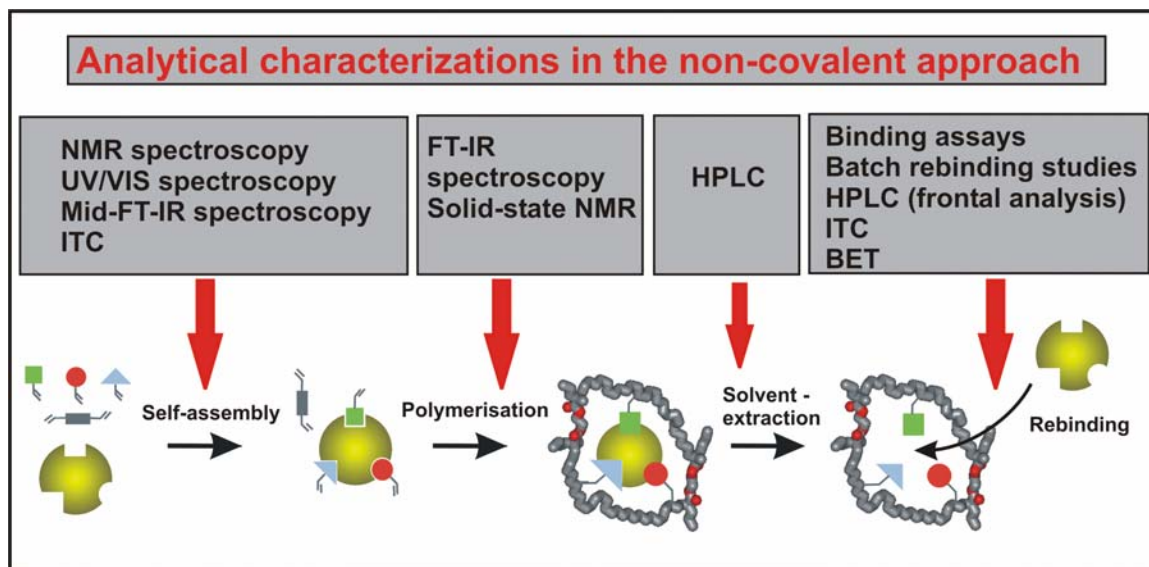
Figure 4 Analytical methodology amenable to the characterization of different processing steps during the preparation of non-covalently imprinted polymers.

Figure 4 schematically summarizes the most relevant analytical techniques available to characterize molecular imprinting processes.

2.1.4.1 Performance characterization of MIPs

The most commonly applied analytical methods assessing MIP specificity and affinity include HPLC chromatographic analysis and competitive ligand binding assays. Particularly, the introduction of enantioselective chromatographic separation materials based on MIPs has attracted interest [25,26]. Enantiomers are most difficult to separate and require receptor sites capable of discriminating optical isomers. The ability of chiral recognition is a distinctive confirmation of successful imprinting proving the existence of 3D binding cavities complementary in size, shape, and functionality to the template analyte [27]. Molecularly imprinted stationary phases synthesized for enantiomeric separations are among the most widely studied materials in the field of molecular imprinting due to their importance in the field of clinical, pharmaceutical and biotechnological analysis. Many quantitative and semi-quantitative chromatographic studies have been performed to further investigate the influence of template basicity, hydrophobicity, and molecular shape along with selective recognition and binding properties in organic and aqueous media [28,29].

Alternatively, MIPs are frequently applied for binding assays as synthetic alternative to antibodies [30-32] and have demonstrated comparable recognition properties with a $K_d < 10^{-8}$ M in many cases. The advantages of MIPs vs. antibodies include chemical, mechanical, and thermal stability [33], excellent storage endurance, a wider choice of assay solvents (aqueous and organic), and tunable synthesis for specific target analytes [34]. However, further increase in assay sensitivity and reliability is required to compete in performance and commercial viability with currently available immunoassays. While MIPs are more resistant to matrix effects compared to their biological counterparts, their performance during direct application in biological samples is usually not competitive

[35]. Furthermore, template bleeding remains a problem particularly at low concentrations, since complete template removal remains difficult [36]. 'Dummy imprinting' is a strategy avoiding this problem using a structural analogue of the target analyte as template during the imprinting process [37,38].

2.1.4.2 Thermodynamic characterization: modeling of binding isotherms

Relatively few attempts are reported assessing the thermodynamic and kinetic parameters of binding events in MIP based receptors. The performance of an imprinted polymer is usually compared to a control polymer in the application of choice for demonstration of selectivity. Trial-and-error is still the most common approach permutating parameters such as the porogen properties, the functional monomer, and the ratio between template/functional monomer/cross-linker to vary polymer binding properties. Since MIPs are amorphous materials, the structure of binding sites cannot be determined by crystallographic or microscopic methods, thus, rendering modeling of imprinted polymers difficult. However, analytical determination and rational optimization of the binding site distribution especially in non-covalently imprinted polymers have the potential to greatly improve MIP performance required for routine analytical applications. Therefore, accurate investigations on the mechanisms of molecular recognition in imprinted polymers are fundamental for the development of synthetic receptors with rationally controlled properties.

Binding parameters of MIPs are usually estimated from adsorption isotherms using mathematical models. One strategy to investigate the binding performance is based on saturation experiments and subsequent Scatchard analysis [39]. The free template concentration after incubation with a known amount of polymer is measured and plotted

in a Scatchard plot. With the assumption that all binding sites are identical and independent, the Scatchard plot should result in a line with slope –K. However, this assumption certainly does not apply to currently reported non-covalently synthesized MIPs. Consequently, the Scatchard plot usually results in a curve with the degree of curvature containing information on the heterogeneity of the binding sites within the MIP matrix. Based on Scatchard analysis estimates of the dissociation constant and the number of binding sites can be made considering the limiting assumptions of (a) bimodal distribution of binding sites and (b) that non-specific binding can be neglected within the selected concentration range [40,41]. However, it appears more realistic assuming that non-covalently prepared MIPs have a far more heterogeneous binding site distribution, which is only roughly approximated with mono- or bimodal distributions prerequisited by the applied models.

Alternatively, Freundlich adsorption isotherms were suggested providing a sufficient model fit and viable approximations of the binding isotherms for non-covalently prepared MIPs [42,43]. The Freundlich isotherm assumes a logarithmic decrease in the enthalpy of adsorption with surface coverage and was found to be most accurate in lower concentration ranges determined well below the saturation level of the investigated MIP. Other models such as the Langmuir-Freundlich isotherm [44] and Hunston's numerical approximation method [45] have been used providing values on the average binding affinity and the total number of binding sites. Approximative solutions of the binding models result in affinity distribution functions, which represent the number of binding sites with respect to the association constant. Studies have been performed to assess the effect of increasing template concentration on the binding properties of the resulting non-covalently prepared MIP, while keeping other factors constant [6]. The optimum 1:1 stoichiometry of template:functional monomer determined in the pre-polymerization solution did not match the results obtained using the Freundlich isotherm model and the

resulting affinity distributions indicating that multiple events during co-polymerization contribute to binding site formation. Further studies did not yield conclusive data on the binding mechanisms [46]. Isothermal titration calorimetry (ITC) was applied in combination with equilibrium binding isotherm analysis to investigate the rebinding process of e.g. 2,4-dichlorophenoxyacetic acid in aqueous environments and to quantify the contributions of enthalpy and entropy to the binding event estimating the cumulative contribution of electrostatic interactions and π-π stacking to the binding of 2,4-D and the functional monomer 4-vinylpyridine [47]. Recently, these findings have been confirmed by NMR titration studies providing additional experimental evidence [48].

In summary, batch rebinding studies are an important step during MIP characterization, in particular if appropriate models enable mathematical approximations of the thermodynamic binding characteristics of MIPs. Furthermore, binding studies provide valuable information for computational approaches aiming at rational modeling of governing MIP interactions at molecular levels.

2.1.4.3 Molecular modeling and computational approaches

Besides the approaches described so far, the optimization of MIP synthesis utilizes combinatorial chemistry methods [49] and most recently molecular modeling [50]. In principle, the latter approach may be performed without any a priori knowledge on the modeled system. However, sufficient analytical results are a prerequisite establishing a profound basis for extensive modeling of complex systems, including information on the nature of the pre-polymerization complex in solution or on the binding events. Molecular dynamics methods allow studying complex macroscopic systems or processes by considering small replications of the investigated systems. The relatively small amount of

molecules allows generating optimized configurations on an energy surface providing structural and thermodynamic properties. However, extensive molecular modeling remains a challenge due to limitations of the available computing capacities and the accuracy of the force fields characterizing the interatomic interactions. While predictive modeling is a future aspect, computational approaches certainly have the short-term potential for a more rapid evaluation of parameters intrinsic to molecular imprinting and for facilitating rational design and optimization of MIP synthesis for the template of choice.

Combinatorial libraries of MIPs have been established and screened for high affinity and selectivity to the selected template analyte using semi-automatic approaches. The use of automated procedures for MIP synthesis enables high-throughput preparation and screening of MIPs at a small scale, allowing for testing of the compatibility between a variety of functional monomers and a given template in a library approach. Besides the choice of functional monomer, other factors such as type and amount of cross-linking agent, porogen, and polymerization conditions (e.g. temperature, pressure) may be optimized [51].

A primary objective of molecular modeling of binding sites in molecularly imprinted polymers is developing a tool for predicting the polymer performance aiding rational experimental design alternatively to the labor- and material-intensive approach of permutatively synthesizing bulk polymers followed by characterization. This rational approach is particularly important when working with costly templates, or templates difficult to obtain. Minute structural changes of the functional monomers or templates may result in substantial thermodynamic differences, which renders predictions of binding affinities the most promising albeit complex approach. Considering the case of protein-ligand interactions, a major obstacle in developing effective models of their structure and thermodynamic behavior is the quality and availability of experimental

data. However, in the case of protein-ligand binding accessible 3D structures assist the interpretation of the results obtained by modeling. In the case of amorphous MIP matrices, data on individual binding pockets are not readily available rendering the development of effective models a tedious process. With the structure of the binding pocket being an unknown, predictions on the effect of structural variations of the template or the surrounding matrix on the recognition process in a binding cavity are challenging.

To date, molecular modeling was applied to create virtual libraries of functional monomers screening the selected template against the designed library [52]. Functional monomer-template interactions were simulated with hydrogen bonding, van der Waals, ionic, and dipole-dipole interactions contributing to a binding energy score. Monomers with the highest binding scores were selected and either directly applied in MIP synthesis or subjected to further simulations determining the number of functional monomers interacting with a single template molecule [53]. MIPs prepared by this computationally assisted approach were found to have higher selectivities in comparison to polymers synthesized with commonly used functional monomers.

However, modeling of a system resembling the pre-polymerization mixture with solvated template, functional monomer, and cross-linker is a complex task, which requires extensive computational resources. A novel strategy currently pursued by our research group and collaborators aims at simulating complexation events between template molecules and selected functional monomers in the pre-polymerization mixture using molecular dynamics simulations in the nanosecond (ns) regime. These models are based on an accurate physical representation of the solvent environment explicitly including solvent molecules [54]. This approach focuses on obtaining fundamental insight on the complex formation and behavior with time. Furthermore, the influence of

solvent molecules on the complexation events and the types of occurring molecular interactions are investigated.

So far, computational approaches based on combinatorial libraries or molecular modeling are limited to few applications only. However, their importance in elucidating the mechanisms of binding site formation and molecular recognition of molecularly imprinted polymer is undoubted. Furthermore, despite the capabilities of state-of-the-art modeling techniques appropriate analytical evidence provides the boundary conditions for the development of accurate computational approaches.

Given the diversity of reported results, it is evident that new insights via molecular modeling and rational design considerations for next-generation non-covalent MIPs prerequisite thorough investigation and analytical description of pre- and post-imprinting processes. In particular, information on the interactions of template, functional monomer and cross-linker in the porogen, along with their ratios and the properties of the porogen at a molecular level are demanded as they govern the achievable MIP selectivity.

2.1.4.4 Analysis of the pre-polymerization mixture: the key to optimized MIPs?

In the non-covalent approach, the efficient formation and stability of template/functional monomer complexes formed in the pre-polymerization solution will govern the resulting binding site distribution and the recognition properties of the imprinted polymer matrix [55]. Hence, analytically characterizing the molecular mechanisms occurring in the pre-polymerization solution is probably the most important step for rational understanding of self-assembly based imprinting.

In depth analysis of the pre-polymerization solution provides fundamental insights on the preferred ratios between template and functional monomer within the formed complexes, solvent effects, the influence of the cross-linker on the complexation events, and the types of occurring molecular interactions. Consequently, spectroscopic studies of pre-polymerization mixtures provide prevalent information on the imprinting process. So far, mainly NMR and UV spectroscopic studies, and to a much lesser extent IR spectroscopic studies have investigated the interactions of template and functional monomers in the porogenic solvent of choice. Complementing NMR and UV studies by isothermal titration calorimetric (ITC) and FT-IR spectroscopic investigations should consolidate the obtained results for a rational assessment of optimized polymerization conditions based on additional validation/confirmation of the derived molecular interactions (see Table 5).

Table 5 Analytical information provided by the most prevalent methods studying molecular self-assembly processes at a molecular level in the pre-polymerization mixture.

Method	Observed	Association constants
NMR spectroscopy	Hydrogen bonding (e.g. ion pair interaction) and π-π stacking	✔
UV/VIS spectroscopy	Interactions involving chromophoric groups (H-bonding, ionic interactions)	✔
IR spectroscopy	Hydrogen bonding	✔
Isothermal titration calorimetry	Changes in enthalpy upon complexation	✔

The formation of multiple non-covalent bonds between the template molecule and the functional monomer, such as hydrogen bridge bonds, are crucial for the success of a non-covalent imprinting strategy [19]. Thus, the observation of bond formation during

30

self-assembly in solution aids in predicting the suitability of a functional monomer to associate with a particular target species. NMR titration experiments facilitate observing H-bond formation confirmed by studies on the bonding between nucleic acid bases and carboxylic acids [56], and H-bonding properties of monosaccharides [57]. Proton NMR has been introduced in molecular imprinting for investigating the extent of complex formation in pre-polymerization solutions [58-60]. Evaluating the shift of a proton signal due to participation in a hydrogen bond was used as selection criterion for a suitable monomer deriving data on complex formation, ratios, and interacting forces [61]. Furthermore, the investigation of chemical shifts with NMR enables the calculation of association constants [62]. The self-assembly process of the system L-phenylalanine/methacrylic acid was studied by ^{1}H-NMR titration experiments and FT-IR spectroscopy [4] indicating the formation of a 1:1 complex. Another chromatographic and ^{1}H-NMR study of the system L-phenylalanine anilide/methacrylic acid concluded that complexes with up to three methacrylic acid monomers coexist in solution prior to polymerization [58]. Furthermore, the complex formed between 4-L-phenylalanylamino-pyridine was determined using ^{1}H-NMR titration studies and UV/VIS spectroscopy [63] investigating the mechanisms of chiral recognition. While these and similar experiments reveal the potential of NMR spectroscopy for elucidating the nature of molecular level interactions in pre-polymerization mixtures, the results also indicate the limitations when dealing with more complex systems. Simple NMR titration experiments are useful to quickly identify interaction/binding to a template molecule. More advanced NMR techniques, such as nuclear Overhauser effect spectroscopy (NOESY) or rotating frame Overhauser enhancement spectroscopy (ROESY) may also render beneficial when examining systems that require enhanced sensitivity. Furthermore, NMR based refinements of molecular dynamics simulations allow incorporating experimental results

obtained from techniques such as NOESY into optimization procedures for molecular modeling studies.

UV titration studies have been performed spectroscopically following the saturation of template molecules with functional monomer building blocks by recording changes of absorbance spectra or differential absorption. Based on these studies rapid estimation of the extent of complex formation with templates such as the dipeptide N-acetyl-L-phenylalaninyl-L-tryptophanyl methyl ester [3,64] and nicotine [65] have been reported. Binding plots from UV studies allowed calculating apparent dissociation constants and ΔG values.

Despite the evident potential of individual techniques, correlated UV, NMR, ITC, and FT-IR studies complementary to the chromatographic characterization of synthesized MIPs were not performed to date, although their orchestrated application would provide a more complete picture of the events occurring during MIP formation and target recognition at a molecular level. Extensive systematic studies on the binding mechanisms involved in the pre-polymerization complex formation with an array of analytical methods will provide more conclusive information on binding interactions and stoichiometries ultimately governing the achievable selectivity, and are among the goals of this study. Furthermore, thus obtained information will provide the basis for more accurate molecular models leading to computational bottom-up approach for the development of next-generation MIP technology.

2.1.4.5 Investigation of the spatial arrangements of functional groups within binding pockets: is it possible?

Ultimately, it would be of substantial interest to analytically confirm whether the functional groups within a binding cavity maintain the spatial arrangement of the complexes formed in the pre-polymerization solution. FT-IR studies, single-molecule fluorescence microscopy [66], and solid-state NMR are among the most suitable techniques to address this challenging question. FT-IR has been used together with ^{13}C-CP/MAS NMR (cross-polarization magic angle spinning NMR) to quantitatively study the binding modes of 1,3-diacetylbenzene to templated polymers showing that binding of difunctional molecules to a difunctional site occurs in a stepwise process [67].

Current efforts focus on improved characterization of both the pre-polymerization solution and the resulting MIPs. Molecular level understanding of the complexation events in the pre-polymerization solution, during rebinding events, and on the binding site properties is the fundamental basis for a more rational approach to molecular imprinting, enabling the development of thoroughly optimized MIPs with enhanced selectivity. However, to date the MIP literature only briefly discusses the events occurring during the radical polymerization process cross-linking the present components, without paying too much attention to the extent at which the complexes formed in the pre-polymerization solution survive such polymerization conditions. In general, MIPs synthesized by thermal initiation or by UV-irradiation do not show identical recognition properties. In order to understand this diverse behavior on-line monitoring of the polymerization process utilizing methods such as FT-IR spectroscopy in combination with evanescent field techniques and in-situ NMR spectroscopy may provide new insights on the governing mechanisms of molecular imprinting. Furthermore, single-

molecule fluorescence microscopy along with orientational studies [66] might be the only viable technique capable of characterizing single binding events in real-time within the polymer matrix.

2.1.5 MIPs in analytical chemistry

Besides the previously described applications in chromatography and binding assays, MIPs have been used in a variety of applications ranging from solid phase extraction and micro-extraction, to capillary electrochromatography and chemical sensing. However, thermodynamic and kinetic considerations of the rebinding mechanisms, along with factors such as diffusion and polymeric permselectivity already indicate that MIPs may only render suitable for selected applications. Due to the heterogeneity of the obtained binding sites and their potentially restricted accessibility, the provided separation path length will be the limiting parameter for the achievable efficiency of the MIP. This consideration is supported by the fact that reports on successful MIP applications are dominated by separation techniques such as HPLC and SPE providing sufficient separation path lengths and/or column diameters. Likewise, MIP based binding assays involve long incubation times with micro-sized particles during successful operation.

Efficient solid phase extraction is certainly among the most promising applications of MIPs. Molecularly imprinted solid phase extraction (MISPE) facilitating selective sample clean-up and pre-concentration offers the potential of reducing multiple and frequently tedious sample preparation steps. This is of particular interest in food and beverage analysis, environmental analysis and biomedical analysis, where the introduction of highly selective sorbent materials reduces time-consuming sample preparation. Furthermore, MISPE can easily be combined with on-line procedures [68]. Drawbacks

encountered in MIP based chromatography such as peak broadening are of minor importance in SPE, while template-bleeding at trace and ultra-trace levels remains a critical issue addressed by 'dummy imprinting' with structural analogues [69]. Although real-world samples were usually spiked or pre-treated, the feasibility of MISPE was demonstrated for liver extract [70], blood serum [71], red wine [72], chewing gum [73], vegetable extracts [74], and river water samples [75].

While conventional MIPs have also been used as selective recognition layers in sensing devices, slow diffusion and rebinding kinetics are limiting parameters and may even render the application of MIPs in chemical sensor technology unfeasible. Few approaches such as surface imprinting techniques forming recognition sites at the membrane surface may in future lead to more efficient sensing layers. Specificity, their stability, and potentially low production costs are certainly the strongest arguments for MIPs in sensing in contrast to immobilized bioreceptors such as antibodies and enzymes. MIPs have been combined with a variety of transduction schemes such as capacitance [76], impedometric [77], amperometric [78], mass-sensitive [79], and optical sensing platforms [80-82]. The achievable selectivity provides sensing chemistries tuned towards the templated analyte due to e.g. preferential enrichment or transport into the recognition layer. However, polymer specificity, affinity, and capacity have to be greatly improved in order to meet the requirements for real-world applications. Furthermore, most sensors require selective recognition at aqueous conditions for applications in the fields of clinical diagnostics and environmental monitoring, which remains a challenge for most MIP receptors reported to date.

Finally, molecularly imprinted membranes offer the potential for cost effective increased selectivity during concentration, purification, or isolation of chemical species (e.g. chiral drugs in pharmaceutical industry). Molecularly imprinted membranes were prepared by phase inversion precipitation [83,84] and by photopolymerization of an ultrathin MIP film

on a microporous alumina support membrane [85]. Due to the highly porous support, the net flux across the membrane was limited by transport in the polymer film. In analogy, a microfiltration polypropylene membrane was imprinted with desmetryn by photograft copolymerization [86]. In another approach, free-standing membranes of imprinted polymers were prepared with 9-ethyladenine as template molecule [87]. Limitations such as slow mass transfer, low capacity, and limited reproducibility of imprinted membrane properties have so far prevented the practical implementation at a larger scale. While specific transport characteristics are still difficult to obtain, also permeability and selectivity will have to be improved. Nevertheless, the development of novel robust membranes providing selective permeation properties is of ongoing interest [88] attesting to the potential of MIP membranes in sensing and separations.

2.1.6 Toward new applications for MIPs

Surface imprinting of proteins and cells has received great attention over the past few years. Due to the large molecular structures of macromolecules, efficient diffusion into a 3D matrix is prevented in classical molecular imprinting. Therefore, surface imprinting appears the method of choice [89]. Imprinting at a polymer surface allows direct access to the binding sites avoiding problems resulting from slow mass transfer. Furthermore, imprinting at a surface allows immobilizing the template molecule at the surface of e.g. a solid silica gel support prior to polymerization [90]. Using metal-binding monomers, metal ion coordination with N-terminal His residues was used to complex short peptides containing N-terminal His residues [91,92] and RNase A [93]. In another approach, radio-frequency glow-discharge plasma deposition was used to form polymeric thin films on proteins coated with disaccharide molecules [94]. Other methods such as bacteria-

mediated lithography of polymer surfaces [95], soft lithographic techniques [96,97], and surface-grafted MIPs [98] have been used for microorganism or protein recognition at micro-devices by fabricating MIPs in two- and three-dimensional patterns. However, most efforts imprinting proteins or larger entities have shown poor analytical resolution to date. Nevertheless, the potential of templating macromolecules such as proteins or whole cells has been indicated, though, selective recognition at real-world conditions remains to be demonstrated.

Finally, MIPs have been proposed serving as synthetic enzymatic materials by imprinting reaction intermediates, acid-base catalysts or metal complexes [99-101] revealing promising results in molecular recognition based catalysis [102].

Last but not least, new polymeric and sol-gel type materials for imprinting along with a wide variety physical presentations of MIPs including polymer monoliths, ultra-thin films, and beads are continuously investigated for improved recognition in various formats [103]. Novel imprinting approaches such as monomolecular imprinting inside dendrimers proved to be successful and open new routes to rational MIP synthesis [104] leaving little doubt that rational approaches to understanding how MIPs work along with creative method and material development will continue to advance molecular imprinting technology.

2.1.7 Conclusions

Despite the enormous body of work presented in literature, there is still no exclusive answer to 'how MIPs work' and there certainly remain applications where they might not work at all. While non-covalently prepared MIPs come closest to mimicking the behavior of natural receptor systems, we have to deal with the complexity and variety of weak

interactions governing the recognition properties of the resulting biomimetic structures. It is evident to date that the heterogeneity of binding sites prevents non-covalent MIPs from behaving like a highly organized - ideally monomolecular - layer of antibodies. Consequently, MIP applications need to take advantage of a separation pathlength or incubation time in order to achieve practically relevant selective recognition. Derived from these considerations it appears natural that applications of non-covalent MIPs in separations and assays are favorable compared to the demands of chemical sensing technology, which requires rapid and highly selective signal generation despite the absence of a considerable separation pathlength.

Orchestrating a range of analytical methods characterizing pre- and post-polymerization processes along with characterization of binding properties provide the fundamental basis to answering the questions on how and why MIPs work. Advanced molecular modeling taking advantage of boundary conditions resulting from analytical evidence may assist in further understanding binding site formation and binding processes. Investigations of the binding mechanisms involved in template-functional monomer interactions in the very first stages of the imprinting process during complexation in the porogenic solvent clearly govern the resulting selectivity of the polymerized MIP matrix. Hence, the combination of methods including NMR, IR and UV/VIS spectroscopy supported by ITC studies facilitates enhanced modeling of prevalent molecular interactions establishing the basis for rationally predicting the selectivity of next-generation molecularly imprinted polymers and optimized synthesis strategies.

2.2 Characterization methods for molecularly imprinted polymers

2.2.1 Introduction

Characterization of structure and morphology of molecularly imprinted polymers together with characterization of the imprinting effect by HPLC are necessary to determine whether templating was successful and to assess the effect of the different factors related to MIP synthesis on polymer recognition properties. Factors such as accessibility of binding sites within the polymer matrix will be seen in chromatographic studies since they affect mass transfer kinetics and load capacity of the polymeric separation material.

2.2.2 HPLC analysis

Distribution between a stationary and a mobile phase and adsorption/retention of analytes within the stationary phase both contribute to analyte separation in high performance liquid chromatography (HPLC). A stronger interaction with the stationary phase will result in a longer residence time within the separation column.

2.2.2.1 Classic chromatographic theory

The classic chromatographic theory from Martin and Synge [105] can be viewed as the series of discrete partitioning steps translated into a continuous procedure in a

separation column. The plate height H [cm] is the height equivalent to a theoretical plate connected to the number of theoretical plates N by:

$$N = \frac{L}{H} \qquad (5)$$

with L [cm] corresponding to the length of the column. It is assumed that within every theoretical plate equilibrium conditions for each analyte are achieved for partitioning between the stationary and the mobile phase. H and N characterize the efficiency of a column; N can be determined directly determined from a chromatogram with

$$N = 5.54 \left(\frac{t_R}{b_{1/2}} \right)^2 \qquad (6)$$

with t_R as the total retention time and $b_{1/2}$ the width at half-maximum of a (ideally) Gaussian peak.

2.2.2.2 Kinetic chromatographic theory

Nevertheless, the classic chromatographic theory has limitations. It does not explain peak broadening effects, which rely on the limited rate at which mass transfer processes occur between the stationary and the mobile phase. The plate height H is a function of the linear flow rate $\bar{u}$ [cm.s^{-1}] of the mobile phase, as shown in the modified van Deemter equation [106,107]:

$$H = A + \frac{B}{\bar{u}} + C_S \bar{u} + C_M \bar{u} \qquad (7)$$

with   A   Eddy diffusion

        $B/\bar{u}$ longitudinal diffusion

        $C_S\bar{u}$ mass transfer coefficient to and from the solid stationary phase

        $C_M\bar{u}$ transfer coefficient to and from the mobile phase

Equation (7) results in a minimum for H at an optimum mobile phase flow rate $\bar{u}$.

2.2.2.3 Characteristic values of a chromatogram

Following parameters are used to characterize the efficiency of the chromatographic separation (adapted from reference [108]):

- Total retention time t_R

Time required (at peak maximum) for an analyte in the mobile phase to pass through the column (under defined chromatographic conditions).

- Hold-up time t_M

Time required for an analyte in the mobile phase, which does not interact with the stationary phase (void marker), to pass through the column. t_M is also called dead time.

- Capacity factor k'

$$k' = K \frac{V_S}{V_M} = \frac{K}{\beta} = \frac{t_R - t_M}{t_M} \qquad (8)$$

with   K   partition coefficient

              V_S, V_M volume of stationary and mobile phase respectively

              β phase ratio.

- Chromatographic resolution R_S

$$R_S = \frac{t_R^A - t_R^B}{w} \qquad (9)$$

The base width w is determined from the intersection of the tangents of the inflection points with the baseline of the Gaussian peak. R_S describes the selectivity of the system.

2.2.2.4 MIPs as stationary phase for HPLC

HPLC is a suitable method evaluating the properties of a stationary phase comprising a molecularly imprinted polymer (MIP) with respect to its selective recognition/retention properties for the template analyte in contrast to structural analogues. A control polymer (CTL) stationary phase prepared at identical conditions but in absence of the template molecule is used as a reference. Acetone serves as the void marker. The recognition properties of the polymers are assessed by comparing the retention times t and capacity factors k'. For a given MIP and CTL polymer system, the separation factor α and the retention index RI of the analyzed analytes are calculated as follows:

42

- Capacity factor: $$k' = \frac{t - t_{ACETONE}}{t_{ACETONE}} \qquad (10)$$

- Separation factor: $$\alpha = \frac{k'_{pr\,int\,molecule}}{k'_{testsubs\,tan\,ce}} \qquad (11)$$

- Retention index $$RI = \frac{\alpha_{CTL}}{\alpha_{IMP}} \qquad (12)$$

2.2.3 BET analysis of stationary phase materials

The adsorption of gases onto a solid surface in multimolecular layers was first described by S. Brunauer, B. H. Emmett, and E. Teller [109]. The BET isotherm assumes that each unit of surface area consists of n sites, which can adsorb one molecule and that all of the sites are energetically equivalent. Furthermore, BET isotherms account for multilayer adsorption by assuming that the first layer of adsorbate is a site available for the next layer, and so forth. The BET isotherm [8] (13) is the most widely used isotherm dealing with multilayer adsorption.

$$V_{RATIO}(z) = \frac{V}{V_{MONO}} = \frac{c \times z}{(1-z)[1-(1-c)\times z]} \qquad (13) \quad \text{where } z = \frac{p}{p^*} \qquad (14)$$

with V_{MONO} volume corresponding to a monolayer of coverage

        p^* vapor pressure above a layer of adsorbate that is more than one

                       molecule thick resembling a pure bulk liquid

c   constant that is large when the enthalpy of desorption from a monolayer is large compared with the enthalpy of vaporization of the liquid adsorbate.

Surface area analyzers and pore size analyzers may be used to analyze a number of factors such as pore distribution, pore volume, specific surface area, and total surface area of a powdered polymeric material. To determine the surface area of a polymer sample, surface area and pore size analyzers measure samples pretreated by a combination of heat, vacuum and/or flowing gas to remove adsorbed contaminants acquired from atmospheric exposure. The sample is cooled under vacuum conditions usually to cryogenic temperatures. An adsorptive (typically nitrogen gas N_2 at its boiling temperature of 77.3 K) is admitted to the solid in controlled increments and physically adsorbed at the surface of the solid. After each dose of adsorptive, the pressure within the surface/ pore size analyzer is allowed to equilibrate and the quantity of gas adsorbed calculated. The gas volume adsorbed at each pressure (at constant temperature) defines an adsorption isotherm, from which the quantity of gas required to form a monolayer over the external surface of the solid and its pores is determined (V_{MONO}). With the area covered by each adsorbed gas molecule being known, the total surface area A_T can be calculated (for nitrogen, the area per molecule is 16.2 Å^2).The specific surface area A_{SP} or BET surface area of a powder is calculated as

$$A_{SP} = \frac{A_T}{m_t} \qquad [\text{m}^2.\text{g}^{-1}] \qquad (15)$$

with m_t weight of powdered sample.

The pore size distribution may be calculated from desorption steps with methods such as the Barrett-Joyner-Halenda (BJH) method [110]. Different models may be used assuming defined pore geometries (spherical, cylindrical, etc.), which will ultimately affect the obtained results.

2.3 MIPs in solid phase extraction (SPE)

Solid phase extraction (SPE) is a sample preparation technique based on the use of a solid separation material to extract specific compounds by retention allowing rapid sample clean-up or pre-concentration. After conditioning of the packing material, the analyte of interest (or the interferences) are adsorbed onto the solid phase. A washing step allows selective removal of interfering components, followed by an elution step where the analyte of interest is eluted with a different solvent and collected in fractions (see Figure 5). The eluting solvent should facilitate fast dissociation of the analyte from the solid phase. SPE is therefore a three step technique based on complete retention followed by rapid elution from the sorbent.
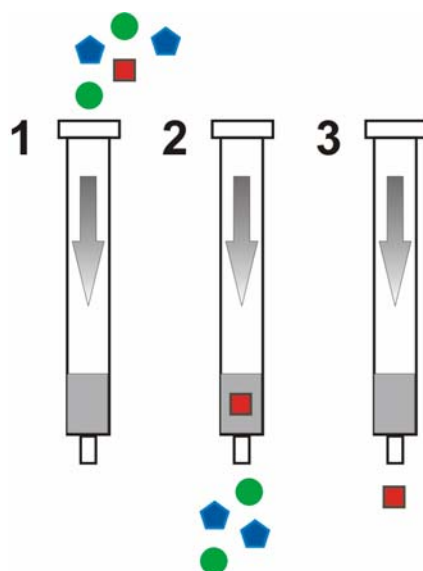
Figure 5 Principles of solid phase extraction; 1: Sample application; 2: Washing step removing interferants; 3: Elution step. Formats may change from SPE columns or cartridges to disks.

Advantages of SPE are the high recoveries rapidly achieved, the ease of automation and compatibility with chromatographic analysis (on-line SPE), and the reduced consumption of organic solvents compared to liquid-liquid extraction. On the other hand, method development is time-consuming and remains one of the major problems in SPE. Reversed phase, normal phase and ion exchange are the three main mechanisms of sorption in SPE based on the same binding interactions utilized in liquid chromatography. Nevertheless, the short column length and low number of theoretical plates make the choice of the sorbent material as along with the washing and eluting solvents crucial to achieve separation. The main parameters affecting the SPE pre-concentration are:

- Type of sorbent material [111,112]
    - Reversed phase sorbents such as chemically bonded C8 or C18 silica and ion exchange sorbents for aqueous samples.

- Normal phase sorbents such as silica, alumina, Florisil, and silica chemically modified by polar groups (e.g. cyano, amino, and diol groups) for non-aqueous samples (liquid organic extracts).

- Molecularly imprinted polymers compatible with aqueous as well as non-aqueous samples. Depending on the nature of the interactions involved in the rebinding process, non-specific binding/hydrophobic interactions contribute to the retention of molecules contained in aqueous samples due to non-specific adsorption to the polymer surface. Washing with an organic solvent allows selective binding due to recognition of functionalities. As a final step, the analyte of interest is eluted with an appropriate elution solvent which may contain a defined amount of modifier to improve the elution properties of the solvent for the extractant.

- Further sorbent materials include carbon-based sorbents, restricted access matrix sorbents, mixed-mode sorbents, apolar poly(styrene-divinylbenzene) co-polymer sorbents, and immunoaffinity extraction sorbents.

- Washing and eluting solvents

- Breakthrough volume V_B

The breakthrough volume V_B is the maximum sample volume which can be applied with a theoretical recovery of 100%. The recovery is given as the ratio between the amount extracted and the amount applied. V_B can be determined by pre-concentrating standard samples of increasing volume containing the same amount of analyte and measuring the peak-areas eluted from the solvent [113]. V_B can also be determined by monitoring continuously or discretely the collected aliquots from the

47

SPE cartridge after applying standard sample aliquots of same concentration C_0 [114]. By plotting the applied sample volume against the detector response or concentration of eluate respectively, a breakthrough curve is observed, starting at V_B (1% of initial signal e.g. concentration of standard solution applied C_0) up to a volume V_M (99% of C_0) as shown in Figure 6.
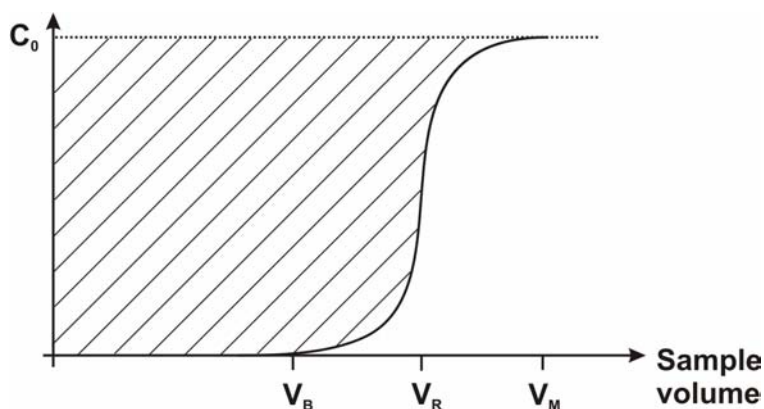
Figure 6 Breakthrough curve obtained by plotting the applied sample volume vs. the detector signal of the collected samples. The shaded area represents the maximum amount that can be pre-concentrated with the SPE column.

The breakthrough curve ideally has a bilogarithmic shape, with the inflection point giving the retention volume of the analyte V_R. The analyte concentration should not overload the capacity of the sorbent.

The more selective the SPE step is, the more sensitivity is gained in the subsequent analysis. Nowadays, SPE is among the most widely used sample preparation techniques with applications ranging from environmental and clinical analysis [115] to food analysis [116].

2.4 Fundamentals of methods applied to the characterization of complex formation in the pre-polymerization solution

2.4.1 Introduction

Spectroscopic methods allowing the determination of stoichiometric coefficients m and n in complex structures of type S_mL_n and of the associated binding constants play an important role in assessing and monitoring complex formation at a molecular level. Following techniques are most widely used to study equilibria in host-guest chemistry and were discussed in chapter 2.1.4.4 according to their relevance for the investigation of MIP pre-polymerization solutions:

- UV-VIS spectroscopy

- NMR spectroscopy

- Fluorescence spectroscopy

- Mass spectrometry

- IR spectroscopy

Further non-spectroscopic methods include electrochemical and calorimetric methods.

For the purpose of the investigations described in this thesis, IR and NMR spectroscopy were selected. IR spectroscopy is not widely applied in supramolecular chemistry and in MIP pre-polymerization analysis. Nevertheless, especially in the MIR (mid infrared) range, IR spectroscopy is molecule specific and provides information on functional groups and their interactions, offering quantitative information at a molecular level. As one of the most widely used methods in the study of complexation events, NMR spectroscopy measures parameters directly related to structure and structural changes,

providing complementary information to IR spectroscopic measurements in a variety of solvents.

2.4.2 MIR spectroscopy

2.4.2.1 Introduction

The mid-IR (MIR) range covers the spectral region from 4000 cm^{-1} (2.5 μm) to 400 cm^{-1} (25 μm). In this region of the electromagnetic spectrum, radiation stimulates fundamental transitions between the ground state of vibrational and rotational modes of specific molecular bonds or whole molecules and their excited states. IR active vibrations are accompanied by a change of the dipole-moment of the molecule. Depending on the strength of the bond, each mode is excited at a specific energy level manifesting as a characteristic band in the absorption spectrum. As vibrations of whole molecules usually require considerably lower excitation energies, they produce highly substance specific absorption patterns at longer wavelengths within the so-called fingerprint region (1200 cm^{-1} – 400 cm^{-1}) of the IR spectral range. Therefore, vibrational spectroscopy is inherently a molecule specific analytical method providing information on chemical functionalities and molecular structures.

2.4.2.2 IR spectroscopy of complex formation processes

The timescale of MIR spectroscopy allows studying molecular interaction processes that take place within a timeframe on the order of up to the nano- and picosecond regime by using ultra-fast lasers (time-resolved spectroscopy). As a result of this susceptibility to

short-time processes, differences in molecular conformations are often reflected in the corresponding IR spectra, allowing hydrogen bonded and free states of the molecules to be discriminated. Therefore, MIR spectroscopy is ideally suited for the analysis of dynamical equilibria at a molecular scale, e.g. phenomena of association, self-association, and dissociation. Nevertheless, infrared spectroscopy is not widely applied in host-guest chemistry, although the potential of vibrational modes in general, and the X-H stretching modes (X= O, N) in particular, have been shown to be very useful for the analysis of hydrogen bonding. A major limitation is the often encountered problem of overlapping absorption features of substrate, ligand, and complexes. However, IR spectroscopy is applicable to sub-millimolar concentration levels, which is often problematic for other analytical techniques such as NMR due to a lack of sensitivity. Quantitative IR absorption spectroscopy is based on the Lambert-Beer law determining the absorbance A [A.U.] of the free (A_{free}) and complexed ($A_{complex}$) states:

$$A = \varepsilon \cdot c \cdot d \qquad (16)$$

with ε molar absorptivity at a selected wavelength [$M^{-1}cm^{-1}$]

      c   compound concentration [mol/L]

      d   optical pathlength [cm].

Assuming a 1:1 complex formation, the measured absorbance at a given wavenumber is provided by:

$$A = \varepsilon_S \cdot d \cdot [S]_0 + \Delta\varepsilon_{SL} \cdot d \cdot [SL] \qquad (17)$$

with $\Delta\varepsilon_{RS} = \varepsilon_{RS} - \varepsilon_R - \varepsilon_S$

Combining $K = \dfrac{[SL]}{[S] \cdot [L]}$ with equation (17) gives

$$\Delta A = A - A_0 = K \cdot \Delta \varepsilon_{SL} \cdot d \cdot [S] \cdot [L] \qquad (18)$$

Combining $[S] = \dfrac{[S]_0}{1 + K \cdot [L]}$ and equation (18) further gives

$$\frac{\Delta A}{d} = \frac{[S]_0 \cdot K \cdot \Delta \varepsilon_{RS} \cdot [L]}{1 + K \cdot [L]} \qquad (19)$$

Taking the reciprocal plot of (17) results in the Benesi-Hildebrand equation (20), from which further binding plots such as the Scott or the Scatchard equations can be derived.

$$\frac{d}{\Delta A} = \frac{1}{[S]_0 \cdot K \cdot \Delta \varepsilon_{RS}[L]} + \frac{1}{[S]_0 \cdot \Delta \varepsilon_{RS}} \qquad (20)$$

Note, that if different complexes coexist in solution, K becomes wavelength dependent.

2.4.3 ^{1}H-NMR spectroscopy

2.4.3.1 Introduction

NMR is an absorption spectroscopic technique involving the absorption of electromagnetic radiation in the radiofrequency range. A sample placed in a static magnetic field is exposed to a second superimposed transverse oscillating magnetic

field inducing transitions between energy levels at the respective resonance frequencies. The magnetic field experienced by a nucleus in a molecule is different from the external field with the exact resonance frequency being characteristic for the chemical environment of the nucleus (chemical shift δ). Chemically non-equivalent nuclei in a molecule are therefore differently shielded leading to separate signals in the NMR spectrum (only for nuclei with a spin quantum number I $\neq$ 0). The applied magnetic fields are in the range of 1.4 to 14.1 T leading to proton resonance frequencies of 60-600 MHz. Intermolecular interactions will change the chemical environment of a nucleus, inducing changes in the chemical shift which can be monitored. NMR spectroscopy has become the main method used for structure elucidation, kinetics, and dynamics of supramolecular complexes in solution.

2.4.3.2 NMR titration studies: molar ratio method

Complexation events such as hydrogen bond formation and π-π stacking may be observed by ^{1}H-NMR titration experiments. This method of studying hydrogen bonding is a well-researched field having been used in the past for applications such as studying bonding between nucleic acid bases and carboxylic acids [117] and H-bonding properties of monosaccharides [118]. In NMR titration studies, measurements are performed at variable concentration of one component and at a fixed concentration of the other component. The experimental conditions are selected such that the degree of complexation is preferably high. The changes of NMR shifts of independent signals upon complex formation are used to monitor complex formation and calculate association constants. Given a rapid exchange between ligand L and substrate S, a sharp signal is

observed at a mean weighted shift between the signals for free and complexed compound:

$$\delta_{OBS} = \delta_0 N_S + \delta_{SL} N_{SL} \qquad (21)$$

with δ_0 and δ_{SL} chemical shifts of a monitored nucleus in the free (S) and complexed (SL) state

    N_S and N_{SL} molar fractions of the free and complexed state.

With a large excess of ligand and for the model of a 1:1 complexation:

$$\delta_{OBS} = \frac{(\delta_0 + \delta_{SL} \cdot K \cdot [L])}{1 + K \cdot [L]} \qquad (22)$$

with   K   equilibrium constant

    [L]   ligand concentration.

Computational methods allow obtaining the association constant and the complexation induced shift for the fully complexed compound from the fitting procedure for a fast ligand exchange. A non-linear curve-fitting method by Atwood [119] gives

$$\delta_{OBS} = \delta_0 + \frac{(\delta_0 - \delta_{SL})}{2[S]_0} \cdot \left\{ [S]_0 + [L]_0 + \frac{1}{K} - \sqrt{\left[\left([S]_0 + [L]_0 + \frac{1}{K} \right)^2 - 4 \cdot [S]_0 \cdot [L]_0 \right]} \right\} \qquad (23)$$

for a 1:1 complex S+L↔SL

With an initially estimated K, the shift is calculated at all given data points. This procedure is repeated until convergence of experimental and calculated values is achieved.

For a slow exchange between S and L, which is less frequent, the separate signals for free and complexed species may be used to directly determine K and the stoichiometries of the complex.

2.4.3.3 Spin lattice relaxation time (T_1) studies

Measurements of the spin-lattice relaxation time T_1 allow following the complex formation due to changes in the local magnetic fields [120,121].

Spin-lattice relaxation allows nuclear spins to return to equilibrium following a disturbance. It enables the spins to flip amidst their energy levels within a time T_1, according to the Boltzmann statistics. Relaxation occurs by the loss of energy from the excited nuclear spins to the surrounding molecular lattice. After a pulse, a nucleus relaxes toward its equilibrium value at an exponential rate and T_1 is the time constant of the exponential curve quantifying the rate of transfer of energy from the nuclear spin system to the lattice. In the T_1 process, the magnetization remaining along the z-axis relaxes back to its equilibrium value (M_z component of the total magnetization). The spin-lattice relaxation depends on the local magnetic fields which are generated by the other molecules in the sample. The predicted relaxation rate $1/T_1$ for an idealized random field mechanism is [122]:

$$R_1 = \frac{1}{T_1} = \gamma^2 \cdot <B^2> \cdot J(\omega_0) \qquad (24)$$

with spectral density $J(\omega_0)$ and mean square value of the local fluctuating fields $<B^2>$. If the local fluctuating fields have components in the appropriate Larmor frequency, they can interact and cause spin relaxation. Slow motions such as the Brownian motion (rotational, diffusional) and molecular torsional and rotational motions play an important role. Furthermore, the principal source of nuclear relaxation for spin ½ nuclei such as ^1H are dipole-dipole interactions.

Spin lattice relaxation data can be used to obtain information on molecular motions and dynamics since the structure of the analyte of interest is known. T_1 characterizes the overall molecular mobility and specific internal motions determined by the internal degree of freedom of the analyte. Due to complex formation, the intermolecular contributions to the relaxation change, affecting the spin-lattice relaxation time. Under the conditions where an exchange equilibrium is rapidly reached, the relaxation rate measured R_1 is a weighted average of the rates of free and complexed species. T_1 is calculated by a non-linear fitting model as shown in equation (26) using the inversion-recovery method [123], where the equilibrium magnetization M_{equ} is first inverted by a 180˚ pulse (p_1) and then allowed to recover for a period τ. A 90˚ pulse (p_2) follows and the longitudinal magnetization M_z is measured. Before repeating the sequence nt times, a delay $d_1 \geq 5 \cdot T_{1max}$ is necessary in order to restore the equilibrium magnetization. A monitoring pulse measures peak height following recovery. The sequence is repeated nt times for each value of τ arrayed ($[d_1 - p_1 - \tau - p_2]\cdot nt$).

According to the Bloch equation $\dfrac{dM_z}{d\tau} = \dfrac{M_{eq} - M_z}{T_1}$ a steady state is reached after the second pulse and the magnetization $M_z(\tau)$ is given as:

$$M_z(\tau) = M_{eq}(1 - 2\exp(-\frac{\tau}{T_1}))\qquad (25)$$

Consequently we can derive

$$I(\tau) = C_1 + C_2 \cdot \exp\left(-\frac{\tau}{T_1}\right) \qquad (26)$$

with C_1, C_2:   parameters

       τ: delay time (interval between the 180˚ and the 90˚ pulses) [s]

       $I(\tau)$:   NMR peak intensity.

The binding constant can be calculated from the spin-lattice relaxation time measurements as follows [124]:

Combining the observed relaxation rate $R_{(obs)}$

$$R_{(obs)} = N_{free} \cdot R_{10} + N_{complex} \cdot R_{11} \qquad (27)$$

with the molar ratios N_{free} and $N_{complex}$

$$N_{free} = \frac{[S]_{free}}{[S]_{free} + [SL]} = \frac{[S]_{free}}{[S]_{total}}$$

$$N_{complex} = \frac{[SL]}{[S]_{free} + [SL]} = \frac{[SL]}{[S]_{total}}$$

$$N_{free} + N_{complex} = 1$$

gives equation (28):

$$R_{obs} = N_{complex} \cdot (R_{11} - R_{10}) + R_{10} \qquad (28)$$

57

With the binding constant K_{11} for a 1:1 interaction

$$K_{11} = \frac{[SL]}{[S] \cdot [L]} \qquad (29)$$

and

$$N_{complex} = \frac{[SL]}{[S]_{total}} \qquad (30)$$

follows

$$N_{complex} = \frac{K_{11}[L]}{1 + K_{11}[L]} \qquad (31)$$

From (27) and (30) we can calculate:

$$(R_{obs} - R_{10}) = \frac{(R_{11} - R_{10}) \cdot K_{11} \cdot [L]}{1 + K_{11} \cdot [L]} \qquad (32)$$

as 1:1 NMR binding isotherm.

The double reciprocal plot of (31) gives the Benesi-Hildebrand equation [125] (33)

$$\frac{1}{(R_{obs} - R_{10})} = \frac{1}{(R_{11} - R_{10}) \cdot K_{11} \cdot [L]} + \frac{1}{(R_{11} - R_{10})} \qquad (33)$$

from which K_{11} can be calculated. Note that equation (33) is different from the corresponding IR equation since different physical properties are probed.

2.4.4 Method of continuous variation - Job's plot analysis

In the method of continuous variation [126,127], a series of mixed solutions of S and L are prepared such as the total concentration [S]+[L] is kept constant, while the ratio [S]/[L] varies. A property of the mixtures such as the absorbance (optical spectroscopy) or the complex concentration (NMR spectroscopy) is plotted as a function of the molar fraction of one of the two components. If both S and L have a non-zero absorbance at the measured wavelength, the absorbance of the free species at each molar fraction is subtracted from the observed value of the mixture. An extreme value in the graph - maximum or minimum – indicates the presence of a complex with a composition of S_mL_n where the molar ratio x at the extremum represents the complexation stoichiometry according to:

$$x = \frac{n}{n+m} = \frac{1}{\frac{m}{n}+1} \qquad (34)$$

A maximum appearing at e.g. x = 0.5 indicates that a 1:1 (or 2:2) complex is the predominant structure at equilibrium conditions. Job's plot analysis is a valuable tool in determining complex stoichiometries since it also allows determining stoichiometries other than 1:1.

2.4.5 Case study of binding isotherms

Given the equation $S + L \leftrightarrow SL$ for a simple equilibrium assuming a 1:1 interaction between substrate S and ligand L with $[S]_0 = [S] + [SL]$ and $[L]_0 = [L] + [SL]$, the dissociation constant K_d is described by $K_d = \dfrac{[S] \cdot [L]}{[SL]}$.

Two different equations for K_d can be derived for two different cases:

- Case 1: if [L] can be measured or if experimental conditions are such that

  $[L]_0$ » $[S]_0$ the assumption $[L] \sim [L]_0$ can be made.

Therefore, $K_d = \dfrac{([S]_0 - [SL]) \cdot [L]}{[SL]}$ (35)

From (35) follows $[SL] = \dfrac{[S]_0 \cdot [L]}{(K_d + [L])}$ or $[SL] = \dfrac{[S]_0 \cdot [L]_0}{(K_d + [L]_0)}$ (36)

- Case 2 (more general): [L] is not known and $[L]_0$ is not » $[S]_0$.

Therefore, $K_d = \dfrac{([S]_0 - [SL])([L]_0 - [SL])}{[SL]}$ (37), which allows calculating K_d if

[SL], $[S]_0$, and $[L]_0$ are known or calculating [SL] if K_d, $[S]_0$, and $[L]_0$ are known.

The presented equations are applicable if they can be solved, which is usually only the case for a 1:1 stoichiometry.

2.4.6 Complexes with stoichiometries other than 1:1 and multiple equilibria

Methods for stoichiometry determination were previously discussed in chapter 2.4.4 and allow obtaining the ratio m/n for a complex S_mL_n The overall binding constant β_{mn} is given as

$$\beta_{mn} = \frac{[S_mL_n]}{[S]^m[L]^n} \qquad (38)$$

For simple systems such as complexes between two small molecules, models based on the assumption of a 1:1 stoichiometry are frequently used. Nevertheless, additional complex species may also be found in the investigated systems and should be taken into consideration. Accordingly, appropriate isotherms describing multiple equilibria should be used. However, obtaining reliable models is not trivial and external factors may strongly affect the models leading to erroneous results. Nevertheless, computational methods using iterative procedures as well as extrapolation methods such as Poë's method of successive approximation [128] may allow an evaluation of such stepwise binding constants.

2.4.7 Conclusions

Both MIR and ^{1}H-NMR spectroscopy allow studying complex formation in solution. Complex stoichiometries, interacting sites on the investigated compounds, and binding constants may be obtained using the same data evaluation methods such as Job's plot analysis and the molar ratio method. Nevertheless, both spectroscopic techniques target

different physical properties of the analyzed molecules, making MIR and ^{1}H-NMR ideal

complementary methods studying complex formation in pre-polymerization solutions.

2.5 Molecular dynamics simulations

2.5.1 Introduction

Molecular dynamics (MD) methods and Monte Carlo (MC) methods are the two most common simulation techniques used in molecular modeling. These simulation methods allow studying complex macroscopic systems or processes by reducing the data space considering small replications of the system. The small amount of molecules allows generating minimum configurations on an energy surface providing structural and thermodynamic properties within reasonable computational expenses.

In molecular dynamics simulations [129], successive configurations of a selected system are generated by integrating Newton's equations of motion. The Newtonian equations of motion, a potential energy function and associated force fields enable following the displacement of atoms in a molecule over a certain period of time, at a certain temperature and for a given pressure. Force field methods allow calculating the energy of a system as a function of the nuclear positions ignoring the electronic motions. MD simulations result in a trajectory, defining the positions and velocities of each particle in the system with time. The system is under the influence of a continuous potential and the motions of all particles in the system are coupled creating a many-body problem that cannot be analytically solved. The equations of motion have to be integrated using finite difference methods based on algorithms such as the Verlet [130,131] or the leap-frog

algorithm [132-134]. A wide variety of algorithms are available for this purpose, depending on the accuracy and efficiency requirements for the application of choice. Starting velocities can be calculated at random (necessary when starting at 0 Kelvin where the kinetic energy is 0) or by scaling the initial forces on the atoms. Simulations can also be performed at a variety of simulated temperatures to obtain different families of conformers. At higher temperatures, more conformers are possible and crossing over energy barriers is facilitated (see chapter 2.5.5 Simulated annealing).

The results from the MD simulations shown within this work were obtained by using the AMBER7 (Assisted Model Building with Energy Refinement) MD simulation package [135]. The AMBER package consists of over 60 programs; the AMBER programs relevant to this work along with the AMBER parameter and topology file formats are described in Appendix A. Furthermore, a comprehensive description of the capabilities of each of the programs in the AMBER7 suite, as well as definitions of each of the commands can be found in the AMBER7 manual, which is available online at http://amber.scripps.edu. For visualizing the trajectories, a molecular visualization program (*VMD*, [136]) has been applied for displaying, animating, and analyzing large biomolecular systems using 3-dimensional graphics and built-in scripting. Detailed information can be found at http://www.ks.uiuc.edu/Research/vmd/.

Four main processing steps characterize a MD simulation. After finding an initial configuration of the system of interest, an equilibration phase is performed in order to obtaining a stable system. Atoms of the macromolecules and of the surrounding solvent are subjected to a relaxation phase usually lasting for tens or hundreds of picoseconds before the system reaches a stationary state. Thermodynamic properties such as temperature, energy, and density are monitored until these values appear stable. The initial non-stationary segment of the simulated trajectory is discarded in the calculation of

equilibrium properties. Before performing long (i.e. period of a nanosecond) MD simulations, the system must be equilibrated using volume, pressure and temperature control to adjust e.g. the density of the solvent to experimental values and the temperature of the system to the selected temperature. After equilibration, the production phase is started, which will produce the actual simulation results with an MD simulation of approximately 1 ns duration. Basically, the same protocol as in the final stage of equilibration can be used. The MD simulation is simply continued until one is satisfied with the obtained molecular configuration. The production MD run is performed at conditions of a constant number of particles (N), volume (V), and energy (E) representing a microcanonical NVE ensemble and allows observation of the molecule(s) of interest interacting with their environment during a pre-determined time interval – usually at the order of nanoseconds. Finally, the simulation is analyzed.

2.5.2 Empirical force field models and solvent models used in AMBER7 MD simulations

Energy models are used to describe the molecular interactions within the system. The inter- and intra-molecular interactions are usually described using empirical energy models derived from molecular mechanics considerations. The main contributions to a force field are bond stretching, angular bending, torsional terms, and non-bonded interactions. A potential energy function as described in equation (39) together with the parameters used in the function defines the force field. At each step of the simulation, the force on each atom is calculated by differentiating the potential function. The force fields 'leaprc.ff99' [137] and 'leaprc.gaff' [138] (gaff, General Amber Force Field) were used within the AMBER package. The 'ff99' and 'gaff' are probably the best "general

purpose" force fields included and were both sourced in *LEaP*, which is the X-windows-based program in the AMBER7 package that provides for basic model building and AMBER coordinate and parameter/topology input file creation. Functional forms and parameters of the 'ff99' and gaff force fields are defined in the AMBER7 manual and in references [137,138].

The basic force field implemented in *Sander* – the main program used for molecular dynamics simulations within the AMBER package - is the simplest functional form preserving the nature of molecules in condensed phases and describing the intra- and inter-molecular forces within the system (equation (39)):

$$U(R) = \sum_{bonds} K_r (r - r_{eq})^2 + \sum_{angles} K_\theta (\theta - \theta_{eq})^2 + \sum_{dihedrals} \frac{V_n}{2} (1 + \cos[n\phi - \gamma]) + \sum_{i<j}^{atoms} (\frac{A_{ij}}{R_{ij}^{12}} - \frac{B_{ij}}{R_{ij}^{6}}) + \sum_{i<j}^{atoms} \frac{q_i q_j}{\varepsilon R_{ij}}$$

where U(R) is the potential energy as a function of the position R of N particles.

The first two energy contributions are energetic penalties associated with the deviation of bonds (bond stretching) and angles (angular bending) from reference values r_{eq} and Θ_{eq}. The interactions between pairs of bonded atoms (bond contribution) and the summation over all valence angles (angle contribution) are modeled by a harmonic potential. K_r and K_θ are force constants. The third energy term is a torsional potential modeling changes in energy due to bond rotation (torsion angle ϕ, phase factor γ, barrier height to rotation V_n). The fourth and fifth energy terms are non-bonded terms for non-bonded van der Waals forces (modeled using a Lennard-Jones potential) and non-bonded electrostatic interactions (modeled using a Coulomb potential term; distance R_{ij}, and charge q). These terms are calculated between all pairs of atoms (i,j) in any molecule, or in the same molecule but separated by at least three bonds. The Lennard-Jones 12-6 potential is a pair potential describing the energy of interaction between two

atoms (i,j) as a function of the distance between their centers. It is characterized by an attractive part varying at R^{-6} and a repulsive part varying at R^{-12}. The term R^{-6} dominates at large distance and the attraction is originated by van der Waals dispersion forces while the term R^{-12} dominates at short distance and models the repulsion between atoms (I,j) at very close proximity.

An additional polarization term E_{pol} can also be added to U(R):

$$E_{pol} = -\frac{1}{2}\sum_{i}^{atom} \mu i * E_i^{(o)} \qquad (40)$$

with μ_i atomic polarizability.

AMBER uses a leap-frog version of the Verlet algorithm, in which the coordinates are determined at times t, t + Δt, t + 2Δt,……, and the velocities at times t – Δt/2, t + Δt/2, t + 3Δt/2, etc. Furthermore, AMBER provides direct support for several solvent models. The default water model is 'TIP3P' [139]. The 'TIP3P' model defines a charge of -0.834e at the oxygen atom and 0.417e at each hydrogen atom. 'WATERBOX216' is a pre-equilibrated box of 'TIP3P' water. After building up the structure, minimization and molecular dynamics simulations can be executed.

2.5.3 Boundary conditions

Periodic boundary conditions allow performing MD simulations using only a small amount of molecules thus ensuring minimized boundary effects. At these conditions, the molecules are influenced by forces as if they were surrounded by bulk fluid. The molecule(s) are placed in a solvent box of a specific size. This box is surrounded with an

image of itself in all directions. The solute in the box of interest only interacts with its nearest neighbor images. Since each box is an image of the other, a molecular trajectory resulting in the particle leaving a box would re-enter from the opposite side ensuring the conservation of the total number of molecules and atoms in the box in agreement with the represented microcanonical NVE ensemble. The box size should be large compared to the range of the interactions present in the system. Long-range forces can be a problem in molecular simulations, and require specific attention during modeling. In AMBER7, the particle-mesh Ewald (PME) procedure is used to handle long-range electrostatic interactions [140], while long-range van der Waals interactions are estimated by a continuum model.

2.5.4 Introduction of restraints during equilibration

In restrained molecular dynamics simulations, additional terms called 'penalty functions' are added to the potential energy function. Internal restraints can be applied to bonds, valence angles, and torsions. The force constants and target values for the restraints can vary during the simulation. The penalty function or violation energy can consist of as many as three types of regions comprising a well with a flat bottom between an "inner" set of upper and lower boundaries r2 and r3 (see Figure 7). To the left and right of r2 and r3 the penalty function parabolically rises, if the internal coordinate violates these boundaries. Finally, since large violations may lead to excessive parabolic penalties, these parabolas can turn into linear penalties outside wider upper and lower boundaries (r1 and r4).
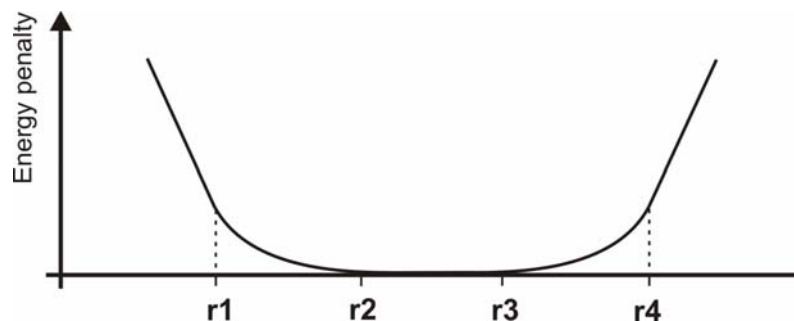
Figure 7 Plot of the penalty function.

The first restraint also specifies the rk2 and rk3 values. rk2 and rk3 are the force constants for the lower and upper boundaries, respectively. They maintain their values throughout the following restraints until rk2 and rk3 are re-defined. Default values defined in AMBER7 along with the penalty functions applied during the studies of this thesis are listed in Appendix B.

2.5.5 Simulated annealing

The main idea in molecular dynamics simulated annealing refinement is to heat up the system such that the molecule of interest has enough energy to explore a wide range in the configuration space facilitating to overcome energy barriers, as relatively large structural rearrangements are permitted at high temperatures. As the temperature is gradually decreased, the structural changes proceed in incrementally smaller steps, continuing to descend toward the global energy minimum. However, one is not guaranteed to reach the global minimum at the end of a simulated annealing procedure, as the optimal achievable annealing schedule may be dependent on the system or even the starting structures.

Usually, simulated annealing utilizes a distance dependent dielectric function. The dielectric function is used to mimic the presence of a high dielectric solvent but has no real physical basis. The next step of improvement from using distance dependent dielectric functions for NMR refinement is applying the generalized Born (GB) implicit solvation model. In this model, the effects of solvent are represented via an electrostatic continuum, and the solvent electrostatic free energy is included as an additional term in the molecular mechanics energetics [141]. However, the most accurate physical representation of the solvent environment is to include all the solvent molecules explicitly.

2.5.6 Conclusions

MD simulations are a widely accepted technique for simulating solvated molecule(s) in atomic detail. However, for specific applications such as the study of complex formation in solution new algorithms better suited for the investigated problems may need to be developed. Furthermore, a statistical problem arises when extending simulation results from a single substrate/ligand complex to the ensemble-averaged data measured in experiments such as the performed NMR and IR spectroscopic studies. Nevertheless, MD simulations have demonstrated the potential providing accurate models for experimental observations in complex systems.

2.6 Investigated template analytes

2.6.1 Deoxynivalenol (DON) and zearalenone (ZON)

Contamination of agricultural products by moulds has been observed for centuries posing a substantial hazard to the health of both humans and animals [142]. Among numerous acute toxic, carcinogenic, mutagenic, teratogenic, and estrogenic secondary metabolites, deoxynivalenol (DON) and zearalenone (ZON) are prominent representatives produced by Fusarium species [143] (see Figure 8).
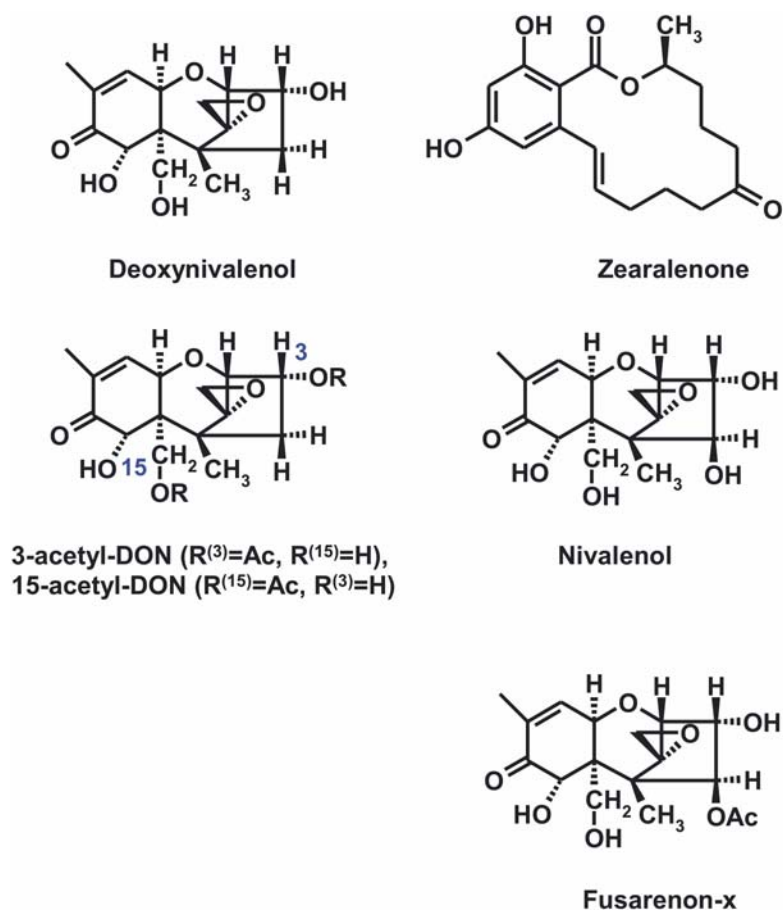
Figure 8 Molecular structures of the mycotoxins DON and ZON and structural analogues.

Most of the mycotoxins are chemically and thermally stable and resist molecular changes at storage conditions and during processing procedures. Mycotoxins may therefore be found in raw products, feed, and processed food and beverages manufactured from cereals. Major food commodities affected are cereals, nuts, coffee, dried fruit, cocoa, oil seeds, spices, dried peas, beans and fruit such as apples. However, mycotoxins may also be found in beer and wine resulting from the use of contaminated barley, other cereals and grapes in their production [144]. Furthermore, they may enter the human food chain via meat or other animal products such as eggs, milk and cheese as the result of livestock eating contaminated feed. The Food and Agricultural Organization of the United Nations (FAO) has estimated that 25% of the global crops are contaminated with mycotoxins. Mycotoxin contamination of US crops is listed in Table 6.

Table 6 Mycotoxin contamination of crops in the USA. Adapted from the Council for Agricultural Science and Technology (CAST) 2003 (Task Force Report No. 139, January 2003).

Crop	Mycotoxin	Action limit (AL)	Samples above AL [%]
Maize	Aflatoxins	20 ppb	6.6
	Fumonisins	2 ppm	2.1
	DON	1 ppm	6.9
Wheat	DON	1 ppm	12.4

Monitoring mycotoxin levels has therefore become of great importance and regulatory levels have been or are being worldwide introduced for many mycotoxins with ongoing efforts to homogenize these regulations on a global basis. Nevertheless, mycotoxin analysis remains a challenge since standard procedures for the determination of mycotoxins involve discontinuously operated laboratory methods based on an extraction step followed by time consuming clean-up procedures, which may need to be

complemented by derivatization steps. Sample preparation techniques include SFE, SPE, and immunoaffinity columns. Chromatographic techniques for mycotoxin analysis include GC-ECD, GC-MS, HPLC-DAD/FLD, and LC-APCI-MS [145-,146,147]. Mycotoxin analysis will therefore strongly benefit from the development of extraction materials for selective and rapid clean-up and pre-concentration from food and beverage samples.

2.6.2 <3,3',4',5,7>Pentahydroxyflavone (quercetin)

The flavonoid group (C_6-C_3-C_6), the cinnamic group (C_6-C_3), and the p-hydroxybenzoic group (C_6-C_1) are the three major groups of phenolic compounds found in plants, vegetables, grains, and fruits as well as processed beverages such as fruit juices and wine [148]. Flavonoids are secondary metabolites present primarily as glycosides and constitute one of the largest groups within the naturally occurring phenolics. Quercetin and the structurally related compounds morin (<2',3,4',5,7>pentahydroxyflavone), rutin (<3,3',4',5,5',7>hexahydroxyflavone, (6-O-α-L-rhamnosyl-β-D-glucoside)), and C-fla (2-carbethoxy-5,7-dihydroxy-4-methoxyisoflavone) are shown in Figure 9.
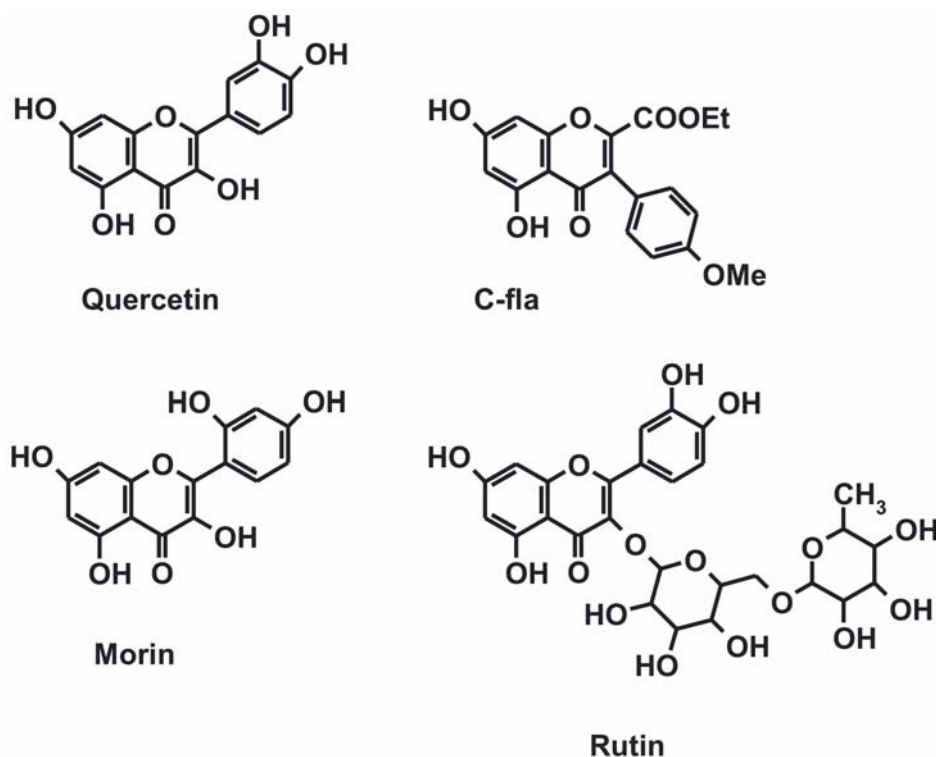
Figure 9 Molecular structure of quercetin and related compounds.

Besides many attributed functions such as light screens and control of plant growth, flavonoid compounds are also naturally occurring pigments and contribute to the flavor and texture of fruits [149]. Because of their metal-chelating capability and their free-radical scavenging properties, flavonoids are potential inhibitors of free-radical mediated diseases responsible for a variety of physiological effects such as vasodilatatory, anti-inflammatory, and anti-arthritic effects [150-152]. Quercetin is among the major flavonols found in fruits and vegetables and is thus considered an important dietary antioxidant. Analysis of flavonoids such as quercetin in food requires tedious pre-chromatographic purification treatments obtaining fractions containing different phenolic subgroups. Furthermore, extractions steps to remove lipids, carotenoids, and chlorophyll from fruit juices, as well as acidic, basic, or enzymatic hydrolysis to remove the sugar moieties

from glycosides are required [153] rendering extraction and monitoring of dietary relevant flavonoids a time-consuming analytical procedure.

2.6.3 2,4-Dichlorophenoxyacetic acid (2,4-D)

Used since 1945, 2,4-D is a selective systemic herbicide used to control broadleaf weeds. This synthetic auxin (plant hormone regulating growth) is among the most studied herbicides worldwide (structure see Figure 10).
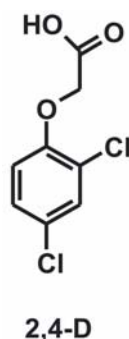
Figure 10 Structure of 2,4-Dichlorophenoxyacetic acid.

The toxicity of 2,4-D is experimentally well studied in mammals. However, although the mode of action of 2,4-D as a plant toxin is well understood, it is not clear in mammals. Adverse human health effects during non-lethal but toxic oral exposure to 2,4-D include irritation to mouth, throat, and gastrointestinal tract, vomiting, chest and abdominal pain, diarrhea, muscle twitches, tenderness, and stiffness. 2,4-D is included in the EPA list of drinking water contaminants with a maximum contaminant level of 0.07 mg/L (http://www.epa.gov).

2.6.4 Nitrophenols

2-and 4-nitrophenol enter the environment during manufacturing and processing, where they are used as reagents. Furthermore, they are found if phenols or cresols and nitrogen oxides are simultaneously present, as e.g. in car exhausts. 3-Nitrophenol is much less prevalent in industry and in the environment in contrast to 2- and especially 4-nitrophenol, which is included in the list of EPA priority phenolic pollutants (http://www.epa.gov).
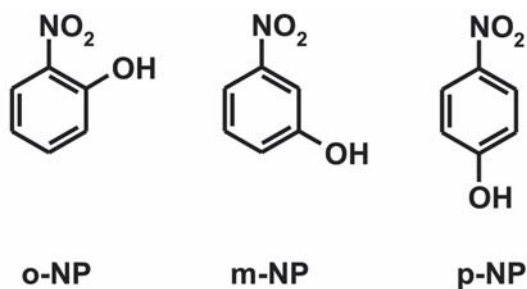
Figure 11 Structure of nitrophenols.

3. RESULTS

3.1 Quercetin MIPs: analysis of parameters affecting successful imprinting

3.1.1 Introduction

Molecularly imprinted polymers used as separation materials in HPLC applications and solid phase extraction are traditionally prepared by bulk polymerization in a trial-and-error approach. In a first step towards rationally designed MIPs, a retrospective analysis of a successful molecular imprint for quercetin [72,154,155] was performed. The focus of this study was to investigate how the ratio between template and functional monomer affects polymer selectivity and to assess the parameters governing the imprinting procedure resulting in an effective MIP. Polymers of varying composition were synthesized using the self-assembly approach and chromatographically characterized. Building on the successful synthesis of a quercetin selective MIP [72], strategies for a rational optimization of this recognition matrix were investigated. In a systematic approach, MIPs based on different ratios of functional monomer to the template quercetin, as well as using different monomers or monomer mixtures were synthesized and characterized.

3.1.2 Experimental

3.1.2.1 MIP synthesis

The quercetin imprinted polymers (see Table 7) were prepared by thermal bulk polymerization using the following components:

- Template: quercetin dihydrate [MW=338.3 g/mol], 1 mmol

- Porogen: acetone, 15 mL

- Functional monomers:

   4-vinylpyridine (4-VP) [MW=105.10 g/mol]

   acrylamide (AA) [MW=71.08 g/mol]

   methacrylic acid (MAA) [MW=86.09 g/mol]

- Crosslinker: ethylene glycol dimethacrylate (EGDMA) [MW=198.20 g/mol]

- Initiator: azobis-(isobutyronitrile) (AIBN) [MW=164.20 g/mol], 2 %

All chemicals were supplied by Sigma-Aldrich. 4-vinylpyridine was distilled under vacuum prior to use; all other chemicals were used as supplied.

For each polymerization, 1 mmol (0.3383 g) of quercetin was dissolved in 15 mL acetone in a glass tube. The functional monomer, the crosslinker and the initiator were then added to the solution. The solution was then cooled in an ice bath and purged with nitrogen for 5 min. The thermal polymerization was performed in a water bath at 60° C over night.

Table 7 MIPs imprinted with quercetin.

Polymer Ref. Nr	Functional monomer	Template: monomer: cross-linker [molar ratio]
Fla 1	4-VP	1 : 8 :40
Fla 2	4-VP	1 : 10 : 40
Fla 3	4-VP	1 : 4 : 20
Fla 4	4-VP	1 : 6 : 30
Fla 5	4-VP	1 : 2 : 10
Fla 6	4-VP and AA	1 : (4 : 4) : 40
Fla 7	4-VP	1 : 12 :60
Fla 8	MAA	1 : 4 : 40
Fla 9	4-VP	1 : 16 : 60
Fla 10	4-VP	1 : 20 : 100

The same procedure without template was used to prepare non-imprinted control polymers.

3.1.2.2 Grinding, sieving, and sedimentation

The obtained block polymer was crushed, ground for 2-3 min in a mechanical mortar (Retsch, Haan, Germany), and wet-sieved with acetone until particles < 25 μm were obtained. The polymer was then sedimented to eliminate particles < 5 μm removing the fines and for obtaining a narrower particle size distribution. The sedimentation was performed in ~250 mL acetone; after one hour the supernatent was discarded and fresh acetone was added to the precipitated MIP particles. The fines were separated after 5 to 6 sedimentations.

3.1.2.3 Packing of HPLC columns

The obtained molecularly imprinted polymers and the control polymers were used as stationary phase for HPLC measurements for characterization. Three grams of the sieved polymer particles were sonicated in acetone and packed into stainless-steel HPLC columns (250 x 4.6 mm) with acetone at 200 bar using an air driven fluid pump (Alltech, USA).

3.1.2.4 Characterization of the MIPs via HPLC

The HPLC analysis was performed using a Dionex HPLC (Dionex, Sunnyvale, CA, USA) with a P580 low pressure mixing pump and an UVD-340S diode array detector with a spectral range from 200 to 600 nm.

In order to extract the template molecule from the molecularly imprinted (IMP) polymer, the prepared column was washed on-line with methanol:acetic acid (7:1, v/v) at 1 mL/min until a stable baseline was obtained. The control columns were treated in the same way as the imprinted columns. After complete extraction of the template quercetin, the imprinted and the control columns were equilibrated with acetonitrile:water:acetic acid (80:10:10, v/v/v) as mobile phase. The elutions were performed at room temperature at a flow rate of 1 mL/min and monitored spectro-photometrically at 200-450 nm. The injection volume was 20 μL and the preferred DAD channel was set at 265 nm.

All measurements were performed with the molecularly imprinted (IMP) and the control polymer (CTL). The quercetin imprinted polymer was evaluated with respect to its selective recognition properties for quercetin and structural analogues of the flavonoid class. Following analytes were used for column characterization:

- Quercetin

- Rutin

- Morin

- 2-Carbethoxy-5,7-dihydroxy-4-methoxyisoflavone (C-fla)

The control polymer was used to confirm the obtained results. For each standard solution, 2 mg of the compounds were dissolved in 20 mL of the mobile phase (100 mg/L). Acetone was used as void marker (stock solution 20 μL in 4 mL mobile phase). A standard stock solution of quercetin, morin (140 mg/L respectively), and acetone (5 μL/mL) was used to determine the separation efficiency of the imprinted columns, since quercetin and morin are strongly related compounds differing only by the position of one OH-group (see Figure 9). The elution of the flavonoid compounds was confirmed by their characteristic UV-spectrum consisting of two absorption maxima in the ranges 300-380 nm (band I) and 240-285 nm (band II).

3.1.2.5 BET characterization

A defined amount of MIP or control polymer (0.03 g - 0.05 g) was degassed at 100 ºC for a period of 4 h prior to analysis removing adsorbed gases and moisture. A Beckman-Coulter (Fullerton, CA) instrument was utilized for BET studies (Coulter SA-3100 Surface Area and Pore Size Analyzer) enabling the determination of polymer surface areas from multi-point N_2 adsorption isotherms.

3.1.2.6 ^{1}H-NMR T_1 relaxation time studies

^{1}H-NMR spectra were recorded on a Varian Mercury Vx 300 spectrometer at 300 MHz equipped with a 5 mm broadband probehead. Chemical shifts were referenced to the solvent reference signal. T_1 values were measured using the inversion-recovery method at 293 K with a relaxation delay d_1= 5·T_1 (T_{1min}= 1, T_{1max}= 5, t= 0.3 h; d_1 calculated with the longest expected T_1, T_{1max}). The standard inversion-recovery experiment supplied by Varian was used and the T_1 values were calculated using the Mestre-C software (http://www.mestrec.com). Measurements were performed in d-acetone with 256 repetitive scans. For the T_1 studies with pyridine-d5, the quercetin concentration was 0.04 M and corresponding equivalents of pyridine-d5 were added.

3.1.3 Results and discussion

Molecularly imprinted polymers and control polymers for the template quercetin were synthesized with an increasing molar ration between the template and the functional monomer ranging from 1:2 to 1:20.

The imprinted and control polymers # Fla 5 (ratio 1:2:10) and # Fla 3 (ratio 1:4:20) were fine and brittle, resulting in substantial losses of polymer during the grinding and sieving procedures and a very high back-pressure during column packing. It was concluded that the ratios 1:4:20 and below produce a polymer that is not suited for column packing. The MIPs with ratios 1:6:30 to 1:20:100 showed good to moderate imprinting effects for quercetin. The retention indices are listed in Table 8.

Table 8 Evaluation of the imprinting effect: retention index for quercetin and structural analogues.

	Retention Index (RI = $\alpha_{CTL}/\alpha_{IMP}$)							
	Fla 8 1:4:40	Fla 6 1:(4:4):40	Fla 4 1:6:30	Fla 1 1:8:40	Fla 2 1:10:40	Fla 7 1:12:60	Fla 9 1:16:60	Fla 10 1:20:100
Quercetin	1	1	1	1	1	1	1	1
Morin	2.63	1.11	0.55	0.55	0.62	0.47	0.47	0.90
C-fla	0.86	0.72	0.16	0.14	0.14	0.21	0.15	0.37
Rutin	0.71	0.58	0.20	0.23	0.20	0.29	0.28	0.54

The polymers # Fla 6, and 8, followed by # Fla 10 showed a high cross-reactivity with morin, with retention indices > 1. The functional monomer MAA used in # Fla 8 did not allow successful templating of quercetin (see Table 9). Furthermore, it is evident that the retention times do not significantly vary from control to imprinted polymer.

Table 9 Capacity factors, separation factors, and retention indices of the IMP- and CTL-columns (25 cm, 4.6 mm ID) for polymer # Fla 8.

Fla 8	logK$_{OW}$	t$_{CTL}$ [min]	k'$_{CTL}$	t$_{IMP}$ [min]	k'$_{IMP}$	α_{CTL}	α_{IMP}	RI
Acetone	-0.24	3.66	-	3.62	-	-	-	-
Quercetin	1.5	4.58	0.25	4.87	0.35	1	1	1
Morin	1.5	4.29	0.17	5.92	0.63	1.47	0.56	2.63
C-fla	3.5	4.22	0.15	4.28	0.18	1.67	1.94	0.86
Rutin	-1.1	3.55	-0.03	3.51	-0.03	-8.33	-11.67	0.71

Using a mixture of different functional monomers also resulted in polymers with no selectivity for the template. Only a difference in retention times between imprinted and control polymer could be observed (see Figure 12).
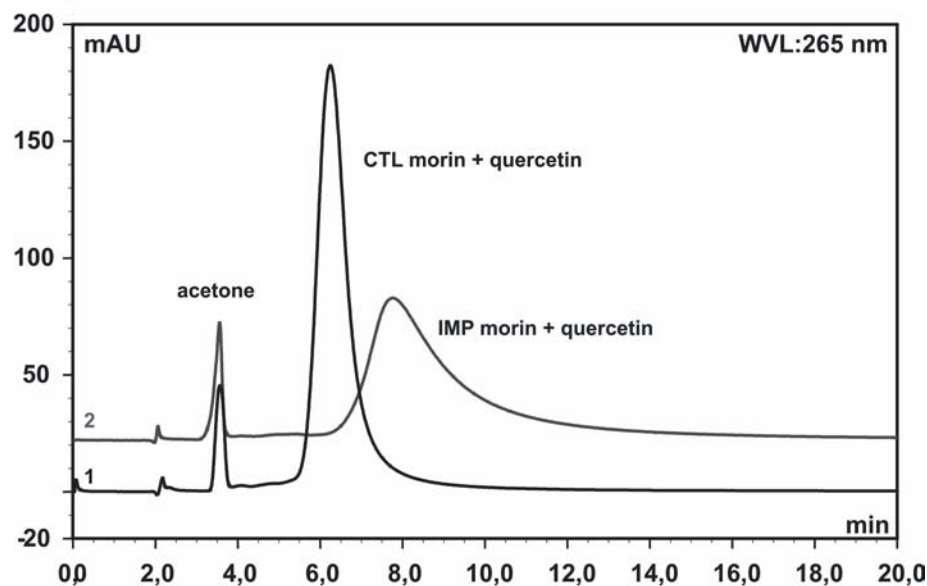
Figure 12 Chromatograms of a mixture of acetone, quercetin, and morin with (1) control polymer # Fla 6 and (2) imprinted polymer # Fla 6 in MeCN:H_2O:HAc (80:10:10, v/v/v) as mobile phase; flow rate 1 mL/min. Elution of acetone at 3.6 min.

The imprinted polymer synthesized with an equimolar mixture of 4-VP and AA as compared to 4-VP only (same total functional monomer concentration) resulted in complete loss of selectivity (see # Fla 6 and # Fla 1). Injected as a mixture, quercetin and morin were not separated by the imprinted polymer but were retained longer compared to the control polymer. The flavonoid peak (chromatogram Nr. 2, Figure 12) showed tailing, which is an indication for a higher affinity of quercetin and morin with the MIP compared to the CTL. This example nicely illustrates the importance of shape and size during imprinting, since quercetin and morin are structurally very similar differing only by the position of one OH group on a ring structure. Separation of quercetin and morin from the other flavonoids C-fla and rutin are predominantly based on size and shape recognition, with retention indices dropping from 1 for quercetin and morin to 0.72 for the isoflavonoid C-fla and further to 0.58 for the larger molecule rutin (see Table 8).

The polymers # Fla 1, 2, 4, 7, and 9 showed selectivity towards quercetin. Both MIPs # Fla 1 and 4 have similar retention indices. Nevertheless, since retention times on imprinted and control columns strongly vary from ratio to ratio, the polymers will be separately discussed.

3.1.3.1 Ratio 1:6:30 (quercetin:4-VP:EGDMA).

The capacity factors, separation factors, and retention indices characterizing the effectiveness of the imprinting, are given in Table 10.

The retention time of quercetin in the imprinted polymer column was approx. 5 times higher than in the column packed with the control polymer. This results in a much higher k' value for the imprinted polymer (k'$_{IMP}$=9.77).

Table 10 Capacity factors, separation factors, and retention indices of the IMP- and CTL-columns (25 cm, 4.6 mm ID) for polymer # Fla 4.

Fla 4	logK$_{OW}$	t$_{CTL}$ [min]	k'$_{CTL}$	t$_{IMP}$ [min]	k'$_{IMP}$	α$_{CTL}$	α$_{IMP}$	RI
Acetone	-0.24	3.78	-	3.43	-	-	-	-
Quercetin	1.5	8.12	1.15	~37.0	9.77	1	1	1
Morin	1.5	8.68	1.30	24.35	6.09	0.88	1.60	0.55
C-fla	3.5	4.83	0.28	4.73	0.38	4.11	25.71	0.16
Rutin	-1.1	4.20	0.12	4.11	0.20	9.58	48.85	0.20

The retention time for acetone, C-fla and rutin remained the same in the imprinted and control columns. Only morin showed a strong cross-reactivity with the generated anti-quercetin imprinted polymer resulting from the similar molecular structure. The pronounced tailing of quercetin and morin (see Figure 13) is an indication of a

heterogeneous binding site distribution within the imprinted polymer, with binding sites ranging in affinity from highly selective to non-specific ones.
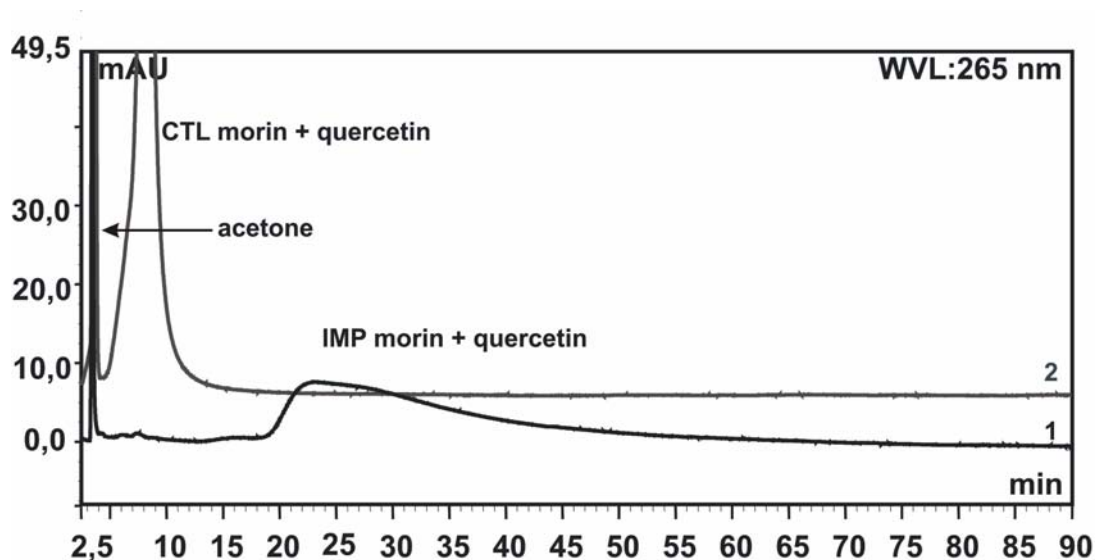
Figure 13 Chromatograms for (1) imprinted polymer # Fla 4 and (2) control polymer # Fla 4 with a mixture of acetone, quercetin, and morin in MeCN:H_2O:HAc (80:10:10, v/v/v) as mobile phase; flow 1 mL/min.

Due to the strong interactions with specific binding sites, quercetin and morin were strongly retained in the column compared to the other flavonoids rutin and C-fla and quantitative elution could not be attained with the selected mobile phase. Since quercetin elutes slowly over time, the retention time of quercetin is only an approximate time used in order to assess the control/imprinted polymer system. Furthermore, when applied as a mixture (Figure 13), morin and quercetin were not separated due to the strong peak tailing.

3.1.3.2 Ratio 1:8:40 (quercetin: 4-VP: EGDMA)

As previously reported [72], the ratio 1:8:40 resulted in the best imprinting effect, showing a high selectivity for quercetin compared to the structural analogues. Quercetin and morin were separated, eluting at 47.7 min and 27.8 min respectively in the imprinted column as compared to both co-eluting at 8.4 min in the control column (see Table 11).

Table 11 Capacity factors, separation factors, and retention indices of the IMP- and CTL-columns (25 cm, 4.6 mm ID) for polymer # Fla 1.

Fla 1	$logK_{OW}$	t_{CTL} [min]	k'_{CTL}	t_{IMP} [min]	k'_{IMP}	α_{CTL}	α_{IMP}	RI
Acetone	-0.24	3.50	-	3.60	-	-	-	-
Quercetin	1.5	8.40	1.40	47.70	12.25	1	1	1
Morin	1.5	8.40	1.40	27.80	6.80	1	1.80	0.55
C-fla	3.5	4.50	0.30	4.70	0.30	4.67	33.33	0.14
Rutin	-1.1	4.30	0.20	4.90	0.40	7.00	30.63	0.23

Rutin and C-fla also showed no difference in retention time between the imprinted and the control polymer. Results for this MIP are summarized in references [72] and [154].

To further compare the affinity of rutin and C-fla for all the synthesized MIP and CTL polymers, the retention times of the investigated compounds are given in Table 12.

Table 12 Comparing retention times of quercetin and structural analogues (IMP and CTL columns 25 cm, 4.6 mm ID)

	Retention time [min]							
	Fla 8	Fla 6	Fla 4	Fla 1	Fla 2	Fla 7	Fla 9	Fla 10
	1:4:40	1:(4:4):40	1:6:30	1:8:40	1:10:40	1:12:60	1:16:60	1:20:100
Acetone IMP	3.62	3.56	3.43	3.60	3.40	3.48	3.28	3.39
Acetone CTL	3.66	3.57	3.78	3.50	3.59	3.28	3.18	3.52
Quercetin IMP	4.87	7.94	~37.00	47.70	43.10	39.23	46.24	22.23
Quercetin CTL	4.58	6.31	8.12	8.40	8.79	8.58	9.25	7.75
Morin IMP	5.92	7.99	24.35	27.80	28.46	21.00	25.44	20.52
Morin CTL	4.29	6.06	8.68	8.40	8.89	8.81	9.77	7.80
C-fla IMP	4.28	4.37	4.73	4.70	4.66	4.89	4.15	4.77
C-fla CTL	4.22	4.29	4.83	4.50	4.75	4.28	3.99	4.38
Rutin IMP	3.51	4.05	4.11	4.90	4.30	4.19	4.30	4.08
Rutin CTL	3.55	4.09	4.20	4.30	4.18	3.63	3.69	3.79

The retention times for acetone, C-fla and rutin remained approx. the same in the imprinted columns # Fla 1 through Fla 10. Furthermore, the retention times of C-fla and rutin were only slightly higher compared to the void marker acetone. Results indicate a shape and size selectivity of the MIPs since besides the template quercetin only morin with similar size and shape showed changes in retention time in the different imprinted polymers. Due to size and shape discrimination in the MIPs, rutin and C-fla showed for all polymers no difference in retention time between the imprinted and the control polymer. Furthermore, the changes in retention time of quercetin and morin in the imprinted columns # Fla 1 to Fla 10 are an indication for changes in polymer selectivity based on recognition of functionalities. While the retention times of quercetin in the control polymers do not vary, the retention times in the imprinted polymers strongly increase when the appropriate ratios for successful imprinting are selected. A successfully imprinted MIP such as # Fla 1 shows the highest selectivity for the templated analyte with baseline separation of structural isomers.

3.1.3.3 Ratio 1:10:40 (quercetin: 4-VP: EGDMA)

Increasing the ratio of template to functional monomer from 1:8 to 1:10 resulted in a slight decrease in retention time of quercetin in the imprinted polymer, while no changes were observed for the other flavonoids. An increase in retention index of morin from 0.55 to 0.62 (see Table 13) was observed due to a slight increase in retention time in the imprinted polymer # Fla 2 compared to # Fla 1.

Table 13 Capacity factors, separation factors, and retention indices of the IMP- and CTL-columns (25 cm, 4.6 mm ID) for polymer # Fla 2.

Fla 2	$\log K_{OW}$	t_{CTL} [min]	k'_{CTL}	t_{IMP} [min]	k'_{IMP}	α_{CTL}	α_{IMP}	RI
Acetone	-0.24	3.59	-	3.40	-	-	-	-
Quercetin	1.5	8.79	1.45	43.10	11.67	1	1	1
Morin	1.5	8.89	1.47	28.46	7.36	0.98	1.59	0.62
C-fla	3.5	4.75	0.32	4.66	0.37	4.53	31.54	0.14
Rutin	-1.1	4.18	0.16	4.30	0.26	9.06	44.88	0.20

Similar to # Fla 4, the retention time of quercetin in the imprinted polymer column was 5 times higher than in the column packed with the control polymer, and morin showed a significant cross-reactivity with the generated anti-quercetin imprinted polymer (RI of 0.62). As for all the MIPs showing an imprinting effect for quercetin and to a lesser extent for morin, the peak of C-fla is sharp and does not show any tailing (see Figure14). The acetone peak is also always sharp.
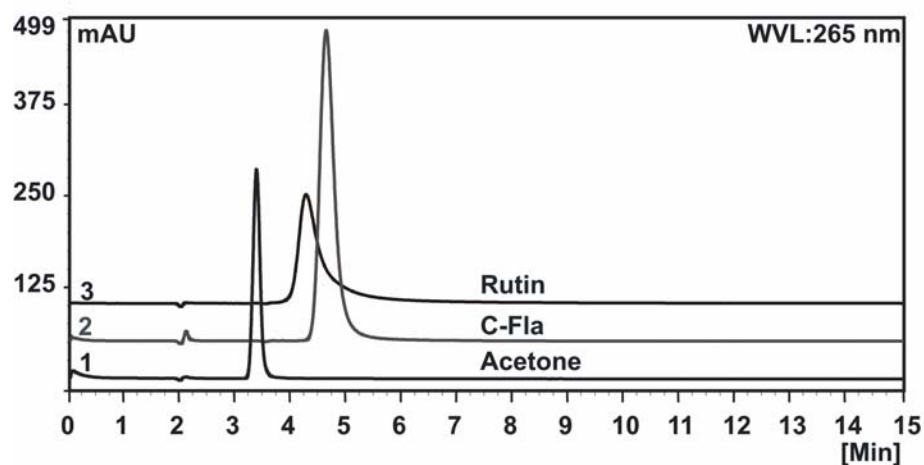
Figure 14 Chromatograms of acetone, rutin, and C-fla, for the imprinted polymer # Fla 2. Mobile phase MeCN: H_2O: HAc (80:10:10, v/v/v); flow rate 1 mL/min.

The peak corresponding to rutin shows slight tailing, which indicates minute cross-reactivity due to recognition of the flavonoid substructure. The tailing is strongest for quercetin and morin, an indication for selectivity with binding sites of different affinity such as a small number of high-affinity binding sites [3,72] with slow exchange kinetics together with binding sites of lower affinity with rapid exchange kinetics. Tailing is therefore an indication for a heterogeneous binding site distribution with gradual release of molecules during elution from a variety of different binding sites (see Figure 15).
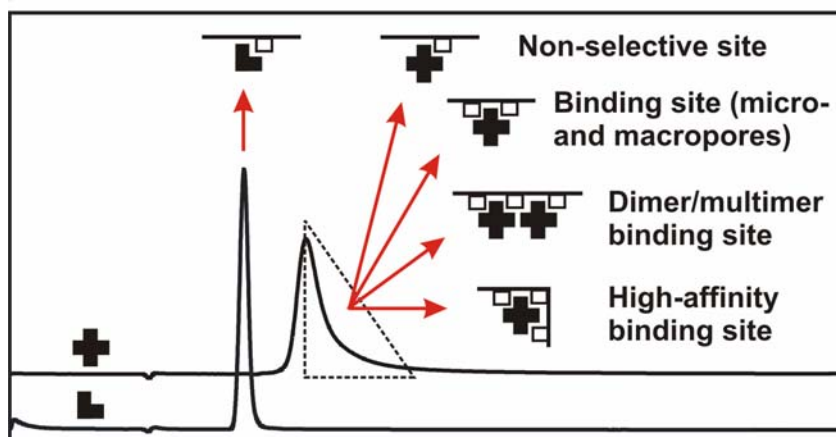
Figure 15 Contribution of the heterogeneity of binding sites in non-covalent imprinted MIPs to the tailing of chromatographic peaks.

Site accessibility, homogeneity of binding sites (e.g. low to high affinity), binding kinetics, and desorption rate contribute to the spreading of the observed chromatographic peaks.

3.1.3.4 Ratios 1:12:60 and higher (quercetin: 4-VP:EGDMA)

An increase from 1:10 to 1:12 and up to 1:16 (MIPs # Fla 7 and 9) resulted in a decrease of the retention index for morin (see Table 8). Both the MIPs # Fla 7 and 9 showed similar results. A further increase of the ratio to 1:20 resulted in complete loss of selectivity for quercetin, which co-eluted with morin in the MIP column (see Table 14) as well as in the control column.

Table 14 Capacity factors, separation factors, and retention indices of the IMP- and CTL-columns (25 cm, 4.6 mm ID) for polymer # Fla 10.

Fla 10	$logK_{OW}$	t_{CTL} [min]	k'_{CTL}	t_{IMP} [min]	k'_{IMP}	α_{CTL}	α_{IMP}	RI
Acetone	-0.24	3.52	-	3.39	-	-	-	-
Quercetin	1.5	7.75	1.20	22.23	5.55	1	1	1
Morin	1.5	7.80	1.21	20.52	5.05	0.99	1.10	0.90
C-fla	3.5	4.38	0.24	4.77	0.41	5.00	13.54	0.37
Rutin	-1.1	3.79	0.08	4.08	0.20	15.00	27.75	0.54

Nevertheless, the MIP # Fla 10 still shows shape and size recognition for quercetin and morin, with a 3-fold increase in retention time compared to the control polymer while C-fla and rutin show no difference in retention time between the control and the imprinted polymer (see Figure 16).
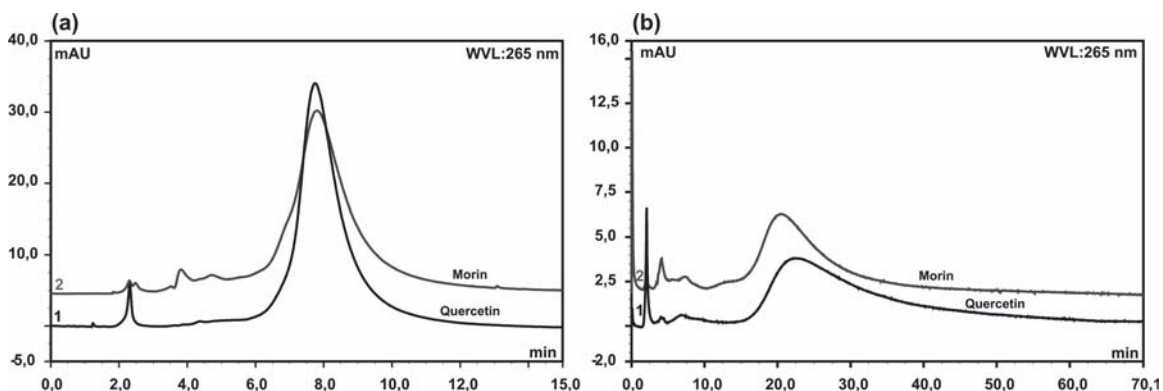
Figure 16 Chromatograms of quercetin (1) and morin (2) with the control # Fla 10 (a) and the imprinted polymer # Fla 10 (b); MeCN:H_2O:HAc (80:10:10, v/v/v) as mobile phase; flow 1 mL/min.

3.1.3.5 BET analysis of quercetin-MIPs

The BET surface area of the synthesized imprinted and control polymers was investigated to ensure that the superior retention observed at a selected ratio is not simply a surface area effect. The results are shown in Figure 17.
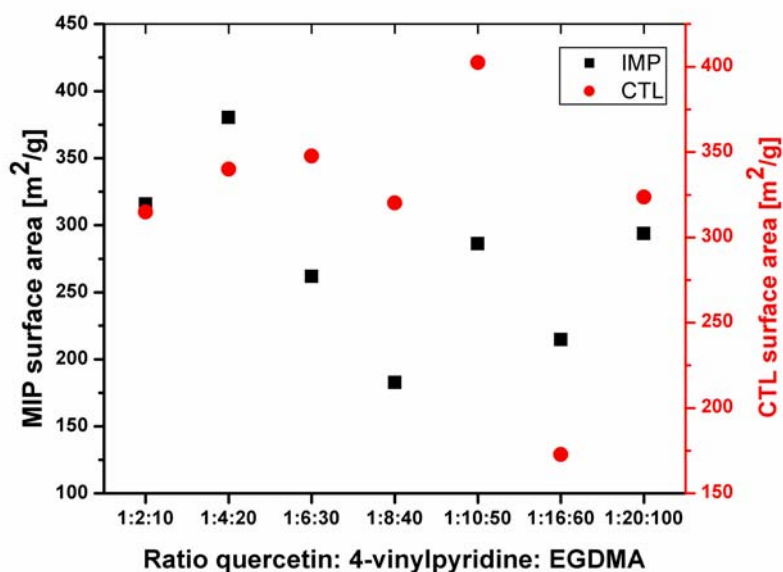
Figure 17 Comparison between surface areas of imprinted and corresponding control polymers at various template:monomer ratios via BET adsorption isotherm studies.

The surface area of the MIPs in comparison with the corresponding control polymers reveals no significant correlation. In fact, the MIP composition with the optimum 1:8 ratio displays the largest difference in surface area between MIP and CTL, with the control polymer revealing the higher surface area thereby ruling out surface area effects.

3.1.3.6 T$_1$ investigation in pre-polymerization solution

Increasing ratios between quercetin and pyridine-d5 were used in this study in analogy to the ratios used for molecularly imprinted polymer synthesis in order to identify quercetin interaction sites. Pyridine-d5 was used instead of 4-vinylpyridine to facilitate the observation of quercetin proton signals. Once equilibrium conditions are reached, the rate of relaxation of quercetin represents a weighted average of free and complexed species reaching a maximum at the ratio where the formation of the quercetin/pyridine-d5 complex is most favored. Since T$_1$ values may be used as a measure of the rate of molecular tumbling, T$_1$ should reach a minimum as complexation occurs to the greatest extent. However, the T$_1$ value increases after addition of increasing equivalents of pyridine-d5, with a maximum at the ratio of 1:8 (see Figure 18).
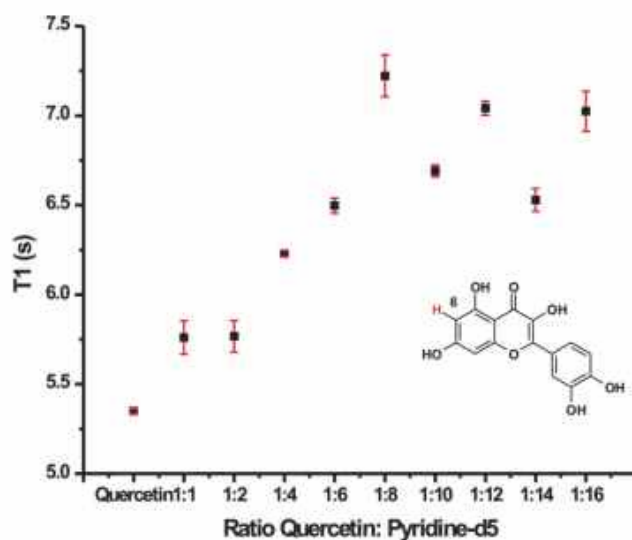
Figure 18 Spin-lattice relaxation time studies of quercetin (0.04 M) monitoring the proton at position C6 (highlighted in red). The titration study was performed with increasing pyridine-d5 ratio in d-acetone at 294 K. The data points represent the average of two measurement series.

Figure 18 summarizes the result for the proton at position C6. The T_1 values seem to reach a plateau at the ratio 1:8. The ratio 1:8 allowed obtaining a MIP with the best imprinting effect for quercetin as shown in the chromatographic studies shown in chapter 3.1.2.4. A direct correlation between the optimum monomer-template ratio derived from the chromatographic studies and the monomer-template ratio of 1:8 observed via ^{1}H-NMR T_1 relaxation time measurements can be made, suggesting the formation of stable pre-polymerization complexes is responsible for an increased formation of selective binding sites during the polymerization step. Since the spin-lattice relaxation time T_1 directly reflects the mobility of quercetin, molecular tumbling may be accelerated due to the addition of functional monomer. This effect may result from the formation of micro-environments of lower viscosity in contrast to the solvent medium.

In fact, visually following the polymerization process taking place in a glass vial as shown in Figure 19 already reveals the formation of aggregates apparent as a macroscopic phase separation effect.
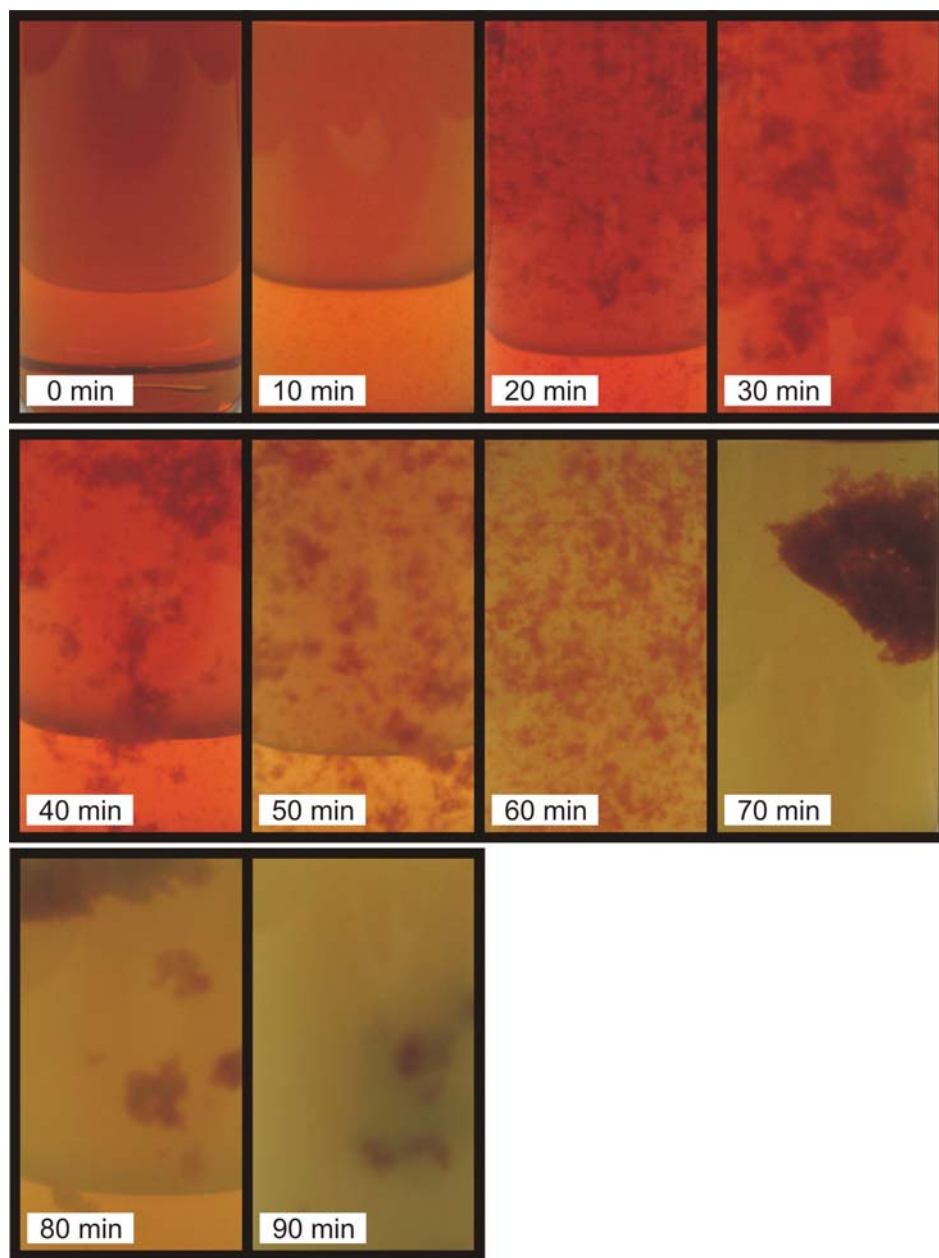
Figure 19 Phase separation observed during quercetin-MIP synthesis from t= 0 min (prior to thermally starting the polymerization) to t= 90 min. Ratio 1:8:40 (quercetin: 4-vinylpyridine:ethyleneglycol dimethacrylate, 1 mmol:8 mmol:40 mmol), 0.175 g AIBN, 15 mL acetone. Thermal polymerization at 60 ˚C.

As the polymerization progresses aggregates form, which subsequently coagulate and frequently result in a single polymer cluster, as demonstrated in Figure 19 at 70 min. These observations complement the T_1 NMR results indicating the formation of

microenvironments, and suggest the formation of monomer-template clusters based on similar hydrophobicity. It was therefore concluded that the observed trend for T_1 with increasing pyridine-d5 concentration was a consequence of the visually observed macroscopic phase partitioning of hydrophobic monomer/template aggregates within the polar solvent environment. The increase in size of the complex was measured as increase in spin-lattice relaxation time, independently from the nature of interactions stabilizing the complex.

3.1.4 Conclusions

The results of the investigations on the imprinting of quercetin are summarized in Figures 20 and 21. Figure 20 shows the retention times of quercetin and of the structural analogues in the imprinted polymers.
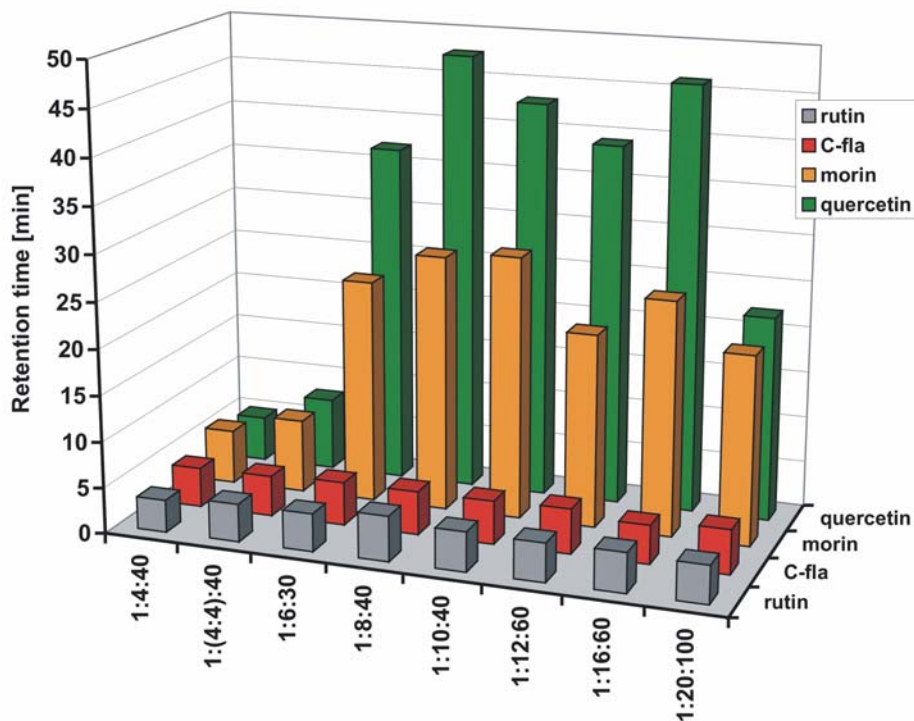
Figure 20 Retention times of quercetin and structural analogues for imprinted polymers packed as stationary phase material into HPLC columns (250 mm x 4.6 mm ID).

4-Vinylpyridine was the functional monomer resulting in polymers with a very high imprinting effect for quercetin. When used in a mixture with acrylamide the imprinting effect strongly decreased. While the retention times for C-fla and rutin do not change significantly within the permuted MIP composition, the retention times for quercetin and morin strongly vary indicating changes in selectivity for quercetin correlated to the ratio of the building blocks used during the imprinting procedure. Furthermore, it also indicates the importance of size and shape recognition, which is an important contributing factor to MIP selectivity.

The obtained retention times of quercetin for imprinted and control columns are summarized in detail in Figure 21.
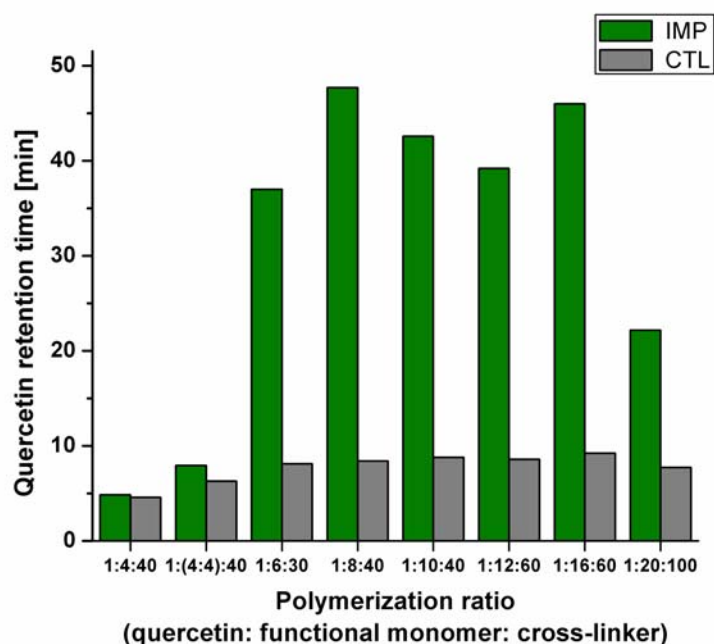
Figure 21 Retention times of quercetin in imprinted and control polymer HPLC columns.

The lower limit of the system quercetin:4-vinylpyridine:EGDMA was found to be the ratio 1:6:30. The polymers synthesized with a lower amount of cross-linker EGDMA were not suited to serve as stationary phase material for HPLC applications. The upper ratio 1:20:100 resulted in a polymer with a much lower imprinting effect compared to the results obtained with the lower ratios. BET studies revealed no significant correlation between the surface area and the polymer performance.

Studying the effect of the amount of functional monomer 4-VP used in MIP synthesis showed that the ratio 1:8 allowed obtaining the MIP with superior selectivity for quercetin. However, better understanding of the interactions governing the complex formation in the pre-polymerization solution and the cavity formation during the polymerization event is needed for a more rational approach to imprinting compared to the labor intensive experimental permutation of mixing ratios. Hence, the question arises why a ratio of 1:8 (quercetin:4-VP) is leading to the most selective molecular imprint?

Therefore, the next step in this study was focused on thorough investigations of the ratios used for imprinting in the pre-polymerization solution by monitoring the complex formation and determining the binding strength. ^{1}H-NMR T1 studies of the pre-polymerization mixture yielded further insight on the nature of the complexes formed prior to the polymerization step. A direct correlation between the optimum ratio of monomer:template in the chromatographic study (1:8), and the most stable ratio of the pre-polymerization complexes was observed via ^{1}H-NMR T_1 relaxation time studies, suggesting the formation of a particularly stable pre-polymerization complex at this ratio of building blocks. This circumstance is considered responsible for the formation of selective binding sites during the polymerization step [156]. Further studies within this thesis using the model analytes 3-acetyl-deoxynivalenol, 2,4-dichlorophenoxyacetic acid and 4-nitrophenol will allow a better understanding of the imprinting procedure by analyzing pre-polymerization complexation events.

3.2 MIPs for mycotoxin analysis

3.2.1 Introduction

For both DON and ZON, detection methods require extensive clean-up procedures [147]. Only for immunoassays, prior clean-up is usually not required [157]. A novel approach using molecularly imprinted polymers (MIPs) as highly selective separation and enrichment materials will therefore enable the development of high affinity, multiple-use solid phase extraction cartridges for the pre-concentration of DON and ZON from contaminated food and beverages such as beer. Sample preparation using MIPs will allow avoiding time-consuming multi-step clean-up procedures as well as costly

immunoaffinity columns. Besides DON and ZON, the structural analogue 3-ac-DON was used as template. Furthermore, due to the high costs for the pure mycotoxin templates, strategies were developed using structurally related and readily available low-cost analytes as dummy imprints. Specifically, the formerly imprinted molecule quercetin was used as dummy template for ZON-selective MIPs.

Although high incidences (up to 58 %) and high concentrations of zearalenone have been found in beers locally brewed in Africa (Nigeria, $\leq$ 2 mg/L; Swaziland, $\leq$ 53 mg/L; and Zambia with $\leq$ 4.6 mg/L), zearalenone as well as α-and β-zearalenol have not been found in Canadian or European beers with the exception of one French beer, which contained 100 µg/L [158]. Typical limits of detection range from 1 to 5 ppb. Nevertheless, due to the possibility of transmission of mycotoxins into beer from contaminated grains, surveying beer has been of interest since the 1970s, where e.g. US beer was surveyed for Ochratoxin A [159]. While zearalenone is converted largely to α-zearalenol and β-zearalenol by brewing strains of Saccharomyces cerevisae [160], DON has been reported to be the mycotoxin that best survives the beer brewing process [158] with limits of detection in the range of 5 to 25 ppb.

3.2.2 Experimental section

3.2.2.1 MIP synthesis

The mycotoxin imprinted polymers (see Table 15) were prepared by thermal bulk polymerization using the following components:

- Templates: - Deoxynivalenol [MW=296.32 g/mol]

- 3-acetyl-Deoxynivalenol [MW=338.40 g/mol]

- dummy template: quercetin dihydrate [MW=338.3 g/mol]

Porogen: acetonitrile, absoluted over molecular sieve (water content ≤ 0.01 %)

- Functional monomers:

    - 4-vinylpyridine (4-VP) [MW=105.10 g/mol]

    - methacrylic acid (MAA) [MW=86.09 g/mol]

    - methyl methacrylate (MMA) [MW=100.12 g/mol]

- Crosslinker: ethylene glycol dimethacrylate (EGDMA) [MW=198.20 g/mol]

- Initiator: azobis-(isobutyronitrile) (AIBN) [MW=164.20 g/mol], 2 %

Table 15 MIP and CTL polymers for mycotoxins; IMP polymers have uneven Ref. # and CTL polymers have even Ref. #; [(a)] data taken from R. Weiss et al. Food additives and contaminants 2003, 20, 386-395.

Ratios	Template	Functional Monomer	Cross-linker	Polymer Ref #	Imprinting effect (HPLC)
1:8:40[a]	DON	4-VP	EGDMA	DON-1/2	moderate
1:12:60[a]	DON	MAA	EGDMA	DON-3/4	moderate
1:8:40[a]	DON	4-VP	DVB	DON-5/6	no
1:8:40	quercetin	4-VP	EGDMA	ZON-7/8	good
1:10:50[a]	ZON	4-VP	EGDMA	ZON-9/10	poor
1:8:40[a]	ZON	TFM	EGDMA	ZON-11/12	no
1:8:40	3-ac-DON	MAA	EGDMA	DON-13/14	no
1:4:20	DON	MAA	EGDMA	DON-15/16	n. a.
1:4:40	DON	MAA	EGDMA	DON-17/18	poor
1:8:40	DON	MMA	EGDMA	DON-19/20	no

0.2 mmol (61 mg) of 3-ac-DON was dissolved in 3 mL acetonitrile. For DON imprinting, between 0.18 mmol (53 mg) and 0.34 mmol (100 mg) were dissolved in 3 to 5 mL acetonitrile. The functional monomer, the crosslinker and the initiator were then added to the solution. The solution was then cooled in an ice bath and purged with nitrogen for 5 min. The thermal polymerization was performed in a water bath at 60 °C over night. The amount of polymer obtained after grinding, sieving, and sedimentation was enough for packing one 150 mm x 4.6 mm HPLC column (approx. 2.2 g).

3.2.2.2 Characterization of MIPs via HPLC

After grinding and sieving (see 3.1.2.2), the polymer particles were sonicated in acetone and packed into stainless-steel HPLC columns (150 mm x 4.6 mm ID if not specified otherwise) with acetone at 200 bar using an air driven fluid pump (Alltech, USA). In order to extract the template molecule from the IMP polymer, the prepared columns were washed on-line with methanol:acetic acid (7:1, v/v) at 0.5 mL/min until a stable baseline was obtained. After complete extraction of the template, the imprinted and the control columns were equilibrated with acetonitrile as mobile phase. The elutions were performed at room temperature at a flow rate of 0.5 mL/min (acetonitrile) and monitored spectro-photometrically at 200-450 nm. The injection volume was 20 μL and the preferred channel was set at 220 nm. The following analytes were used for column characterization:

- DON
- 3-acetyl-DON
- 15-acetyl-DON
- Fusarenon-x

- Nivalenol

Acetone was used as void marker.

3.2.2.3 Solid phase extraction

SPE cartridges were packed with 50, 200, or 400 mg polymer. Columns with a capacity of 1 mL and a diameter of 0.5 cm were used for 50 mg of packing material and columns with a capacity of 6 mL and a diameter of 1 cm were used for packing higher amounts. Fritted polyethylene disks were used at the top and at the bottom.

The solid phase extraction was performed using a 12-port vacuum manifold from Alltech Associates (Deerfield, IL, USA). The collected SPE aliquots were evaporated at room temperature under a dry air flow with a 12-port drying attachment from Alltech Associates (Deerfield, IL, USA). The residues were then redissolved in 100 μL of HPLC mobile phase.

For SPE analysis of spiked beer samples ('Coors Original'), the beer was sonicated and degassed for 1 h prior to use. The degassed beer was spiked with 1 μg/mL ZON. After sample loading, the SPE cartridges with CTL and IMP polymers # Fla-1 were washed with water and eluted with methanol:water (70:30, v/v) followed by methanol containing 15 % acetic acid. 1 mL aliquot samples were collected, evaporated under a stream of dry, filtered air, and re-dissolved in 250 μL mobile phase (acetonitrile:water (0.1 % acetic acid), 1:1, v/v).

3.2.2.4 HPLC method for the characterization of SPE aliquots

HPLC measurements of the samples collected from the SPE procedure were performed with a Kromasil 100-5 C18 column (250 mm x 4.6 mm ID) at a flow rate of 0.8 mL/min. Isocratic elution with a 1:1 (v/v) mixture of acetonitrile and water containing 0.1 % acetic acid as mobile phase allowed separation of the mycotoxins within 10 min (see Figure 22), except ZON, which eluted after 20 min (see Figure 23).
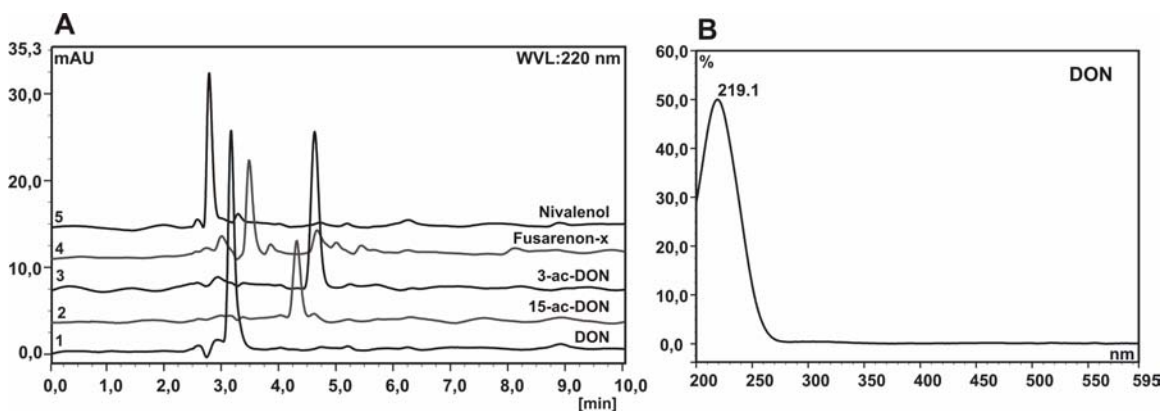
Figure 22 (A) Chromatograms of DON (1), 15-ac-DON (2), 3-ac-DON (3), fusarenon-x (4), and nivalenol (5) with a Kromasil 100-5 C18 column (250x4.6 mm ID). Analyte concentrations were 2.5 μg/mL. Mobile phase acetonitrile:water (1:1, v/v) containing 0.1 % acetic acid. Flow rate 0.8 mL/min. (B) UV/Vis spectrum of DON.

DON and 3-ac-DON (at 2.5 μg/mL) were determined with a relative standard deviation of 5.1 % and 4.8 % respectively.
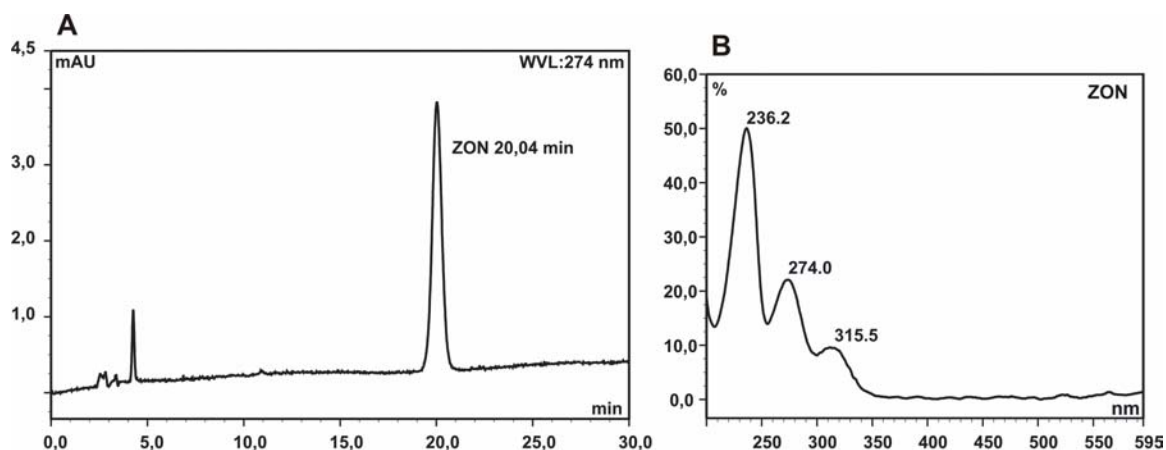
Figure 23 (A) Chromatogram of ZON at 2.5 mg/mL with a Kromasil 100-5 C18 column (250 x 4.6 mm ID). Mobile phase acetonitrile:water (1:1, v/v) containing 0.1 % acetic acid. Flow rate 0.8 mL/min; (B) UV/Vis spectrum of ZON (DAD).

For ZON analysis, the preferred UV/VIS channel was set at 236 nm.

3.2.2.5 ^{1}H-NMR studies with 3-acetyl-DON

^{1}H-NMR studies were performed on a Varian Mercury Vx 300 spectrometer at 300 MHz equipped with a 5 mm broadband probehead. The proton spectra were acquired with a spectral width of 4500 Hz and 16384 data points. Chemical shifts were referenced either to the solvent reference signal or to tetramethylsilane (TMS). Titration studies at room temperature were performed in d-acetone with 256 repetitive scans. For titration studies with d-acetic acid, the ratio of template-to-monomer was systematically varied, using equimolar solutions of 3-ac-DON and d-acetic acid (0.02 M) with a constant sample volume of 0.75 mL.

T_1 values were measured using the inversion-recovery method at 293 K with a relaxation delay $d_1 = 5 \cdot T_1$ ($T_{1min}=1$, $T_{1max}=5$, $t=0.3$ h; d_1 calculated with the longest expected T_1,

T_{1max}). The standard inversion-recovery experiment supplied by Varian was used and the T_1 values were calculated using the *Mestre-C* software (http://www.mestrec.com).

3.2.3 Results and discussion

3.2.3.1 MIPs for mycotoxins: HPLC characterization and optimization of synthetic mycotoxin receptor materials

A systematic approach was used varying functional monomers, cross-linkers and ratios as far as template availability allowed. The synthesized polymers were characterized by HPLC. In general, imprinting of mycotoxins only resulted in MIPs with poor to moderate imprinting efficiency as summarized in Table 15.

The imprinted polymer # DON-1 showed a moderate imprinting effect for DON, with a high cross-reactivity for nivalenol (see Table 16).

Table 16 Capacity factors, separation factors, and retention indices of the IMP- and CTL-columns (250 mm x 4.6 mm ID) for polymers # DON-1/2.

DON-1/2	$logK_{OW}$	t_{CTL} [min]	k'_{CTL}	t_{IMP} [min]	k'_{IMP}	α_{CTL}	α_{IMP}	RI
Acetone	-0.24	7.30	-	7.42	-	-	-	-
DON	-0.71	10.19	0.40	13.08	0.76	1	1	1
Uracil	-0.87	12.21	0.67	12.85	0.73	0.60	1.04	0.58
3-ac-DON	-0.55	8.47	0.16	8.88	0.20	2.50	3.80	0.66
15-ac-DON	0.30	8.51	0.17	9.19	0.24	2.35	3.17	0.74
Fusarenon-x	-1.24	10.25	0.40	10.78	0.45	1	1.69	0.59
Nivalenol	-2.22	13.00	0.78	17.15	1.31	0.51	0.58	1.14

Uracil is used as void marker for C_{18} columns and was added as further compound for column characterization. All analytes showed an increase of the capacity factor from the

CTL to the IMP column. However, only DON and nivalenol showed a marked increase in retention time on the imprinted column compared to the control column. Both DON and nivalenol lack the acetoxy group, which the o-substituted 3-ac-DON, 15-ac-DON, and fusarenon-x feature (see Figure 8). Furthermore, the cross-reactivity with nivalenol (RI value of 1.14) is high confirming shape selectivity of the MIP # DON-1. Also, effective imprinting effect is again supported by evident peak tailing of the DON and nivalenol peaks as shown in Figure 24. Since the retention indices of the investigated compounds are below 1 (besides nivalenol), the MIP is considered to be selective for DON with cross-reactivity to nivalenol.
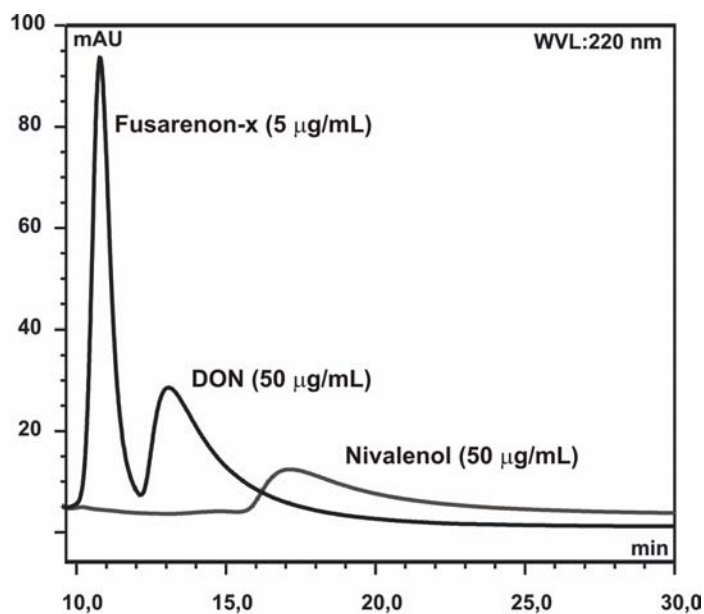
Figure 24 Chromatograms of nivalenol (at 50 μg/mL) and a mixture of DON (at 50 μg/mL) and fusarenon-x (at 5 μg/mL) with the DON-1 imprinted column (150 mm x 4.6 mm ID). Mobile phase: acetonitrile. Flow rate 0.5 mL/min.

Substituting 4-vinylpyridine with methyl methacrylate as functional monomer (# DON-19/20, same ratio 1:8:40) resulted in complete loss of selectivity for DON with all the mycotoxins co-eluting at approx. 5.1 min both in the imprinted and control columns.

107

Substituting the cross-linker EGDMA with DVB also resulted in loss of selectivity (# DON-5/6) [37].

Since promising results were obtained with MAA as functional monomer (# DON-3/4, ratio 1:12:60, [37]), DON and 3-ac-DON were imprinted using MAA as functional monomer reducing the ratios from 1:12 to 1:8 and 1:4 (template:functional monomer). Lowering the ratio for DON imprinting from 1:12 to 1:4 (# DON-17/18) did not improve the imprinting effect for the template. Furthermore, imprinting of 3-ac-DON (# DON-13/14) was unsuccessful revealing no difference between control and imprinted polymers. Nevertheless, the acetylated 3-acetyl-DON lacks an OH functionality compared to DON, which may be responsible for the reduced binding. Hence, the loss of a binding moiety apparently strongly reduces selective recognition due to less interaction sites contributing to complex formation and, ultimately, formation of selective recognition sites.

In contrast to DON and due to similar substructures (see Figure 25), quercetin could successfully be used as dummy imprint for ZON.
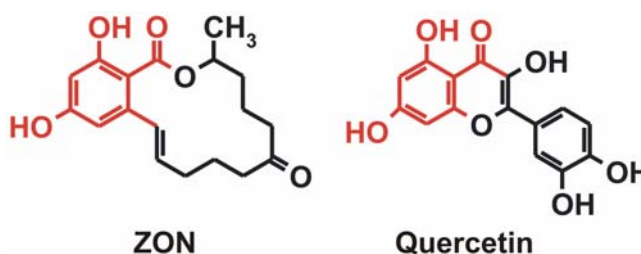
Figure 25 Structures of ZON and quercetin with the identical substructures highlighted in red.

Selectivity of the MIP for ZON was considerably reduced compared to the template quercetin with a ZON retention index of 0.23. Nevertheless, similar size and shape, as well as identical functionalities on the substructure highlighted in Figure 25 allowed

obtaining a higher affinity for ZON in the quercetin-imprinted polymer compared to the control polymer (see Table 17).

Table 17 Retention times of quercetin and ZON in the quercetin imprinted and control polymers (# Fla 1 in Table 7 and # ZON-7/8 in Table 15).

	t(quercetin) [min]	t(ZON) [min]
Quercetin-MIP	39.5	12.1
Quercetin-CTL	8.4	8.6

Furthermore, an increase of the capacity factor of ZON from k'=1.46 for the control polymer (# CTL Fla 1) to k'=2.36 for the imprinted polymer (# IMP Fla 1) confirmed selectivity. The dummy approach for ZON was more successful than previous attempts directly using ZON as template (see Table 15 and [37]).

This dummy approach for ZON illustrates the importance and feasibility of alternate approaches for molecular imprinting of analytes such as mycotoxins where the template is costly and toxic. Using the dummy template quercetin for ZON allowed obtaining a fairly selective MIP for ZON and strongly reducing MIP production costs as well as facilitating handling because of elimination of the toxic analyte within the imprinting procedure. Although some flavonoid compounds from the chalcone group such as xanthohumol have been identified in hops and beer [161], the flavonol quercetin is predominantly found in vegetables and fruit skins and does therefore not interfere with ZON enrichment. Furthermore, template bleeding, which may be a problem in SPE applications when working at trace and ultra-trace levels, does not interfere with ZON detection since the template quercetin and the investigated analyte ZON give two distinct signals.

3.2.3.2 Molecularly imprinted solid phase extraction (MISPE) for improved beverage analysis

Analyte enrichment and sample clean-up can be obtained with molecularly imprinted solid phase extraction (MISPE), if sufficient selectivity and affinity of the polymer for the selected mycotoxin is provided. The synthesized polymers described in Table 15 were tested as solid phase extraction material for the extraction of deoxynivalenol and zearalenone from standard solutions and from spiked beer samples.

3.2.3.2.1 SPE with standard solutions

SPE cartridges were packed with 50, 200, and/or 400 mg polymer (see Table 18). Besides DON, the structural analogue 3-ac-DON was selected to test the cross-reactivity and the affinity of the imprinted polymer cartridges. The mycotoxins were applied in acetonitrile. Applying the same solvent used as porogen during the polymerization process allowed for highest recognition conditions. The elution was performed in acetonitrile leaving the imprinted sorbent wetted by the same solvent. Thus swelling and shrinking of the material was minimized.

Table 18 SPE conditions for the extraction of DON from standard solutions.

Polymer Ref. #	Amount polymer [mg]	Concentrations [μg/mL]	Applied volume [mL]	Elution solvent
DON-1/2	400	2.5	1	Acetonitrile
DON-1/2	400	1.25	1	Acetonitrile
DON-1/2	400	0.625	1	Acetonitrile
DON-15/16	50	5	1	Acetonitrile
DON-17/18	50	2.5	1	Acetonitrile
DON-17/18	200	2.5	1	Acetonitrile

The MIP # DON-1 (1:8:40, DON:4-VP:EGDMA) showed the best results for MISPE of DON from standard solutions. Figure 26 shows the solid phase extraction profile for DON and 3-acetyl-DON from standard solutions containing 2.5 μg/mL in acetonitrile with a 400 mg SPE cartridge.
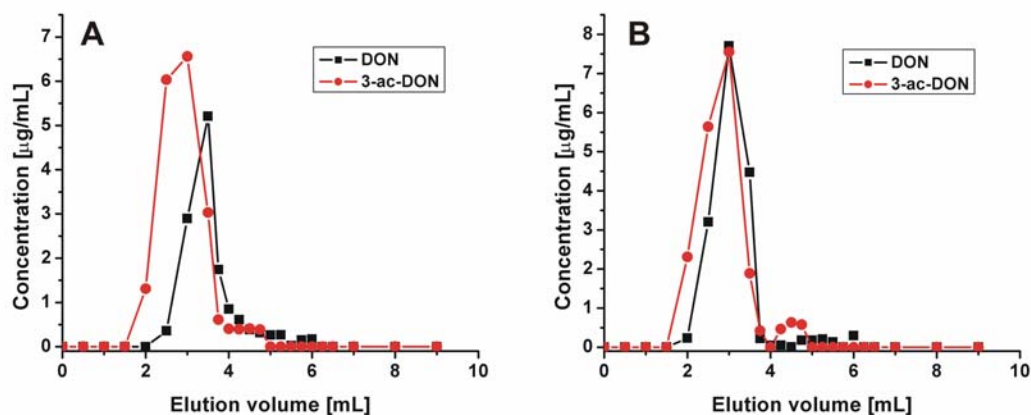
Figure 26 MISPE of DON and 3-ac-DON (2.5 μg/mL) with 400 mg cartridges of imprinted polymer # DON-1 (A) and control polymer # DON-2.

DON was recovered from the imprinted polymer DON-1 to 53% and from the control polymer DON-2 to 67.7 %. There was no significant difference in the recovery of 3-acetyl-DON between the imprinted and the control polymer (76.6 % and 78 %,

respectively). The low recovery rate of deoxynivalenol may result from higher affinity

binding sites causing the strong retention and thus incomplete desorption of DON.

However, higher recovery rates may be obtained with stronger eluents. While there was

no difference between the elution behavior of 3-acetyl-DON in the imprinted and in the

control polymer, DON was stronger retained in the imprinted cartridge, resulting in a shift

of the elution profile compared to the control polymer.

3.2.3.2.2 SPE of spiked beer samples

Molecularly imprinted solid phase extraction enabled selective pre-concentration of ZON

from a spiked beer sample as shown in Figure 27 by using the dummy imprinted

quercetin MIP for ZON, as previously reported in 3.2.3.1. RP-C_{18} HPLC analysis with a

1:1 mixture of acetonitrile:water (0.1 % acetic acid) as mobile phase with a flow rate of

0.8 mL/min enabled to completely separate the elution of zearalenone from the elution of

the beer matrix [162] (manuscript in preparation).
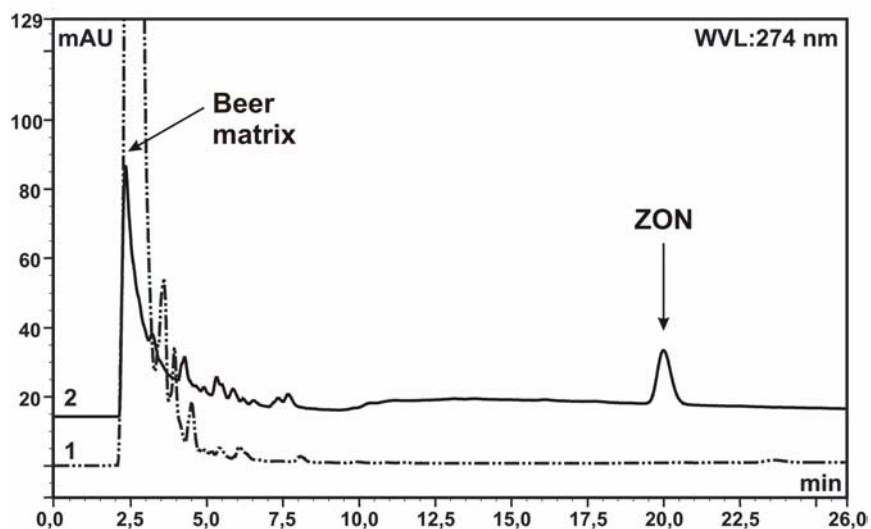
Figure 27 Chromatograms of a beer sample spiked with 1 μg/mL ZON before (1) and after (2) SPE with MIP # Fla-1 (115 mg). MISPE: pre-concentration from 10 mL beer; chromatogram of 1 mL aliquot from the solid phase extraction of a beer sample (Coors Original) spiked with ZON. The aliquots were evaporated to dryness and redissolved in 250 μL mobile phase. Elution with methanol containing 15 % acetic acid. The HPLC analysis was performed with a Kromasil C18 column with a C18 Alltech pre-column. Mobile phase: acetonitrile/water (1:1, v/v) with 0.1 % acetic acid at a flow rate of 0.8 mL/min.

Zearalenone was recovered to 80 % from the imprinted column IMP # Fla-1 and to 74.7 % from the control polymer CTL # Fla-1. Comparing SPE with imprinted and control polymers, the imprinted SPE cartridge showed preferential enrichment of ZON and of a few unidentified beer components compared to the control SPE cartridge (see Figure 28).
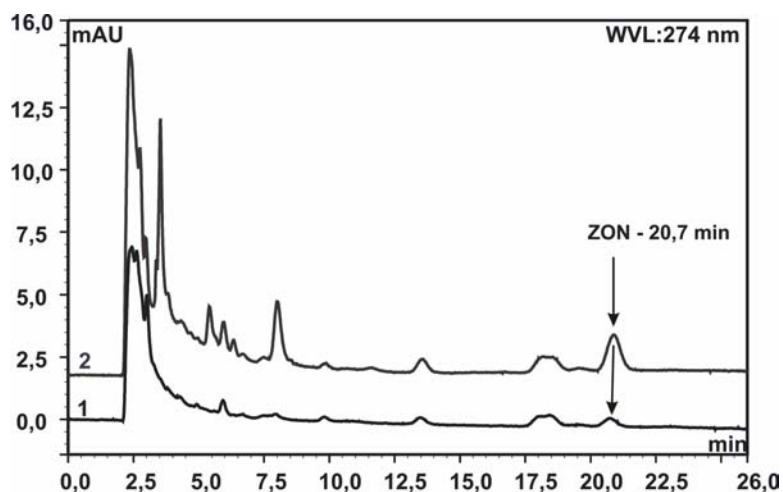
Figure 28 SPE aliquots of control (1) and imprinted (2) cartridges.

Furthermore, the ZON capacity of imprinted and control polymer was determined with 500 mg cartridges and compared to a standard 500 mg C_{18} SPE cartridge (see Figure 29). A total of 15 mL of 10 mg ZON/mL acetonitrile were applied. The cartridges were then washed with acetonitrile and eluted with methanol containing 18 % acetic acid.
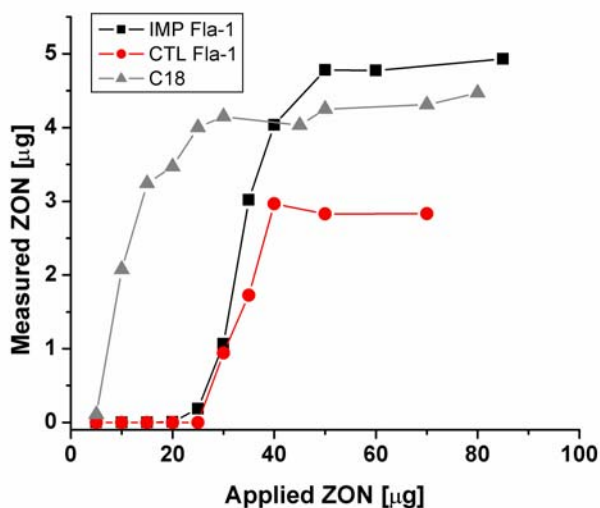
Figure 29 Breakthrough curve for ZON with CTL # Fla-1, IMP # Fla-1, and C_{18} SPE cartridges (500 mg).

Both imprinted and control polymer # Fla-1 showed a markedly higher capacity for ZON compared to the 500-C_{18} cartridge. ZON was not retained in the C_{18} material and could immediately be measured after application. The corresponding recovery rates are shown in Table 19.

Table 19 ZON recovery rates for IMP # Fla-1, CTL # Fla-1, and C_{18} cartridges.

SPE [500 mg]	Recovery ZON [%]		
	IMP # Fla-1	CTL # Fla-1	C_{18}
Total	91.1	71.8	89.3
Application	78.4	42.7	82.8
Washing	10.2	11.8	4.8
Eluting	2.5	17.3	1.7

A total of 91.1 % was recovered from the imprinted cartridge compared to 71.8 % from the control cartridge. These results indicate a high amount of non-specific binding to the polymer matrix, with a recovery during sample application of 42.7 % from the control compared to 78.4 % from the imprinted column, as well as a comparatively high recovery of 17.3 % from the control polymer during the elution step. The imprinted polymer # Fla-1 therefore demonstrated its suitability for SPE applications with a high capacity for ZON together with high recovery rates of approx. 91 %.

3.2.3.3 NMR studies with 3-acetyl-DON

The ^{1}H-NMR spectrum of 3-acetyl-DON was assigned from relative peak intensities and is shown in Figure 30 along with the structural assignments.
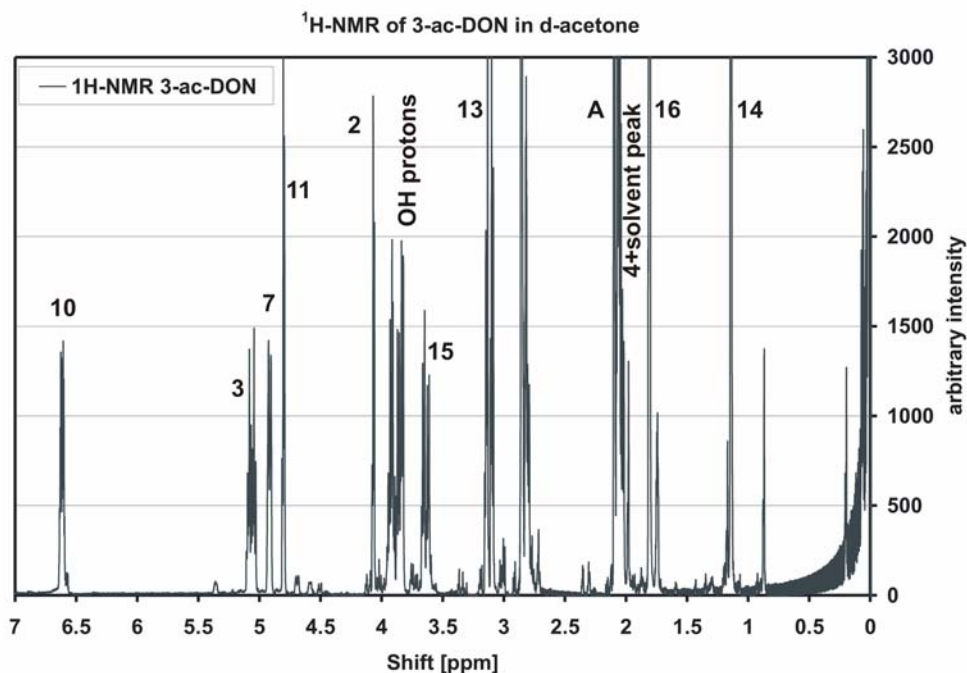
Figure 30 Spectral assignment of ^{1}H-NMR spectrum of 3-acetyl-DON.
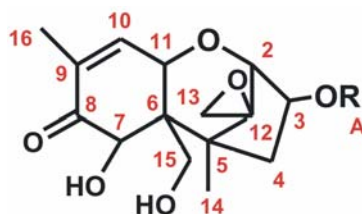
Figure 31 Chemical structure of 3-acetyl-DON with carbon atom numbering. A: CH$_3$ (Ac).

The ^{1}H chemical shift assignments of 3-ac-DON have been previously reported for 250 MHz spectra in CDCl$_3$ [163]. The ^{1}H-NMR spectrum revealed the expected peaks and integration ratios. The solvent shift for d6-acetone is evident at 2.05 ppm.

d-Acetic acid was selected for the titration study instead of the functional monomer methacrylic acid to facilitate the observation of changes in proton signals. Nevertheless, the titration of 3-ac-DON with d-acetic acid only resulted in an increased peak

broadening with increasing acid concentration, which is attributed to a dynamic exchange of protons as shown in Figure 32 for the # C13 protons. The splittings disappear as a result of rapid acid-catalyzed H^+ exchange.
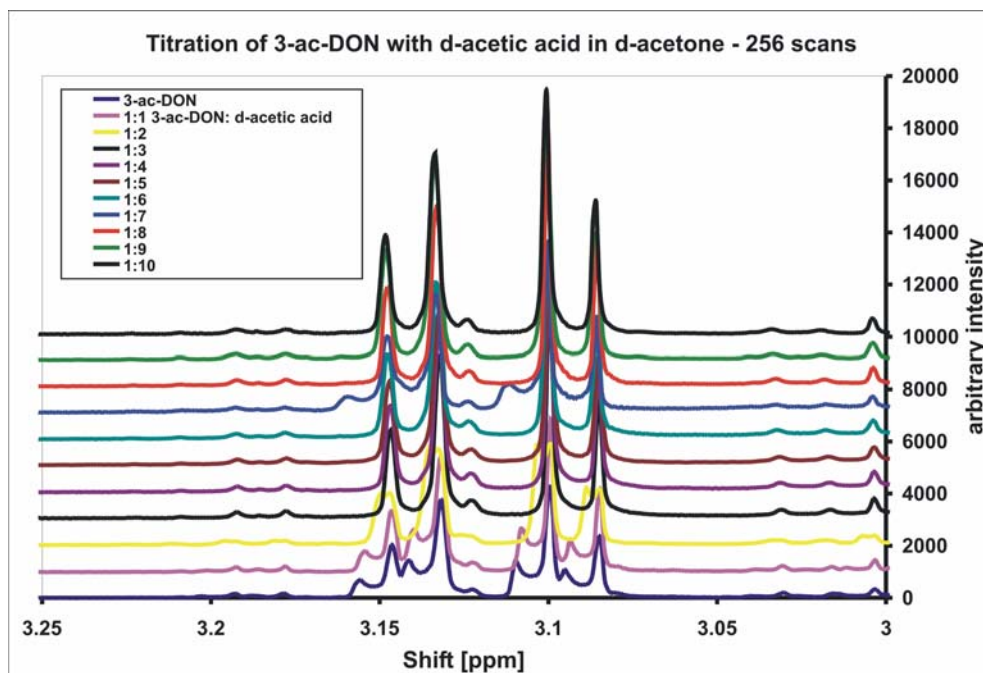
Figure 32 Titration of 3-ac-DON with deuterated acetic acid in acetone-d6. Peaks from the epoxy ring # C13 protons are observed.

No changes in NMR shifts could be observed during the titration study with d6-acetic acid.

Since MIP synthesis is thermally performed at 60 ˚C, a temperature study was performed with the ratio 1:8 across a temperature profile from 20 ˚C to 60 ˚C in increments of 10 ˚C. Figure 33 shows the ^{1}H-NMR spectra at 20 ˚C and 60 ˚C for the protons at position C13 (on the epoxy ring).
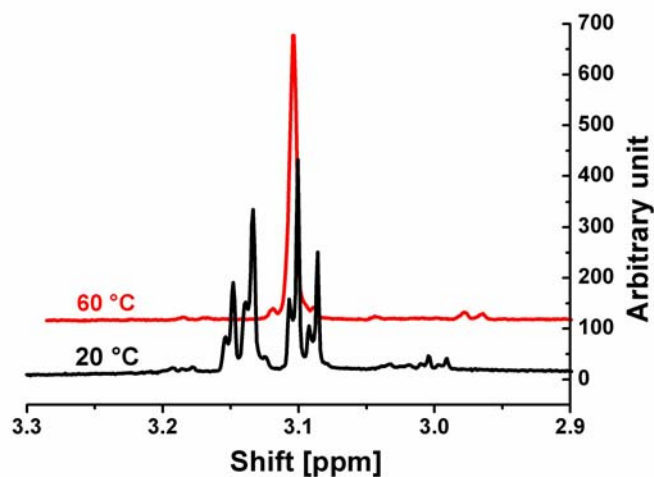
Figure 33 ^{1}H-NMR temperature study with 3-acetyl-DON. Sample 1:8 of 3-ac-DON with d-acetic acid in d-acetone measured at 20 and 60 °C.

Besides a minute upfield shift of the methyl proton signal from the 3-o-acetylated group, no other changes were observed due to the temperature increase. The singlet observed at 60 °C in Figure 33 may result either from increased mobility of the epoxy group at the higher temperature or may be an indication for opening of the epoxy ring at 60 °C. So far, studies on the effect of temperature on the stability of DON have shown no measurable decomposition at 110 °C in aqueous samples [164] or decomposition in whole barley powder samples heated at elevated temperatures such as 220 °C [165]. Temperatures in this study did not exceed 60 °C. However, due to the presence of d-acetic acid, acid-catalyzed H^+ reactions with 3-acetyl-DON may accelerate decomposition.

Spin lattice relaxation time studies of the prepared samples showed a strong increase in T_1 after addition of d-acetic acid to 3-ac-DON (see Figure 34).
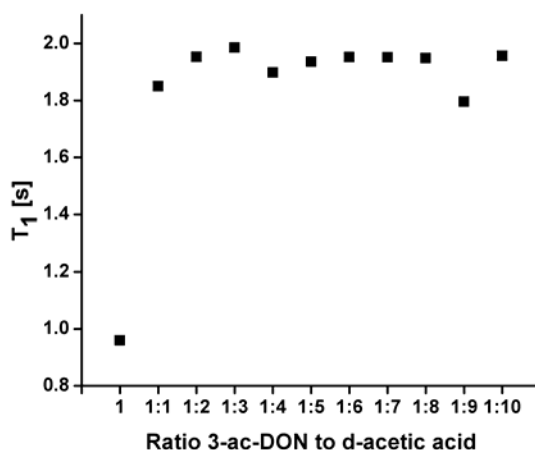
Figure 34 Spin-lattice relaxation time studies of 3-acetyl-DON (0.02 M) monitoring the proton at position C7 (see Figure 29). The titration study was performed with increasing d-acetic acid ratio in d-acetone at 294 K.

Since T_1 values may be used as a measure of the rate of molecular tumbling, T_1 should reach a minimum as complexation occurs to the greatest extent. However, the T_1 value strongly increases immediately after addition of d-acetic acid in a 1:1 ratio with 3-ac-DON and rapidly saturates at a plateau value as previously observed for the T_1 studies of quercetin (see chapter 3.1.3.6). This increase in T_1 was measured for multiple protons of the 3-ac-DON molecule. The T_1 relaxation studies offer a direct reflection of the immediate environment of the 3-ac-DON molecule in d-acetone. Therefore, the increase in T_1 may also be attributed to a change in viscosity of the micro-environment of 3-ac-DON, due to increasing amounts of d-acetic acid leading to a change in mobility of the molecule.

These studies clearly indicate that thorough NMR investigations provide in depth insight on the behavior and interactions of challenging templates such as the mycotoxins 3-acetyl-DON and zearalenone in pre-polymerization solutions. In the case of DON and 3-acetyl-DON the instability of the epoxy ring at the elevated polymerization temperatures may provide an explanation for the medium to low selectivities obtained during

imprinting. For ZON, it has been proposed that a reactive double bond present in the molecular structure could be responsible for an incorporation of ZON in the polymerization reaction resulting in a poor imprinting effect when templating ZON [37]. Template stability under the harsh polymerization conditions is therefore an important factor to be taken into consideration when choosing a template analyte. Structural or conformational changes of the template occurring during the imprinting process will result in templating structures or conformations different from those exposed to the MIP during the batch rebinding process. The presented results have shown that polymerization conditions such as increased temperature have structural implications on the template and will affect imprinting results. The MIPs imprinted with DON, 3-acetyl-DON and ZON (see Table 15) have shown only poor to moderate affinity for the template analyte when re-exposed to the MIP as opposed to the successful imprinting of quercetin. Furthermore, besides the template itself, the number of variable parameters affecting self-assembly in solution is considerable, ranging from electrostatic interactions to hydrophobic effects, which may lead to aggregation and changes in the micro-environment of the template as demonstrated in the T_1 studies with quercetin and 3-acetyl-DON. Hence, the importance of such extensive NMR studies substantiates by the generation of analytical evidence for a direct correlation of molecular level pre-polymerization complexation events with the post-polymerization chromatographic performance of the synthesized MIP. Results have demonstrated that analytical investigations of the template behavior in the pre-polymerization solution is a valuable tool in molecular imprinting directed towards rational understanding of pre-polymerization events for optimum selection of template and functional monomer.

3.2.4 Conclusions

This first study on mycotoxin imprinted polymers promise the future application of molecularly imprinted polymers as selective material for the separation and enrichment of DON and ZON from natural sources such as grains and processed beverages such as beer offering a viable alternative to conventional sample clean-up and pre-concentration methods. While the obtained results demonstrate the potential of molecularly imprinted materials for mycotoxin analysis, their implementation for real-world applications remains a challenge due to the medium to low selectivities achieved so far. DON-imprinted solid phase extraction cartridges revealed enhanced retention of DON compared to control cartridges with recovery rates of up to 88%. Molecularly imprinted solid phase extraction with dummy-imprinted ZON cartridges using quercetin as structural imprinting analogue enabled effective sample clean-up and the pre-concentration of ZON (1.25 µg/mL) from spiked beer samples directly applied onto the cartridge with recovery rates of 80 %. Next to these results only one other molecular imprinting approach for the mycotoxin ochratoxin A has been reported [166].

Especially for templates which are costly or difficult to obtain such as DON and ZON, careful consideration of the imprinting procedure is necessary. Hence, a more rational approach to molecular imprinting was investigated, based on thorough NMR studies of 3-acetyl-DON. However, because of the toxicity and high costs of pure mycotoxins required for these investigations, the analytical method development and studies of the pre-polymerization solution were shifted to less costly model templates (2,4-dichlorophenoxyacetic acid, and 2-, 3-, and 4-nitrolphenol), which have successfully been imprinted in our research group in recent years. It is anticipated to resume studies

on cost extensive template molecules once the analytical strategy is well defined and a minimum set of experiments have been identified.

From these first studies it is evident that the mode and strength of the non-covalent binding interactions between the template and the functional monomers in the pre-polymerization mixture are to a large extent responsible for the formation of high affinity binding sites during the polymerization process. Hence, detailed NMR titration experiments and IR-spectroscopic studies have been devised to observe the monomer-template complex formation at a molecular level and to further advance in depth understanding of the imprinting procedure facilitating the development of more efficient imprinting matrices.

3.3 The nature of MIPs: analyzing the mechanisms of selectivity in 2,4-dichlorophenoxyacetic acid imprints

3.3.1 Introduction

Most MIPs are synthesized in weakly polar aprotic solvents such as acetonitrile, which favour polar interactions. In contrast, 2,4-D was the first template successfully imprinted and applied in acetonitrile as well as aqueous solutions using the functional monomer 4-vinylpyridine [13,82]. Templated polymers synthesized in the self-assembly approach rely on complex formation between the target analyte and functional monomers in porogenic solution prior to radical polymerization. Consequently, the achievable selectivity is governed by the nature and stability of these complexes. In addition to van der Waals interactions and hydrophobic effects, comparatively weak electrostatic interactions such as π-π stacking may occur between aromatic rings in polar solvents

such as water and methanol. Hence, it was postulated that the 2,4-D complex formation results from both hydrophobic and electrostatic interactions. Imprinting in aqueous solutions is of substantial interest as such synthetic receptors would enable templating of e.g. biomolecules in their natural environment. Since the three-dimensional structure and activity of biomolecules is defined by relatively weak non-covalent interactions, which are usually restricted to aqueous environments, imprinting of biomolecules can only be performed in aqueous porogenic solutions.

In this study, the nature of non-covalent interactions responsible for complex formation during imprinting of the template 2,4-dichlorophenoxyacetic acid (2,4-D) with the functional monomers 4-vinylpyridine and methacrylic acid was investigated in aqueous and apolar aprotic solvents. Furthermore, the effect of the cross-linker on complex formation was analyzed. Fourier transform infrared (FT-IR) and ^{1}H-NMR spectroscopy provide the fundamental analytical basis for rationalizing the mechanisms of recognition during the imprinting process and for probing the governing interactions for selective binding site formation at a molecular level [167]. Chromatographic studies of the synthesized MIPs further allowed investigating the importance of size, shape, and functional molecular moieties during selective 2,4-dichlorophenoxyacetic acid re-binding processes.

3.3.2 Experimental section

3.3.2.1 MIP synthesis and HPLC characterization

The functional monomer 4-vinylpyridine (4-VP) together with the cross-linker ethyleneglycol dimethacrylate (EGDMA) were used for radical block co-polymerization in

a ratio of 1:4:20, 2,4-D:4-VP:EGDMA (mM ratios) [82]. A methanol:water mixture (4:1, v/v) was used as porogen (5 mL). Azobis-isobutyronitrile (AIBN) was used as polymerization initiator. The pre-polymerization solution was degassed by sonication and purged with nitrogen for 5 min. A pre-polymerization solution without template was used for the synthesis of the control polymer. The polymerization was performed thermally at 45 °C (imprinted polymer Ref. # IMP1) and compared to UV initiated polymerization (imprinted polymer Ref. # IMP2).

The polymer monoliths were grinded in an electrical mortar, wet sieved through a 25 μm sieve and sedimented in acetone until the fines were removed. Thus processed particles were packed into 150 mm x 4.6 mm ID HPLC steel columns for characterization as described in chapter 2.2.2.4. The packed columns were washed for 12 h with methanol containing 12 % acetic acid as mobile phase at 0.5 mL/min prior to use. The mobile phase used for column characterization was acetonitrile containing 1 % acetic acid at a flow rate of 1 mL/min. Acetone was used as void marker.

3.3.2.2 MIR spectroscopy

The IR data was recorded on a Bruker Equinox 55 Fourier transform infrared (FT-IR) spectrometer (Bruker Optics, Billerica/MA) equipped with a liquid nitrogen cooled mercury-cadmium-telluride (MCT) detector in the spectral range of 400-4000 cm^{-1} at a spectral resolution of 1 cm^{-1}. The transmission absorption measurements were performed in a thin film liquid cell (Pike Technologies, WI, USA) at room temperature with a 200 μm teflon spacer and NaCl windows (32 x 3 mm). The spectrometer was purged with dry air and 100 repetitive scans were averaged.

The hydrogen-bonded complexes between 2,4-D and the functional monomers MAA and 4-VP along with the influence of the cross-linker ethyleneglycol dimethacrylate on the complex formation were investigated in CCl_4 by transmission absorption FT-IR spectroscopy, which enabled identifying the free and hydrogen bonded species. The reaction of a protic acid and a base in a non-dissociating solvent such as chloroform or carbon tetrachloride leads to the formation of a hydrogen-bonded complex (weak acids/bases) [168] or an ion-pair bonded salt associated via a hydrogen bond (stronger acids/bases) [169]. The two extremes of these interactions can be written as A-H···B and BH^+···A^-. In order to identify the nature of 2,4-D/4-VP complexes, two types of titrations were performed keeping either the 2,4-D concentration or the functional monomer concentration constant. Both the spectral features of the acid 2,4-D and the base 4-VP can be traced during the complexation event. The absorption bands of free and complexed 4-VP, respectively, were utilized for qualitative analysis. In addition to investigate effects on 4-VP spectra during complex formation a solution with a fixed concentration of 4-VP (2.10^{-3} M) was titrated with solutions of variable 2,4-D concentration. The measurements were performed with a 200 μm spacer and started after 25 min of equilibration time for steady background conditions. For Job's plot analysis of IR data, stock solutions of 4.10^{-3} M 4-VP and 2,4-D, respectively, in CCl_4 were used and mixed from 0 to 100 % to a constant total volume of 1 mL. The absorbance of 4-VP was measured at 1597 cm^{-1} in the mixture and for 4-VP alone. The absorbance observed in absence of 2,4-D (4-VP only) was subtracted from the absorbance of each mixture and the absolute value was plotted against the molar ratio of 2,4-D.

3.3.2.3 ^{1}H-NMR spectroscopy

In addition to the IR studies, complementary NMR spectroscopic investigations were performed. 1D ^{1}H measurements were performed on a Varian Mercury Vx 300 spectrometer at 300 MHz equipped with a 5 mm broadband probehead. The proton spectra were acquired with a spectral width of 4500 Hz and 16384 data points. Chemical shifts were referenced to the solvent reference signal if TMS was not present in the deuterated solvent. For Job's plot analysis the ratios of functional monomer and template were systematically varied between 0:1 to 8:1 using equimolar solutions (0.04 M) with a constant sample volume of 0.75 mL. Titration measurements for the determination of association constants were performed using a constant amount of template (0.04 M) titrated with increasing amounts of functional monomer from 1 to 20 equivalents.

T_1 relaxation studies were performed using the inversion-recovery method (supplied by Varian) at 293 K with a relaxation delay $d_1 = 5 \cdot T_1$ (T_{1min}= 1, T_{1max}= 5, t= 0.3 h; d_1 calculated with the longest expected T_1, T_{1max}). The interval between the 180° and the 90° pulses was varied in the range of 0.125-32 s (p_1=180). Sixteen scans were acquired into 32 K data points. The relaxation rates were calculated by a non-linear fitting model using the peak intensities to fit a two-parameter exponential equation available in the program *MestReC 3.3*.

3.3.3 Results and discussion

3.3.3.1 Assessing the role of molecular size, shape, and functionality to the polymer recognition

Besides the template 2,4-D, the structural analogues shown in Figure 35 were investigated in order to assess the role of size, shape, and functionality during the molecular recognition in the synthesized MIP.
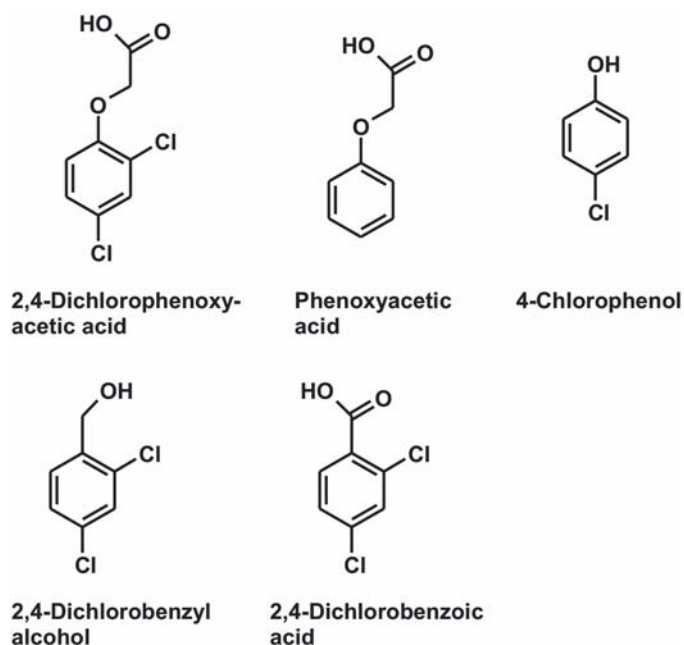
Figure 35 Structure of 2,4-D and structural analogues.

Furthermore, in order to identify the best polymerization conditions, thermal (at 45 ˚C) and UV-polymerization was performed. The resulting block-polymers were characterized as shown in Figure 36. Retention times are summarized in Figure 37. Both imprinted and control polymers showed tailing of the analyte peaks indicating non-specific interaction

with the polymer matrix. Nevertheless, retention times for 2,4-D (chromatogram 1) and 2,4-dichlorobenzoic acid (chromatogram 3) strongly increased from the control to the imprinted polymers, which is characteristic for MIP selectivity.
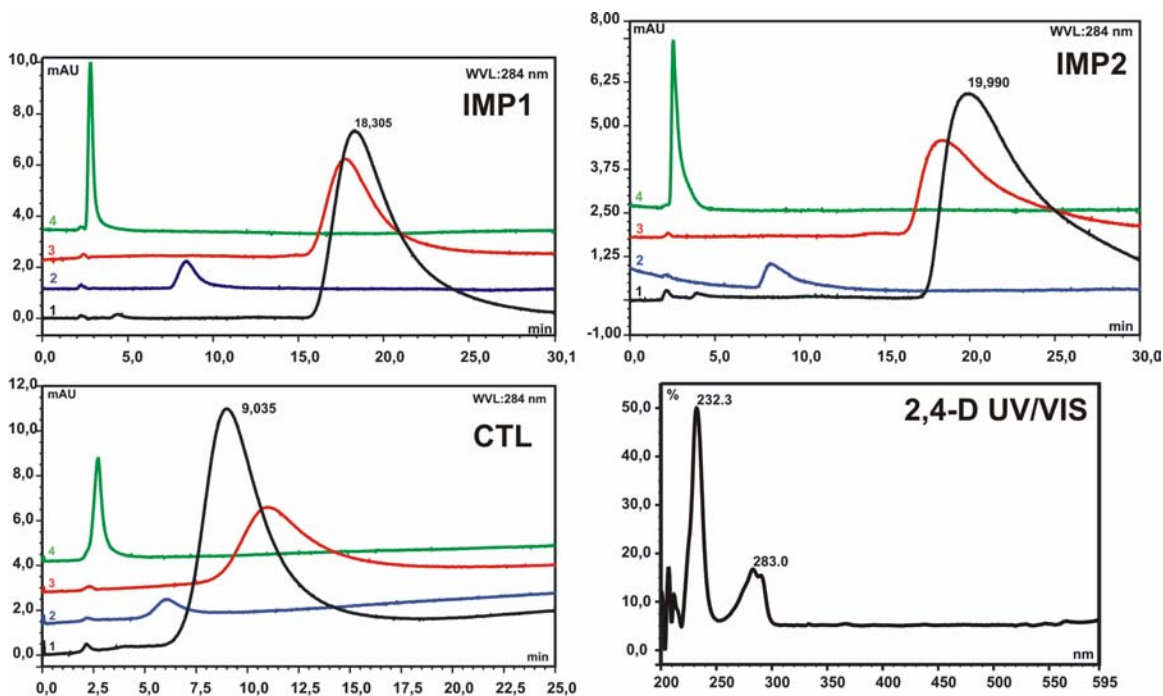
Figure 36 Chromatograms of standard solutions of 0.25 mg/mL of
1) 2,4-dichlorophenoxyacetic acid; 2) phenoxyacetic acid; 3) 2,4-dichlorobenzoic acid; and 4) 2,4-dichlorobenzyl alcohol with the imprinted polymer columns IMP1 (thermal) and IMP2 (UV polymerization) and a control polymer CTL (thermal). Mobile phase: acetonitrile containing 1 % acetic acid at 1 mL/min. Bottom right: UV/VIS spectrum of 2,4-D.

The imprinted polymer IMP2 (UV polymerization) is characterized by a more pronounced tailing compared to IMP1 (thermal polymerization) indicating slightly higher affinity. The temperature at which the polymerization is performed affects the complex stability in the pre-polymerization solution and during polymerization, which in turn has impact on the binding cavity formation. Nevertheless, the overall selectivity and separation behavior towards 2,4-D and the structural analogues used for HPLC characterization was the

same. Furthermore, both the UV and thermal polymers showed a higher BET surface area for the imprinted polymer compared to the control polymer. While the control polymers had approximately the same surface area (121.13 m^2/g for CTL1 and 113.02 m^2/g for CTL2), the thermal polymerization yielded an imprinted polymer with higher surface area compared to the UV polymerization (255.93 m^2/g for IMP1 and 160.15 m^2/g for IMP2). Nevertheless, the difference in surface area does not seem to affect retention properties and selectivity of the MIP. At these conditions, the C_{18} column showed no particular affinity for any of the compounds. 2,4-D and 2,4-dichlorobenzoic acid were strongly retained in IMP1 and IMP2 compared to the control polymer CTL, followed by phenoxyacetic acid (see Figure 37).
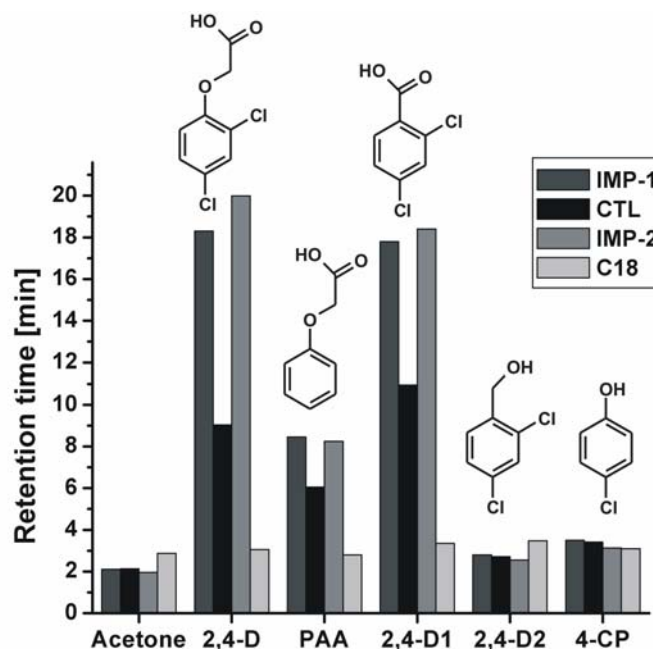
Figure 37 Retention time of 2,4-D and structural analogues phenoxyacetic acid (PAA), 2,4-dichlorobenzoic acid (2,4-D1), 2,4-dichlorobenzyl alcohol (2,4-D2), and 4-chlorophenol (4-CP) in the imprinted (thermal IMP1 vs. UV IMP2 polymerization) and control (CTL) columns (150 mm x 4.6 mm ID), compared to a standard C18 HPLC column (250 mm x 4.6 mm ID). Mobile phase: acetonitrile containing 1 % acetic acid at a flow rate of 1 mL/min.

The imprinted columns showed no difference in retention time for 2,4-dichlorobenzyl alcohol and 4-chlorophenol compared to the control polymer and the C_{18} column. The capacity factors k', separation factors α and the retention index RI were calculated assuming similar retention properties of both control polymers (Table 20).

Table 20 Capacity factors, separation factors, and retention indices of the 2,4-D IMP- and CTL-columns (150 mm x 4.6 mm ID).

2,4-D	k'_{CTL}	k'_{IMP} IMP1	k'_{IMP} IMP2	α_{CTL}	α_{IMP} IMP1	α_{IMP} IMP2	RI (IMP1)	RI (IMP2)
Acetone	--	--	--	--	--	--	--	--
2,4-D	3.22	7.70	9.21	1	1	1	1	1
Phenoxyacetic acid	1.83	3.02	3.21	1.76	2.55	2.87	0.69	0.61
2,4-Dichlorobenzoic acid	4.12	7.46	8.40	0.78	1.03	1.10	0.76	0.71
2,4-Dichlorobenzyl alcohol	0.27	0.33	0.30	12.16	23.33	30.29	0.52	0.40
4-Chlorophenol	0.60	0.66	0.60	5.39	11.60	15.43	0.46	0.35

The imprinted polymer showed significantly enhanced affinity for 2,4-dichlorophenoxyacetic acid, 2,4-dichlorobenzoic acid, and phenoxyacetic acid in contrast to the control polymer. This effect was most pronounced for the template 2,4-D (capacity factor k'_{IMP}= 9.21 vs. k'_{CTL}= 3.22) and for 2,4-dichlorobenzoic acid (k'_{IMP}= 8.40 vs. k'_{CTL}= 4.12). The results are summarized in Figure 38 with annotation of the retention index for each investigated analyte. Based on the results obtained with 2,4-D and its structural analogues during HPLC experiments, a first assessment of the importance of shape, size and functionality on MIP recognition is enabled.
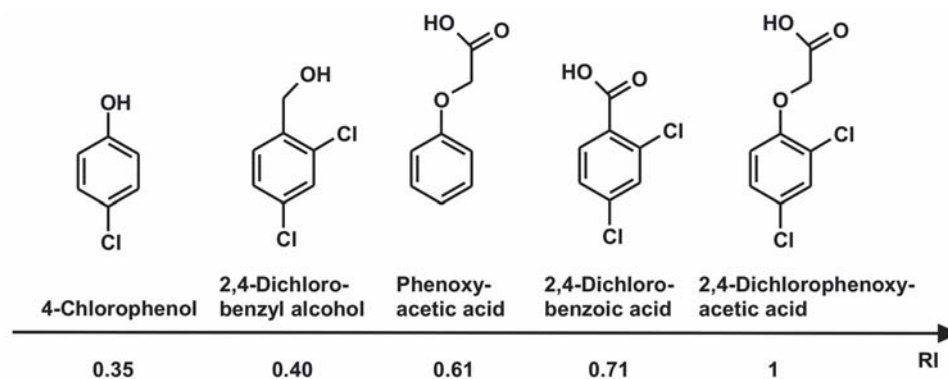
Figure 38 Affinity of the 2,4-D imprinted polymer towards structural analogues of 2,4-D. RI: retention index given as ratio of separation factors in control vs. imprinted polymer.

4-Chlorophenol had the lowest retention index and also represents the smallest molecule in this study. As the alcohol group did not allow for specific binding, molecular size is an important factor in MIP recognition. 2,4-Dichlorobenzyl alcohol has a longer side chain by one $-CH_2-$ unit, which is considered responsible for the slight increase in retention index. The carboxylic functionality is accountable for selective recognition, since – besides 2,4-D – the compounds with a carboxylic group exhibited distinctly higher affinities compared to analytes with an alcohol group. Surprisingly, phenoxyacetic acid is characterized by a lower RI than 2,4-dichlorobenzoic acid. Hence, the two -Cl groups in ortho- and para-position to the side chain may also play a role during recognition. The two –Cl groups are also present in both 2,4-dichlorobenzoic acid and 2,4-dichlorophenoxyacetic acid contributing to the overall polarity of the ring, which may have an effect on π–π stacking of the aromatic moieties. Nevertheless, if the main interacting functional group (carbonyl group) is absent, such as in 2,4-dichlorobenzyl alcohol the contribution of the –Cl groups to molecular recognition is minor as confirmed by the comparatively low RI values. Since phenoxyacetic acid has a lower RI than 2,4-dichlorobenzoic acid in the MIP, apparently the aromatic ring is the second main site of interaction involved in the re-binding process. Therefore, π-π stacking should be a

main effect contributing to selective template recognition besides hydrogen bonding or ionic interaction via the carboxylic group.

Consequently, the obtained HPLC results investigating a series of structural analogues suggest a 3-point interaction within the high affinity binding sites. Further evidence for these findings will be provided in the following by MIR and NMR studies of the 2,4-D/4-VP pre-polymerization solution.

3.3.3.2 MIR studies of pre-polymerization mixtures

An IR titration approach was established to identify and monitor complex formation in the pre-polymerization solution and to calculate apparent macroscopic binding constants. The mid-infrared spectra of hydrogen-bond complexes between 2,4-D and 4-VP as well as 2,4-D and MAA were investigated and the spectroscopic features elucidated in detail. Furthermore, the influence of the cross-linker ethyleneglycol dimethacrylate on the complex formation was studied.

3.3.3.2.1 Dimerization of 2,4-dichlorophenoxyacetic acid

The dimerization of 2,4-D was studied in CCl_4, $CHCl_3$, and $CDCl_3$ considering the following equations:

$$2,4-D + 4-VP \leftrightarrow Complex(2,4-D/4-VP) , \quad K_b = \frac{[Complex]}{[2,4-D][4-VP]} \quad (1)$$

$$2,4-D + 2,4-D \leftrightarrow Dimer(2,4-D) , \quad K_{dim} = \frac{[Dimer(2,4-D)]}{[2,4-D]^2} \quad (2)$$
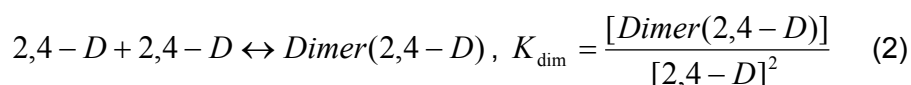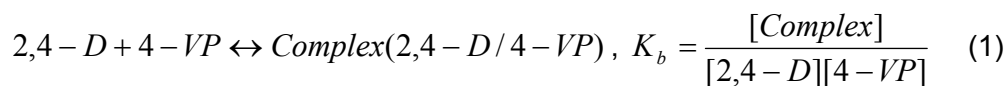
With $[2,4-D]_0 = [2,4-D]_{free} + [Complex] + 2[Dimer(2,4-D)]$ (3)

Both dimers and chains of the carboxylic acids may be possible. In order to investigate K_{dim}, solutions of increasing concentration of 2,4-D in CCl_4 have been studied within the solubility range of 2,4-D in carbon tetrachloride (see Figure 39).
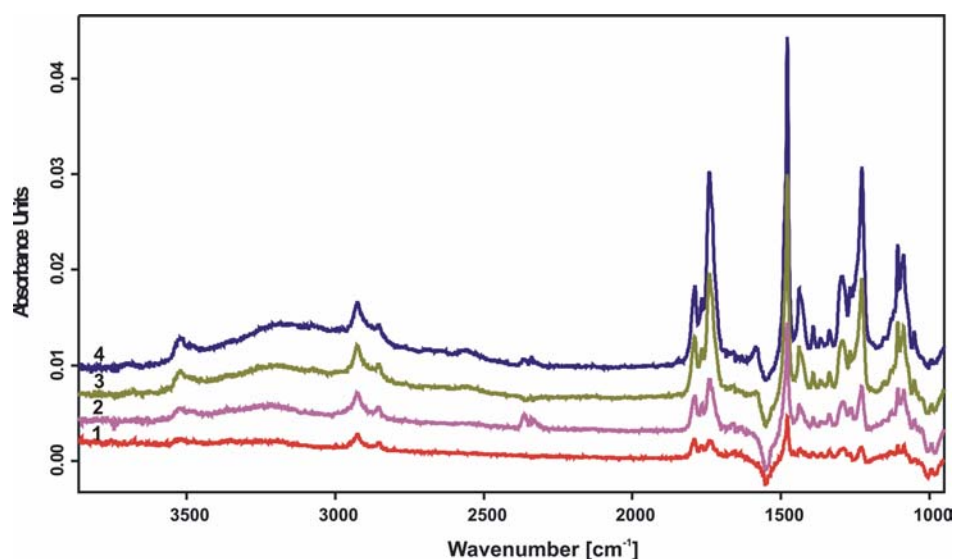
Figure 39 Absorbance MIR spectra (200 μm spacer, NaCl windows, in CCl_4) of 2,4-dichlorophenoxyacetic acid; 1) $0.5 \cdot 10^{-3}$ M; 2) $1 \cdot 10^{-3}$ M; 3) $2 \cdot 10^{-3}$ M; 4) $3 \cdot 10^{-3}$ M.

Characteristic for the carboxylic acid group are:

- OH stretch band (3400 cm^{-1})

- C=O stretch band (1740 cm^{-1})

- C-O stretch bands (1315-1280 cm^{-1})

- OH in-plane bend bands (1440-1395 cm^{-1})

- OH out-of-plane wag bands (960-875 cm^{-1})

These bands are sensitive to the H-bonding state of the COOH-group, which can exist as carboxylic acid dimer, unbonded monomer, and as H-bonded polymeric form. The H-bonded dimer is the most common form. When the two monomer compounds of the dimer vibrate out-of-phase, the vibration is IR active, while the in-phase vibration is Raman-active. If further H-bond donor or acceptor groups are introduced by adding the template, other variations in H-bondings may occur.

The 2,4-D aromatic ether aryl-O-CH$_2$ shows two strong IR bands at 1310-1210 cm^{-1} from the aryl-O and at 1050-1010 cm^{-1} from the O-CH$_2$. The aryl-O band is a coupling of different ring vibrations and stretching such as C-O-C out-of-phase stretching, aromatic ring vibrations, and aryl-O stretch making the interpretation of the spectra comparatively difficult. The carboxylic acid C=O stretch is a strong band occurring at 1740 cm^{-1}. The carboxylic OH stretching band is strong and very broad, and centered around 3400 cm^{-1}. In dilute CCl$_4$ solution, the band resulting from the monomeric OH stretch absorption can be located around 3550-3500 cm^{-1}. The monomeric OH stretch is only a weak sharp band since the dimer is the predominant form. Other carboxylic acid dimer bands are difficult to identify due to the complexity of the 2, 4-D IR spectra.

In addition, substituted benzenes show substituent-sensitive bands: the meta-Cl benzene absorbs at 1078-1074 cm^{-1} and 1073-1065 cm^{-1}. The C-H stretching vibrations of the substituted benzene ring result in bands in the 3100-3000 cm^{-1} range, which are superimposed by the broad O-H stretch band of the dimeric acid. Other C-H bands such as C-H in-plane bending (1600-1000 cm^{-1}) and C-H out-of-plane bending ('wag', at 1000-700 cm^{-1}) are difficult to identify. Various C-C vibrations of the aromatic ring are also coupling with the C-H bending modes.

The variation of the absorption intensities of the bands corresponding to the free and complexed species versus concentration were investigated to determine the degree of

association and the equilibrium constant of the dimerization reaction [170]. Both the monomeric and dimeric OH bands increase in intensity with increasing 2,4-D concentration (see Figure 40).
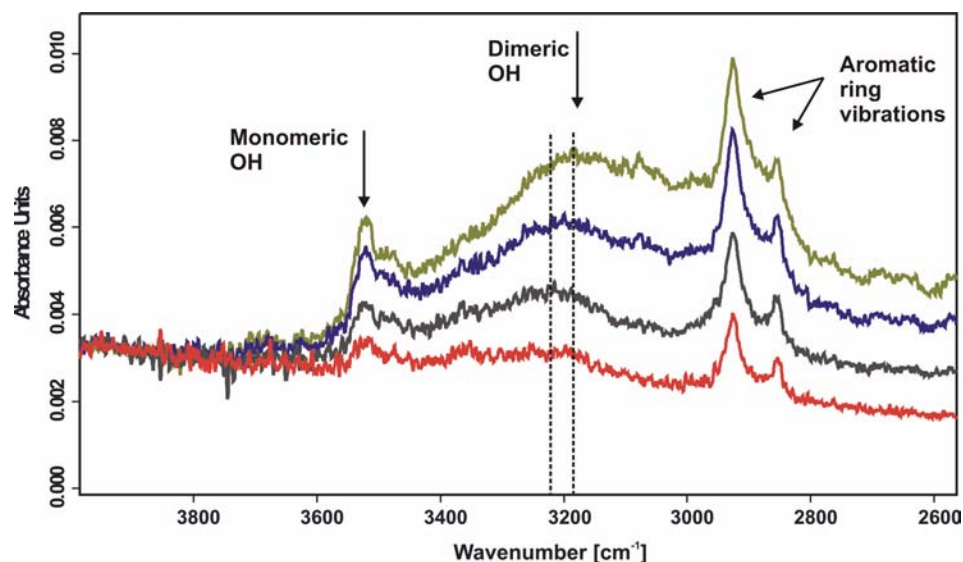
Figure 40 Absorbance MIR spectra (200 μm spacer, NaCl windows, in CCl$_4$) of 2,4-dichlorophenoxyacetic acid. From bottom to top: $0.5 \cdot 10^{-3}$ M; $1 \cdot 10^{-3}$ M; $2 \cdot 10^{-3}$ M; and $3 \cdot 10^{-3}$ M 2,4-D.

In dilute CCl$_4$ solution, the band resulting from the monomeric OH stretch absorption can be located at 3521.7 cm^{-1}. A red shift of the dimeric OH band was also observed. The band intensity of the monomeric OH band was plotted against the 2,4-D concentration as shown in Figure 41.
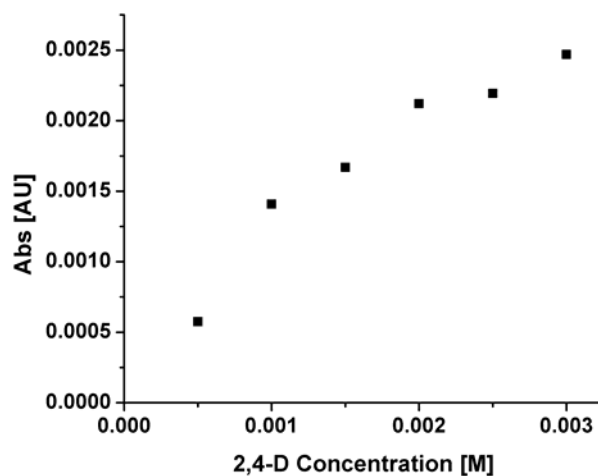
Figure 41 MIR absorbance of the monomeric ν(OH) stretch band of 2,4-D at 3521.7 cm^{-1} vs. 2,4-D concentration in CCl$_4$ solution.

It was not possible to determine a dimeric OH band below the concentration of $1\cdot10^{-3}$ M. This may indicate the presence of predominantly monomeric species at lower concentrations within the analyzed concentration range. Furthermore, a band of medium intensity at 873 cm^{-1} was attributed to the dimeric OH$\cdots$O out-of-plane wag as shown in Figure 42.
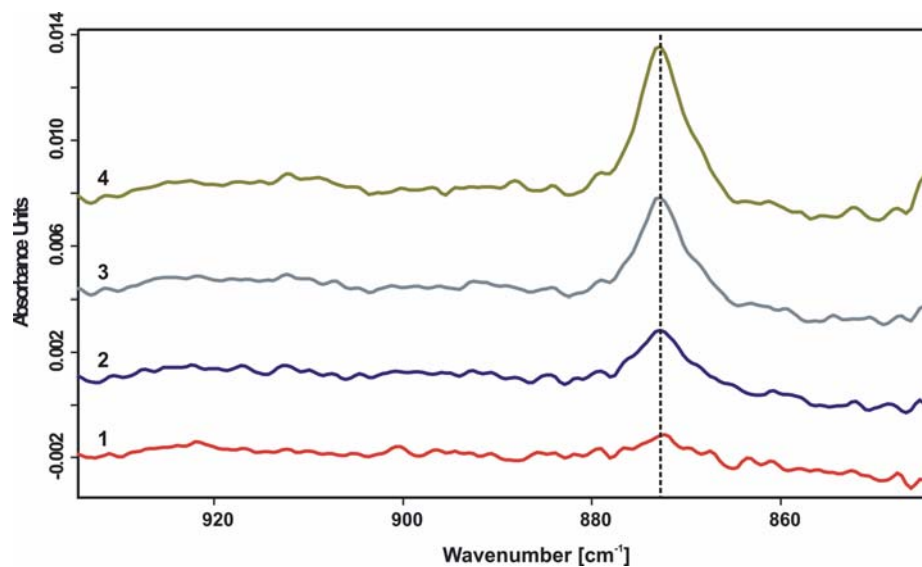
Figure 42 Transmission MIR spectra (200 μm spacer, NaCl windows, in CCl_4) of 2,4-dichlorophenoxyacetic acid in the spectral range 930-850 cm^{-1}. The band at 873 cm^{-1} is attributed to the dimeric OH$\cdots$O out-of-plane wag. From bottom to top: 2,4-D at $0.5\cdot10^{-3}$ M; $1\cdot10^{-3}$ M; $2\cdot10^{-3}$ M; and $3\cdot10^{-3}$ M.

The absorbance at peak maximum of the band at 873 cm^{-1} was plotted against the 2,4-D concentration (Figure 43) and revealed a linear increase vs. 2,4-D concentration.
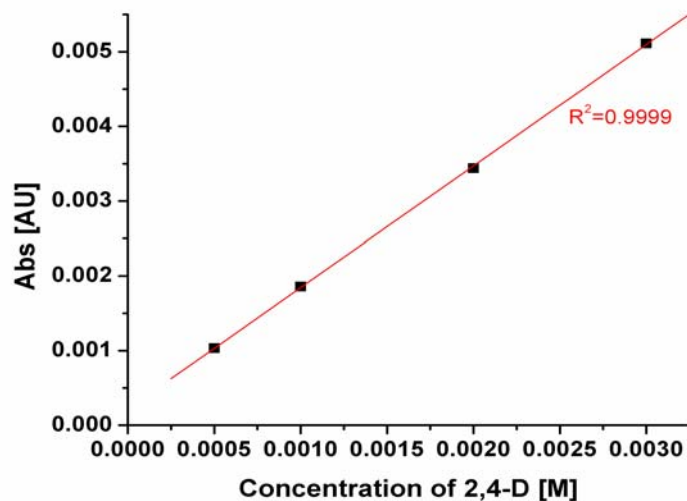
Figure 43 MIR absorbance of the 2,4-D band attributed to the dimeric OH$\cdots$O out-of-plane wag vs. 2,4-D concentration in CCl_4 solution.

Also, the absorbance of the asymmetric C=O stretch corresponding to the dimeric form at 1740.8 cm^{-1} was monitored at increasing 2,4-D concentration. The C=O dimeric band overlaps with the much smaller bands at 1791 and 1767 cm^{-1} (left shoulders, see Figure 39). A Levenberg-Marquardt algorithm was therefore applied for curve fitting of the spectral region 1840-1680 cm^{-1} to confirm the linearity between absorption intensity and 2,4-D concentration. The Levenberg-Marquardt algorithm [171,172] is available from the Bruker OPUS software (Bruker Optics Inc., Billerica, MA) for model optimization. This algorithm is based on the least squares method and the quadratic deviation $X^2(S)$ for the deviation between measured and calculated curve is defined as

$$\mathbf{X}^2(S) = \sum_{i=1}^{N}[Y_G - y(x;S)]^2 \qquad (4)$$

with S as the set of curve parameters, x the frequency, and Y_G the measured data. $X^2(S)$ is minimized by iteration.

While the C=O monomeric stretch absorbance may not further increase with increasing 2,4-D concentration (at c > 3·10[-3] M), the absorbance of the C=O dimeric band linearly increases at concentrations of 2,4-D ≥ 0.5·10[-3] M. The C=O dimeric band, which is a band of strong intensity compared to the weak C=O monomeric band, is present – even if relatively weak - at low concentrations of 2,4-D and linearly increases with higher 2,4-D concentrations indicating the presence of dimerized 2,4-D in the analyzed concentration range.

The dimerization of 2,4-D was therefore calculated according to the following equations using the absorbance of the monomeric OH stretch band of 2,4-D:

$$M + M \leftrightarrow D \quad K_{\text{dim}} = \frac{[D]}{[M]^2} \qquad (5)$$

With   M: 2,4-D monomer

D: 2,4-D dimer.

If A_0 is the total amount of 2,4-D: $\qquad [A_0] = 2[D] + [M]$

$$D = \frac{[A_0] - [M]}{2}$$

Then $\quad K_{\text{dim}} = \dfrac{[A_0] - [M]}{2[M]^2} \quad$ or $\quad K_D = \dfrac{2[M]^2}{[A_0] - [M]} \quad$ and with $\quad [M] = \dfrac{Abs(M)}{\varepsilon \cdot d} \qquad (6)$

ε: molar extinction coefficient [L mol^{-1} cm^{-1}]

d: path length [cm].

Follows: $\qquad [A_0] \cdot K_D - \dfrac{Abs(M)}{\varepsilon \cdot d} \cdot K_D = 2 \cdot \dfrac{Abs(M)^2}{\varepsilon^2 d^2} \qquad (7)$

$$Abs(M) = \frac{[A_0] \cdot K_D \cdot \varepsilon^2 d^2}{2 \cdot Abs(M)} - \frac{K_D \cdot \varepsilon \cdot d}{2} \qquad (8)$$

Since the OH vibration is most sensitive to changes, the absorbance (Abs) of the monomeric OH band at 3521.7 cm^{-1} was plotted against $[A_0]$/Abs according to equation 4 (Figure 44).
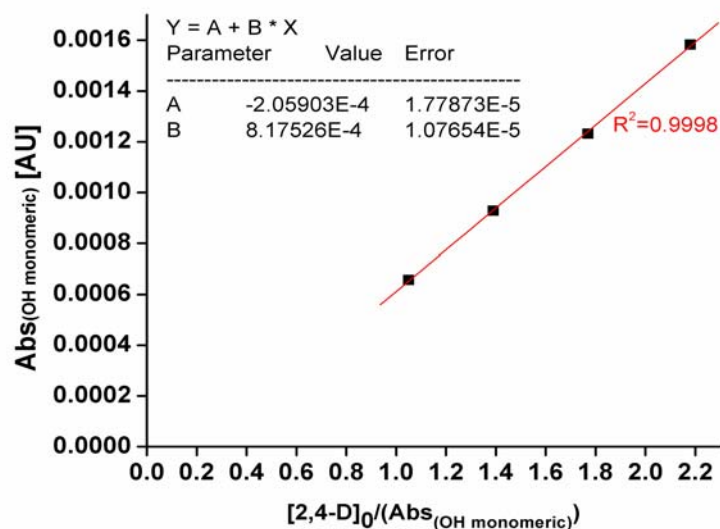
Figure 44 Absorbance of the monomeric OH stretch band of 2,4-D plotted against the initial 2,4-D concentration divided by the absorbance of the monomeric OH stretch band according to equation (4).

From the slopes and intercept [173] a K_{dim} value of 8943 M^{-1} ± 17 % in CCl_4 was obtained from three repeated measurement series.

Since NMR studies of the 2,4-D system in pre-polymerization solution were mainly performed in $CDCl_3$, and dimerization as well as binding constants strongly vary according to the solvent used, the behavior of 2,4-D was also investigated in $CDCl_3$. Since the monomeric $\nu(OH)$ band is located between two regions where the solvent $CHCl_3$ strongly absorbs, deuterated chloroform furthermore allowed shifting the interfering absorbing C-H stretch of chloroform at 3021 cm^{-1} to a C-D stretch at 2254 cm^{-1}. Spectra of 2,4-D at increasing concentrations in $CDCl_3$ are given in Figure 45 for the spectral region 4000-2400 cm^{-1}.
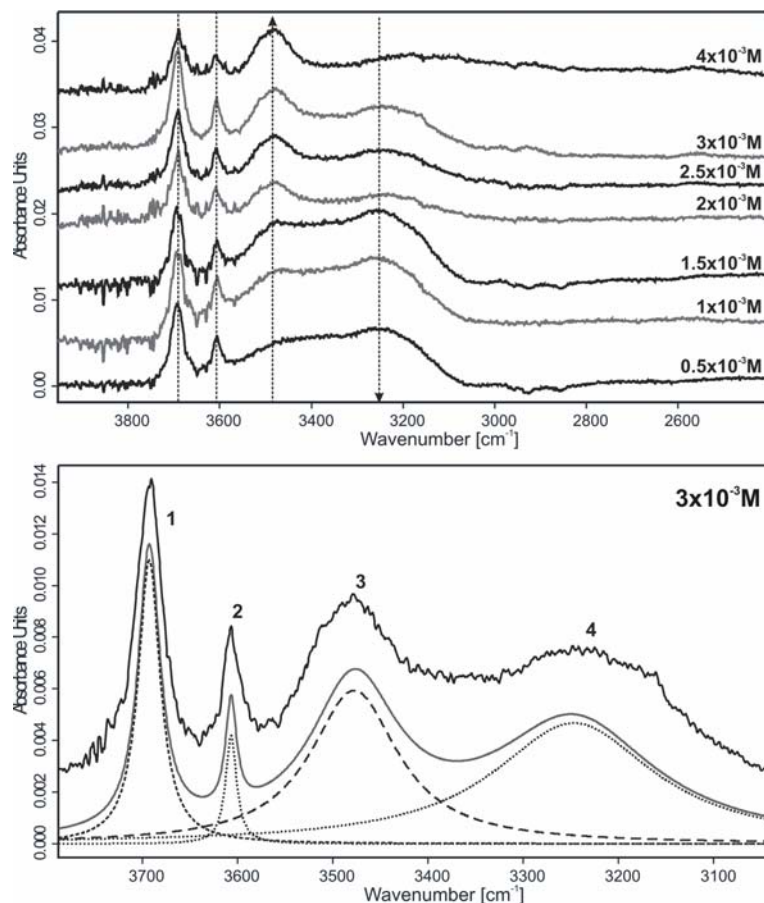
Figure 45 MIR spectra of 2,4-D (from 0.5 to $4 \cdot 10^{-3}$ M) in $CDCl_3$ (top) and band deconvoluted spectrum of 2,4-D at $3 \cdot 10^{-3}$ M (bottom).

Performing curve fitting in the spectral region 3750-3050 cm^{-1} (model FIT.419, Levenberg-Marquardt algorithm, Lorentzian peak shape) resulted in peak deconvolution into four bands. The two broad bands 3 and 4 were attributed to $\nu(OH)$ bound (dimers, multimers) and are strongly affected by increasing the 2,4-D concentration as evident in Figure 45 (top). Bands 1 and 2 did not show any changes in absorbance upon increase of the 2,4-D concentration and may be attributed to traces of $CHCl_3$ in $CDCl_3$ (99.9 atom % D) as shown in Figure 46 thus preventing quantitative analysis of the overlapping $\nu(OH)$ monomeric stretch.
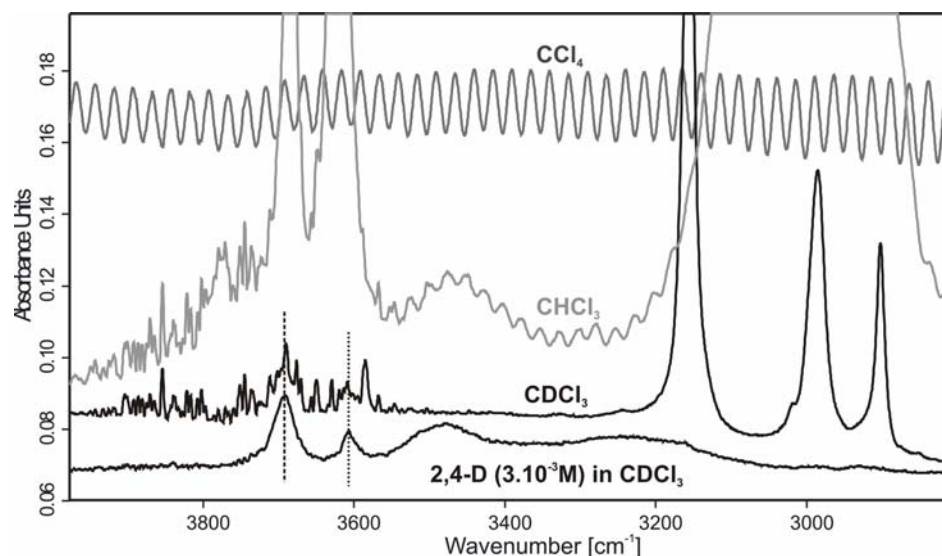
Figure 46 Transmission MIR spectra (200 μm spacer, NaCl windows, in CCl_4) of 2,4-D ($3 \cdot 10^{-3}$ M) in $CDCl_3$ (from bottom), $CDCl_3$, $CHCl_3$, and CCl_4 in the spectral range 4000-2800 cm^{-1}.

Figure 46 shows the absorbance of 2,4-D (3×10^{-3} M) in $CDCl_3$ (bottom spectrum) as well as the $CDCl_3$, $CHCl_3$, and CCl_4 absorbance in comparison. Carbon tetrachloride is definitely the solvent most suited for MIR studies of complex formation in solution without any absorbance in the spectral regions of interest. Only interference fringes are evident, which result from the IR radiation reflected off the thin film cell windows (spacer: 200 μm).

3.3.3.2.2 Interaction of 2,4-dichlorophenoxyacetic acid and MAA in the pre-polymerization solution

The MIR spectrum with band assignment of methacrylic acid (MAA) is shown in Figure 47.
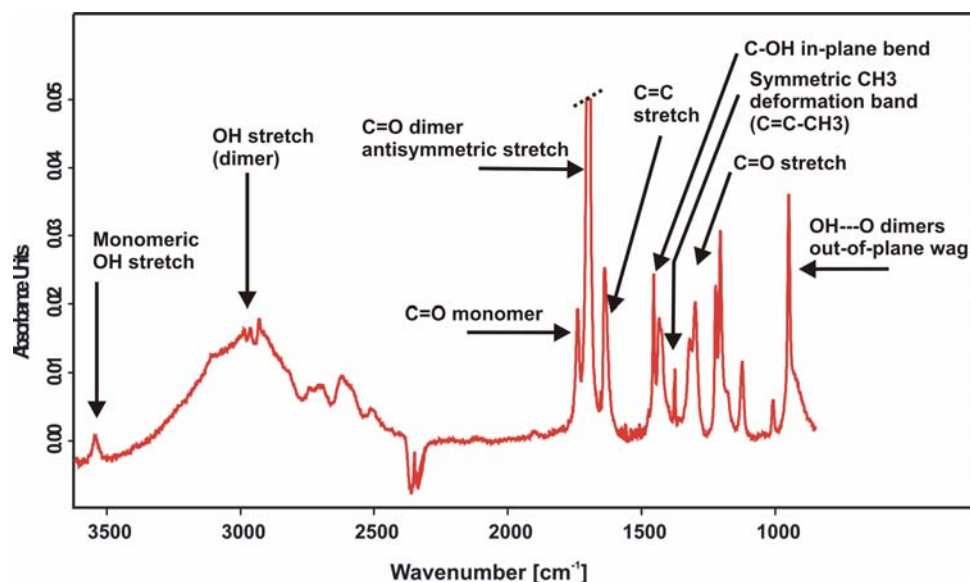
Figure 47 MIR spectrum of methacrylic acid ($8\cdot10^{-3}$ M in CCl_4). Transmission cell, 200 μm spacer.

The carboxylic dimer has a strong band at 1700 cm^{-1}. The dimers also show a band of medium intensity around 960-875 cm^{-1} resulting from the in-phase out-of-plane OH$^{\cdots}$H wag. The monomer C=O band is weak and located at 1739 cm^{-1}. Band clusters between 1315-1200 cm^{-1} are also attributed to the COOH group. The C-O-H in-plane deformation can be located at 1440-1395 cm^{-1}. The C=C stretching frequency of the alkyl-substituted ethylene occurs at 1636 cm^{-1}. It is a medium-strong IR band for 1,1-disubstituted alkenes depending on the local symmetry of the C=C group [174]. In C=C-CH$_3$, the symmetric CH$_3$ deformation band appears near 1375 cm^{-1} and has a medium intensity.

The complex formation of the two acids 2,4-dichlorophenoxyacetic acid (2,4-D) and methacrylic acid (MAA) was spectroscopically monitored and the changes of the bands sensitive to the H-bonding state of the COOH-groups were investigated The asymmetrical C=O band is the strongest in the IR spectra. The carboxylic dimers of 2,4-D and MAA respectively have a strong band around 1740-1660 cm^{-1}. The dimers also show a band of medium intensity at 960-875 cm^{-1} resulting from the in-phase out-of-

plane OH···H wag. In dilute CCl_4 solution, the band assigned to monomeric OH stretch absorption can be determined around 3550-3500 cm^{-1}. It is only a weak sharp band since the dimer is the predominant form. The monomer C=O band of MAA is weak compared to the dimeric C=O and can be seen at 1739 cm^{-1} (Figure 48).
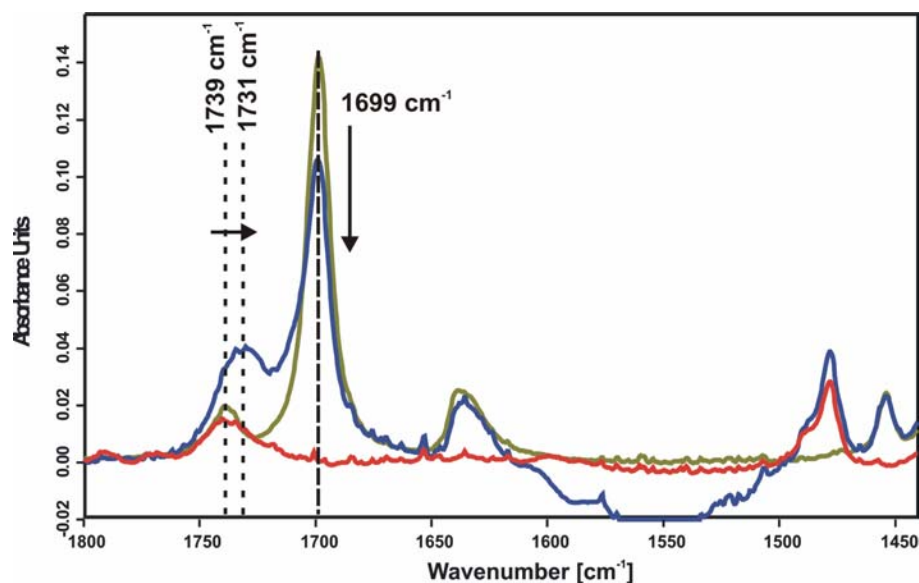
Figure 48 IR spectra of MAA, 2, 4-D, and a mixture of 2, 4-D and MAA. Green: 2, 4-D at $2 \cdot 10^{-3}$ M; red: MAA at $8 \cdot 10^{-3}$ M; blue: 2, 4-D at $4 \cdot 10^{-3}$ M and MAA at $8 \cdot 10^{-3}$ M. Spectral region: 1800-1600 cm^{-1}.

Compared to the spectra of 2, 4-D (2×10^{-3} M) or MAA (8×10^{-3} M), changes in the spectral regions from 1760-1660 cm^{-1} and from 3800-2800 cm^{-1} were observed in the solution containing both 2, 4-D (4×10^{-3} M) and MAA (8×10^{-3} M) (see Figure 48). A band shift in the 2,4-D/MAA mixture from 1739 cm^{-1} to 1731 cm^{-1} was observed. The band may correspond to a C=O band for the hydrogen bonded but not dimerized carboxylic acid MAA. Furthermore, a decrease in intensity is observed for the band at 1699 cm^{-1} corresponding to the antisymmetrical C=O stretch of the (dominating) dimer form of the carboxylic acid MAA. This may indicate a decrease of the MAA dimeric form due to complexation with 2, 4-D.

An increase in solubility of 2,4-D with the presence of MAA also indicates complex formation. When titrating from 100 % 2,4-D ($2x10^{-3}$ M) to 100 % MAA ($2x10^{-3}$ M), monitoring of the C=O monomeric band of MAA allows following a peak shift shown in Figure 49.
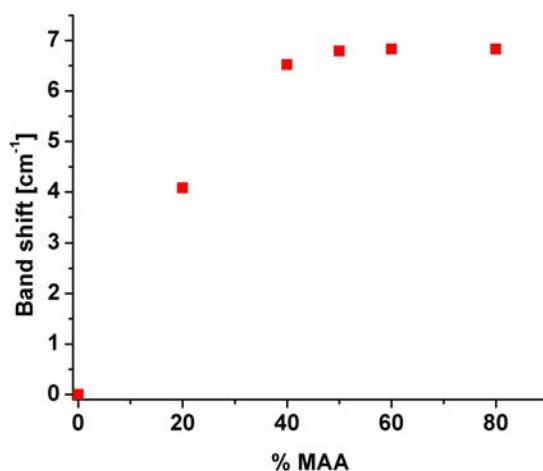
Figure 49 IR shift of MAA C=O band at 1739 cm^{-1}. Method of continuous variation with stock solutions of $2 \cdot 10^{-3}$ M in CCl$_4$.

The band shift of the C=O band during the titration with MAA reaches a maximum at 50% corresponding to the fully complexed template and functional monomer indicating a 1:1 complex formation between 2,4-D and MAA.

When increasing the concentration of 2,4-D from $2x10^{-3}$ M to a maximum of $8x10^{-3}$ M while keeping the concentration of MAA constant at $8x10^{-3}$ M and titrating with increasing amounts of 2,4-D (from $1x10^{-3}$ M to $8x10^{-3}$ M), a more complex spectrum with four bands develops as shown in Figure 50. The curves shown in Figure 50 also have a small superimposition of a periodic structure resulting from interference fringes.
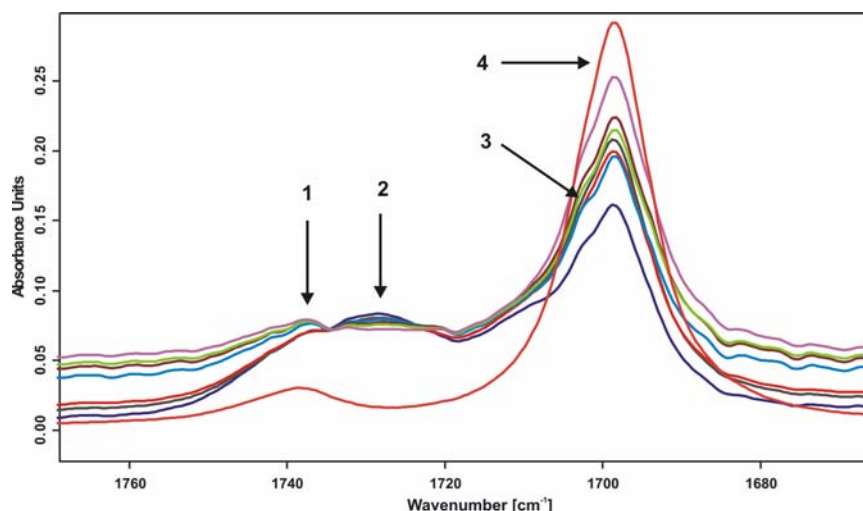
Figure 50 IR titration of MAA ($8 \cdot 10^{-3}$ M) with 2,4-D in the range of 0 to $8 \cdot 10^{-3}$ M. Spectral range of the C=O stretching bands.

The bottom spectrum in Figure 50 corresponds to neat MAA at a concentration of 8×10^{-3} M in CCl_4. Peak #4 (1699 cm^{-1}) can therefore be identified as the dimeric C=O band of MAA. The C=O band from 2,4-D as well as the monomeric C=O band from MAA are both located around 1739 cm^{-1} and are therefore entirely overlapping in a mixture of 2,4-D and MAA (peak #1). Due to complex formation, a broadening of the C=O dimeric band of MAA can be observed along with a decrease of band intensity. Band deconvolution of the bands in the spectral region 1780-1660 cm^{-1} was performed since the carboxylic bands of the two acids strongly overlap (Figure 51).
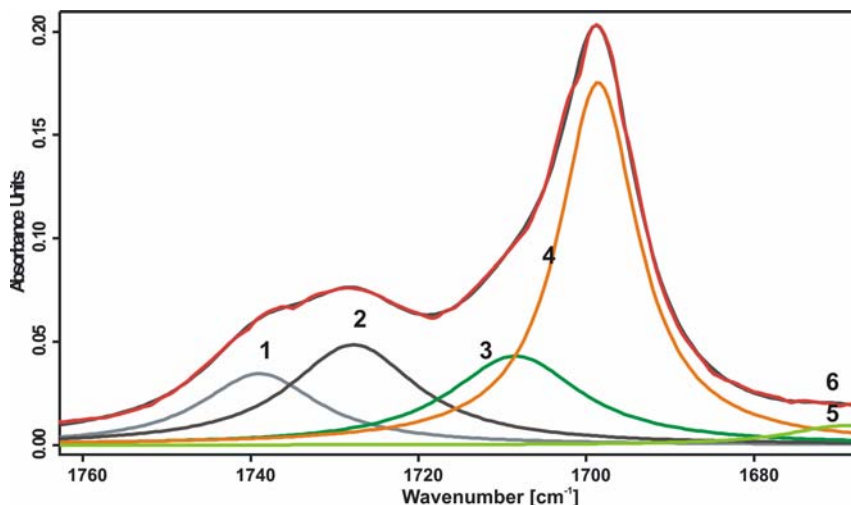
Figure 51 Curve fitting in the spectral region 1780-1660 cm^{-1} with a Levenberg-Marquardt algorithm with a residual RMS error of 0.00135. The fitted spectrum corresponds to a mixture of 2,4-D (6·10^{-3} M) and MAA (8·10^{-3} M). Spectrum #6 shows the result of the curve fitting.

The peak fitting was performed with a Levenberg-Marquardt algorithm. Since the spectral region in which the peak fitting was performed has multiple peaks due to the carboxylic acids and since total overlapping of bands is expected, the fitted model will only be used to identify spectral trends during the titration of MAA with 2,4-D. Peak #4 (1699 cm^{-1}) is the dimeric C=O band of MAA. The C=O band from 2,4-D as well as the monomeric C=O band from MAA are both located around 1739 cm^{-1} and are totally overlapping in a mixture of 2,4-D and MAA (peak #1). If the carboxyl C=O is H-bonded but not dimerized, this is evident at 1730-1705 cm^{-1} (peaks #2 and/or #3). While peak #3 only slightly increases in intensity during the titration, peak #2 strongly increases, probably due to complex formation. The increase in intensity of peak #1 during the titration is due to the increase in 2,4-D concentration. Peak #4 broadens and strongly decreases in intensity due to a decrease in the MAA dimeric C=O band resulting from complex formation. Furthermore, peaks #2 and #3 are slightly blue shifted. The

147

carboxylic C=O bands can be qualitatively attributed to MAA dimeric C=O, monomeric C=O, and complexed C=O bands.

The OH group is more sensitive to changes in the group environment than the C=O group. Nevertheless, changes in the bands corresponding to O-H are difficult to follow in this case. The spectra are only characterized by a broadening of the O-H band during the titration. A MAA carboxylic acid dimeric band of medium intensity is located at 949.5 cm^{-1} and corresponds to the OH···O out-of-plane wag. A slight hypsochromic shift (Figure 52) is evident along with a decrease in band intensity upon addition of 2,4-D.
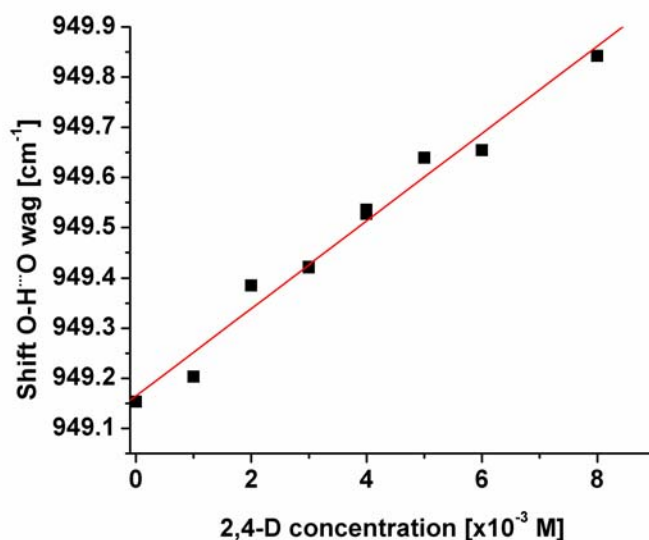
Figure 52 Shift of the OH···O out-of-plane wag of MAA during the titration with 2,4-D.

Based on the spectral changes occurring during the titration of 2,4-D or MAA respectively, it is evident that 2,4-D and MAA interact and that complex formation in CCl_4 due to hydrogen bonding of the carboxylic groups is monitored. Nevertheless, due to strongly overlapping absorption features corresponding to the carboxylic groups of the

two acids, and due to the low solubility of 2,4-D in CCl_4, it was not possible to quantitatively determine the extent of the complexation.

3.3.3.2.3 Interaction of 2,4-dichlorophenoxyacetic acid and 4-VP in the pre-polymerization solution

The IR spectrum of 4-VP (pure, transmission cell, 50 μm spacer) is shown in Figure 53 along with a detailed band assignment.
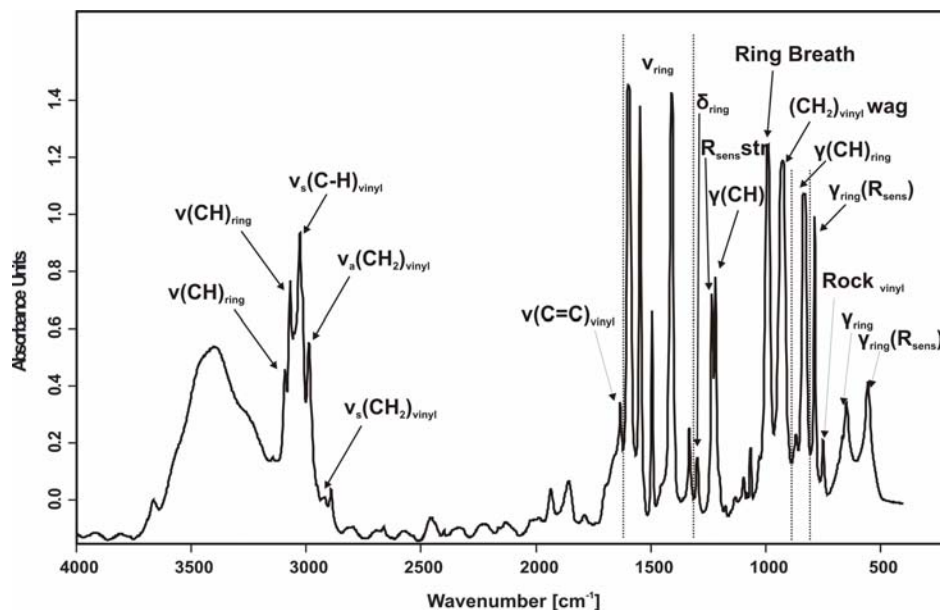
Figure 53 IR spectrum of 4-VP at 4000-400 cm^{-1} (transmission cell, NaCl windows, 50 mm spacer).

The six-membered pyridine ring gives rise to many benzene-like absorption features such as aryl-type C-H stretch bands in the 3100-3000 cm^{-1} region. According to literature [174], the C=N- stretching mode of e.g. methyleneimine ($H_2C=NH$) occurs at 1638 cm^{-1} and a red shift occurs when the C=N group is included as part of a ring system. For

pyrrolines, the C=N stretching occurs at 1653-1613 cm^{-1} in CCl$_4$ and further red shifts occur if the ring strain increases. The C=N stretching mode of 4-VP occurs at 1597 cm^{-1}. In a mixture of 2,4-D and 4-VP, the protonated carboxyl group is characterized by two main vibrational features, which are the O–H stretch (ν_{OH}) at 3251 cm^{-1} and the C=O stretch (ν_{COOH}) at 1739 cm^{-1}. The spectra of 2,4-D complexed with 4-VP are characterized by broad ν(C=O) and ν(OH) bands. Furthermore, the C=O stretching vibration at 1739 cm^{-1} broadens after addition of 4-VP. Additionally, the spectra of the complexes show two characteristic ν(OH) stretching bands of medium intensity centred around 2495 cm^{-1} and 1895 cm^{-1} resulting from self-association of 2,4-D and 4-VP together with a strong decrease of the broad ν(OH) at 3251 cm^{-1}. Furthermore, no absorption features corresponding to the deprotonated carboxylate group ν(COO$^-$) could be detected indicating that the complex is of type A-H$^{...}$B. The governing interaction results from self-association of 2,4-D and 4-VP in a 1:1 ratio via intermolecular hydrogen bonding [175]. In comparison, Barrow showed that the infrared spectra of 1:1 reaction products of acids of intermediate strength with pyridine result from a simple hydrogen bonded complex in tautomeric equilibrium with an ion-pair species, rather than a single resonating species [176]. In contrast, weak acids only form non-proton-transferred hydrogen bonded species. Also, it has been reported in literature that benzoic acid (pK$_a$ of 4.2) and 2,4-dichlorobenzoic acid (pK$_a$ of 2.68) can yield H-bonded complexes with pyridine derivatives [175]. The pK$_a$ of 2,4-D is located in between these values at 2.87 and will therefore be able to form a complex with 4-VP.

The spectral characteristics of 4-VP reveal distinct changes upon addition of 2,4-D (see Figure 54A).
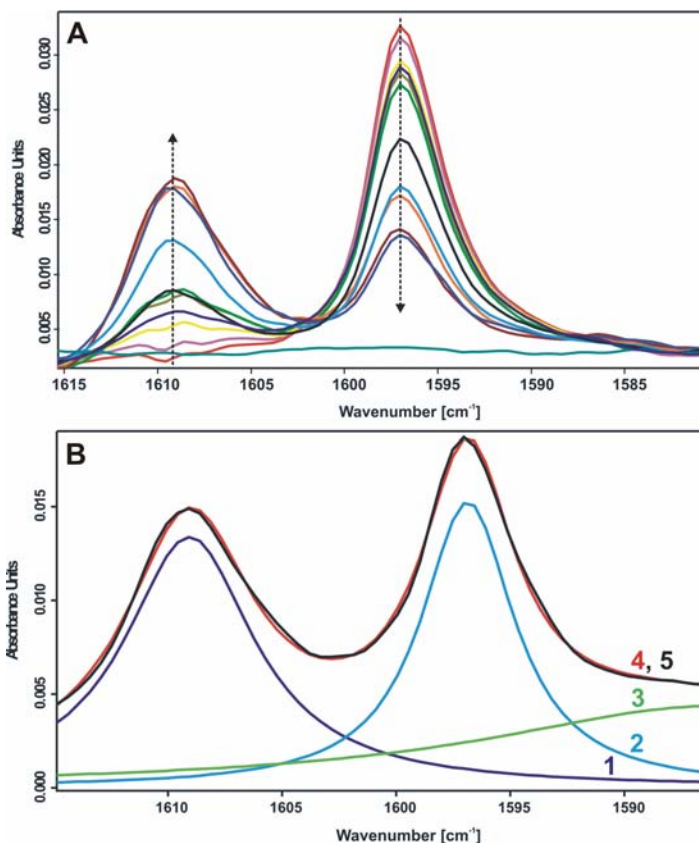
Figure 54 IR titration study of 2,4-D/4-VP mixture. A: Spectral region 1615-1585 cm^{-1}. Titration of 4-VP ($2 \cdot 10^{-3}$ M) with 2,4-D (concentration range 0 to $4 \cdot 10^{-3}$ M). Bands of free (1597 cm^{-1}) and complexed (1609 cm^{-1}) 4-VP in CCl$_4$. B: Levenberg-Marquardt curve fitting of a spectrum with a three peak model with a residual RMS error of 0.000215; 4: original spectrum; 1, 2, 3: model resolved peaks; 5: sum of resolved peaks.

The IR spectrum of the free 4-VP moiety exhibits an intense band at 1597 cm^{-1} resulting from the ν(C=N) mode. When compared to the spectra of free 4-VP, the 2,4-D/4-VP complexes show hypsochromically shifted new bands within the ν(C=N) mode. The peaks at 1597 cm^{-1} and 1609 cm^{-1} were assigned to monomeric 4-VP and hydrogen-bonded 4-VP, respectively. This shift strongly suggests the formation of intermolecular H-bonding between the carboxylic group of 2,4-D and the nitrogen of the 4-vinylpyridine ring. Furthermore, the intensity of the absorption at 1597 cm^{-1} decreases with increasing complex formation. However, it is also possible that the C=C and the C=N stretching

151

modes couple with each other since their resonance frequencies are in close range. In order to confirm the nature of the new band observed at 1609 cm^{-1}, the measurements were performed by adding increasing amounts of acetic acid to 4-VP in analogy to the measurements performed with the system 2,4-D/4-VP by replacing the acid 2,4-D with acetic acid. Since the same effect was observed due to complexation, it can be concluded that the ring heteroatom in 4-VP is the interaction site of 4-VP involved in hydrogen-bonded complex formation. Furthermore, H-bonding interaction was also confirmed by titrations of 4-VP with methanol. Hence, 4-VP forms complexes of the type N$\cdots$H-O resulting from self-association in a 1:1 ratio via intermolecular hydrogen bonding. The complex formation of 2,4-D/4-VP resulted in sufficient changes of the corresponding IR spectrum, which enables the calculation of an equilibrium constant for the reaction. The spectral region of interest (1615-1585 cm^{-1}) was deconvoluted into three distinct Lorentzian peaks using the Levenberg-Marquardt algorithm [177,178] for optimization of the model. The fitted spectrum of the mixture in CCl$_4$ at room temperature is shown in Figure 54B with a residual RMS error of 0.000215.

The absorbance measured at different concentrations has an experimental error of 3.4 to 11.2 % RSD. The fitted data of the titration of 2x10^{-3} M 4-VP with 2,4-D in CCl$_4$ is plotted in Figure 55.
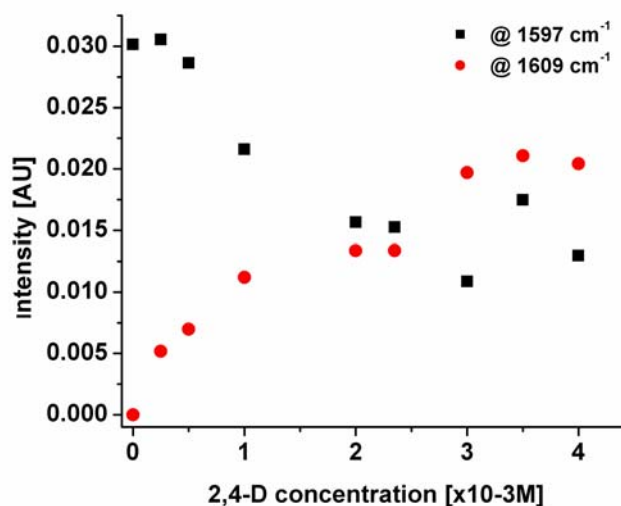
Figure 55 Absorption of free and complexed 4-vinylpyridine after peak deconvolution; squares: @ 1597 cm^{-1} (free 4-VP); circles: @ 1609 cm^{-1} (complexed 4-VP).

Using the fitted absorbance data for the absorption of free (1597 cm^{-1}) and complexed (1609 cm^{-1}) 4-VP, information on the complex stoichiometry, the absorption coefficients, and the binding constant K_b can be derived.

Since $[2,4\text{-D}]_0$ never exceeds the 5-fold $[4\text{-VP}]_0$ concentration, the assumption $[2,4\text{-D}]_{free}\sim[2,4\text{-D}]$ cannot be used (case 1). The free 2,4-D concentration is therefore not known (case 2). Using the following equations:

$$[4-VP]_0 = [4-VP]_{free} + [4-VP]_{compl} \qquad (1)$$

$$[2,4-D]_0 = [2,4-D]_{free} + [2,4-D]_{compl} \qquad (2)$$

the dissociation constant K_d can be written as

$$K_d = \frac{[4-VP]_{free}[2,4-D]_{free}}{[4-VP]_{compl}} = \frac{([4-VP]_0 - [4-VP]_{compl})([2,4-D]_0 - [2,4-D]_{compl})}{[4-VP]_{compl}} \quad (3)$$

Consequently,

$$\frac{[4-VP]_{compl}}{[4-VP]_{free}} = \frac{1}{K_d}([2,4-D]_0 - [4-VP]_{compl}) \quad (4)$$

Equation (4) can be written as

$$\frac{A_{1609}}{A_{1597}}\left(\frac{\varepsilon_{free}}{\varepsilon_{compl}}\right) = \frac{1}{K_d}\left([2,4-D]_0 - \frac{A_{1609}}{\varepsilon_{compl}*d}\right) \quad (5)$$

with   d: absorption pathlength (0.02 cm) and

   ε: extinction coefficient [L mol^{-1} cm^{-1}].

Equation (5) can be used to estimate K_d. The results are summarized in Figure 56.
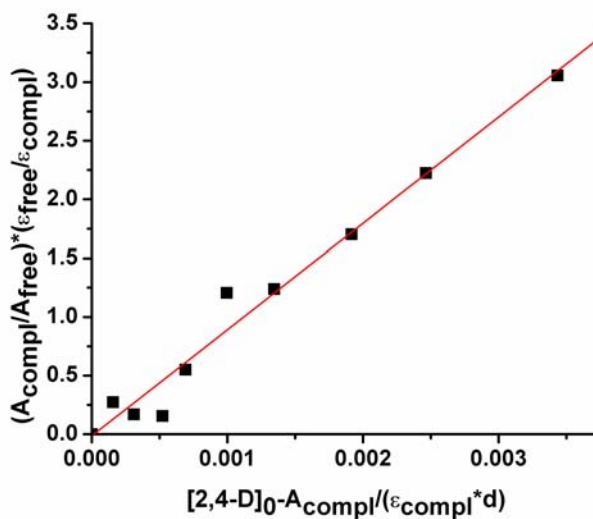
Figure 56 Fitted absorbance A of the absorption bands at 1597 cm^{-1} and 1609 cm^{-1} for the determination of the apparent binding constant K_b.

A K_d value in carbon tetrachloride of $1.11 \cdot 10^{-3}$ M was obtained from the slope and intercept of the linear plot ($R^2=0.98$) at room temperature. Therefore, the apparent binding constant K_b was found to be 898.75 M^{-1}, which is in the range expected for strongly H-bonded complexes [179,180]. It should be noted that errors in the curve fitting will result in relatively large errors of the K_b value on the basis of error propagation. Hence, the obtained values should be viewed as a first approximation.

Furthermore, besides the spectroscopic changes evaluated for quantitative analysis, further changes could be observed. New bands of medium intensity only appear in the 2,4-D/4-VP mixture as shown in Figure 57B at 1011.9 cm^{-1}. Other new bands are observed at 1201 cm^{-1} and at 837 cm^{-1}.
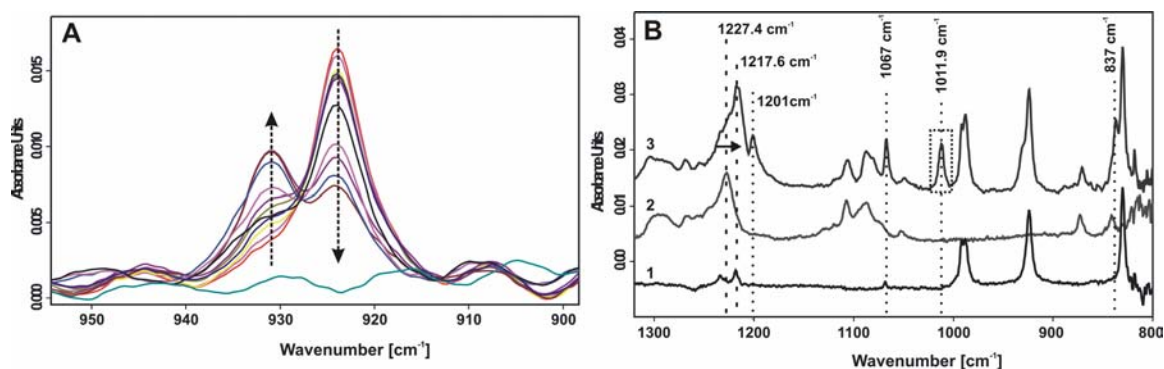
Figure 57 IR spectroscopic changes during titration of 4-VP with 2,4-D; A) Bands of 4-VP at $2 \cdot 10^{-3}$ M (924/930 cm^{-1}) revealing changes due to complex formation; B) Spectral region 1300-800 cm^{-1}. IR spectra of 4-VP, 2,4-D, and a mixture of 2,4-D and 4-VP: (1) 4-VP at $1 \cdot 10^{-3}$ M; (2) 2,4-D at $2 \cdot 10^{-3}$ M; (3) 2,4-D at $2 \cdot 10^{-3}$ M and 4-VP at $1 \cdot 10^{-3}$ M.

A band at 924 cm^{-1} attributed to 4-VP strongly decreases in intensity during the titration with 2,4-D and a new hypsochromically shifted band arises at 930 cm^{-1} (Figure 57A). Most likely, these spectral features result from changes in the aromatic ring bands of 4-VP and 2,4-D.

Furthermore, the complex stoichiometry was determined by Job's plot analysis showing a maximum at x=0.5 (Figure 58).
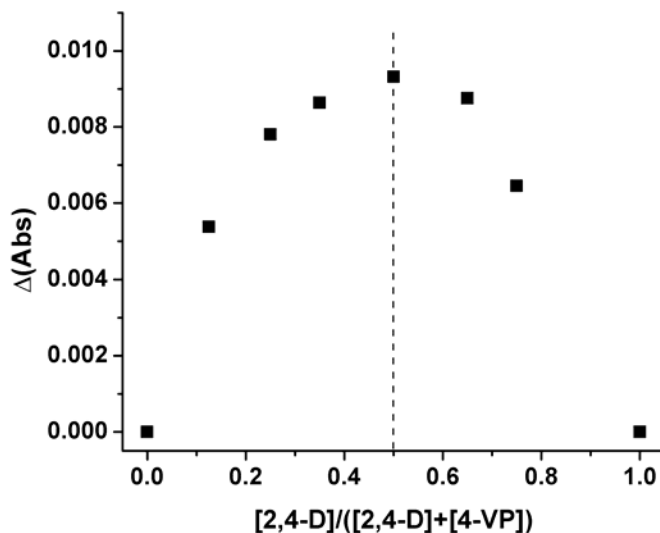
Figure 58 Job's plot analysis from IR titration of 4-VP with 2,4-D in CCl$_4$ following the method of continuous variation using the absorbance of 4-VP at 1597 cm^{-1}.

The maximum at a molar ratio of 0.5 indicates a 1:1 complex formed in CCl$_4$.

3.3.3.2.4 Interaction of 2,4-dichlorophenoxyacetic acid and the cross-linker EGDMA in the pre-polymerization solution

The interaction of the cross-linker ethyleneglycol dimethacrylate (EGDMA, Figure 59) with the template 2,4-D and with the functional monomer 4-VP was also investigated in carbon tetrachloride solution.
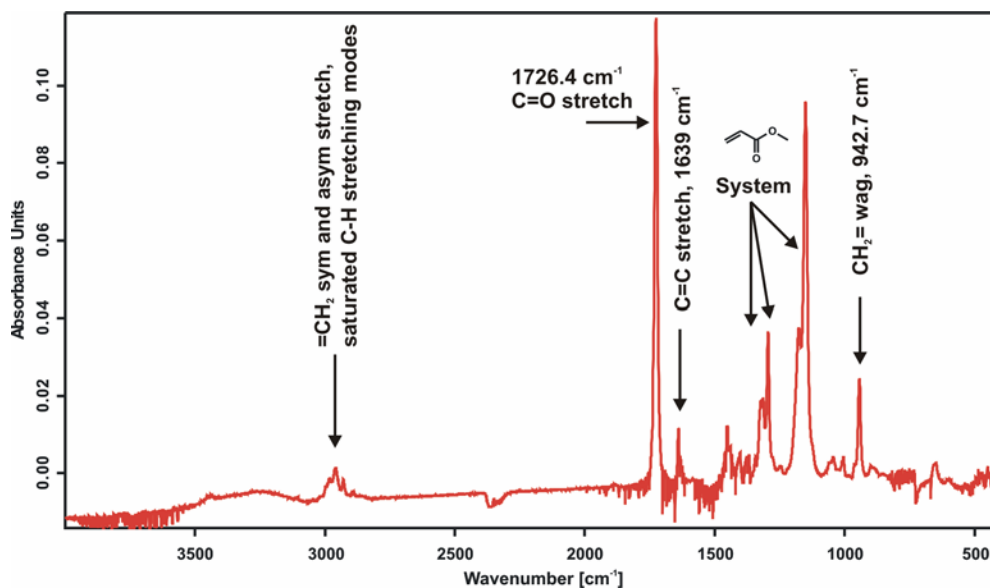
Figure 59 IR spectrum of EGDMA ($4 \cdot 10^{-4}$ M in CCl_4), transmission, 200 μm spacer.

The concentration range for the IR spectroscopic studies was much lower (2 to 4×10^{-3} M) than the concentration range usually encountered in the actual pre-polymerization solution (4 M) due to the solubility limitations in CCl_4. Also, a maximum ratio of 2,4-D to EGDMA of 1:6 was used instead of 1:20. Nevertheless, this study allowed investigating the effect of the presence of cross-linker on the complex formation. Ideally, the cross-linker should not interact with the other components of the system, ensuring low non-specific binding. No significant changes of the monitored spectral features were evident, as shown in Figure 60.
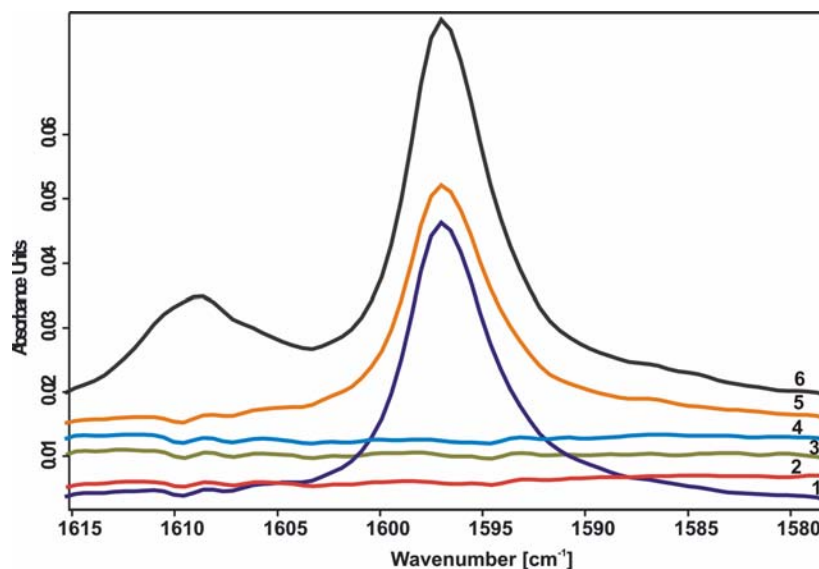
Figure 60 IR transmission spectra of EGDMA, 4-VP, and 2,4-D (200 μm spacer, in CCl_4. (1) 4-VP ($2 \cdot 10^{-3}$ M) and EGDMA ($2 \cdot 10^{-3}$ M); (2) 2,4-D ($2 \cdot 10^{-3}$ M); (3) EGDMA ($2 \cdot 10^{-3}$ M); (4) 2,4-D ($2 \cdot 10^{-3}$ M) and EGDMA ($2 \cdot 10^{-3}$ M); (5) 4-VP ($2 \cdot 10^{-3}$ M); (6) 4-VP ($2 \cdot 10^{-3}$ M), EGDMA ($2 \cdot 10^{-3}$ M), and 2,4-D ($2 \cdot 10^{-3}$ M).

EGDMA (3) and 2,4-D (2) do not have characteristic bands in the investigated spectral region. The functional monomer 4-VP has a characteristic C=N band at 1597 cm^{-1} (5). The spectrum of 4-VP and of the mixture of 4-VP and EGDMA (1) are identical and have one band at 1597 cm^{-1} showing no complexation due to hydrogen bonding between the functional monomer 4-VP and the cross-linker EGDMA. Also, taking the EGDMA spectrum (2×10^{-3} M) as a new background for the mixture of 4-VP (2×10^{-3} M) and EGDMA (2×10^{-3} M) resulted in a 4-VP spectrum identical to the one of only 4-VP at 2×10^{-3} M. Only the mixture of 4-VP, EGDMA, and 2,4-D (6) showed a new band formed at 1609 cm^{-1} which is due to the interaction of 4-VP and 2,4-D (hydrogen bonded complex formation). Therefore, in the selected concentration range it was concluded that the cross-linker EGDMA does not have any impact on the 2,4-D/4-VP or 2,4-D/MAA complex formation in CCl_4. Furthermore, Nicholls previously followed the self-assembly process with UV spectroscopic studies in chloroform indicating that the "crosslinking

agent [EGDMA] does not significantly interact with the template", which supports the findings of the present study [3,64].

3.3.3.3 ^{1}H-NMR studies of pre-polymerization mixtures

Figure 61 shows the ^{1}H-NMR spectrum of 2,4-D in D_2O at a concentration of $6.6 \cdot 10^{-3}$ M acquired at room temperature with sixteen scans. The reference was set with the residual HDO peak.
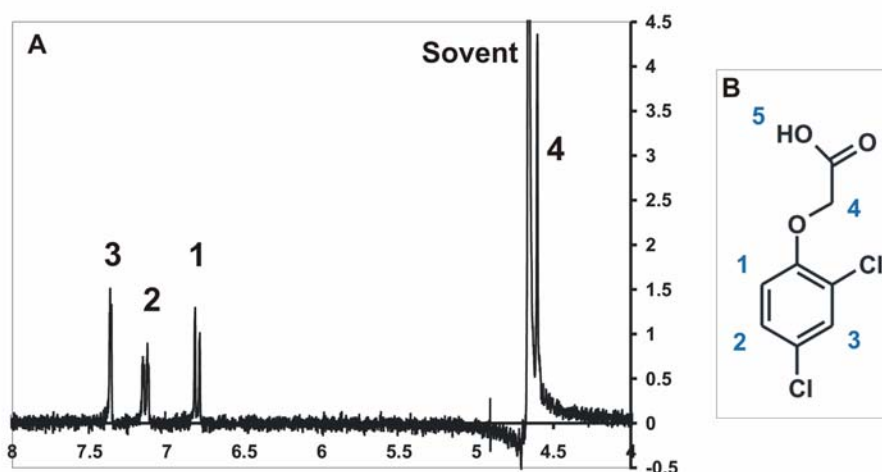
Figure 61 (A) 300 MHz ^{1}H-NMR spectrum of 2,4-D ($6.6 \cdot 10^{-3}$ M) in D_2O, 16 scans, room temperature, and (B) 2,4-D structure with correspondingly numbered hydrogens.

Five signals were observed in the ^{1}H-NMR spectrum. The signals 1, 2, and 3 correspond to the aromatic protons of 2,4-D (see Figure 61B). A singlet at low field (7.36 ppm) was assigned to H3, and two doublets assigned to H1 (~6.8 ppm) and H2 (~7.15 ppm). Another singlet at 4.61 ppm was assigned to H4. The proton H5 interchanges rapidly with D_2O and is therefore not apparent in the NMR spectrum.

In order to confirm and validate the results obtained during the IR and HPLC studies and to assess the molecular interactions in aqueous pre-polymerization solutions, ^{1}H-NMR

titration studies were performed investigating the type and strength of 2,4-D/4-VP interactions in deuterated water and deuterated chloroform. These studies allowed identifying individual molecular interactions contributing to the complex formation complementary to the IR studies. The complex stoichiometry was determined by Job's plot analysis, where the ratios of 2,4-D and 4-VP were systematically varied from 0:1 to 8:1 using equimolar 0.04 M solutions with a constant sample volume of 0.75 mL (see Figure 62).

For the aromatic protons, an upfield shift of less than 0.003 ppm was observed upon increasing the 2,4-D concentration from 0.0002 M to 0.02 M suggesting that self-stacking effects are negligible. During the ^{1}H-NMR titration studies performed in deuterated chloroform, the signal of the acidic proton of the carboxylic acid strongly migrated upfield, as 4-VP was increasingly protonated (see Figures 62 and 63-A1). For these studies, 4-VP was substituted with deuterated pyridine (pyr-d5) facilitating the observation of aromatic proton shifts.
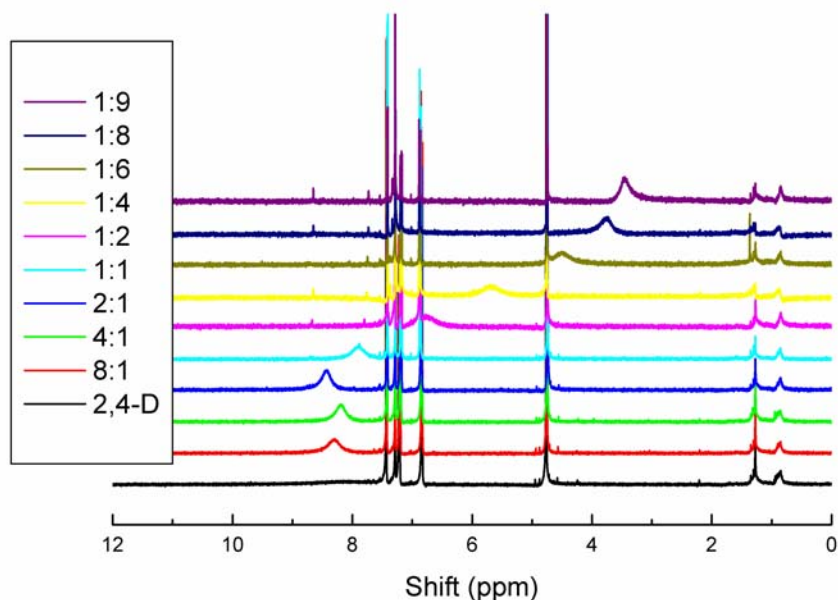
Figure 62 ^{1}H-NMR shifts of 2,4-D acid exchangeable protons in CDCl$_3$.

The signal of the acidic proton of the carboxylic acid 2,4-D strongly migrates upfield as the titration progresses towards higher 4-VP concentrations (see Figure 63-A1) with 4-VP in solution being increasingly protonated. It can be concluded that the primary interaction mechanism is based on hydrogen bonding/electrostatic effects between the basic pyridine molecule and the acidic 2,4-D molecule forming a strong hydrogen bonded complex.
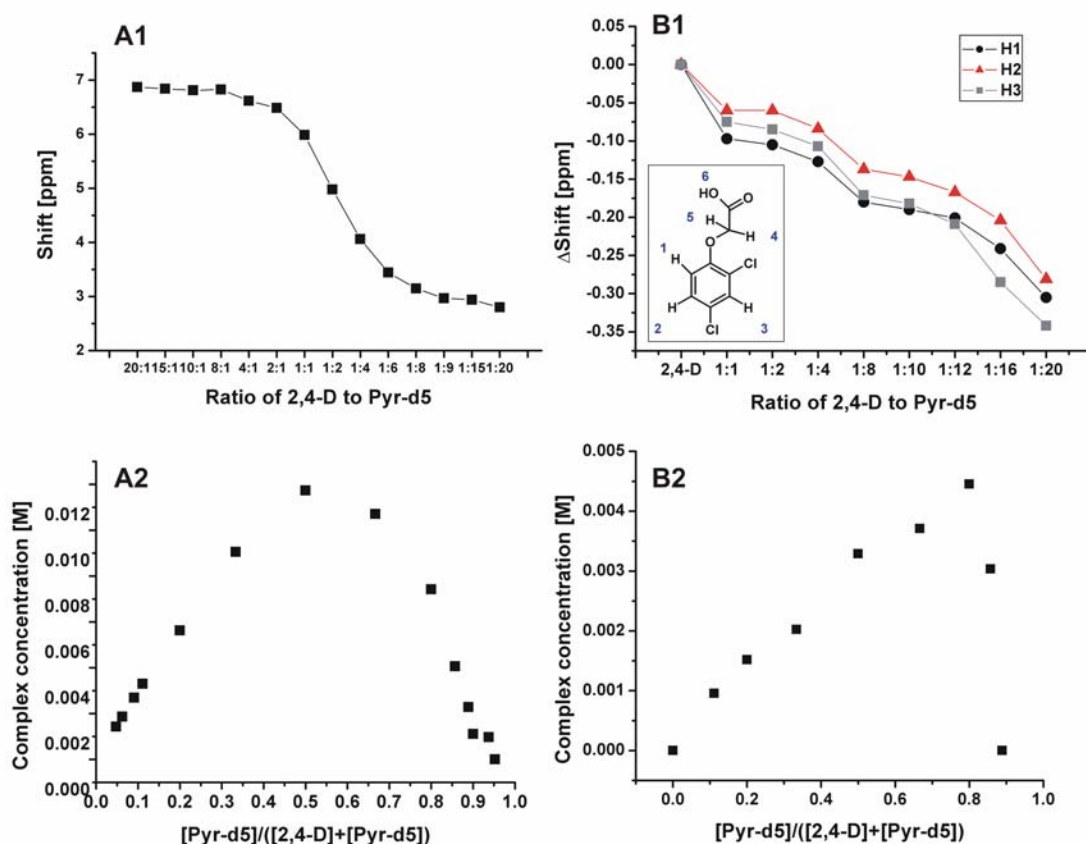
Figure 63 Titration measurements (1) and Job's plot analysis (2) of 2,4-D/pyridine-d5 from ^{1}H-NMR titration studies in CDCl$_3$ (ionic interaction, A) and in D$_2$O (hydrophobic interaction, B). ^{1}H-NMR measurements were performed at 25 °C with 16 repetitive scans. A1) Shift of 2,4-D acidic protons. B1) Shift of 2,4-D aromatic protons.

The complex concentration for Job's plot analysis was calculated as

$$[complex] = [template]_{tot} \times (\delta_{OBS} - \delta_{template})/(\delta_{complex} - \delta_{template}) \qquad (1)$$

where [template]$_{tot}$ is the total template concentration, $\delta_{template}$ is the shift of the free template molecule, $\delta_{complex}$ is the chemical shift of the complex and δ_{obs} is the observed chemical shift. The Job's plot analysis of the observed interaction (Figure 63-A2)

indicates a 1:1 2,4-D:4-VP stoichiometry. Following, the association constants were calculated using the model described by Atwood calculating association constants in weak complexes based on changes in the observed NMR signal shifts. Furthermore, dilution experiments were performed to exclude self-association effects during the titrations. The corresponding association constant was determined to be 172 M^{-1} in $CDCl_3$. Furthermore, ^{1}H-NMR line width measurements as described by K. Mosbach et al. [58] monitoring line widths during titration showed the presence of three maxima attributed to the formation of 1:1, 1:2, and 1:3 complexes [48].

In order to identify interactions predominantly occurring in polar protic solvents, ^{1}H-NMR titration studies in deuterated water were performed. An upfield shift of the aromatic protons of 2,4-D was observed (see Figure 64) and attributed to participation in π-π stacking interactions [181], as aggregated oligomers form in solution due to hydrophobic effects along with electrostatic interactions such as π-π stacking and van der Waals interactions.

Titration of 1M 2,4-D with 1M Pyridine-d$_5$ in D$_2$O

Legend:
— 1:20
— 1:16
— 1:14
— 1:12
— 1:10
— 1:8
— 1:6
— 1:4
— 1:2
— 1:1
— 2,4-D

Shift (ppm)
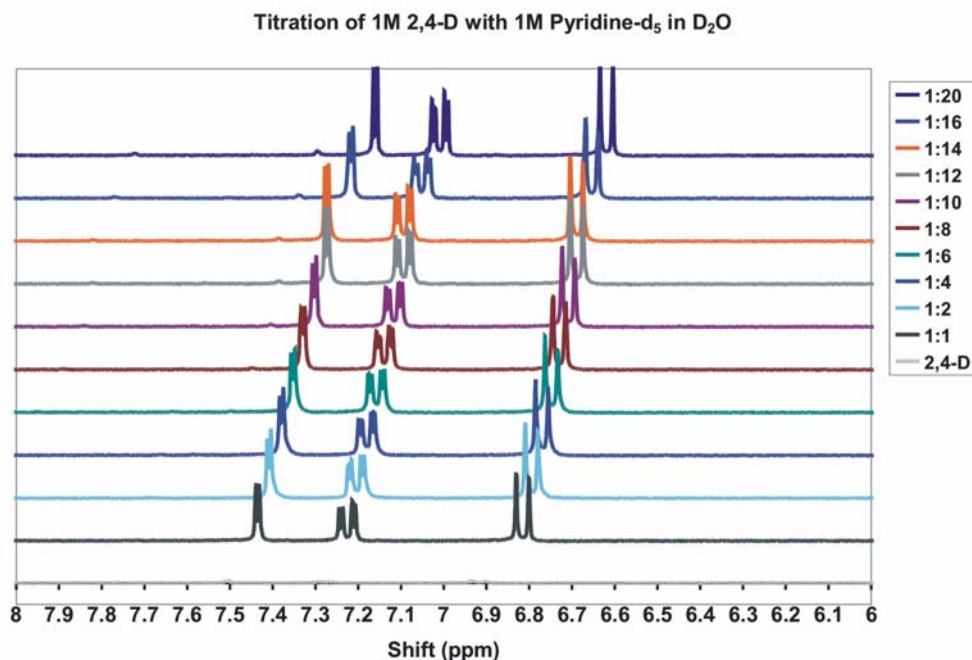
Figure 64 ^{1}H-NMR shifts of aromatic protons in D$_2$O.

Control experiments were performed in d-chloroform resulting in only minute shifts of the aromatic protons related to 2,4-D. The Job's plot of this interaction (Figure 63-B2) results in a maximum at 0.75-0.8 suggesting that a 1:3 (2,4-D:4-VP) complex - and possibly higher order complexes - are being formed. The additional stabilization of the pre-polymerization complexes resulting from π-π stacking was determined to be 27 M^{-1} in D$_2$O. Therefore, in aqueous solution NMR studies suggest that the complex formed in solution is primarily based on electrostatic interactions, which are stabilized by secondary aggregation of aromatic moieties. In summary, hydrogen bonding, hydrophobic interactions and π-π stacking strongly contribute to the complex formation.

In the following, the dynamics of the 2,4-D/4-VP interactions were investigated by measuring relative changes of the ^{1}H-spin-lattice relaxation time (T$_1$) of the aromatic and non-aromatic 2,4-D protons. These studies were performed with 2,4-D as the probe

molecule, while increasing the ratio of functional monomer 4-VP relative to 2,4-D. At conditions where an exchange equilibrium is rapidly reached, the measured relaxation time is a weighted average of the rates of free and complexed 2,4-D. T_1 values were measured using the inversion-recovery method at 293 K with a relaxation delay of d= $5 \cdot T_1$ (see Figure 65).
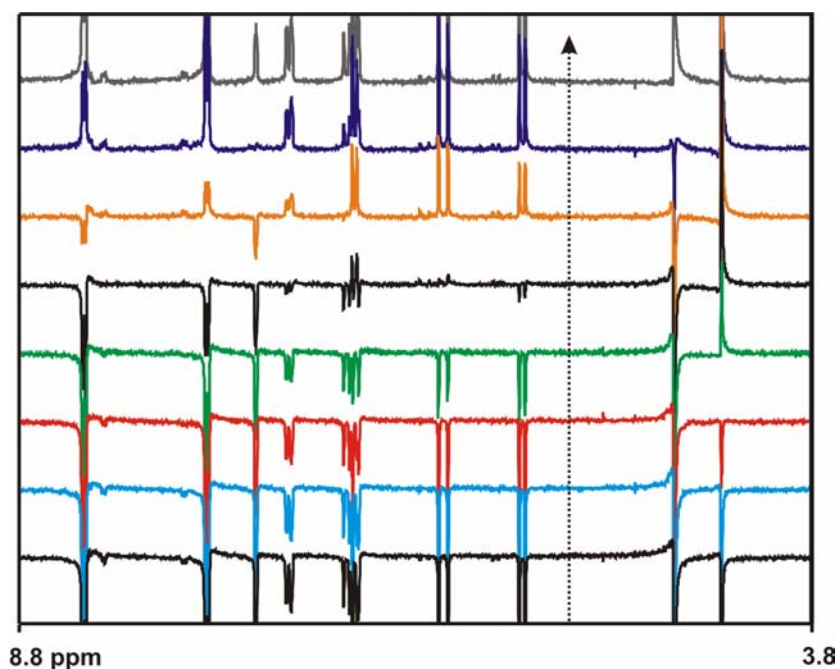
Figure 65 ^{1}H-NMR inversion recovery measurement for a 1:1 ratio of 2,4-D and 4-VP (0.02 M in D2O). From bottom to top: delay τ = 0.125, 0.25, 0.5, 1, 2, 4, 8, 16, and 32 s. 16 scans, 293 K.

The aromatic 2,4-D protons are located downfield of the vinyl protons. Nevertheless, the aromatic protons of 2,4-D may participate in π-π stacking interaction, since an upfield shift is observed. With an increase of the 4-VP concentration, 2,4-D/4-VP aggregated oligomers may form in solution. The aromatic protons H1, H2, and H3 of 2,4-D are shifted upfield and the duplet assigned to H1 merges with the 4-VP signal at 6.65 ppm. The relaxation rates were calculated by a non-linear model fitting the peak intensities to

a two-parameter exponential equation. The changes in the ^{1}H spin-lattice relaxation time at three different molecular sites were investigated to identify interaction sites between 2,4-D and the functional monomer 4-VP (see Figure 66).
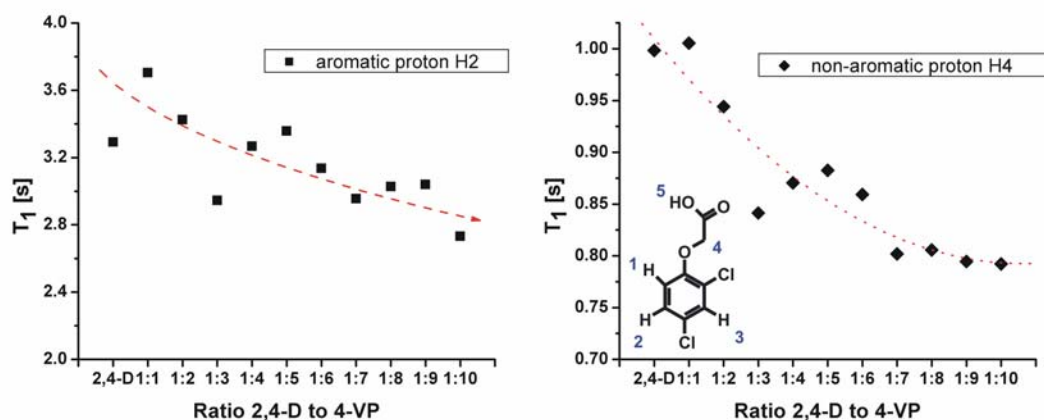
Figure 66 ^{1}H-NMR spin-lattice relaxation time (T$_1$) values for aromatic (left) and non-aromatic (right) 2,4-D protons in the presence of increasing amounts of 4-VP.

In a solution of 0.02 M 2,4-D in D_2O, the aromatic protons H1, H2, and H3 had spin-lattice relaxation times of 1.685, 3.293, and 9.076 s, respectively. The RSD was < 2 %. The non-aromatic proton H4 had a T_1 of 1.025 s. The T_1 values of the aromatic protons H1 (1.685 s), H2 (3.293 s) and H3 (9.076 s) are larger than the T_1 value of the non-aromatic proton H4 (1.025 s). Isolated protons have much longer T_1 values since fewer pathways available for a proton to relax result in larger T_1 values. Consequently, aromatic protons are characterized by longer T_1 times than alkyl groups. The addition of 4-VP resulted in a strong decrease of the T_1 value for the aromatic protons. For the non-aromatic proton H4, the T_1 values only slightly decreased during titration. If an association product is formed by complexation that rotates as a unit, the spin-lattice relaxation time is expected to decrease since the rotational mobility of the complexed molecule is smaller compared to the free molecule [182]. Consequently, the results in

this study indicate that the initial interaction of 2,4-D and 4-VP at low ratios - such as 1:1 and 1:2 - occurs at the non-aromatic interaction moiety of 2,4-D via the carbonyl group. At higher concentrations of 4-VP, the strong decrease of T_1 for the aromatic protons and the small changes of T_1 for the non-aromatic proton indicate π-π stacking of the aromatic moiety. Therefore, it is concluded that the molecular interactions during pre-polymerization shift from the carboxylic group at low 2,4-D:4-VP ratios to the aromatic ring at higher 2,4-D:4-VP ratios. The hydrophobic/π-π stacking contribution to the binding event was determined to be 4 ± 0.8 M^{-1} in D_2O derived from the decrease in T_1 of the aromatic protons using the Benesi-Hildebrand equation (33) as discussed in section 2.4.3.3 (Figure 67). Errors in relaxation data are usually estimated to be approx. 20 % [183]. Furthermore, changes in viscosity and pH also affect T_1 values. Hence, the 10-fold increase in 4-VP concentration from 0.02 to 0.2 M may therefore also contribute to slight changes of the T_1 values and will therefore contribute to an error in the calculation of the binding constant.
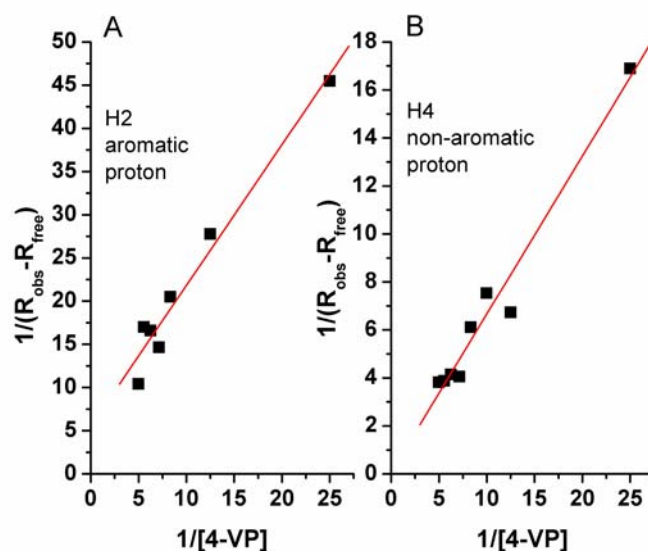
Figure 67 T_1 NMR studies: Benesi-Hildebrand plot for aromatic (A) and non-aromatic (B) 2,4-D protons in D_2O.

The non-aromatic proton H4 gives a value of 0.12 M^{-1} indicating an extremely weak contribution from the non-aromatic sites of the molecule in D_2O. These results are in reasonable agreement with the titration ^{1}H-NMR studies performed on the 2,4-D/4-VP system.

The binding constants of the complexes in the pre-polymerization solution determine their ability to withstand the polymerization process, which subsequently results in the formation of binding pockets or binding sites within the polymer matrix. It is expected that polymers with a heterogeneous binding site distribution will be formed ranging from binding sites with high affinity for the template to non-specific binding to the cross-linked polymer matrix. The estimated apparent K_b values obtained from IR (898.75 M^{-1} in CCl_4) and NMR (172 M^{-1} in $CDCl_3$) titration measurements are in the range of $1\text{-}10\cdot10^2$ M^{-1}. While the IR studies suggest a simple hydrogen bonded complex possibly in tautomeric equilibrium with an ion-pair bonded species, the NMR results confirmed the presence of a 1:1 ionic interaction. Nevertheless, the difference in K_b derived from the IR and NMR experiments indicates possible further interactions, which contribute to the observed IR spectroscopic changes during the 2,4-D/4-VP titration. The strength and type of the acid-base hydrogen interaction is mainly dependent on the pK_a of the acid and on the polarity of the environment. Depending on the resulting polarity of the selected protic or aprotic porogen, the combination of two or more interaction modes is assumed. Furthermore, higher association constants are frequently obtained by multiple bonding or by stoichiometric non-covalent interactions ($K_b > 900$ M^{-1}), where template and functional monomer are almost entirely associated in a 1:1 molar ratio [19].

In conclusion, the obtained results permit proposing the predominant existence of a 1:3 (2,4-D:4-VP) complex in aqueous solution prior to polymerization. The proposed ratio is in accordance with the optimum ratio of 1:4 determined during polymer synthesis of the 2,4-D-MIP, which provides the highest selectivity for the template molecule. Slight

excess (1:4) of functional monomer apparently facilitates shifting the equilibrium toward the preferred 1:3 complex. Furthermore, HPLC studies with 2,4-D imprinted stationary phases and the corresponding control polymers investigating the retention behaviour of 2,4-D and structural analogues confirmed the presence of two types of binding interactions involving the carboxylic group and the aromatic moiety.

The investigations performed in this study serve as fundamental analytical basis for preliminary work focusing on molecular dynamics simulations of the 2,4-D/4-VP system in explicit solvents with the aim of establishing predictive models ultimately incorporating experimentally determined restraints from NMR and IR studies.

3.3.3.4 Molecular modeling studies

3.3.3.4.1 Hardware specifications

The computer nodes in the cluster used to perform the simulations (ARC Seibersdorf, Austria) were dual-processor machines with 1 GHz Pentium III CPUs and 2 GB RAM. The front-end node computer had the same processor (single) with 512 MB RAM.

3.3.3.4.2 General considerations

In the following, the modeling procedure of the 2,4-D/4-VP system is discussed as a sequence of several processing steps required for first molecular dynamics calculations on these molecules in explicit solvent.

- Generation of the basic structure files

Topology files of 2,4-D and 4-VP were created in Brookhaven Protein Data Bank format (PDB) containing essential information on atom type, charge, connectivity, and starting Cartesian coordinates (see Appendix B). A common problem when working with the AMBER7 software is the fact that depending on their origin the generated PDB files may require some modification before being accepted by the programs for further processing. In particular, labeling issues appeared to be the most common source of incompatibility. For each input file a force field description was generated, which is compatible with the usual AMBER force fields. The 2,4-D and the 4-VP molecule were defined as two residues within a unit (the system of interest), with solvent molecules as further residues. Each residue must be defined as such unit. Therefore, in the respective 'prepin' files, 2,4-D was defined as residue "24D" and 4-VP was defined as residue "4VP". The program *Parmchk* was then used to read in the 'prepin' files as well as the force field files generating two output files ('frcmod') for the missing parameters. Such modified PDB structures were opened with *ViewerLite* and the two molecules were positioned in the desired starting configuration. The new PDB file for the "complex" was then saved and inspected for compatibility with the *LEaP* program. *LEaP* allowed to solvate the complex creating an AMBER coordinate and parameter/topology input file for the main MD program *Sander*. The following starting configurations were selected for 2,4-D and 4-VP:
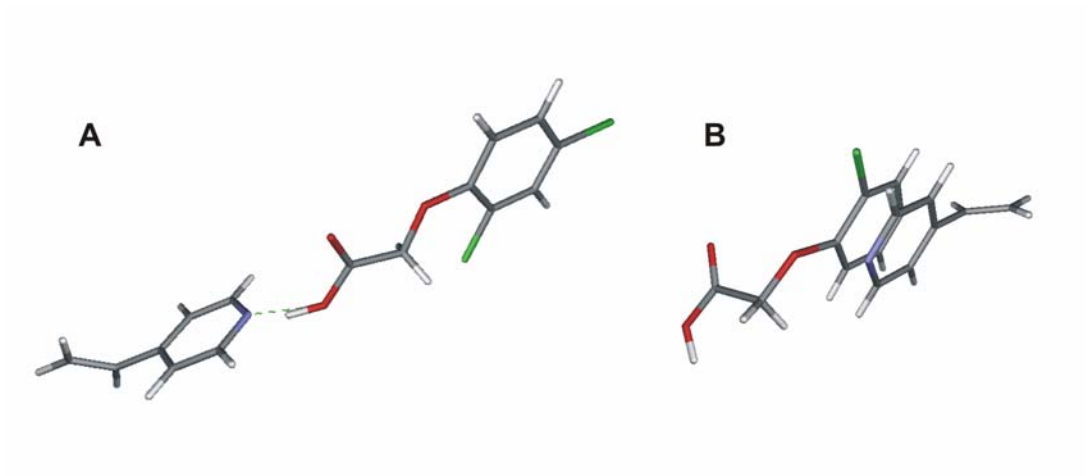
Figure 68 Initial configurations: (A) model of hydrogen bonding interaction between 2,4-D and 4-VP, and (B) π-π stacking configuration.

Residue 1 (24D 1): 2,4-D.

Residue 2 (4VP 2): 4-VP.

- Solvatization and preparation of structural files

Periodic boundary conditions were defined and the molecules placed in a solvent box (water or chloroform) with ten angstrom of solvent added around the complex in each direction.

Residues 3 to x: solvent molecules (e.g. water molecules WAT 1 to WAT x).

- Energy minimization

Energy minimization involved the following steps before starting the system equilibration prior to molecular dynamics runs:

1) Energy minimization with restrained solvent

2) Short MD run

3) Energy minimization with restrained solute

4) Short MD run

5) Energy minimization of solute and solvent without any restraints

First, the positions of the atoms were relaxed to get rid of corrupt van der Waals (non-bonded) contacts without causing substantial changes to the structures. Prior to executing molecular dynamics simulations, it was necessary to ensure that any large steric overlaps or electrostatic inconsistencies are minimized, since the placement in a solvent box does not consider possible conflicts. Large steric overlaps lead to initially large forces, which will lead to large velocities frequently resulting in distortion of the structure or localized "hot spots". During solvent energy minimization, the solute molecules were restrained to their initial positions in order not to distort their structure. The solvent was then restrained and the solute molecules were energetically minimized. For the example of water as a solvent, the solvent energy minimization only minimizes the positions of the hydrogens. A force constant of up to 5000 kcal/mol can be selected for the restraint. For minimization any value is possible, however, the force constants should not be too large since the frequency of the (effective) bond vibration increases with increasing force constant, which may lead to MD integration failures unless the time step for the molecular dynamics simulation is short enough to represent the high frequency motions. A force constant of 100 kcal/mol was selected for the restrained minimization steps. To conclude the minimization procedure, the whole system energy was minimized with no restraints applied. Constant pressure dynamics were used allowing the box size to change. If only constant volume simulations are executed, "vacuum" bubbles may appear in the box. The minimization steps as well as the applied restraints were written into one text input file (see Appendix B), from where the program Sander reads all commands and applies them to the system.

- Equilibration of the system

Following MD runs were performed during equilibration:

1) MD run at constant volume

2) MD run at constant pressure with very strong pressure coupling constant

3) MD run at constant pressure with medium pressure coupling constant

4) MD run at constant pressure with weak pressure coupling constant

5) Longer MD run at constant pressure with restraints to equilibrate the system

Since during longer equilibration runs (e.g. 250 ps) the 2,4-D and 4-VP molecules slowly drifted apart, following distance restraint forces were introduced between the two molecules to prevent drifting during the equilibration step:

- 2,4-D/4-VP (1:1) in water

Atoms defining the ring are treated as a group and the distance between the two rings was restrained.

- 2,4-D/4-VP (1:1) in chloroform

The restraint was placed on the distance between a pair of matched atoms and was incorporated into the energy function as additional penalty term. A distance restraint of three Å was placed between the hydrogen bond donor (the nitrogen atom of the pyridine ring) and the acceptor (the acidic proton of the 2,4-D molecule).

- MD simulation (production run)

For the MD production run of 1 ns, all restraints were removed and the system was allowed to freely evolve. Following properties were monitored:

- Density: for water as the solvent, a density of 1 g/mL should be reached and remain stable after the equilibration step. A density of 1.49 g/mL should be reached for chloroform.

- EPtot: the total potential energy should be stable after the equilibration step. If the conformation of the molecules is not in a stationary phase, the potential energy is subjected to drifts.

- Temperature: the temperature ramping is defined in the input file for the MD calculations in Sander (mdin). The default starting temperature is 0 K. The reference temperature, at which the system is to be kept through a weak coupling scheme, is 300 K. The time constant for heat bath coupling is set between 0.5 and 5.

- RMSd: the RMSd values (in Å) are calculated and plotted using *ptraj* and provide information whether the conformation has reached a stationary state. The RMS deviation of each frame in the trajectory to the first frame in the trajectory is calculated. This is a useful value in determining how far the structures have drifted during the MD run.

EPtot and RMSd were used as criteria to decide how much equilibration was needed before production data was collected and analyzed. Furthermore, the configurations were stored every 25-50 steps and visually examined to make sure the simulations execute well.

3.3.3.4.3 MD results of the system 2,4-D/4-VP (1:1) in water

The two starting configurations for the 2,4-D/4-VP complex as shown in Figure 68 were used for the MD simulations. When using the H-bonding configuration in water, the 2,4-D and 4-VP molecules drifted apart and no complex re-formation could be observed. The following results were obtained using the π-π stacking starting configuration (SC π-π

stacking) (see Figure 68). After energy minimization following MD runs were performed with restraints (see Appendix B):

1) 5 ps equilibration at constant volume

2) 3x 5 ps equilibration at constant pressure with decreasing pressure coupling constant with a pressure relaxation time of 0.05, 0.5, and 5 ps.

3) 250 ps equilibration at constant pressure with a pressure relaxation time of 1 ps.

The temperature, total potential energy, and density values for the MD runs were plotted against the total MD simulation time of 270 ps as shown in Figures 69 and 70.
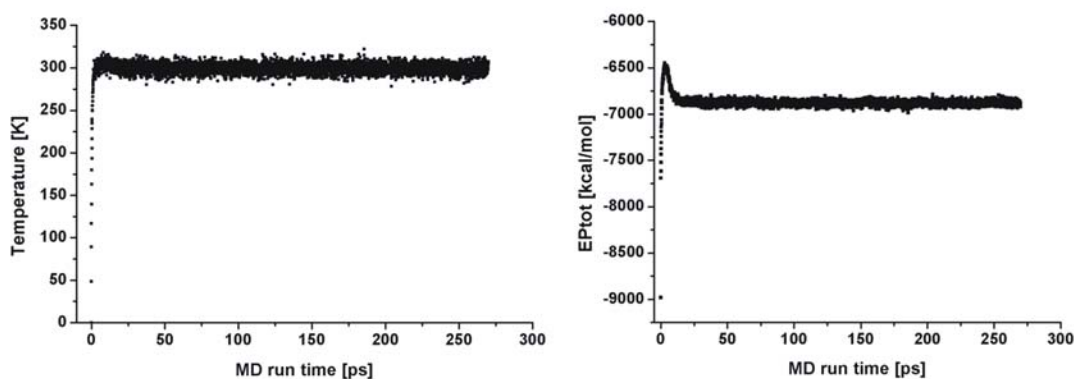
Figure 69 2,4-D/4-VP (1:1) in water (SC π-π stacking). Temperature and total potential energy of the MD runs after equilibration plotted against MD run time.
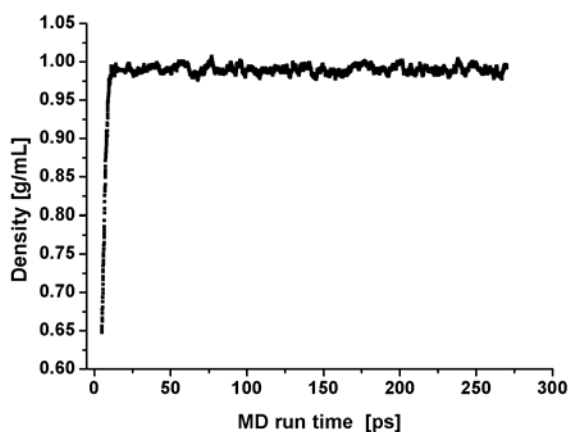
Figure 70 Density of the system in water during the MD runs plotted against MD run time (SC π-π stacking).

The temperature and density plots indicated that after the selected equilibration process the set temperature of 300 K was reached and the density was stable and close to the real value of 1 g/mL. Furthermore, the total potential energy plot and the RMSd plot indicated that the system had reached an equilibrium state. Therefore, a production simulation was started. The production MD simulation was performed at constant volume and constant energy (NVE) with no restraints for a total time of 1 ns. Temperature and total potential energy were constant during the MD simulation period as shown in Figure 71.
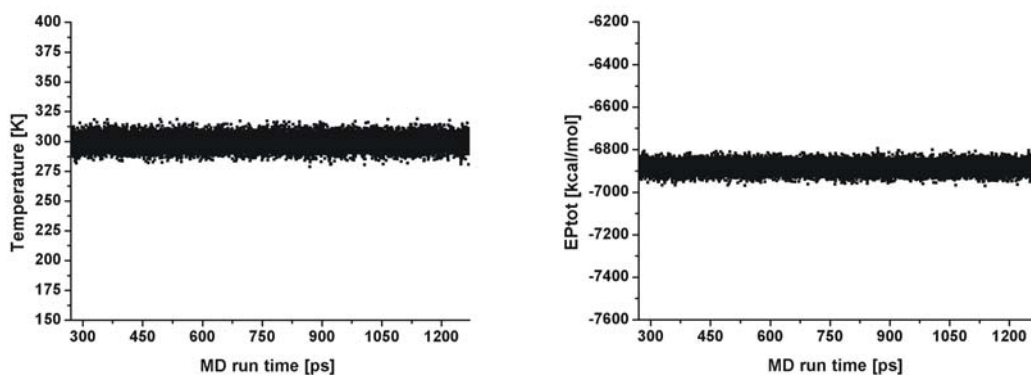
Figure 71 2,4-D/4-VP (1:1) in water (SC π-π stacking): temperature and total potential energy against MD run time during production MD run.

The RMSd increased during the production MD simulation (see Figure 72) indicating a drift of the 2,4-D/4-VP complex from its initial position (residues :1-2).
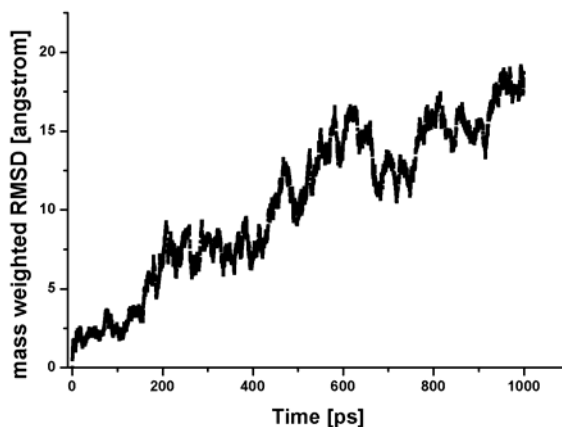
Figure 72 Mass weighted RMSd of the 2,4-D/4-VP complex in water in the NVE production simulation (SC π-π stacking).

Many orientations have been observed for aromatic dimers, ranging from face-to-face structures to edge-on (T-shaped) structures with several proposed models for aromatic interactions [184-186]. An aqueous solution of a benzene dimer was investigated by

means of molecular dynamics simulations and the T-shaped structure was found to be the most favorable [187]. The angle α was measured as angle between the coordinates of the mass centered 2,4-D and 4-VP rings and a ring C atom of 2,4-D (atom I.D. #14, see Appendix B). The 2,4-D and 4-VP rings seem to oscillate between two extremes which are the face-to-face and the edge-on configuration (see Figure 73). The rings alternate from face-to-face/center-to-center, to face-to-face/center-to-edge, to edge-on, and finally to non-stacked conformations.
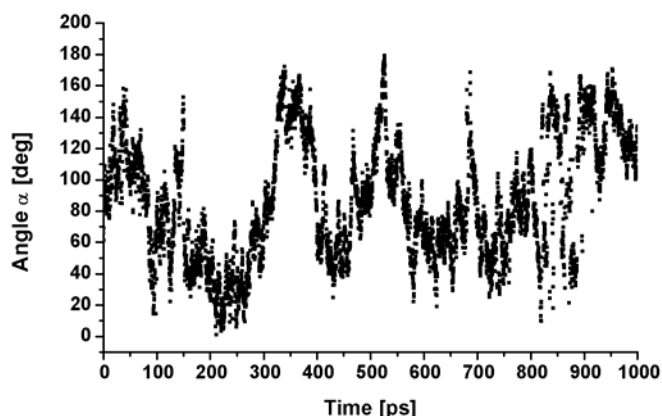
Figure 73 Angle α between the coordinates of the mass centered 2,4-D and 4-VP rings and a ring C atom of 2,4-D (atom I.D. #14) plotted against MD run time (SC π-π stacking).

The distance between the rings was also plotted against the MD run time. The distance d_1 was measured as distance between two atoms (see Figure 74, left) defined as atom 12 (C with I.D. #12 from 2,4-D ring) and atom 25 (C with I.D. #25 from 4-VP ring). The distance d_2 was measured as distance between the mass centered 2,4-D and 4-VP rings (see Figure 74, right).
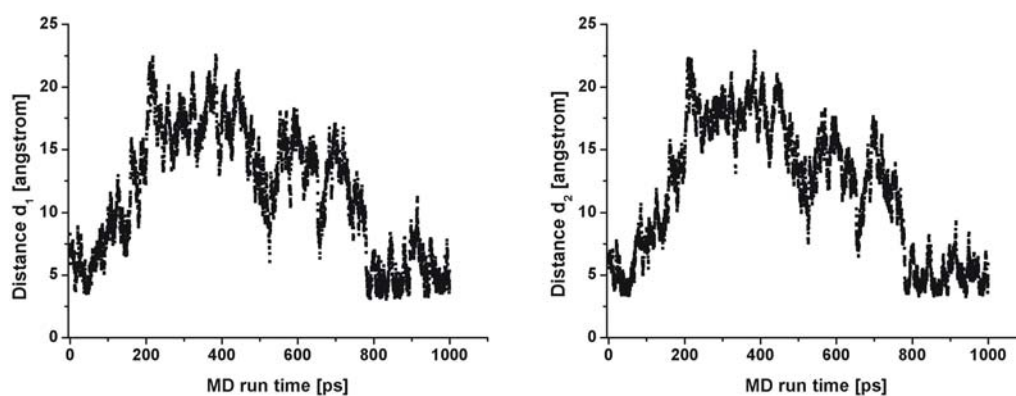
Figure 74 Distances d1 (left) and d2 (right) between the 2,4-D and the 4-VP rings (SC π-π stacking).

From the observed distance plots and trajectories from the MD runs of 1 ns, the 2,4-D and 4-VP molecules seem to slowly drift apart, however, remaining in sufficiently close proximity to interact again. The distance at close proximity is around 3.2-3.8 Å, which is within the π-stacking range. For the trajectory, 5000 frames were recorded. The trajectory can be observed with 5 frames per picosecond. Some exemplary frames are shown in Figure 75.
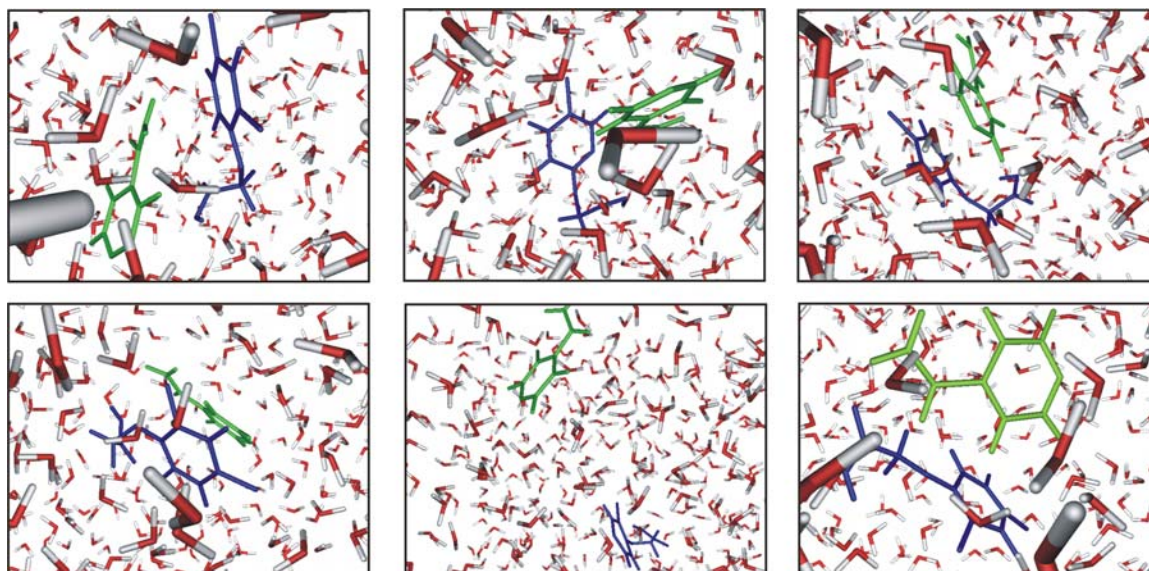
Figure 75 2,4-D/4-VP (1:1) in water (SC π-π stacking). Clockwise: frames Nr. 1 (0 ps), 100 (20 ps), 200 (40 ps), 300 (60 ps), 2466 (493.2 ps), and 5000 (1 ns) from the recorded trajectory of the 1 ns MD simulation.

The face-to-face (3rd frame) and the edge-on (2nd and 4th frames) configurations can be observed in the frame-shots. Also, 2,4-D and 4-VP drift apart (5th frame) and recombine within the box (6th frame).

The 1 ns molecular dynamics simulations of the system 2,4-D/4-VP in water have modeled aromatic π-π stacking interactions demonstrating that π-π stacking is a dominating interaction between the 2,4-D and the 4-VP molecules with the aromatic rings oscillating between a face-to-face and an edge-on configuration. These results are furthermore confirmed by experimental evidence as demonstrated in the ^{1}H-NMR studies presented in chapter 3.3.3.3.

3.3.3.4.4 MD results of the system 2,4-D/4-VP (1:1) in chloroform

Equilibration was started applying a constant pressure constraint to the system. As shown in Figure 76, the temperature and potential energy of the system were monitored at each step to ensure thermodynamic stability, which was obtained after 10 ps (starting configuration (SC): H-bonding interaction, see Figure 68).
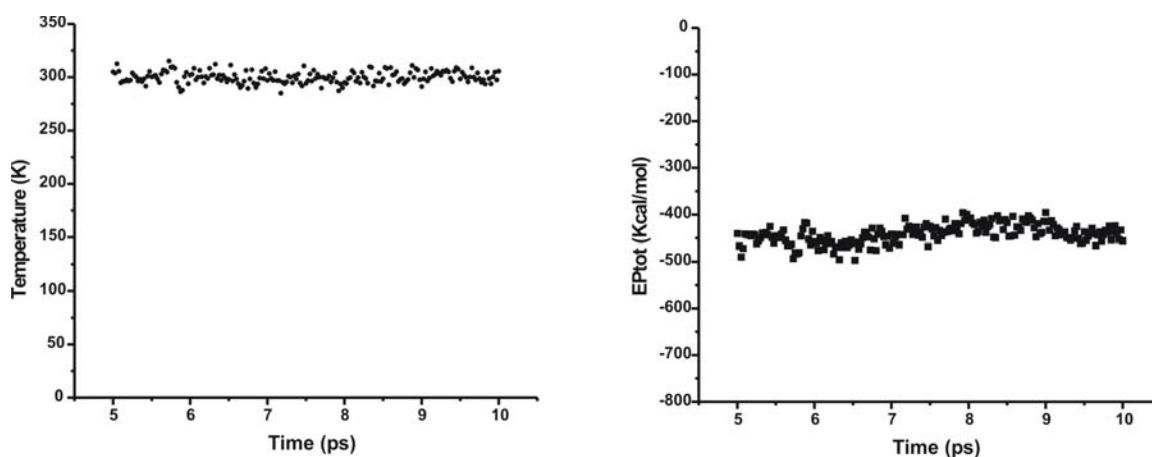
Figure 76 2,4-D/4-VP (1:1) in chloroform (SC H-bonding): temperature and total potential energy against MD run time during equilibration MD simulation.

After an equilibration time of 250 ps, an overall density value close to the experimental value of 1.49 g/cm^3 was obtained as shown in Figure 77.
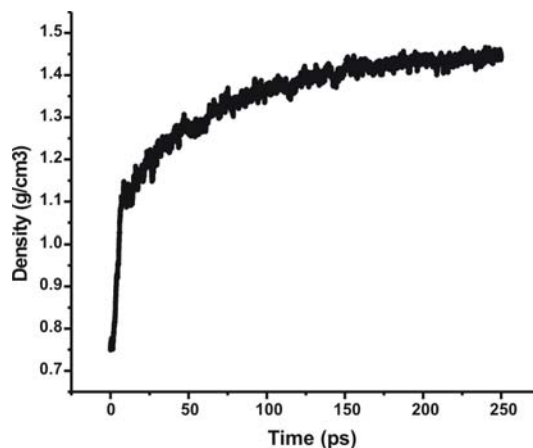
Figure 77 Density of the system in chloroform during the MD runs plotted against MD simulation time (SC H-bonding).

Also, observing the root mean square deviation of the coordinates for 2,4-D and 4-VP revealed that the coordinate deviations had stabilized within the 250 ps suggesting that the system had achieved an equilibrium (see Figure 78).
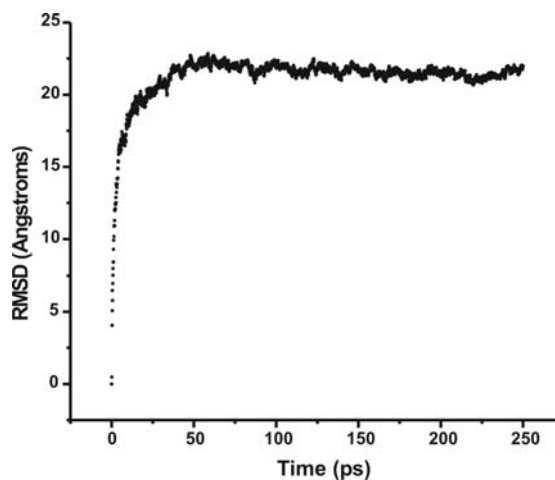
Figure 78 Mass weighted RMSd of the 2,4-D/4-VP complex in chloroform in the NVE production simulation (SC H-bonding).

The results indicated that the system 2,4-D/4-VP in chloroform was equilibrated after 250 ps enabling to start a production MD simulation.

After equilibration of the system, it was possible to execute the simulation at constant energy (NVE ensemble) and examine the 'true' trajectory of the complex during a 1 ns period without any artificial restraints being imposed upon the system. As before, the first parameters analyzed were the temperature and the potential energy behavior of the system. Both parameters were constant during the 1 ns simulation confirming stability of the system during the MD simulation. Ptraj allowed the observation of changes in the distance of the H-bond donor-acceptor pair (the nitrogen atom of the pyridine ring and acidic proton of the 2,4-D). Figure 79 shows how this interaction varied for the duration of the simulation (Note: after the equilibration had been completed, the molecular dynamics simulation was a continuation of this simulation, rather than a restart. Hence, the timescale (x-axis in Figure79) starts at 1000ps).
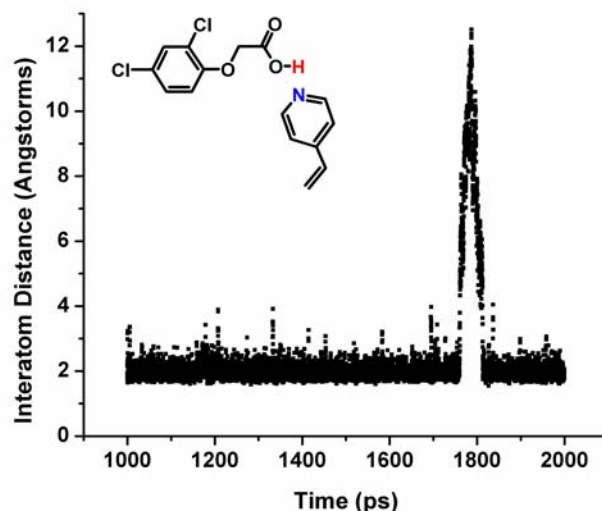
Figure 79 2,4-D/4-VP (1:1) in chloroform. Variations of inter-atomic distance of H-bonding pair during MD run.

The H-bonding interaction does not remain intact for the entire run. 2,4-D and 4-VP can drift apart as indicated in Figure 79, however, eventually recombine and remain in close

183

proximity due to the hydrogen bonding interaction. *Ptraj* allowed evaluating the integrity of this interaction. In this case, the molecular interaction was intact for a total of 98.56 % of the duration of the MD simulation.

Short simulated annealing runs were performed proving the feasibility of simulated annealing with the solvated 2,4-D/4-VP systems. A simulated annealing run was performed prior to performing a 1 ns NVE MD production simulation using the temperature profile specified in Appendix B. The system was heated from a starting temperature of 300 K up to a maximum of 600 K, prior to gradual cooling until to the final phase of the simulation (18 ps) with a rapid cooling step to 0 K at 20 ps. During simulated annealing, the hydrogen bond experiences variations in length and integrity as shown in Figure 80A.
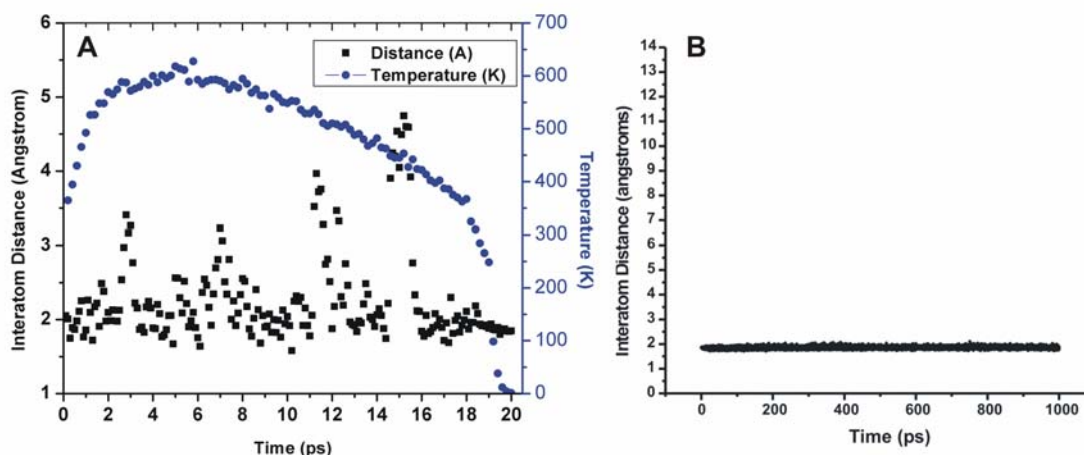
Figure 80 2,4-D/4-VP in chloroform. Hydrogen bond distance between the pyridine N-atom and 2,4-D acidic H-atom during the 20 ps simulated annealing (A) and distance during the following 1 ns NVE MD simulation (B).

After simulated annealing, a 1 ns NVE MD simulation was started to examine the stability of the complex. The interatomic distance between the pyridine N-atom and the 2,4-D acidic H-atom was plotted against the MD simulation time as shown in Figure 80B.

An interesting effect of the annealing is that the complex seems to have achieved its most stable configuration without any break-up of the hydrogen bond during the MD simulation. A snapshot of the system (see Figure 81) at the end of the 1 ns MD simulation shows that the complex remained intact indicating an energetically minimized stable configuration for the system with the H-bond still existing after the observation period.
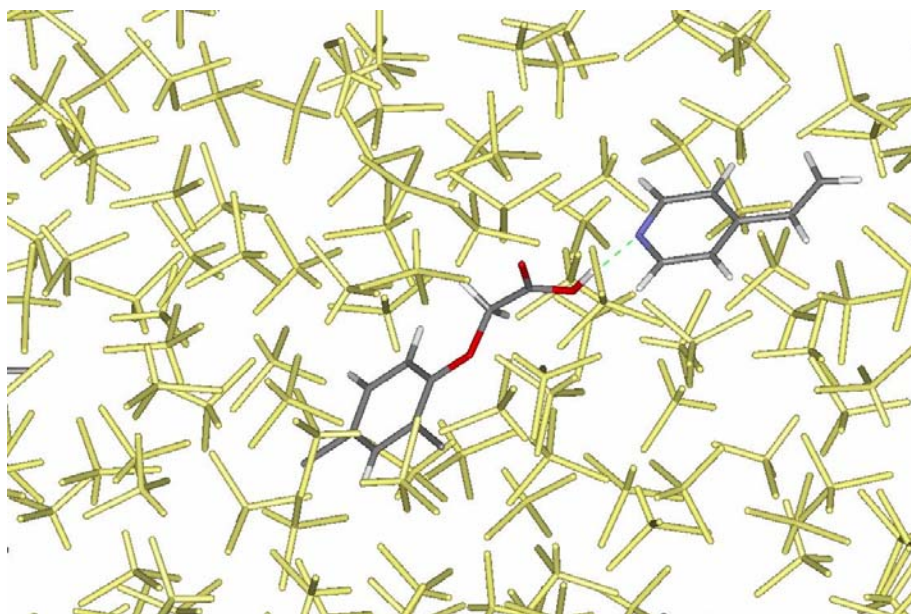
Figure 81 2,4-D/4-VP complex (SC H-bonding) at the end of the 1 ns NVE MD simulation after simulated annealing (chloroform in yellow). The hydrogen bond is indicated by a dashed line (interatomic distance 1.85 Å).

During the MD simulation at constant high temperature, frame shots may be performed every picosecond. The saved structures may then be used as starting structure for the cooling procedure allowing different minimum energy configurations to be obtained.

Molecular dynamics simulations of 2,4-D and 4-VP in explicit chloroform indicated that hydrogen bonding is a strong binding interaction for the 2,4-D/4-VP system. The 2,4-D/4-VP complex remained intact for a total of 98.56 % of the duration of the MD simulation.

Furthermore, results have indicated the potential of simulated annealing in explicit solvent for exploring configurations of minimum energy.

3.3.3.4.5 Conclusions and outlook

The first examination of the applicability of molecular modeling techniques to the elucidation of the structure and nature of pre-polymerization complexes revealed encouraging results. The following statements can be made from the results obtained for the molecular dynamics simulations of the 2,4-D/4-VP system (2,4-D:4-VP, 1:1) in water and in chloroform:

- H-bonding interactions between 2,4-D and 4-VP in a polar solvent such as water do not play an important role during complex formation

- π-π stacking appears to be the dominating interaction between 2,4-D and 4-VP in a polar, protic solvent such as water. The 2,4-D and 4-VP aromatic rings seem to oscillate between a face-to-face and an edge-on configuration.

- H-bonding is the dominating interaction between 2,4-D and 4-VP in a less polar, aprotic solvent such as chloroform.

The first results from molecular dynamics simulations relevant to molecular imprinting demonstrated the potential of molecular modeling aiding the prediction of the behavior and interactions of template and functional monomer building blocks in solution. Compared to modeling based on 3D database searching-and-docking (Piletsky et al [53]), molecular dynamics simulations enable following the behavior of template and functional monomer molecules in explicit solvent. In future, MD simulations may therefore enable screening of different functional monomers and different ratios between

template and functional monomer, thereby contributing to rational design of MIPs for a given target analyte. Furthermore, such simulations enable incorporating experimentally obtained boundary conditions derived from NMR and IR spectroscopic data. NMR data can be introduced to the MD simulations as harmonic distance restraints or torsional restraints for the generation of conformations consistent with the experimental data. Restraints can also be directly defined in terms of NOESY intensities (calculated with a relaxation matrix technique), residual dipolar couplings, scalar coupling constants and proton chemical shifts, thereby providing a powerful and flexible approach to NMR structural refinements. Furthermore, the MD simulation can be applied to obtain effective modes of vibration from atomic fluctuations from an average structure in quasi-harmonic analysis [188]. An effective force field may be calculated from atomic fluctuations relative to the average dynamic structure yielding the same fluctuation matrix as the one obtained from a normal mode calculation. Incorporating IR spectroscopic data into MD simulations is a more challenging task, especially if empirical force field models are applied. Nevertheless, IR spectroscopic measurements have previously been incorporated into molecular modeling processes as refinement energy terms for orientational restraints when IR data yielded structural information such as e.g. the secondary average structure of proteins [189].

3.3.4 Conclusions

Liquid chromatographic, ^{1}H-NMR and IR spectroscopic studies on the molecular interactions governing 2,4-D/4-VP complex formation and template re-binding along with interactions with the cross-linker in porogenic solution demonstrated that the orchestrated application of analytical methods provides a sound basis for rational

understanding of the mechanisms prevailing molecular imprinting procedures. In contrast to optimization by trial-and-error, the obtained results provided a collection of analytical observations for rational tuning of non-covalent molecular imprinting procedures. It was shown that in the methanol/water (4:1, v/v) mixture used for MIP synthesis, the combination of hydrogen bonding, hydrophobic effects, and weak attractive forces such as van der Waals interactions and π-π stacking dominate complex formation. In particular, spectroscopic titration studies of the pre-polymerization solution such as IR and ^{1}H-NMR Job's plot analysis and spin-lattice relaxation time studies have proven useful for predicting optimized component ratios during molecular imprinting. Results indicated the predominant existence of a 1:3 (2,4-D:4-VP) complex in aqueous solution prior to polymerization, further confirmed by HPLC results suggesting a 3 point interaction within the high affinity binding sites of the 2,4-dichlorophenoxyacetic acid imprinted polymer. BET surface area investigations of the polymer morphology from thermal and UV polymerization methods have shown that differences in surface area do not affect separation selectivity and HPLC column retention confirming the BET results obtained for the quercetin imprinted and control polymers. Furthermore, molecular dynamics simulations of both one molecule of 2,4-D and 4-VP in explicit solvent corroborated the importance of π-π stacking in water, as well as of hydrogen bonding in aprotic solvents such as chloroform during complex formation of the 2,4-D/4-VP system. Consequently, the potential of molecular modeling for future prediction of the governing interactions of template and functional monomer building blocks in solution has been demonstrated.

3.4 Probing the nature of non-covalent imprinting mechanisms with IR spectroscopy: a case study with o-, m-, and p-nitrophenol

3.4.1 Introduction

A molecularly imprinted polymer for 4-nitrophenol (4-NP) was previously successfully prepared by our research group [12] using the conventional trial-and-error approach with 4-vinylpyridine as functional monomer and ethyleneglycol dimethacrylate as cross-linker in acetonitrile. It was proposed that a H-bonding interaction between 4-NP and 4-VP is responsible for polymer recognition in an organic phase with "disturbed [H-bonding interaction] in the presence of water explaining the lower selectivity in aqueous eluent than in organic eluent". Nevertheless, the MIP showed a marked affinity for 4-NP in organic eluent, followed by the structural isomers 3-NP and 2-NP, respectively. 4-Nitrophenol is a small aromatic molecule with two functional groups serving as interaction moieties for molecular imprinting. 4-NP is therefore an ideal model molecule to spectroscopically study interactions in pre-polymerization solution. Furthermore, the effect of the functional group distribution within a 3-dimensional structure, as well as the consequences of the presence of intra-molecular versus inter-molecular interactions could be studied using o-, m-, and p-nitrophenol.

3.4.2 Experimental

The IR spectroscopic data was recorded on a Bruker Equinox 55 Fourier transform infrared (FT-IR) spectrometer with a liquid nitrogen cooled mercury-cadmium-telluride (MCT) detector in the spectral range of 400-4000 cm^{-1} at a spectral resolution of 1 cm^{-1}. The transmission measurements were performed in a thin film liquid cell (Pike Technologies, WI, USA) at room temperature with a 200 μm teflon spacer and NaCl windows (32 x 3 mm). The spectrometer was purged with dry air and 100 repetitive scans were averaged. Measurements were started after 15 min of equilibration time and performed by keeping either the template or the functional monomer at a fixed concentration of 4×10^{-3} M in CCl_4 while titrating with solutions of various concentrations between $0.5\text{-}20 \times 10^{-3}$ M. For Job's plot analysis, stock solutions of 4×10^{-3} M functional monomer and template respectively in CCl_4 were used and mixed from 0 to 100 % maintaining a constant total volume of 1 mL. Relevant spectral absorbances were measured in mixture and for each individual compound. The absorbance observed in absence of the functional monomer was subtracted from the absorbance of each mixture. The resulting absolute value was then plotted against the molar ratio of the functional monomer.

^{1}H-NMR measurements were performed on a Varian Mercury Vx 300 spectrometer at 300 MHz equipped with a 5 mm broadband probehead. The proton spectra were acquired with a spectral width of 4500 Hz collecting 16384 data points. Chemical shifts were referenced to the DHO reference signal. For Job's plot analysis, the ratios of functional monomer and template were systematically varied between 10:1 to 1:10 using equimolar solutions (0.01 M in D_2O) with a constant sample volume of 0.75 mL. Pyridine-

d5 was used instead of 4-VP to facilitate the observation of shifts of the aromatic protons characteristic for nitrophenol.

3.4.3 Results and discussion

3.4.3.1 IR characteristics of nitrophenols

The MIR spectrum of 4-nitrophenol is shown in Figure 82 along with a detailed absorption band assignment.
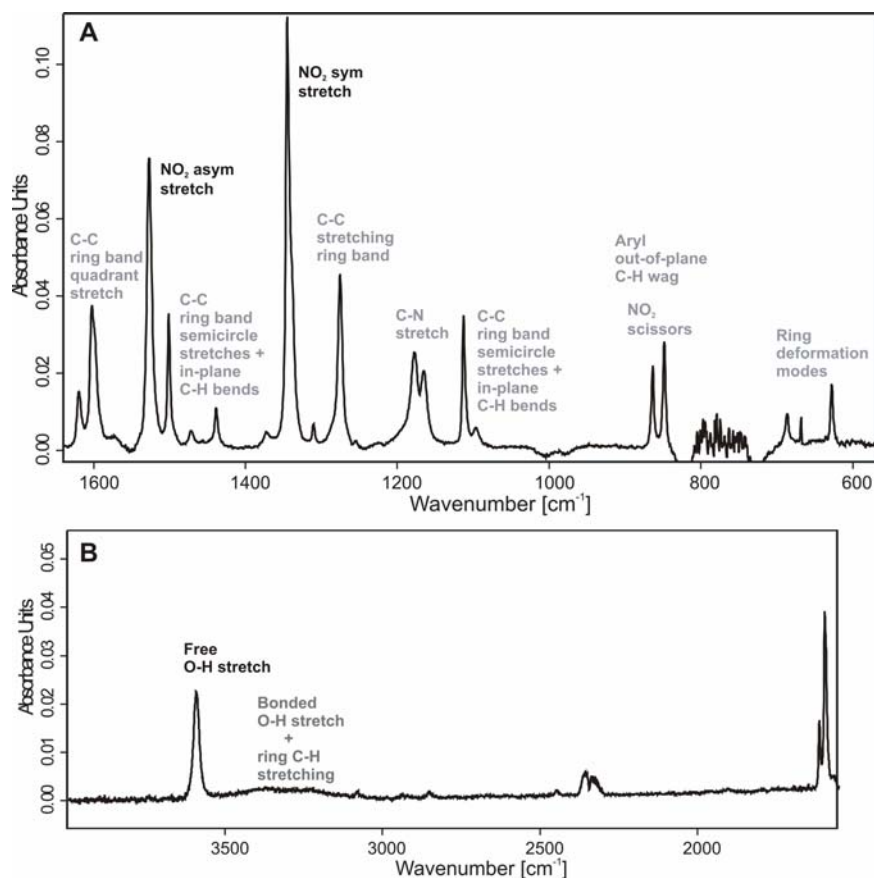
Figure 82 (A) IR spectrum of 4-nitrophenol ($4 \cdot 10^{-3}$ M in CCl_4) in the spectral regions 1600-600 cm^{-1}, and (B) in the spectral range of 4000-1600 cm^{-1}. Transmission cell, 200 μm spacer.

The NO$_2$ stretches are the two most useful group frequencies. There are six main vibrational modes with frequencies which vary according to the structural isomer and are assigned in Table 21:

- NO$_2$ asymmetric stretch
- NO$_2$ symmetric stretch
- C-N stretch
- NO$_2$ scissors
- NO$_2$ wag
- NO$_2$ rock

The NO$_2$ frequencies of substituted nitrobenzenes such as the nitrophenols are affected by the type and position of the substituent. Inductive effects, resonance effects, and hydrogen bonding will affect the stretching frequency. Furthermore, aromatic ring vibrations also couple with the NO$_2$ symmetric stretching mode. The C-N stretching mode of aromatic nitro-compounds has a broad range between 1177-865 cm^{-1} and couples with ring vibrations. The band frequency assignments are summarized in Table 21 for 2-, 3-, and 4-NP. Due to the presence of multiple bands within this spectral region, no specific band could be attributed with absolute certainty to the C-N stretching mode, which is possibly located at 1177.4 cm^{-1} for 4-NP and 3-NP and at 1190.2 cm^{-1} for 2-NP.

Table 21 Absorption band frequency assignments for nitrophenols (m: medium; s: strong; vs: very strong).

Vibrational Mode Regions	From Ref. [174]	4NP	3NP	2NP	IR
	[cm^{-1}]				
Free OH	3600	3595.5	3601	--	vs
Bonded OH	3500-3100	3500-3100		3242	m
NO$_2$ asymmetric stretch	1555-1487	1527	1536.6	1540.6	vs
NO$_2$ symmetric stretch	1357-1318	1344.9	1354.9	1332.7	vs
C-N stretch	1177-865	n.d.	n.d.	n.d.	s
NO$_2$ scissors	857-830	848.1	867.3	870.4	m

From the three NO$_2$ deformation vibrations, the NO$_2$ scissoring band is the most characteristic vibration.

If a heteroatom is present at the ortho-position of an O-H group in phenols, a lower frequency of the free O-H stretching is expected compared to meta- and para-substituted phenols due to intra-molecular hydrogen bonding. In comparison to the observed free O-H stretching frequencies (see Table 21), the ν(OH) band of phenol in dilute CCl$_4$ solution appears at 3611 cm^{-1}. Figure 83 shows the spectral region 4000-2000 cm^{-1} for 2-, 3-, and 4-nitrophenol.
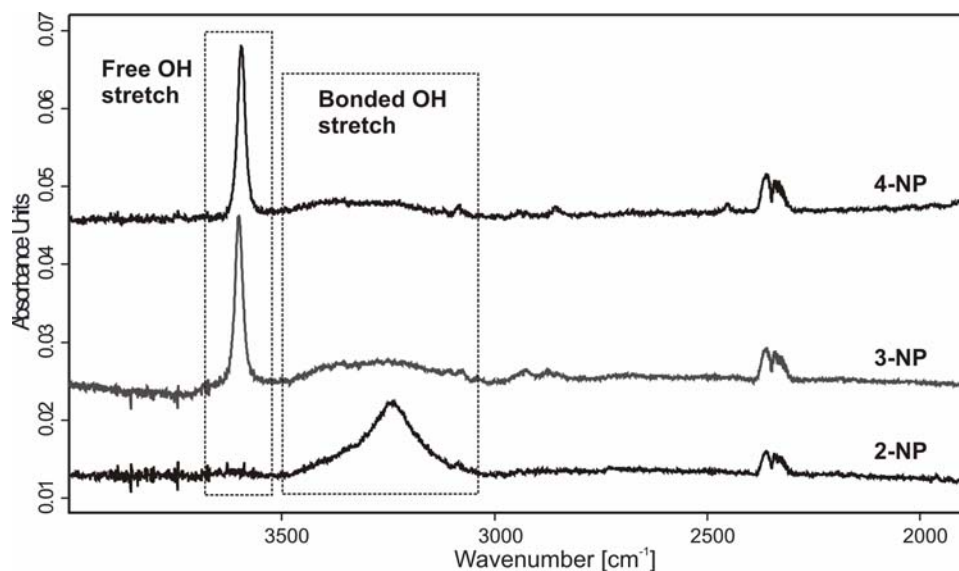
Figure 83 IR spectrum of 2-, 3-, and 4-nitrophenol ($4 \cdot 10^{-3}$ M in CCl_4) in the spectral region 4000-2000 cm^{-1}.

In 2-Nitrophenol, the NO_2 group is in ortho-position to the OH group and is therefore an accessible basic site for the OH group. Therefore, 2-NP shows no band corresponding to the free OH stretching vibration due to intra-molecular hydrogen bonding.

3.4.3.2 Interactions with 4-vinylpyridine

When titrating 4-NP and 3-NP (at 4×10^{-3} M in CCl_4) with increasing amounts of 4-VP (from 0.5×10^{-3} to 20×10^{-3} M in CCl_4), the band corresponding to the free $\nu(OH)$ stretch rapidly disappeared as shown in Figure 84 indicating a hydrogen bonding interaction with 4-VP as soon as it is added.
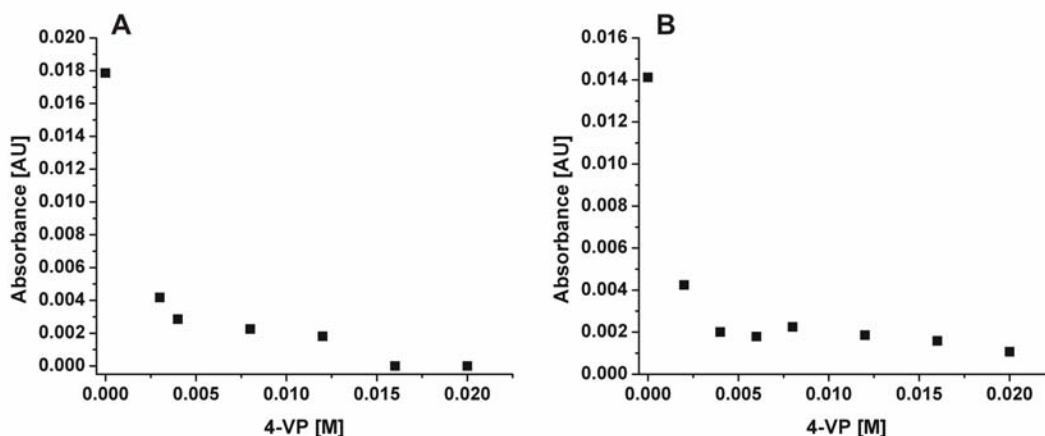
Figure 84 Absorbance of free ν(OH) stretch of 4-NP (A) and 3-NP (B) at a constant concentration of $4 \cdot 10^{-3}$ M in CCl_4 during titration with 4-VP.

In contrast, 2-NP did not show any changes upon addition of 4-VP. Also, no band shift was observed for 2-, 3-, and 4-NP during the titration. However, when monitoring the asymmetric NO_2 stretches a shift towards lower wavenumbers could be observed as shown in Figure 85 for 3-NP and 4-NP.
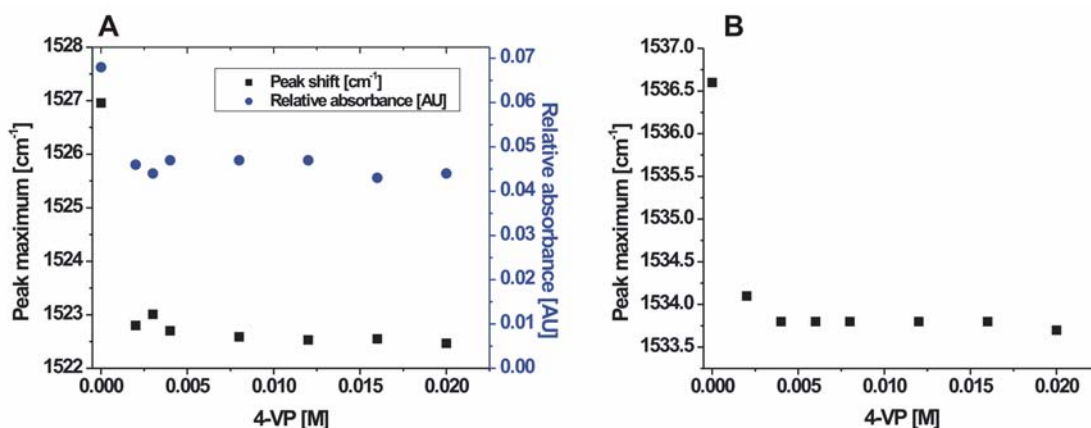
Figure 85 Shift of band corresponding to the asymmetric NO_2 stretch of 4-NP (A) and 3-NP (B) at a constant concentration of $4 \cdot 10^{-3}$ M in CCl_4 during titration with 4-VP.

The shift was more pronounced for 4-NP as compared to 3-NP and indicates a participation of the nitro-group in the complex formation. At constant concentration, the relative absorbance was decreasing during titration as shown in Figure 83A for 4-NP. The peak shifts were strongest after addition of an equimolar amount of functional monomer (1:1). Again, 2-NP did not show any band shifts or changes in intensity during the titration with 4-VP indicating the unavailability of the nitro-group for inter-molecular interactions.

Job's plot analysis was used for the determination of the complex stoichiometry, by monitoring the bands of the free ν(OH) stretch and the symmetric ν(NO$_2$) stretch. The characteristic absorbances were measured in the presence and absence of 4-VP at different nitrophenol concentrations used during preparation of the solutions according to the method of continuous variation. A linear increase in absorbance with increasing concentration was obtained for 2-, 3-, and 4-nitrophenol as shown for the example of 4-NP in Figure 86.
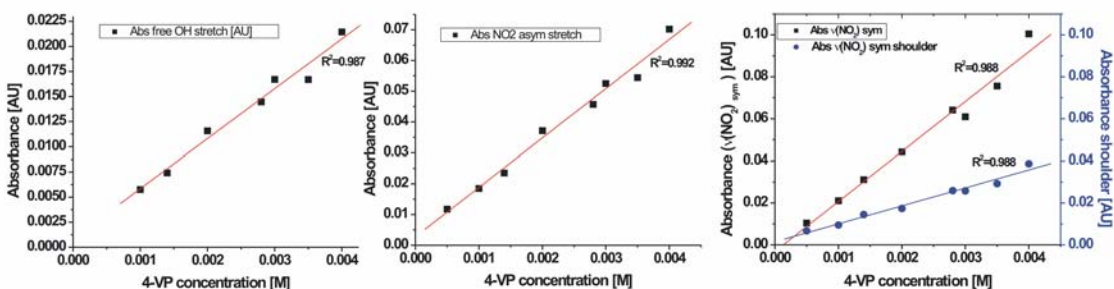
Figure 86 Absorbance of 4-NP bands corresponding to (from left to right) the free ν(OH) stretch, the asymmetric ν(NO$_2$) stretch and the symmetric ν(NO$_2$) stretch with shoulder.

The symmetric NO$_2$ stretching band of nitrophenols revealed a shoulder at lower wavenumbers (at 1339.5 cm^{-1} for 4-NP as shown in Figure 83 and at 1350.5 cm^{-1} for

3-NP). These overlapping bands were resolved using a Levenberg-Marquardt algorithm, which enabled band deconvolution into two separate peaks with a residual RMS error of < 0.001832. For 3- and 4-NP, the absorbance of both the NO_2 stretching band and the shoulder were strongly affected by titration with 4-VP (see Figure 87).
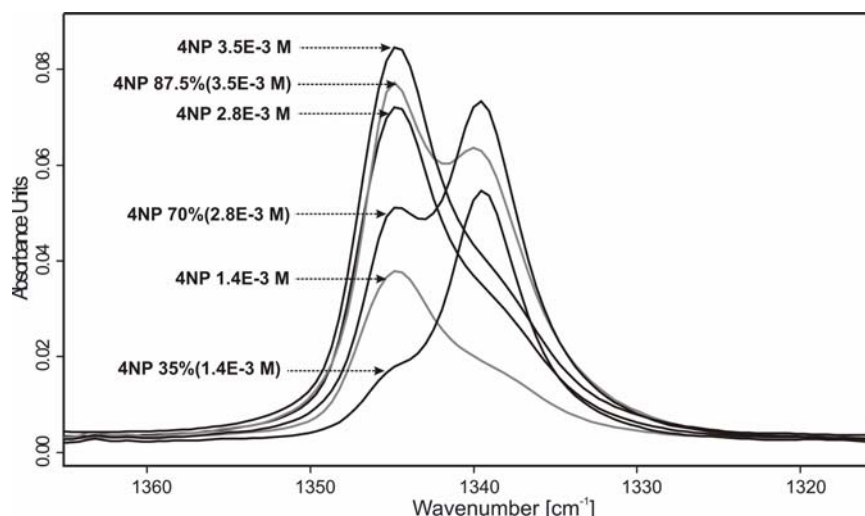
Figure 87 IR spectrum of 4-NP in the region 1365-1315 cm^{-1} showing the NO_2 symmetric stretch at 1344.9 cm^{-1} and the shoulder at 1339.5 cm^{-1}. The functional monomer 4-VP has no bands within this spectral region.

Figure 87 shows a strong difference in absorbance between complexed and non-complexed 4-NP with an increase in absorbance at 1339.5 cm^{-1} in the mixture (shown for 35, 70, and 87.5 % of 4-NP stock solution at 4.10^{-3} M in CCl$_4$) compared to 4-NP only. The 2-NP bands remain unaffected by the 4-VP titration as shown in Figure 88. Job's plot analysis was performed with the changes in absorbances of both the bands corresponding to the free OH stretch and the symmetric NO_2 stretch of the nitrophenols as provided in Figures 88 and 89.
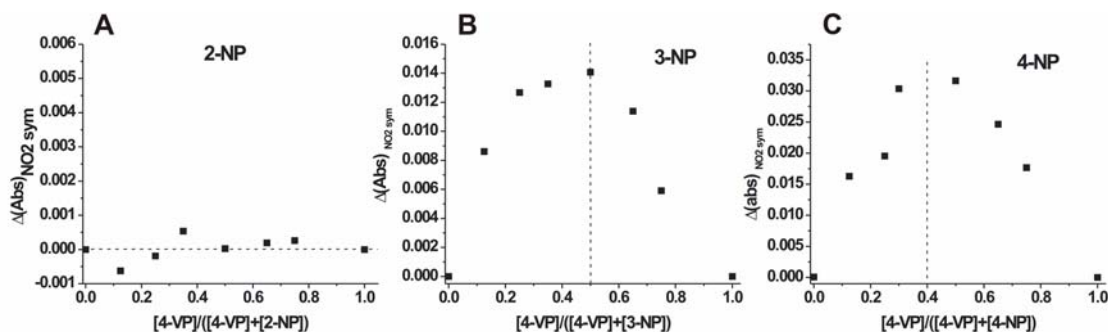
Figure 88 Job's plot analysis with changes in absorbances of the $\nu(NO_2)$ symmetric stretch of 2-NP (A), 3-NP (B), and 4-NP (C).
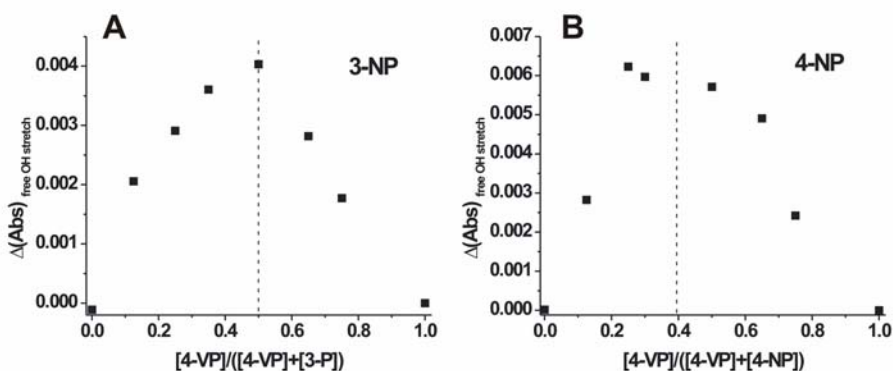
Figure 89 Job's plot analysis with changes in absorbances of the free $\nu(OH)$ stretch of 3-NP (A), and 4-NP (B).

Both the Job's plots based on the $\nu(OH)$ and the $\nu(NO_2)$ show the same results for 3-NP and 4-NP respectively confirming the presence of a single complex since the maximum x_{max} is independent of the wavelength. The Job's plot analysis of the observed 3-NP interactions (Figures 88B and 89A) indicated a ratio of the stoichiometric coefficients of 1 with a maximum at x_{max}= 0.5. Therefore, a 1:1 or possibly a 2:2 (3-NP:4-VP) stoichiometry can be expected, since both of the functional groups of 3-NP have shown changes in spectral features due to complex formation. For 4-NP, the maximum shifts to 0.4, indicating a 3:2 (4-NP:4-VP) stoichiometry. The 2-NP showed no interaction with 4-VP as evident in Figure 88.

Therefore, while in the ortho-position the functional groups are unavailable for complex formation due to intra-molecular hydrogen bonding, moving from the meta- to the para-position results in an increasing number of available molecular interaction sites for complex formation in CCl_4.

Job's plot analysis was also performed by using a characteristic spectral feature of the functional monomer 4-VP. Since the band corresponding to the ν(C=N) frequency overlaps with nitrophenol features, a 4-VP band at 924 cm^{-1} was selected in a spectral region where the nitrophenols do not absorb. The results are shown in Figure 90 for the titration with 4-NP.
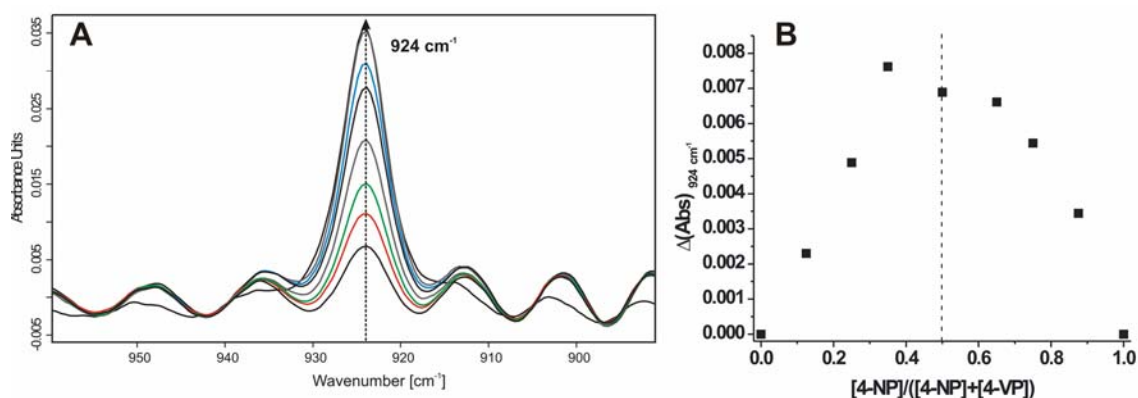
Figure 90 IR spectra of 4-vinylpyridine in the spectral region 960-890 cm^{-1} with increasing 4-VP concentration from $0.5.10^{-3}$ to 4.10^{-3} M in CCl_4 (A) and Job's plot analysis with changes in absorbances of the 4-VP band at 924 cm^{-1} during the titration with 4-nitrophenol (B).

The Job's plot analysis of the observed 4-VP interactions (see Figure 90) indicated a 1:1 or 2:2 (4-VP:4-NP) stoichiometry in CCl_4 with a maximum at $x_{max}= 0.5$. Since the Job's plot analysis of the 4-NP spectral features indicated a 3:2 (4-NP:4-VP) stoichiometry, it may be concluded that two 4-nitrolpenol and one 4-vinylpyridine molecule are probably

involved in complexation with possibly a 4-NP hydroxy group interacting with the nitro group of the second 4-NP molecule as shown in Figure 91.
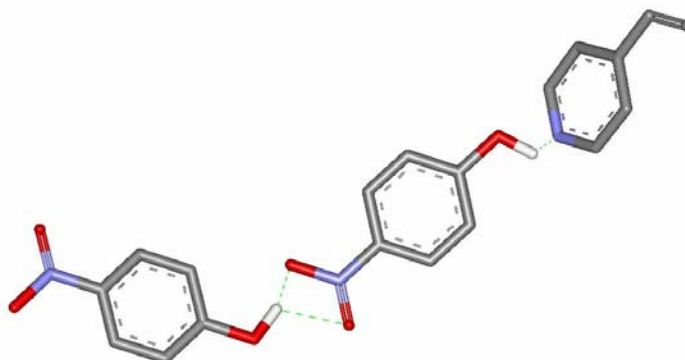
Figure 91 Proposed interactions between 4-nitrophenol and 4-vinylpyridine in CCl$_4$.

In order to confirm the obtained results, Job's plot analysis of ^{1}H-NMR titrations of 4-NP with 4-VP were performed in CD$_3$CN and D$_2$O. During the titration in acetonitrile–d3, the 4-NP hydroxyl proton signal immediately disappeared upon addition of 4-VP as shown in Figure 92(B) for a 1:1 equimolar mixture.
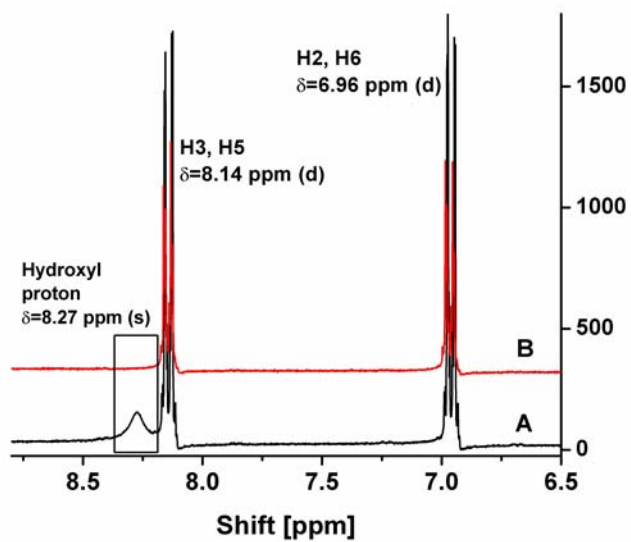
Figure 92 ^{1}H-NMR signals of 4-nitrophenol protons at a concentration of 0.01 M in acetonitrile-d3 (A) and upon addition of one equivalent of 4-vinylpyridine (B). Multiplicities of the signals: (s) singlet, (d) doublet.

The disappearing of the hydroxyl proton signal (δ=8.27 ppm) may suggest a proton exchange occurring faster than the NMR timescale. The OH group therefore interacts with the functional monomer 4-VP, although no further information could be obtained. No shifts are observed for the aromatic protons. In contrast, the titration in D_2O indicated a minute shift of the H2/H6 protons as shown in Figure 93A.
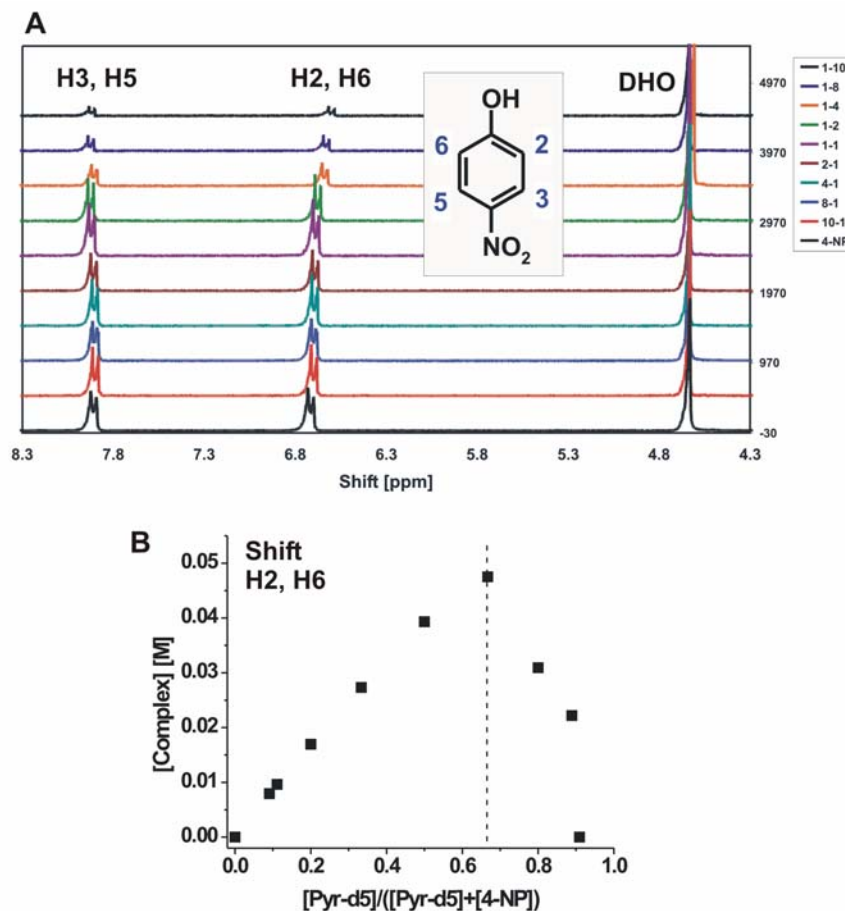
Figure 93 ^{1}H-NMR characterization of 4-NP/4-VP interaction; (A) ^{1}H-NMR spectra of 4-NP in D_2O during titration with 4-VP (bottom: 4-VP only); (B) Job's plot analysis of shift of H2/H6 aromatic protons during titration with 4-VP in D_2O.

The Job's plot analysis of the observed 4-NP interactions (Figure 93B) indicated a 1:2 (4-NP:4-VP) stoichiometry in D_2O with a maximum at x_{max}= 0.67. While studies in CCl_4 (IR) and CD_3CN (NMR) indicated interactions based on the hydroxy- and nitro-functionalities, the study in D_2O (NMR) provided evidence that the aromatic ring is the preferred interaction site in a polar protic solvent with a shift in stoichiometries from 3:2 (CCl_4) to 1:2 (D_2O), probably involving π-π stacking of the 4-NP and two 4-VP rings combined with hydrophobic effects.

The presented results from the IR spectroscopic studies of the nitrophenol/4-vinylpyridine interactions in pre-polymerization solution are in agreement with the HPLC characterization studies of 4-NP and 3-NP imprinted polymers which have previously been performed in our research group [12]. In these studies, the selectivity of imprinted and control HPLC columns for 4-NP, 3-NP, and 2-NP was investigated. The results are summarized in Figures 94 and 95.
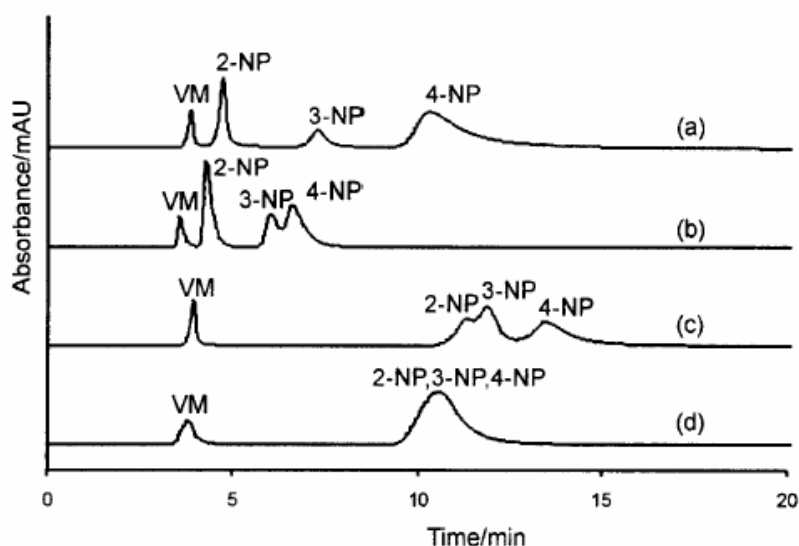
Figure 94 Chromatograms of a mixture of void marker (VM), 2-NP, 3-NP, and 4-NP applying (a) 4-NP imprinted polymer as HPLC stationary phase with an organic mobile phase (acetonitrile:heptane:acetic acid, 94:5:1, v/v/v); (b) control polymer as HPLC stationary phase with the organic mobile phase; (c) 4-NP imprinted polymer as HPLC stationary phase with an aqueous mobile phase (phosphate buffer (40 mmol):acetonitrile:acetic acid, 490:500:10, v/v/v); (d) control polymer as HPLC stationary phase with the aqueous mobile phase. The flow rate was kept constant at 1 mL/min throughout the whole study. From M. Janotta et al, *Intern. J. Environ. Anal. Chem.* **2001**, 80(2), 75-86.

In both organic (Figure 94 (a)) and aqueous (Figure 94 (c)) phase, the 4-NP imprinted polymer showed a markedly stronger affinity for the template 4-NP, separating 4-NP from the other nitrophenols. The selectivity was highest in the aprotic organic phase achieving baseline separation of the structural nitrophenol isomers.
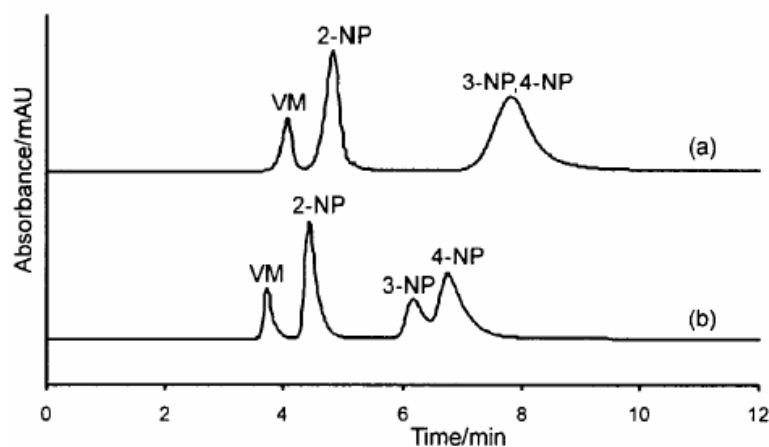
Figure 95 Chromatograms of a mixture of void marker (VM), 4-NP, 3-NP, and 2-NP applying (a) 3-NP imprinted polymer as HPLC stationary phase with an organic mobile phase (acetonitrile:heptane:acetic acid, 94:5:1, v/v/v); (b) control polymer as HPLC stationary phase with the organic mobile phase. The flow rate was kept constant at 1 mL/min throughout the whole study. From M. Janotta et al, *Intern. J. Environ. Anal. Chem.* **2001**, 80(2), 75-86.

In contrast, the 3-NP imprinted polymer did not show any affinity for the template molecule 3-NP compared to 4-NP and did not facilitate chromatographic separation of 3-NP and 4-NP when applied as a mixture (see Figure 95).

Spectroscopic pre-polymerization studies in CCl_4 (IR) and CD_3CN (NMR) indicated that nitrophenol/4-VP interactions were based on the hydroxy- and nitro-functionalities, while the study in D_2O (NMR) provided evidence that the aromatic ring was the preferred interaction site in a polar protic solvent. These findings explain the lower selectivity of the 4-NP imprinted MIP in the aqueous eluent compared to the organic eluent as demonstrated in Figure 94, since the hydrogen bonding interaction is disrupted in the presence of water. Furthermore, Job's plot analysis of the observed 3-NP interactions (Figures 88B and 89A) indicated a 1:1 (4-NP:4-VP) stoichiometry while Job's plot analysis of the observed 4-NP interactions (Figures 88C and 89B) indicated a 3:2 (4-NP:4-VP) stoichiometry. These results are reflected in the chromatograms shown in Figures 94 and 95, with the 4-NP imprinted polymer providing a higher selectivity

towards the templated analyte in contrast to the 3-NP imprinted polymer. Evidently, moving the nitro-group from the meta- to the para-position resulted in an increasing number of available molecular interaction sites for the complex formation in the pre-polymerization solution. In ortho-position, the functional groups are not available for complex formation due to intra-molecular hydrogen bonding, which results in rapid elution from both the 3-NP and 4-NP imprinted columns.

In analogy to the results obtained when comparing the spectroscopic pre-polymerization investigations of the template 2,4-D to the chromatographic characterization of 2,4-D with imprinted and control columns, the results obtained for the nitrophenol studies would have provided optimized imprinting strategies for nitrophenols and again corroborate the feasibility of using IR spectroscopy for predicting the suitability of selected template analytes for successful imprinting. The results also demonstrate that - although the template/functional monomer interactions will vary according to the experimental conditions in the pre-polymerization solution and during the polymerization process - investigating the pre-polymerization solution provides valuable indications on the preferred molecular interactions, which will ultimately lead to the formation of high affinity binding sites.

3.4.3.3 Interactions with methacrylic acid

Besides 4-vinylpyridine, methacrylic acid (MAA) is a very commonly used functional monomer in molecular imprinting and was also tested as monomer for nitrophenol imprinting. The MIPs prepared using MAA did not show an imprinting effect as opposed to the MIPs prepared using 4-VP. The interactions between 2-, 3-, and 4-nitrophenol and MAA were therefore also investigated in pre-polymerization solution by IR spectroscopy.

When titrating 4-NP (at 4×10^{-3} M in CCl_4) with increasing amounts of MAA (from 2×10^{-3} to 20×10^{-3} M in CCl_4), the band corresponding to the free $\nu(OH)$ stretching of 4-NP did not show any changes in absorbance as opposed to the results observed when adding 4-VP. Results therefore indicated no interaction of the OH group of 4-NP with MAA. Furthermore, Job's plot analysis was also performed by using characteristic spectral features from both 4-NP and the functional monomer MAA (see Figure 96).
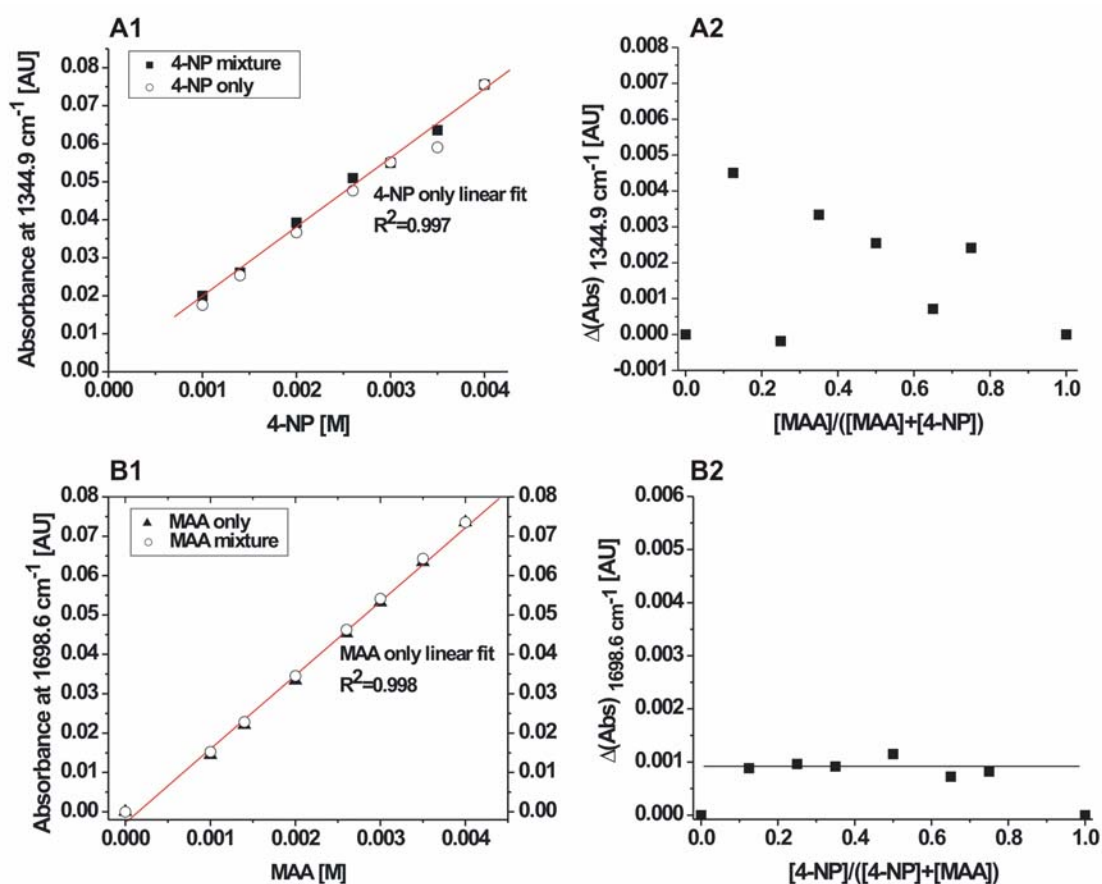
Figure 96 IR Job's Plot analysis (A2 and B2) using (A1) absorbance of the band corresponding to the $\nu(NO_2)$ symmetric stretch of 4-nitrophenol and (B1) corresponding to the $\nu(C=O)$ stretch of methacrylic acid.

Both absorbances of the 4-NP NO_2 symmetric stretch and the MAA C=O stretch linearly increase with increasing concentration (see A1 and B1 respectively in Figure 96). The

Job's plot analysis from 4-NP (Figure 96-A2) gave poorly interpretable results while the Job's plot analysis from MAA (Figure 96-B2) clearly indicated no interaction. Results were confirmed at several wavelengths and indicate unfavorable interaction of MAA with 4-NP in competing with acid self-association. Both 3-NP and 2-NP showed the same results with no changes in spectral features upon titration with MAA.

IR Job's plot analysis of the system nitrophenols/MAA in CCl_4 showed that there was no particular interaction between the nitrophenols and MAA, explaining the absence of selectivity obtained with the MIPs imprinted using MAA as functional monomer.

3.4.4 Conclusions

The vibrational absorbance features of o-, m-, and p-nitrophenol were analyzed by IR spectroscopy in order to investigate non-covalent interactions involved during complex formation with the functional monomers 4-vinylpyridine (used in MIP synthesis with p-nitrophenol) and methacrylic acid (manuscript in preparation). Hydrogen bonds play an important role in complex formation strongly influencing the type of complexes that can be formed based on the steric distribution of functional groups at the template molecule. The presented study with o-, m-, and p-nitrophenol demonstrated the participation of hydrogen bonds in complex formation with the functional monomer 4-vinylpyridine. The reactivity of the individual OH groups is clearly depended on their position relative to the second functionality, the nitro-group. In dilute aprotic solutions, intra-molecular hydrogen bonding strongly competes with inter-molecular hydrogen bonding if sterically favorable conditions are provided, as shown for o-nitrophenol. Furthermore, the participation of the nitro-group in complex formation of m- and p-nitrophenol was demonstrated. Also, the functional monomer MAA showed no interaction with the nitrophenols demonstrating the

unsuitability of MAA as a functional monomer for imprinting of nitrophenols. IR Job's plot

analysis was introduced for the first time as a rapid method for the determination of the

complex stoichiometry, which offers a new route of effective pre-screening for

template/functional monomer selection.

4. CONCLUSION AND OUTLOOK

The self-assembly approach for the synthesis of molecularly imprinted polymers has demonstrated great potential for producing selective, highly cross-linked polymeric biomimetic materials in a straight forward method. By adding a template molecule to a mixture containing the functional monomer and cross-linker in porogenic solution and starting a radical polymerization, molecularly imprinted polymers can be obtained in the required format. Many examples throughout literature demonstrate the successful application of MIPs as synthetic recognition material in sample preparation, chromatographic separation, and as antibody substituents in binding assays [12,72,154,155]. Nevertheless, many factors such as the choice of functional monomer, cross-linker, and porogenic solvent, as well as the ratio between template, functional monomer, and cross-linker will affect the resulting imprinting efficiency, as demonstrated by the example of imprinting the antioxidant quercetin. Especially when using either expensive or toxic templates such as the mycotoxins zearalenone and deoxynivalenol, a trial-and error approach for screening appropriate imprinting components is a limiting option unless 'dummy' templates can be used. Nevertheless, MIPs for mycotoxins offer an interesting alternative to the antibodies used for sample pre-concentration in mycotoxin analysis. Molecularly imprinted solid phase extraction allowed pre-concentration of zearalenone from spiked beer samples without preceding clean-up steps. Despite the general advantages of MIPs including thermal, chemical, and mechanical stability, non-covalently imprinted polymers are characterized by substantial binding site heterogeneity with a low percentage of high affinity binding sites, which has limited their practical application. Based on these considerations, improving the binding characteristics of MIPs by developing highly optimized imprinted polymers is necessary.

Consequently, this thesis aimed at a rational understanding of the principles underlying formation of binding sites investigating molecular level interactions between the components involved in imprinting at the pre-polymerization stage. For this purpose, 2,4-dichlorophenoxyacetic acid, and 2-, 3-, and 4-nitrophenol were used as model templates. The interactions between the templates and the commonly used functional monomers 4-vinylpyridine and methacrylic acid as well as the effect of the cross-linker on complex formation were investigated by FT-IR and ^{1}H-NMR spectroscopic titration measurements. The obtained results demonstrated the feasibility and utility of using two complementary spectroscopic techniques for determining complex stoichiometries, binding interactions and interaction strengths during complex formation based on hydrogen-bonding, π-π stacking, hydrophobic, and electrostatic effects in dependence of the applied solvent. IR spectroscopy was applied for the analysis of hydrogen-bonded complexes in IR transparent carbon tetrachloride solution enabling simultaneous studies of the free and complexed species confirming IR spectroscopy as a powerful technique for investigating molecular level interactions. ^{1}H-NMR spectroscopy is among the most important methods applied in supramolecular chemistry for the determination of association constants and enabled complementary analysis of the complexation events in the pre-polymerization solution. Measurements were performed in more polar or protic solvents (in contrast to carbon tetrachloride) as well as deuterated water. The obtained results demonstrated that the concerted application of IR and NMR spectroscopic techniques offers a powerful strategy for pre-screening the interactions between the imprinting building blocks and their ratios based on the determination of interaction sites, binding constants, and complex stoichiometries. Furthermore, preliminary results of molecular dynamics simulations of the model analyte 2,4-dichlorophenoxyacetic acid modeling the interactions of 2,4-D with 4-vinylpyridine in explicit solvent (water and chloroform respectively) revealed that MD simulations are a promising tool following

molecular-level interactions. The simulations resulted in a trajectory of the molecules at a nanosecond timescale directly visualizing the interacting groups. Furthermore, factors known to affect imprinting such as solvation effects may be assessed with MD simulations by e.g. calculating solvation free energies of selected conformations. The incorporation of IR and NMR data (1D and 2D) into MD simulations would significantly improve the control of the starting configurations rendering MD simulations a useful tool for investigating physical and chemical phenomena. Thereby, appropriate candidate molecules with high selectivity for a specific target analyte can be identified in a predictive process. From the present body of work it can be concluded that monitoring and understanding the non-covalent interactions responsible for complex formation and complex stability in the pre-polymerization solution (and ideally during the polymerization) and effects resulting from variation of the polymerization components, amounts and polymerization conditions on the complex formation are the key towards developing optimized imprinted polymers as these factors directly affect the binding site heterogeneity. Furthermore, the importance of simultaneous multiple-site interactions for increased complex stability was demonstrated. 2,4-dichlorophenoxyacetic acid was investigated as a model analyte confirming that the predicted ratios of MIP building blocks derived from IR and ^{1}H-NMR investigations were in agreement with results obtained for successfully imprinted MIPs. Thereby, it was demonstrated that pre-screening in solution facilitates determining optimized polymerization conditions and has direct impact on the selectivity of the finally obtained biomimetic material.

APPENDIX A

The AMBER7 package [135]

- <u>AMBER7</u>: The AMBER7 package consists of over 60 programs with the most important ones briefly described below.

- *Antechamber***:** This program suite automates the process of developing force field descriptors for most organic molecules. *Antechamber* generates from the respective PDB files (PDB format) new ('prepin') files with a format that can be read into *LEaP* for use in molecular modeling. The force field description that is generated is designed to be compatible with the usual Amber force fields.

- *Parmchk*: *Parmchk* reads in an 'ac' file or a 'prep' input file as well as a force field file. It writes out a 'frcmod' file for the missing parameters.

- *LEaP*: *LEaP* is an X-windows-based program that provides for basic model building and AMBER coordinate and parameter/topology input file creation. It includes a molecular editor which allows for building residues and manipulating molecules.

- *Sander* (simulated annealing with NMR-derived energy restraints): *Sander* is the main program used for molecular dynamics simulations. This program relaxes the structure by iteratively moving the atoms down the energy gradient until a sufficiently low average gradient is obtained. The molecular dynamics portion generates configurations of the system by integrating Newtonian equations of motion. MD will sample more configurational space than minimization, and will allow the structure to cross over small potential energy barriers. Configurations may be saved at regular intervals during the simulation for later analysis, and basic free energy calculations using thermodynamic integration may be carried out. It allows for NMR refinement based on NOE-derived

distance restraints, torsion angle restraints, and penalty functions based on chemical shifts and NOESY volumes.

- *Ptraj* and *Carnal*: programs to analyze MD trajectories, computing (e.g. RMS deviation from a reference structure), hydrogen bonding analysis, time-correlation functions, diffusional behavior, etc.

- **AMBER7 parameter/topology file formats**

The basic files necessary to run sander (named as the default names) are:

- **'prmtop'**: a description of the molecular topology, force field parameters, periodic box type, atom and residue names

- **'prmcrd'**: (or a 'restrt' file from a previous run): a description of the coordinates and optionally the velocities and current box dimensions

- **'mdin'**: the *Sander* input file which is a series of namelists and control variables

- **'mdout'**: output format, user readable state information and diagnostics

- **'restrt'**: final coordinates, velocity, and box dimensions; file used for restarting/continuing an MD run

- **Preparation of structure files for use in *LEaP* with *Antechamber* and *Parmchk***

AMBER7 is supplied with applications (*Antechamber* and *Parmchk*) designed to modify and rectify flaws in imported structural files. The first step in the generation of the 2,4-D/4-VP system for molecular dynamics simulation was therefore to prepare the input in a suitable format. Having created the 'prepin' input file required by *LEaP* for energy minimization, the program *Parmchk* was used to investigate whether the 'prepin' file violates the requirements for application of the force field at the next stage. For this type of application, the 'gaff' (**g**eneral **A**mber **f**orce **f**ield) force field was used. *Parmchk*

213

identifies missing parameters in the 'prepin' file and also creates any necessary force field modifications in an 'frcmod' file.

- <u>Solvatization and preparation of structural files for use in *Sander*, *xLEaP* and *tLEaP*</u>

The structures prepared with *Antechamber* and *Parmchk* were introduced into *LEaP* for visualization. The *LEaP* program is also necessary to generate the two types of file required for the actual minimization run - a list of Cartesian coordinates of all atoms in the file ('prmcrd' file) and a topology file ('prmtop' file). These two files are the only format accepted by *Sander*, employed in energy minimization, molecular dynamics, and simulated annealing analyses.

- <u>Energy minimization</u>

The minimization steps as well as restraints are written into one text input file, from where *Sander* read all commands and applied them to the system. *Sander* also reports on the energy state of the system at regular intervals (the frequency of which is determined by the user) by writing an 'mdinfo' file, which tells the user the energy state of the system at the last step recorded. The coordinates of the atoms at each step recorded are output to a coordinate file ('mdcrd'), permitting the user to later examine the movements of the complex during minimization using molecular dynamics visualization programs (such as the *VMD* package). The final coordinates of the system at the end of the run are written to a file called restart file. The trajectory saved as 'md.crd' file and can be viewed with *VMD*, associated with the 'restrt' file as starting frame and contains five frames per ps. However, of greatest interest to the user will be the 'mdout' file created by *Sander* which documents energy changes for the duration of the minimization run.

- Equilibration

In MD simulations, atoms of the macromolecules and of the surrounding solvent undergo a relaxation that usually lasts for tens or hundreds of picoseconds before the system reaches a stationary state. Thermodynamic properties such as temperature, energy, and density are monitored until the values are stable. The initial non-stationary segment of the simulated trajectory is discarded in the calculation of equilibrium properties. Before running long MD runs, the system must be equilibrated using volume, pressure and temperature control to adjust e.g. the density of the solvent to experimental values. For a periodic system, constant pressure is the only way to equilibrate density if the starting state is not correct. Another potential problem is small gaps at the edges of the box. Every system must be equilibrated first at constant volume to something close to the final temperature, before turning on constant pressure. The system must then be equilibrated at constant pressure (ntb= 2, ntp > 0) to get to a proper density. The pressure may be maintained at a constant defined value by e.g. scaling the volume. In AMBER, the system is coupled to an external bath of constant pressure and/or temperature.

- Simulated annealing

A short simulated annealing run was performed with the 2,4-D/4-VP system in explicit solvent (water and chloroform respectively) after equilibration. Note that with explicit solvent simulations, a significant effort must be made to prepare and equilibrate the sample to obtain reasonable starting structures. The MD run was performed under constant volume conditions and includes some (mild) heating and cooling for simulated annealing. The starting temperature after the equilibration was 300 K. Following simulated annealing algorithm was used in a 20 ps run (20000 steps) after the equilibration run as shown in Figure 97:

- From steps 0 to 5000: heat the system to 600 K ('tautp' = 0.4 ps)

- From steps 5001-18000: re-cool to low temperatures (100 K) with long 'tautp' ('tautp'= 4 ps)

- From steps 18001-20000: final cooling with short 'tautp' (from steps18001 to 19000 'tautp' = 1 ps, and from steps 19001 to 20000 'tautp' = 0.1 ps down to 0.05 ps)
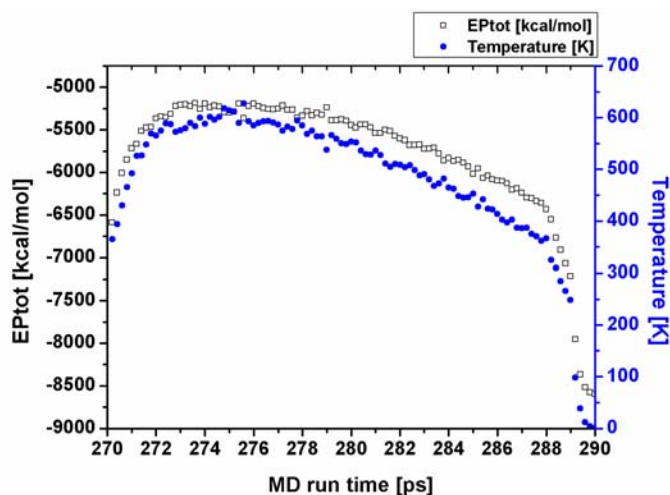
Figure 97 Simulated annealing run for the 2,4-D/4-VP system in water. Temperature and total potential energy against MD simulation time.

APPENDIX B

Starting configurations (PDB) and 'mdin' input files for

MD runs in *Sander*

For details on mdin command lines refer to http://amber.scripps.edu/doc7/amber7.pdf.

- PDB file of 2,4-D/4-VP complex, π-stacking starting configuration

```
ATOM     1 O1   24D   1     3.537  1.423  0.000 1.00 0.00
ATOM     2 H11  24D   1     3.544  1.733  0.950 1.00 0.00
ATOM     3 C3   24D   1     4.764  0.871 -0.315 1.00 0.00
ATOM     4 O2   24D   1     4.963  0.424 -1.452 1.00 0.00
ATOM     5 C4   24D   1     5.851  0.742  0.797 1.00 0.00
ATOM     6 H41  24D   1     6.066  1.662  1.128 1.00 0.00
ATOM     7 H42  24D   1     5.465  0.200  1.544 1.00 0.00
ATOM     8 O5   24D   1     7.109  0.105  0.372 1.00 0.00
ATOM     9 C8   24D   1     7.243 -1.346  0.448 1.00 0.00
ATOM    10 C9   24D   1     8.513 -1.907 -0.081 1.00 0.00
ATOM    11 Cl6  24D   1     9.733 -0.853 -0.629 1.00 0.00
ATOM    12 C10  24D   1     8.700 -3.236 -0.128 1.00 0.00
ATOM    13 H11  24D   1     9.553 -3.611 -0.492 1.00 0.00
ATOM    14 C11  24D   1     7.625 -4.149  0.367 1.00 0.00
ATOM    15 Cl7  24D   1     7.821 -5.842  0.262 1.00 0.00
ATOM    16 C12  24D   1     6.498 -3.649  0.889 1.00 0.00
ATOM    17 H11  24D   1     5.792 -4.263  1.243 1.00 0.00
ATOM    18 C13  24D   1     6.305 -2.196  0.939 1.00 0.00
ATOM    19 H11  24D   1     5.468 -1.824  1.342 1.00 0.00
TER
ENDMDL
TER
ATOM     1 C2   4VP   2     1.242  1.098 -2.107 1.00 0.00
ATOM     2 H10  4VP   2     0.249  1.005 -2.035 1.00 0.00
ATOM     3 C1   4VP   2     2.019  1.160 -0.965 1.00 0.00
ATOM     4 H9   4VP   2     1.590  1.110 -0.063 1.00 0.00
ATOM     5 N3   4VP   2     3.392  1.289 -1.079 1.00 0.00
ATOM     6 C5   4VP   2     3.998  1.358 -2.321 1.00 0.00
ATOM     7 H11  4VP   2     4.990  1.452 -2.394 1.00 0.00
ATOM     8 C6   4VP   2     3.221  1.297 -3.464 1.00 0.00
ATOM     9 H12  4VP   2     3.650  1.346 -4.364 1.00 0.00
ATOM    10 C4   4VP   2     1.847  1.168 -3.352 1.00 0.00
ATOM    11 C7   4VP   2     1.023  1.102 -4.572 1.00 0.00
ATOM    12 H13  4VP   2     1.086  0.378 -5.258 1.00 0.00
```

```
ATOM    13 C8   4VP   2     0.112  2.052 -4.824 1.00 0.00
ATOM    14 H14  4VP   2    -0.444  2.003 -5.654 1.00 0.00
ATOM    15 H15  4VP   2    -0.010  2.811 -4.185 1.00 0.00
TER
ENDMDL
```

- PDB file of 2,4-D/4-VP complex, H-bonding starting configuration

```
ATOM     1 C18  24D   1     2.568 -1.315 -1.108 1.00 0.00
ATOM     2 C1   24D   1     0.864 -1.096 -1.033 1.00 0.00
ATOM     3 C2   24D   1     0.017 -2.075 -1.530 1.00 0.00
ATOM     4 H14  24D   1     0.396 -2.909 -1.931 1.00 0.00
ATOM     5 C4   24D   1    -1.355 -1.897 -1.469 1.00 0.00
ATOM     6 Cl7  24D   1    -2.407 -3.111 -2.086 1.00 0.00
ATOM     7 C6   24D   1    -1.879 -0.742 -0.911 1.00 0.00
ATOM     8 H16  24D   1    -2.871 -0.614 -0.867 1.00 0.00
ATOM     9 C5   24D   1    -1.031  0.236 -0.416 1.00 0.00
ATOM    10 H15  24D   1    -1.412  1.070 -0.015 1.00 0.00
ATOM    11 C3   24D   1     0.343  0.061 -0.476 1.00 0.00
ATOM    12 O9   24D   1     1.169  1.033  0.014 1.00 0.00
ATOM    13 C10  24D   1     2.586  0.944 -0.090 1.00 0.00
ATOM    14 H17  24D   1     2.825  0.932 -1.061 1.00 0.00
ATOM    15 H18  24D   1     2.875  0.087  0.336 1.00 0.00
ATOM    16 C11  24D   1     3.235  2.122  0.597 1.00 0.00
ATOM    17 O13  24D   1     4.592  2.204  0.658 1.00 0.00
ATOM    18 H19  24D   1     5.025  2.990  1.101 1.00 0.00
ATOM    19 O12  24D   1     2.552  2.996  1.080 1.00 0.00
TER
ATOM     1 C1   4VP   1     6.681  6.107  1.002 1.00 0.00
ATOM     2 H9   4VP   1     7.424  6.513  1.537 1.00 0.00
ATOM     3 C2   4VP   1     6.618  4.735  0.832 1.00 0.00
ATOM     4 H10  4VP   1     7.315  4.147  1.243 1.00 0.00
ATOM     5 N4   4VP   1     5.588  4.186  0.090 1.00 0.00
ATOM     6 C6   4VP   1     4.618  4.991 -0.484 1.00 0.00
ATOM     7 H12  4VP   1     3.878  4.585 -1.018 1.00 0.00
ATOM     8 C5   4VP   1     4.681  6.361 -0.313 1.00 0.00
ATOM     9 H11  4VP   1     3.985  6.951 -0.724 1.00 0.00
ATOM    10 C3   4VP   1     5.712  6.913  0.429 1.00 0.00
ATOM    11 C7   4VP   1     5.776  8.373  0.609 1.00 0.00
ATOM    12 H13  4VP   1     5.080  8.918  1.078 1.00 0.00
ATOM    13 C8   4VP   1     6.815  9.069  0.129 1.00 0.00
ATOM    14 H14  4VP   1     6.853 10.062  0.254 1.00 0.00
ATOM    15 H15  4VP   1     7.553  8.598 -0.354 1.00 0.00
TER
```

- Energy minimization, no restraints

```
minimization
 &cntrl
   imin=1,
   ntc=1, ntb=1,
   maxcyc=500, ntpr=25,
 &end
```

- Energy minimization, restraints: e.g. water restrained

```
 minimization
 &cntrl
   imin=1,
   ntr=1,
   ntc=1,
   ntb=1,
   maxcyc=500, ntpr=25,
 &end
Group input for restrained water atoms
100.0
WAT 3 718
END
END
```

- Equilibration MD run, constant volume (cV1)

```
molecular dynamics run
 &cntrl
   imin=0, irest=0, ntx=1,
   ntt=1, temp0=300.0, tautp=2,
   ntp=0, taup=0.2,
   ntb=1, ntc=2, ntf=2,
   nstlim=5000,
   ntwe=200, ntwx=200, ntpr=50,
 &end
```

- Equilibration MD run, constant pressure (cP1)

```
molecular dynamics run
 &cntrl
   imin=0, irest=1, ntx=7,
   ntt=1, temp0=300.0, tautp=2,
   ntp=1, taup=0.05,
   ntb=2, ntc=2, ntf=2,
   nstlim=5000,
   ntwe=200, ntwx=200, ntpr=50,
```

&end

For cP2 and cP3, 'taup' was changed to 0.5 and 5 respectively. After energy minimization, cV1, cP1, cP2, and cP3, a long equilibration run cP4 was performed. The runs cV1, cP1, cP2, and cP3 were performed with 50000 steps. For cP4, 'taup' was changed to 1 and 'nstlim' to the required run time e.g. 250000 steps (250 ps with 0.001 ps per step).

- Equilibration MD run with distance restraint

```
MD
&cntrl
imin=0, nmropt=1,
ntx=7, iwrap=1,
irest=1, temp0=300,
tautp=0.2, ntt=1,
ntb=2, ntp=1, taup=0.05,
ntc=2, ntf=2,
nstlim=250000,
ntwe=100, ntwx=100, ntpr=25
&end
&wt
  type='REST',
  istep1=1,
  istep2=5000,
  value1=1,
  value2=1
&end
&wt type='END'  &end
LISTIN=POUT
LISTOUT=POUT
DISANG=RST.dist
```

The file 'RST.dist' has to be defined with the 'mdin' file:

Distance restraint between the 2,4-D aromatic ring and the 4-VP ring (atoms of a ring defined as a group):

```
&rst
  ixpk= 0, nxpk= 0, iat=  -1, -1, 0, 0, r1= 1.30, r2= 1.80, r3= 3.40, r4= 3.90,
     igr1=  9,  10,  12,  14,  16,  18, igr2=  20,  22,  24,  25,  27,  29,
     rk2=20.0, rk3=20.0, ialtd=0
```

```
 &end
 &rst
  iat=0,0,0,0
 &end
```

Distance restraint between 2,4-D (residue 1, atom H19) and 4-VP (residue 2, atom N4):

```
#
#  1  24D H19     2  4VP N4          3.0
 &rst
  ixpk= 0, nxpk= 0, iat=  18,  24, r1= 1.30, r2= 1.80, r3= 3.00, r4= 3.50,
     rk2=20.0, rk3=20.0, ir6=1, ialtd=0,
 &end
```

'Make DIST_RST' gives the default value 20.0 kcal/mol.A for rk2 and rk3 (if rk2 = 0 kcal/mol.A there will be no lower bound between two atoms. This is reasonable with molecular mechanics refinement because the van der Waals parameters in the force field will not allow two non-bonded atoms to get closer than they should be). In the command line, IAT(1) to IAT(4) are the atoms defining the restraint. If IAT(3) ≤ 0, it is a distance restraint. If IAT(4) ≤ 0, it is an angle restraint. Otherwise, it is a torsional (or J-coupling, if desired) restraint. If a distance restraint is chosen, and IAT(1) < 0, then a group of atoms is defined as well, and the coordinate-averaged position of this group will be used in place of the coordinates of atom 1 [IAT(1)]. Similarly, if IAT(2) < 0, a group of atoms will be defined below whose coordinate-averaged position will be used in place of the coordinates for atom 2 [IAT(2)].

- Simulated annealing

```
simulated annealing protocol, 20 ps
 &cntrl
   imin=0, irest=1, ntx=7,
   nstlim=20000, pencut=0.1,
   nmropt=1, ntb=1, tautp=2.0,
   ntpr=200, ntt=1, ntwx=200,
   iwrap=1, scee=1.2, ntc=2,
   vlimit=10,
```

```
 &end
#
#Simple simulated annealing algorithm:
#
#from steps 0 to 5000: heat the system to 600K
#from steps 5001-18000: re-cool to low temperatures with long tautp
#from steps 18001-20000: final cooling with short tautp
#
 &wt type='TEMP0', istep1=0,istep2=5000,value1=600.,
       value2=600.,    &end
 &wt type='TEMP0', istep1=5001, istep2=18000, value1=600.0,
       value2=100.0,    &end
 &wt type='TEMP0', istep1=18001, istep2=20000, value1=0.0,
       value2=0.0,    &end

 &wt type='TAUTP', istep1=0,istep2=5000,value1=0.4,
       value2=0.4,    &end
 &wt type='TAUTP', istep1=5001,istep2=18000,value1=4.0,
       value2=4.0,    &end
 &wt type='TAUTP', istep1=18001,istep2=19000,value1=1.0,
       value2=1.0,    &end
 &wt type='TAUTP', istep1=19001,istep2=20000,value1=0.1,
       value2=0.05,   &end

 &wt type='END'  &end
LISTOUT=POUT
```

APPENDIX C

LIST OF PUBLICATIONS

1) Weiss, R.; <u>Molinelli, A</u>.; Jakusch, M.; Mizaikoff, B. Molecular imprinting and solid phase extraction of flavonoid compounds. *Bioseparation* **2002**, 10, 379-387.

2) <u>Molinelli, A</u>.; Weiss, R.; Mizaikoff, B. Advanced solid phase extraction using molecularly imprinted polymers for the determination of quercetin in red wine. *J. Agric. Food Chem.* **2002**, 50(7), 1804-1808.

3) <u>Molinelli, A</u>.; Janotta, M.; Mizaikoff, B. Molecularly imprinted polymers for biomolecular recognition. Chapter 11; Protein nanotechnology: protocols, instrumentation, and applications; Ed. T. Vo Dinh (Methods in molecular biology, Vol. 300). Humana Press Inc.: Totowa, NJ, USA; in press **2004**.

4) O'Mahony, J.; <u>Molinelli, A</u>.; Nolan, K.; Smyth, M. R.; Mizaikoff, B. Towards the rational development of molecularly imprinted polymers: ^{1}H-NMR studies on hydrophobicity and ion-pair interactions as driving forces for selectivity. *Biosens. Bioelectron*.; in press **2004**.

5) Krska, R.; Welzig, E.; Berthiller, F.; <u>Molinelli, A</u>.; Mizaikoff, B. Advances in analysis of mycotoxins and its quality assurance. *Anal. Bioanal. Chem*.; accepted **2004**.

6) <u>Molinelli, A</u>.; Mizaikoff, B. How molecularly imprinted polymers work…or why they might not work. *Anal. Chem*.; accepted **2004**.

7) <u>Molinelli, A</u>.; O'Mahony, J.; Nolan, K.; Smyth, M. R.; Mizaikoff, B. The nature of molecularly imprinted materials: analyzing the mechanisms of selectivity in 2,4-dichlorophenoxyaceetic acid imprints. *Anal. Chem*.; submitted **2004**.

8) O'Mahony, J.; <u>Molinelli, A</u>.; Nolan, K.; Smyth, M. R.; Mizaikoff, B. Anatomy of a successful imprint: analyzing the recognition mechanisms of a molecularly imprinted polymer for quercetin. *Biosens. Bioelectron.*; submitted **2004**.

9) Wei, S.; <u>Molinelli, A</u>.; Mizaikoff, B. Imprinted micro- and nanospheres for β-estradiol. *Anal. Chem.*; submitted **2004**.

10) <u>Molinelli, A</u>.; Mizaikoff, B. IR Job's plot analysis for probing pre-polymerization complex formation during non-covalent molecular imprinting. Manuscript in preparation to *J. Am. Chem. Soc.* **2004**.

11) <u>Molinelli, A</u>.; Weiss, R.; Mizaikoff, B. Molecularly imprinted solid phase extraction for the determination of 2,4-dichlorophenoxyacetic acid in red wine. Manuscript in preparation to *J. Agric. Food Chem*. **2004**.

12) <u>Molinelli, A</u>.; Krska, R.; Mizaikoff, B. Synthetic receptors based on molecularly imprinted polymers for mycotoxin analysis in food and beverages. Manuscript in preparation to *J. Agric. Food Chem*. **2004**.

13) <u>Molinelli, A</u>.; Mizaikoff, B. Understanding molecular imprints: IR spectroscopy for probing molecular interactions in pre-polymerization solutions. Manuscript in preparation to *Appl. Spectrosc*. **2004**.

REFERENCES

[1] Molinelli, A.; Mizaikoff, B. *Anal. Chem*.; submitted **2004**.

[2] Nicholls, I. A. *Anal. Chim. Acta* **2000**, 435, 9-18.

[3] Andersson, H. S.; Nicholls, I. A. *Bioorganic Chemistry* **1997**, 25, 203-211.

[4] Spivak, D. A.; Simon, R.; Campbell, J. *Anal. Chim. Acta* **2004**, 504, 23-30.

[5] Katz, A.; Davis, M. E. *Macromolecules* **1999**, 32, 4113-4121.

[6] Kim, H.; Spivak, D. A. *J. Am. Chem. Soc*. **2003**, 125, 11269-11275.

[7] Andersson, H. S.; Karlsson, J. G.; Piletsky, S. A.; Koch-Schmidt, A. C.; Mosbach, K.; Nicholls, I. A. *J. Chrom. A* **1999**, 848, 39-49.

[8] *Physical chemistry*. Atkins, P. W.; VCH: Weinheim, 1996.

[9] *Supramolecular chemistry*; Steed, J. W.; Atwood, J. L.; John Wiley & Sons: England, 2000.

[10] Perrin, C. L.; Nielson, J. B. „Strong hydrogen bonds in chemistry and biology". *Annu. Rev. Phys. Chem*. **48**, 511-544 (1997).

[11] Chapuis, F.; Pichon, V.; Lanza, F.; Sellergren, S.; Hennion, M.-C. J*. Chrom. A* **2003**, 999, 23-33.

[12] Janotta, M.; Weiss, R.; Mizaikoff, B.; Brüggemann, O.; Ye, L.; Mosbach, K. *Intern. J. Environ. Anal. Chem.* **2001**, 80(2), 75-86.

[13] Haupt, K.; Dzgoev, A.; Mosbach, K. *Anal. Chem*. **1998**, 70, 628-631.

[14] Fischer, E.; *Ber. Deutsch. Chem. Gesell*. **1894**, 27, 2985.

[15] Koshland, D. E., Jr.; *Proc. Natl Acad. Sci. USA* **1958**, 44, 98.

[16] Davies, D. R.; Cohen, G. H. *Proc. Natl. Acad. Sci. USA* **1996**, 93, 7-12.

[17] *Monolothic materials. Preparation, properties and applications*; Svec, F., Ed.; Tennikova, T. B., Ed.; Deyl, Z., Ed.; Journal of Chromatography Library, 64; Elsevier: Amsterdam, 2003.

[18] Viklund, C.; Ponten, E.; Glad, B.; Irgum, K.; Hörstedt, P.; Svec, F. *Chem. Mater*. **1997**, 9, 463-471.

[19] Wulff, G.; Knorr, K. *Bioseparation* **2002**, 10, 257-276.

[20] Andrews, P. R.; Craik, D. J.; Martin, J. L. *J. Med. Chem*. **1984**, 27, 1648-1657.

[21] Nicholls, I. A. *J. Mol. Recogn*. **1998**, 11, 79-82.

[22] Williams, D. H.; Cox, J. P. L.; Doig, A. J.; Gardner, M.; Gerhard, U.; Kaye, P. T.; Lal, A. R.; Nicholls, I. A.; Salter, C. J.; Mitchell, R. C. *J. Am. Chem. Soc*. **1991**, 113, 7020-7030.

[23] *Molecularly imprinted polymers. Man-made mimics of antibodies and their applications in analytical chemistry*; Sellergren, B., Ed.; Elsevier: Amsterdam, 2001.

[24] *Immunology*; Eisen, H. F.; Harper and Row: Hagerstown, Md., 1974.

[25] Yu, C.; Mosbach, K. *J. Chrom. A* **2000**, 888, 63-72.

[26] Sellergren, B.; Shea, K. J. *J. Chrom*. **1993**, 635, 31-49.

[27] Kempe, M.; Mosbach, K. *J. Chrom. A* **1995**, 694, 3-13.

[28] Yu, C.; Mosbach, K. *J. Mol. Recogn*. **1998**, 11, 69-74.

[29] Dauwe, C., Sellergren, B. *J. Chrom. A* **1996**, 753, 191-200.

[30] Ye, L.; Cormack, P. A. G.; Mosbach, K. *Anal. Commun*. **1999**, 36, 35-38.

[31] Vlatakis, G.; Andersson, L. I.; Müller, R.; Mosbach, K. *Nature* **1993**, 361, 645-647.

[32] Haupt, K. *Chem. Commun*. **2003**, 2, 171-178.

[33] Svenson, J.; Nicholls, I. A. *Anal. Chim. Acta* **2001**, 435, 19-24.

[34] Takeuchi, T.; Dobashi, A.; Kimura, K. *Anal. Chem*. **2000**, 72, 2418-2422.

[35] Andersson, L. I. *J. Chrom. B* **2000**, 739, 163-173.

[36] Ellwanger, A.; Berggren, C.; Bayoudh, S.; Crecenzi, C.; Karlsson, L.; Owens, P. K.; Ensing, K.; Cormack, P.; Sherrington, D.; Sellergren, B. *Analyst* **2001**, 126, 784-792.

[37] Weiss, R.; Freudenschuss, M.; Krska, R.; Mizaikoff, B. *Food Additives and Contaminants* **2003**, 20, 386-395.

[38] Matsui, J.; Fujiwara, K.; Takeuchi, T. *Anal. Chem*. **2000**, 72, 1810-1813.

[39] Scatchard, G.; *Ann. N. Y. Acad. Sci*. **1948**, 51, 660-672.

[40] Matsui, J.; Miyoshi, Y.; Doblhoff-Dier, O.; Takeuchi, T. *Anal. Chem*. **1995**, 67, 4404-4408.

[41] Dong, H.; Tong, A.; Li, L. *Spectrochim. Acta A* **2003**, 59, 279-284.

[42] Umpleby II, R. J.; Baxter, S. C.; Bode, M.; Berch Jr., J. K.; Shah, R. N.; Shimizu, K. D. *Anal. Chim. Acta* **2001**, 435, 35-42.

[43] Szabelski, P.; Kaczmarski, K.; Cavazzini, A.; Chen, Y.-B.; Sellergren, B.; Guiochon, G. *J. Chrom. A* **2002**, 964, 99-111.

[44] Umpleby II, R. J.; Baxter, S. C.; Chen, Y.; Shah, R. N.; Shimizu, K. D. *Anal. Chem*. **2001**, 73, 4584-4591.

[45] Umpleby II, R. J.; Bode, M.; Shimizu, K. D. *Analyst* **2000**, 125, 1261-1265.

[46] Baggiani, C.; Giraudi, G.; Giovannoli, C.; Tozzi, C.; Anfossi, L. *Anal. Chim. Acta* **2004**, 504, 43-52.

[47] Chen, W.-Y.; Chen, C.-S.; Lin, F.-Y. *J. Chrom. A* **2001**, 923, 1-6.

[48] O'Mahony, J.; Molinelli, A.; Nolan, K.; Smyth, M. R.; Mizaikoff, B. *Biosensors & Bioelectronics* **2004**, in press.

[49] Takeuchi, T.; Fukuma, D.; Matsui, J. *Anal. Chem.* **1999**, 71, 285-290.

[50] Piletsky, S.A.; Karim, K.; Piletska, E.V.; Day, C.J.; Freebairn, K.W.; Legge, C.; Turner, A.P.F. *Analyst* **2001**, 126, 1826-1830.

[51] Lanza, F.; Sellergren, B. *Anal. Chem.* **1999**, 71, 2092-2096.

[52] Chianella, I.; Lotierzo, M.; Piletsky, S. A.; Tothill, I. E.; Chen, B.; Karim, K.; Turner, A. P. F. *Anal. Chem*. **2002**, 74, 1288-1293.

[53] Subrahmanyam, S.; Piletsky, S. A.; Piletska, E. V.; Chen, B.; Karim, K.; Turner, A. P. F. *Biosensors & Bioelectronics* **2001**, 16, 631-637.

[54] Molinelli, A.; O'Mahony, J.; Nolan, K.; Smyth, M. R.; Jakusch, M.; Mizaikoff, B.; **2004**, *private communications*.

[55] Nicholls, I.A.; Adbo, K.; Andersson, H.S.; Andersson, P.O.; Ankerloo, J.; Hein-Dahlstrom, J.; Jokela, P.; Karlsson, J.G.; Olofsson, l.; Rosengren, J.; Shoravi, S.; Svenson, J.; Wikman, S. *Anal. Chim. Acta* **2001**, 435, 9-18.

[56] Lancelot, G. *J. Am. Chem. Soc*. **1977**, 99, 7037-7042.

[57] Hawley, J.; Bampos, N.; Aboitiz, N.; Jiminez-Barbero, J.; Lopez de la Paz, M.; Sanders, J.K.M.; Carmona, P.; Vicent, C. *Eur. J. Org. Chem.* **2002**, 1925-1936.

[58] Sellergren, B.; Lepistö, M.; Mosbach, K. *J. Am. Chem. Soc.* **1988**, 110, 5853-5860.

[59] Idziak, I.; Benrebouh, A.; Deschamps, F. *Anal. Chimica. Acta* **2001**, 435, 137-140.

[60] Svenson, J.; Karlsson, J. G.; Nicholls, I. A. *J. Chromatogr*. A **2004**, 1024, 39-44.

[61] Jie, Z.; Xiwen, H. *Anal. Chim. Acta* **1999**, 381, 85-91.

[62] Whitcombe, M. J.; Martin, L.; Vulfson, E. N. *Chromatographia* **1998**, 47, 457-464.

[63] Lu, Y.; Li, C.; Zhang, H.; Liu, X. *Anal. Chim. Acta* **2003**, 489, 33-43.

[64] Svenson, J.; Andersson, H. S.; Piletsky, S. A.; Nicholls, I. A. *J. Mol. Recogn*. **1998**, 11, 83-86.

[65] Liu, Y.; Liu, X.; Wang, J. *Anal. Lett*. **2003**, 36, 1631-1645.

[66] Bartko, A. P.; Dickson, R. M. *J. Phys. Chem. B* **1999**, 103, 3053-3056.

[67] Shea, K. J.; Sasaki, D. Y. *J. Am. Chem. Soc*. **1991**, 113, 4109-4120.

[68] Caro, E.; Marcé, R. M.; Cormack, P. A. G.; Sherrington, D. C.; Borrull, F. *J. Chrom. A* **2003**, 995, 233-238.

[69] Andersson, L. I.; Paprica, A.; Arvidsson, T. *Chromatographia* **1997**, 46, 57-62.

[70] Muldoon, M. T.; Stanker, L. H. *Anal. Chem.* **1997**, 69, 803-808.

[71] Mullett, W. M.; Lai, E. P. C. *Anal. Chem.* **1998**, 70, 3636-3641.

[72] Molinelli, A.; Weiss, R.; Mizaikoff, B. *J. Agric. Food Chem*. **2002**, 50, 1804-1808.

[73] Zander, Å.; Findlay, P.; Renner, T.; Sellergren, B. *Anal. Chem.* **1998**, 70, 3304-3314.

[74] Cacho, C.; Turiel, E.; Martín-Esteban, A.; Pérez-Conde, C.; Camara, C. *Anal. Bioanal. Chem*. **2003**, 376, 491-496.

[75] Masqué, N.; Marcé, R. M.; Borrull, F.; Cormack, P. A. G.; Sherrington, D. *Anal. Chem*. **2000**, 72, 4122-4126.

[76] Panasyuk, T. L.; Mirsky, V. M.; Piletsky, S. A.; Wolfbeis, O. S. *Anal. Chem.* **1999**, 71, 4609-4613.

[77] Panasyuk-Delaney, T.; Mirsky, V. M.; Ulbricht, M.; Wolfbeis, O. S. *Anal. Chim. Acta* **2001**, 435, 157-162.

[78] Sode, K.; Ohta, S.; Yanai, Y.; Yamazaki, T. *Biosensors and Bioelectronics* **2003**, 18, 1485-1490.

[79] Haupt, K.; Noworyta, K.; Kutner, W. *Anal. Commun*. **1999**, 36, 391-393.

[80] Kriz, D.; Ramström, O.; Svensson, A.; Mosbach, K. *Anal. Chem*. **1995**, 67, 2142-2144.

[81] Nopper, D.; Lammershop, O.; Wulff, G.; Gauglitz, G. *Anal. Bioanal. Chem*. **2003**, 377, 608-613.

[82] Jakusch, M.; Janotta, M.; Mizaikoff, B.; Mosbach, K.; Haupt, K. *Anal. Chem*. **1999**, 71, 4786-4791.

[83] Wang, H. Y.; Kobayashi, T.; Fujii, N. *Langmuir* **1996**, 12, 4850-4856.

[84] Ramamoorthy, M.; Ulbricht, M. *J. Membr. Sci*. **2003**, 217, 207-214.

[85] Hong, J.-M.; Anderson, P. E.; Qian, J.; Martin, C. R. *Chem. Mater.* **1998**, 10, 1029-1033.

[86] Piletsky, S. A.; Matuschewski, H.; Schedler, U.; Wilpert, A.; Piletska, E. V.; Thiele, T. A.; Ulbricht, M. *Macromolecules* **2000**, 33, 3092-3098.

[87] Mathew-Krotz, J.; Shea, K. J. *J. Am. Chem. Soc*. **1996**, 118, 8154-8155.

[88] Sergeyeva, T. A.; Piletsky, S. A.; Piletska, E. V.; Brovko, O. O.; Karabanova, L. V.; Sergeeva, L. M.; El'skaya, A. V.; Turner, A. P. F. *Macromolecules* **2003**, 36, 7352-7357.

[89] Glad, M.; Norrlöw, O.; Sellergren, B.; Siegbahn, N.; Mosbach, K. *J. Chromatogr*. **1985**, 347, 11-23.

[90] Yilmaz, E.; Haupt, K.; Mosbach, K. *Angew. Chem. Intl. Ed*. **2000**, 39, 2115-2118.

[91] Hart, B. R.; Shea, K. J. *J. Am. Chem. Soc*. **2000**, 123, 2072-2073.

[92] Hart, B. R.; Shea, K. *Macromolecules* **2002**, 35, 6192-6201.

[93] Kempe, M.; Mosbach, K. *J. Chrom. A* **1995**, 691, 317-323.

[94] Shi, H.; Tsai, W.-B.; Garrison, M. D.; Ferrari, S.; Ratner, B. D. *Nature* **1999**, 398, 593-597.

[95] Aherne, A.; Alexander, C.; Payne, M. J.; Perez, N.; Vulfson, E. N. *J. Am. Chem. Soc.* **1996**, 118, 8771-8772.

[96] Dickert, F. L.; Hayden, O. *Anal. Chem.* **2002**, 74, 1302-1306.

[97] Conrad II, P. G.; Nishimura, P. T.; Aherne, D.; Schwartz, B. J.; Wu, D.; Fang, N.; Zhang, X.; Roberts, M. J.; Shea, K, J. *Adv. Mater.* **2003**, 15, 1541-1544.

[98] Bossi, A.; Piletsky, S. A.; Piletska, E. V.; Righetti, P. G.; Turner, A. P. F. *Anal. Chem.* **2001**, 73, 5281-5286.

[99] Krebs, J. F.; Borovik, A. S. *J. Am. Chem. Soc.* **1995**, 117, 10593-10594.

[100] Matsui, J.; Nicholls, I. A.; Karube, I.; Mosbach, K. *J. Org. Chem.* **1996**, 61, 5414-5417.

[101] Sellergren, B.; Karmalkar, R. N.; Shea, K. J. *J. Org. Chem.* **2000**, 65, 4009-4027.

[102] Emgenbroich, M.; Wulff, G. *Chem. Eur. J.* **2003**, 9, 4106-4117.

[103] Fireman-Shoresh, S.; Avnir, D.; Marx, S. *Chem. Mater.* **2003**, 15, 3607-3613.

[104] Zimmerman, S. C.; Wendland, M. S.; Rakow, N. A.; Zharov, I.; Suslick, K. S. *Nature* **2002**, 418, 399-403.

[105] Synge, R. L. M.; Martin, A. J. P. *Journal of Biochemistry* **1941**, 35, 1358-1368.

[106] Van Deemter, J. J.; Zuiderweg, F. J.; Klinkenberg, A. *Chem. Eng. Sci.* **1956**, 5, 271-289.

[107] Van Deemter, J. J.; Zuiderweg, F. J.; Klinkenberg, A. *Chem. Eng. Sci.* **1995**, 50(24), 3869-3882.

[108] *Analytical Chemistry*. Kellner, R.; Mermet, J.-M.; Otto, M.; and Widmer, H. M. Wiley VCH, Weinheim, 1998.

[109] Brunauer, S.; Emmett, P. H., Teller, E. *J. Am. Chem. Soc*. **1938**, 60, 309-319.

[110] Barrett, E. P.; Joyner, L. G.; Halenda, P. P. *J. Am. Chem. Soc*. **1951**, 73, 373-380.

[111] Hennion, M.-C.; *J. Chrom. A* **1999**, 856, 3-54.

[112] *Sampling and sample preparation techniques for field and laboratory*. Ed. Pawliszyn, J. Elsevier, Amsterdam, The Netherlands, 2002.

[113] Liska, I. *J. Chrom.* **1993**, 655, 163-176.

[114] Hennion, M.-C.; Cau-Dit-Coumes, C.; Pichon, V. *J. Chrom. A* **1998**, 823, 147-161.

[115] Liu, R.; Zhou, J. L.; Wilding, A. *J. Chrom. A* **2004**, 1022, 179-189.

[116] Chapuis, F.; Pichon, V.; Lanza, F.; Sellergren, B.; Hennion, M.-C. *J. Chrom. B* **2004**, 804, 93-101.

[117] Lancelot, G. *J. Am. Chem. Soc* **1977**., 99, 7037-7042.

[118] Hawley, J.; Bampos, N.; Aboitiz, N.; Jiminez-Barbero, J.; Lopez de la Paz, M.; Sanders, J. K. M.; Carmona, P.; Vicent, C. *Eur. J. Org. Chem.* 2002, 12, 1925-1936.

[119] *Comprehensive supramolecular chemistry*. Ed. Atwood, J. L.; Davies, J. E. D.; MacNicol, D. D.; Vögtle, F. Volume 8, Pergamon, New York, 1996.

[120] Correia, I.; Bezzenine, N.; Ronzani, N.; Platzer, N.; Beloeil, J.-C.; Doan, B.-T. *J. Phys. Org. Chem*. **2002**, 15, 647-659.

[121] Martins de Carvalho, E.; Velloso, M. H. R.; Tinoco, L. W.; Figueroa-Villar, J. D. *Journal of Magnetic Resonance* **2003**, 164, 197-204.

[122] *Nuclear Magnetic Resonance*. Hore, P. J. Oxford University Press Inc., New York, 1995.

[123] Martin, M. L.; Martin, G. J.; Delpuech, J.-J. *Practical NMR Spectroscopy*. Heyden & Son Ltd, London, 1980.

[124] *Binding Constants. The Measurement of Molecular Complex Stability*. Connors, K. A. John Wiley & Sons, New York, 1987.

[125] Benesi, H. A.; Hildebrand, J. H. *J. Am. Chem. Soc.* **1949**, 71, 2703-2707.

[126] Job, P. *Ann. Chim.* **1928**, 9, 113-199.

[127] Vosburgh, W. C.; Cooper, G. R. *J. Am. Chem. Soc.* **1941**, 63, 437-442.

[128] Poë, A. J. *J, Phys. Chem*. **1963**, 67, 1070-1073.

[129] *Molecular Modeling, Principles and Applications*. Leach, A. R.; Pearson education, second edition, 2001.

[130] Verlet, L.. *Physical Review* **1967**, 165, 201-204.

[131] Rodger, P. M. *Mol. Sim*. **1989**, 3, 263.

[132] Hockney, R. W. *Methods in Computational Physics* **1970**, 9, 136-211.

[133] Bolton, K.; Nordholm, S. *J. Comput. Phys*. **1994**, 113(2), 320-335.

[134] *Computer Simulation of Liquids*. Allen, M. P.; Tildesley, D. J.; Oxford: Clarendon, 1987.

[135] Case, D. A.; Pearlman, D. A.; Caldwell, J. W.; Cheatham III, T. E.; Wang, J.; Ross, W. S.; Simmerling, C. L.; Darden, T. A.; Merz, K. M.; Stanton, R. V.; Cheng, A. L.; Vincent, J. J.; Crowley, M.; Tsui, V.; Gohlke, H.; Radmer, R. J.; Duan, Y.; Pitera, J.; Massova, I.; Seibel, G. L.; Singh, U. C.; Weiner, P. K.; and Kollman, P. A. (2002), AMBER 7, University of California, San Francisco.

[136] Humphrey, W.; Dalke, A; Schulten, K. *J. Molec. Graphics* **1996**, 14, 33-38.

[137] Wang, J.; Cieplak, P.; Kollman, P. A. *J. Comput. Chem.* **2000**, 21, 1049-1074.

[138] Pearlman, D. A.; Case, D. A.; Caldwell, J. W.; Ross, W. S.; Cheatham, T. E., III; DeBolt, S.; Ferguson, D.; Seibel, G.; Kollman, P. *Comp. Phys. Commun*. **1995**, 91, 1-41.

[139] Jorgensen, W. L.; Chandrasekhar, J.; Madura, J.; Klein, M. L. *J. Chem. Phys.* **1983**, 79, 926-935.

[140] Ewald, P. *Annalen der Physik* **1921**, 64, 253-287.

[141] Tsui, V.; Case, D. A. *J. Am. Chem. Soc.* **2000***,* 122, 2489-2498.

[142] Pittet, A. *Revue de Médecine Vétérinaire* **1998***,* 149(6), 479-492.

[143] Creppy, E. E. *Toxicology Letters* **2002**, 127(1-3), 19-28.

[144] Scott, P. M. *Journal of AOAC International* **1996**, 79, 875-882.

[145] Krska, R.; Josephs, R. *Fresenius J. Anal. Chem.* **2001**, 369, 469-476.

[146] Schuhmacher, R.; Krska, R.; Weingaertner, J.; Grasserbauer, M. *Fresenius J. Anal. Chem.* **1997**, 359, 510-515.

[147] Langseth, W.; Rundberget, T. *J. Chrom. A* **1998**, 815, 103-121.

[148] Hollman, P. C. H.; Arts, I. C. W. *J. Sci. Food Agric*. **2000**, 80, 1081-1093.

[149] *The Flavonoids, Parts 1 and 2*. Harborne, J. B.; Mabry, T. J.; Mabry, H.; Academic Press, New York, 1975.

[150] McDonald, M. S.; Hughes, M.; Burns, J.; Lean, M. E. J.; Matthews, D.; Crozier, A. *J. Agric. Food Chem*. **1998**, 46, 368-375.

[151] Burns, J. et. al. *J. Agric. Food Chem*. **2000**, 48, 220-230.

[152] Wattel, A.; Kamel, S.; Prouillet, C.; Petit, J.-P.; Lorget, F.;Offord, E.; Brazier, M. *J. Cellul. Biochem*. **2004**, 92, 285-295.

[153] Merken, H, M.; Beecher, G. R. *J. Agric. Food Chem*. **2000**, 48, 577-599.

[154] Weiss, R.; Molinelli, A.; Jakusch, M.; Mizaikoff, B. *Bioseparation* **2002**, 10, 379-387.

[155] Molinelli, A.; Janotta, M.; Mizaikoff, B. Molecularly imprinted polymers for biomolecular recognition. Chapter 11; Protein nanotechnology: protocols, instrumentation, and applications; Ed. T. Vo Dinh (Methods in molecular biology, Vol. 300). Humana Press Inc.: Totowa, NJ, USA. In press **2004**.

[156] O'Mahony, J.; Molinelli, A.; Nolan, K.; Smyth, M. R.; Mizaikoff, B. *Anal. Chim. Acta*, submitted 2004.

[157] Krska, R.; Baumgartner, S.; Josephs, R. *Fresenius J. Anal. Chem*. **2001**, 371, 285-299.

[158] Scott, P. M. *J. AOAC Int*. **1996**, 79, 875-882.

[159] Fischbach, H.; Rodricks, J. V. *J. AOAC* **1973**, 56, 767-770.

[160] Moller, T. E.; Gustavsson, H. F. *J. AOAC Int*. **1992**, 75, 1049-1053.

[161] Miranda, C. L.; Stevens, J. F.; Ivanov, V.; McCall, M.; Frei, B.; Deinzer, M. L.; Buhler, D. R. *J. Agric. Food Chem*. **2000**, 48, 3876-3884.

[162] Krska, R.; Welzig, E.; Berthiller, F.; Molinelli, A.; Mizaikoff, B. *Anal. Bioanal. Chem*.; submitted **2003**.

[163] Blackwell, B. A.; Greenhalgh, R.; Bain, A. D. *J. Agric. Food. Chem*. **1984**, 32, 1078-1083.

[164] Lauren, D. R.; Smith, W. A. *Food Add. Cont*. **2001**, 18, 1011-1016.

[165] Yumbe-Guevara, B. E.; Imoto, T.; Yoshizawa, T. *Food Add. Cont*. **2003**, 20, 1132-1140.

[166] Jodlbauer, J.; Maier, N. M.; Lindner, W. *J. Chrom. A* **2002**, 945, 45-63.

[167] Molinelli, A.; O'Mahony, J.; Nolan, K.; Smyth, M. R.; Mizaikoff, B. *Angew. Chem., Int. Ed*.; submitted 2004.

[168] Tamres, M., Searles, S., Leighly, E. M.; Mohrman, D. W. *J. Am. Chem. Soc*. **1954**, 76, 3983-3985.

[169] Barrow, G. M.; Yerger, E. A. *J. Am. Chem. Soc*. **1954**, 76, 5211-5216.

[170] Abraham, M. H.; Prior, D. V.; Schulz, R. A.; Morris, J. J.; Taylor, P. J. *J. Chem. Soc., Faraday Trans*. **1998**, 94, 879-885.

[171] Levenberg, K. *Quart. Appl. Math*. **1944**, 2, 164-168.

[172] Marquardt, D. *SIAM J. Appl. Math*. **1963**, 11, 431-441.

[173] Harris, Jr., J. T.; Hobbs, M. E. *J. Am. Chem. Soc.* **1954**, 76, 1419-1422.

[174] *The handbook of IR and Raman characteristic frequencies of organic molecules.* Lin-Vien, D., Colthup, N. B., Fateley, W. G., Grasselli, J. G. Academic Press, Boston (1991).

[175] Johnson, S. L.; Rumon, K. A. *J. Phys. Chem.***1965**, 69, 74-86.

[176] Barrow, G. M. *J. Am. Chem. Soc.* **1956**, 78, 5802-5806.

[177] Levenberg, K. *Q. Appl. Math.* **1944**, 2, 164-168.

[178] Marquardt, D. W. *J. Soc. Indust. Appl. Math.* **1963**, 11, 431-441.

[179] Pei, K., Li, Y.; Li, H. *J. Mol. Struct.* **2003**, 660, 113-118.

[180] Drichko, N. V., Kerenskaia, G. Y.; Schreiber, V. M. *J. Mol. Struct.* **1999**, 477, 127-141.

[181] *Introduction to NMR Spectroscopy*. Abrahams, R. J.; Fisher, J.; Loftus, P. 1st Ed. Wiley, New York, 1988.

[182] Anderson, J. E. *J. Chem. Phys.* **1969**, 51, 3578-3581.

[183] Pogliani, L. *Computers Chem.* **1996**, 17(3), 283-286.

[184] Hunter, C. A.; Saunders, J. K. M.; *J. Am. Chem. Soc.***1990**, 112, 5525-5534.

[185] Martin, C. B.; Mulla, H. R.; Willis, P. G.; and Cammers-Goodwin, A. *J. Org. Chem.* **1999**, 64, 7802-7806.

[186] Sinnokrot, M. O.; Sherrill, C. D. *J. Am. Chem. Soc.* **2004**, 126, 7690-7697.

[187] Linse, P. *J. Am. Chem. Soc.* **1992**, 114, 4366-4373.

[188] Guillot, B. *J. Chem. Phys*. **1991**, 95, 1543-1551.

[189] Kukol, A.; Adams, P. D.; Rice, L. M.; Brunger, A. T.; Arkin, I. T. *J. Mol. Biol*. **1999**, 286, 951-962.